Formation control for a group of underactuated vehicles

Dang Hao Nguyen

Département de formation doctorale en automatique **École doctorale IAEM Lorraine**
UFR Sciences et Technologies

Formation control for a group of underactuated vehicles

THÈSE

présentée et soutenue publiquement le 7 Décembre 2015

pour l'obtention du

Doctorat de l'Université de Lorraine

(Spécialité automatique)

par

NGUYEN Dang Hao

Composition du jury

Rapporteurs :	Mohammed CHADLI	Maître de conférences HDR, Université de Picardie, AMIENS
	Rogelio LOZANO	Directeur de recherche, HEUDIASYC, CNRS, Compiègne
Examinateurs :	Fréderic KRATZ	Professeur, INSA Centre Val de Loire
	Mohamed BOUTAYEB	Professeur, Université de Lorraine (Directeur de thèse)
	Hugues RAFARALAHY	Maître de conférences, Université de Lorraine

Centre de Recherche en Automatique de Nancy —CNRS UMR 7039

Mis en page avec la classe thloria.

Acknowledgments

First and foremost, I am indebted to my supervisor Professor Mohamed BOUTAYEB and my external supervisor Maître de conférences Hugues RAFARALAHY, at the Research Center for Automatic Control of Nancy, Lorraine University, for their guidance, help, support, comments and sharing their technical knowledge. In supervising my research, both of my supervisors gave me freedom and encouraged me to manage my research on my own.

I would like to thank committee members, Professor Rogelio LOZANO - Directeur de recherche, HEUDIASYC, Compiègne; Maître de conférences HDR, Mohammed CHADLI - Université de Picardie, AMIENS; Professeur Fréderic KRATZ - INSA Centre Val de Loire and my two supervisors for their careful reading and constructive comments to my thesis.

I wish to express my gratitude to the staff of CRAN-Longwy: Michel Zasadzinski, Harouna Souley Ali, Mohamed Darouach, Marouane ALMA, BOUTAT-BADDAS Latifa, ZEMOUCHE Ali. For my external supervisor, I am grateful for his French abstract translation. I also would like to thank all the PhD students whom I have encountered during the last four years: Lama HASSAN, Adrien Drouot, Nan Gao, Yassine BOUKAL, Ghazi BEL HAJ FREJ, Bessem BHIRI, GUELLIL Assam, Asma Barbata, CHAIB DRAA Khadidja, Gloria Lilia Osorio-Gordillo,...

I would like to give thanks to my coworkers of Thai Nguyen University of Technology for their help and encouragement. My acknowledgments are also sent to Professor Nguyen Dang Binh - Viet Bac University, Vietnam and Professor Do Khac Duc - Department of mechanical engineering, Curtain University, Australia for their guidance, support, help and encouragement.

I thank those people in my personal life whose love and support made this dissertation possible. My parents and sisters encourage me to do research. I am grateful for my wife Gia Thi Dinh for her patience love and sacrifice that she has given to me, my son Nguyen Dang Quang and my daughter Nguyen Gia Binh An.

The work presented in the thesis was supported by the 322 project - Vietnamese government and Research Center for Automatic Control of Nancy, Lorraine University, France.

To my parents,
my sister Huong - Doan and Dao - Hai,
to my wife Dinh, and to Dang Quang - Binh An

Contents

Notation and acronyms

Acronyms

2D	2 Dimensions
3D	3 Dimensions
UAVs	Unmanned aerial vehicles.
VTOL UAV	A vertical take-off and landing unmanned aerial vehicle.
GPS	Global Positioning System
IMU	Inertial Measurement Unit
LIDAR	Light Detection And Ranging
RADAR	Radio Detection And Ranging
SLAM	Simultaneous Localization And Mapping

Notations and Variables

$\odot$	The quaternion product between two unit quaternions
NED	Ortho-normal coordinate system where the x-axis is directed towards the Earth's magnetic North pole, the y-axis directed towards the East, and the z-axis is directed downwards.
E	Inertial (Fixed) Coordinate Frame rigidly attached to a position on the Earth (assumed flat) expressed in NED coordinates.
B	Body Coordinate Frame rigidly attached to the rigid-body center of gravity, where the x-axis is directed towards the front of the rigid-body, the y-axis is directed towards the right-hand-side of the rigid-body, and the z-axis is directed towards the bottom of the rigid-body.
$\boldsymbol{p}$	Position of the frame B expressed in the frame E.
x, y, z	Elements of vector $\boldsymbol{p}$.
$\boldsymbol{v}$	Linear velocity of the frame B expressed in the frame E.
v_1, v_2, v_3	Elements of vector $\boldsymbol{v}$.
$\boldsymbol{Q}$	The set of unit-quaternion, or equivalently, the set of unit length vectors in $\mathbb{R}^4$, or equivalently the set of vectors contained in S3 (4-dimensional unit-sphere). The unit-quaternion belonging to the set $\mathbb{Q}$ which describes the relative orientation of B taken with respect to E.
η, $\boldsymbol{q}$	Elements of vector $\boldsymbol{Q}$.
q_1, q_2, q_3	Elements of vector $\boldsymbol{q}$.
$\boldsymbol{\eta}$	Orientation vector in Euler angles
$\boldsymbol{\omega}$	Angular velocity of the frame B expressed in the frame E.
g	Acceleration due to gravity ($9.81m/s^2$).
m, J_1	Mass of quadrotor.
$\boldsymbol{J}$	Inertia matrix of quadrotor.
T	Thrust force.
$\boldsymbol{\tau}$	Torque.
$\boldsymbol{e}_3$	The unit vector $[0, 0, 1]^T$.
$\boldsymbol{R}_{\eta}^{T}(\boldsymbol{\eta})$	Transformation matrix of the translational subsystem in Euler angles.
$\boldsymbol{K}_{\eta}(\boldsymbol{\eta})$	Transformation matrix of the rotational subsystem in Euler angles.
$\boldsymbol{R}_{Q}^{T}(\boldsymbol{Q})$	Transformation matrix of the translational subsystem in quaternions.
$\boldsymbol{K}_{Q}(\boldsymbol{Q})$	Transformation matrix of the rotational subsystem in quaternions.
ϕ, θ, ψ	Elements of vector $\boldsymbol{\eta}$.
K_t, K_d	Thrust and drag coefficients
l	The distance between the center of mass of the quadrotor and the center of a propeller.
G_1, G_2, G_3, G_4	The angular velocity of propeller 1, 2, 3, 4.
f_1, f_2, f_3, f_4	Forces generated by propeller 1, 2, 3, 4.

$S(\cdot)$	Sine of $(\cdot)$.
$C(\cdot)$	Cosine of $(\cdot)$.
$T(\cdot)$	Tangent of $(\cdot)$.
$\boldsymbol{F}$	Intermediate control input.
$\boldsymbol{\alpha}_\eta$	Orientation vector in Euler angles
α_ϕ, α_θ, and α_ψ	Elements of vector $\boldsymbol{\alpha}_\eta$.
$\boldsymbol{p}_d$	Reference position vector.
ψ_d	Reference heading angle.
$\boldsymbol{Q}_d$	Reference unit quaternion vector.
$\boldsymbol{\omega}_d$	Reference angular velocity vector in quaternions.
$\boldsymbol{p}_e$	Position tracking errors.
$\boldsymbol{Q}_e$	Attitude tracking errors.
$\boldsymbol{v}_e$	Linear velocity tracking errors.
$\boldsymbol{\omega}_e$	Angular velocity tracking errors.
$\boldsymbol{d}_v$	Disturbance acting on the translational subsystem.
$\boldsymbol{d}_\omega$	Disturbance acting on the rotational subsystem.

List of Figures

CHAPTER

1

Introduction

Contents

1.1 Introduction

A cooperative system is defined to be multiple dynamic entities that share information or tasks to accomplish a common task. Some cooperative control systems might include: robots operating within a manufacturing cell, unmanned aircraft in search and rescue operations or military surveillance and attack missions. The term entity is most often associated with vehicles capable of physical motion such as mobile robots, underwater vehicles, and aircraft, but the definition extends to any entity concept that exhibits a time dependent behavior. The ability to maintain the position of a group of autonomous vehicles relative to each other or relative to references is referred as formation control. A team of manned or unmanned vehicles working together is often more effective than a single agent acting alone in applications like surveillance, search and rescue, perimeter security, and exploration of unknown and/or hazardous environments. For example, a team of these vehicles each with a variety of sensors offers the opportunity for increased sensor coverage when compared to a single mobile sensor or multiple stationary sensors.

Formation control relates with the motion control of multiple vehicles to accomplish a common task. The study of formation control is motivated by the advantages achieved by using a formation of vehicles, instead of a single vehicle. The common unmanned vehicles would be a variety of kinds of vehicles from on the ground, in the water to in the space. The formation of vehicles may be constructed as centralized or decentralized control. In both schemes, the communication and transition information keep a crucial key. In centralized control, a main station is used to plan tasks for agents in formation to perform. This can be advantageous because it has all information receiving from network so that the optimal tasks can be centralized and generated to achieve a global objective. However, centralized control requires more power of computation and multi-directional information flow. In contrast, decentralized control requires local information exchange between agents to achieve the control objective goal. Comparing with centralized control, the multi-directional information flow is divided to the agents in the decentralized control. However, there usually exists delay in exchange information between agents. Several formation control approaches have been considered in the literature such as leader-follower [AT13, BMF+11, BM02, EBOA04], behavior-based [BLH01, BSZX12], virtual structure [CMSW11, BLH01, AT09], Geometric formation based on graph theory [ZK12], on flocking [BVV11], and on swam aggregation [PAR05, HC08]. These approaches can be cataloged into three main group [SHP04]: leader-follower, behavioral, and virtual structure.

The leader-follower approach ([AT13, BMF+11, BM02, EBOA04]) uses several agents as leaders and others as followers. The common task consists of forcing the followers tracking the leaders. There are variety of successful publications using this approach for teams of mobile robots [DL12, MS13], underwater vehicles [CS11, Sho15], and UAVs [YCLL08, RCC+14, AT13]. This approach ensures coordination maintenance if the leaders are disturbed but the desired coordination shape can not be maintained if the followers are perturbed unless a feedback is implemented [EH01].

The behavior-based approach consisting of prescribing several desired behaviors such as neighbor tracking, collision and obstacle avoidance, and formation keeping is assigned for each individual agent [Ark98]. This approach can naturally be used to design control strategies for robots with multiple competing objectives. Moreover, it is suitable for large groups of robots, since it is typically a decentralized strategy. A disadvantage of this method is that the complexity of the dynamics of the group of robots does not lend itself for simple mathematical stability analysis [LRH$^+$08]. This approach has been employed in interesting applications applying for mobile robots [CL98, LRH$^+$08, LSZ14], underwater vehicles [SB00], and UAVs [CSW12, KK07, KKT09]. The flocking and swam aggregation can be cataloged in the behavioral group.

Virtual structure approach treats all the agents as a single entity, and is amenable to mathematical analysis but has difficulties in controlling critical points. The application of this approach can be found in [Do11, SHK$^+$11, Low14] for mobile robots, [Do12] underwater vehicles , and [Low11, Do15] for UAVs.

The above approaches and applications of formation control consist of several issues in cooperative control. Formation control for aerial vehicles is also relative with motion control of whole group of vehicles to accomplish the common task and with motion control of each individual vehicle. An autonomous underactuated quadrotor is an aerial vehicle which usually has three to five fixed propellers or actuators. The quadrotor used in this thesis has four fixed propellers and is one kind of VTOL UAVs. The formation control design for this kind of vehicles has been developed in both theory and experiment. It can be classified into three layers. The first layer is responsible for generating reference trajectories or creating a common task. Depending on the formation control structure and approach, the suitable trajectory or task is formed. The communication is extremely important to the success of the formation control task. The data receiving from sensors for common task and the data exchanging among formation can be used for many purposes such as collision avoidance or collecting sampling data. The communication delay problem in leader-follower formation of VTOL UAVs can be referred in [AT13]. The collision avoidance based on the exchanging information among VTOL UAVs can be found in [Do15]. The third layer contains individual quadrotors which are the most basic element of the formation. An underactuated quadrotor has only four actuators when the degree of freedom to be controlled is six. One can refer the difficulty in the control design for the underactuated vehicles in [DP09]. Since the quadrotor dynamics is underactuated and no general method exists to design efficient autonomous navigation system for these vehicles. In fact, the position of quadrotor is modeled in SE(3) and the Euler angles or quaternions are usually used to represent its attitude. The singularity, using Euler angles for representing attitude, is a challenging problem when desiring the global or semi-global results. Moreover, although the attitude describing in quaternions can avoid the singularity in the model, it still also is a daresay problem to achieve the global results. The control strategies have proposed in the literature including feedback linearization [Kha02], backstepping [KKK95], slide-mode [Kha02], high gain [SDFC01] and nested saturation [Tee92] method. Since the dynamics of quadrotor can be separated into two subsystems, the translational subsystem and the rotational subsystem. The rotational subsystem has three actuators

with three degree of freedom to be controlled whereas the translational has only one actuator to control for three remained degree of freedom. This mean that it can directly apply the control technique to design control for the rotational subsystem while the coordinate transformation techniques [OSM98, DP09] must be used for the translational subsystem.
The attitude controllers assume that the system attitude and angular velocity are accurately known [WKD91, JKW95]. A number of authors also developed the attitude controller without the system angular velocity measurements [Tay08, Tsi98]. To deal with the absence of angular velocity measurements, an auxiliary system, lead filter, or attitude observer [Rob11], are used to provide these values to the controller.
Position control for VTOL UAVs has been focused in several groups in the research community. Due to the underactuated nature of VTOL UAVs, the system attitude must be used in order to control the position and velocity of the system. The objective for this case is design control inputs such that the position and velocity errors comparing with the reference converging to zero. The authors [MDTMC09] use a thrust vector, a function of the attitude and system thrust which is associated with the system acceleration, to attempt this objective. In other cases, the authors [Rob11] employ a thrust and attitude extraction algorithm to generate suitable thrust and reference attitude for the rotational subsystem as the reference inputs. This algorithm makes the control design process simpler. However, the heading angle of the vehicle is not concerned. Thus, the problem of self-rotation around the vertical axis may be occurred. To overcome this problem, the author [DP13] uses the standard backstepping control design technique and a combination of Euler angles and quaternions to achieve the global results. However, the designed control is quit complicated. It can be seen that the control design for VTOL UAVs is complicated for a number of reasons, for instance, the coupling between two subsystems, the effect of external disturbance, uncertainties of the dynamics, the singularities and requirement of achieving the global results.

1.2 Thesis contributions and organization

The thesis consists of five chapters and two appendices. The contributions are presented two main parts. The first part consists chapter 3 presenting two controllers for a single quadrotor and introducing a new thrust and attitude extraction algorithm. The second part consists of chapter 4. This part presents new results of formation control for multiple quadrotors where the thrust and attitude extraction is embedded in the designed controllers.
The thesis is organized as follows:

- **Chapter 1** presents an overview of formation control, formation control for VTOL UAVs, control of a single VTOL UAV, and summary of contributions of the thesis.
- **Chapter 2** provides an overview of the mathematical background used in development and analysis of the control laws. The basic equations of motion of an underactuated quadrotor and of multiple quadrotors are described in the form of Euler angles and quaternions. It

also introduces some other mathematical tools such as projection operation, smooth and smooth step function, and an adaptive controller for second order system.

- **Chapter 3** contains two controllers for a single quadrotor, one using Euler angles and one employing quaternions. By using conversion between Euler angles and quaternions, a thrust and attitude extraction algorithm is generated. This algorithm is embedded in the formation controller in the next sections.

- **Chapter 4** consists of some formation controllers. In this chapter, two formation control design approaches are presented. The first approach uses the virtual structure to develop three formation controllers and the second approach employs the leader-follower combining with virtual structure to expand two adding formation controllers. The collision avoidance function based on the smooth step function and pairwise smooth step function is embedded in the controller to avoid collision among quadrotors and obstacles.

- **Chapter 5** provides a summary of the work in the thesis and discusses some research areas in the future.

- **Appendix 1 and 2**: consists of some proof of lemma and theorem in the thesis.

CHAPTER

2

Mathematical Preliminaries

Contents

In this chapter we review some of the mathematical background that is used in the development and analysis of the control and estimation laws. The equations of motion for a single quadrotor and for multiple quadrotors are presented in Section 2.1. Some preliminary results used in the control design and stability analysis are illustrated in the next sections such as projection operation, backstepping controller, saturation functions, smooth step function, and pairwise collision avoidance functions.

2.1 Equations of motion of quadrotor

To represent the position and orientation of a quadrotor, we use two reference frames:

- **Inertial or fixed to earth frame E**: A frame rigidly attached to a position on the Earth in NED coordinates (NED: North-East-Down coordinate system: Refers to the right-handed frame where the x axis is directed towards North, y axis is directed towards the East, and the z axis is directed downwards to the Earth).
- **Body fixed frame B**: A frame which is rigidly attached to the quadrotor where the origin of the body fixed frame is coincident with the center of mass of the quadrotor. The x axis is directed towards the front of the quadrotor, the y axis is taken towards the right side, and the z axis is directed downwards.

The quadrotor used to model in this section is an X-type fixed pitch copter. It has four fixed propellers mounted on the respective electric motors as shown in Figure 2.1. With this configuration, the lift coefficient provided by each propeller is fixed. Therefore the change of angular velocity of the motors is chosen to produce control input for the quadrotor. To avoid gyroscopic effects and aerodynamic torques, the rotate direction of the motor one and three is installed opposite with the motor two and four as shown in Figure 2.2. It can be seen from this figure that there are no actuators on sway and surge. The actuators acting on heave, roll, pitch and yaw are functions of f_i, including total forces generated by four propellers, the torques created by $(f_4 - f_2)$, $(f_3 - f_1)$, and $(-f_1 + f_2 - f_3 + f_4)$, respectively.
The earth-fixed frame and a body-fixed frame are defined as described in Figure 2.2. To simplify the effects of internal and external disturbances are omitted and the following assumptions are employed.

Assumption 2.1.

- *The quadrotor structure is rigid and symmetric.*
- *The gravity center of the rigid is coincided with the origin body-fixed frame coordinate.*
- *The propellers are rigid, the thrust and drag forces in each propeller are proportional to the square of speed of the propellers* $(f_i = K_t G_k^2; k = 1, \ldots, 4)$*, and all propellers have the same coefficient,* K_t*.*

Figure 2.1: A X-type quadrotor.

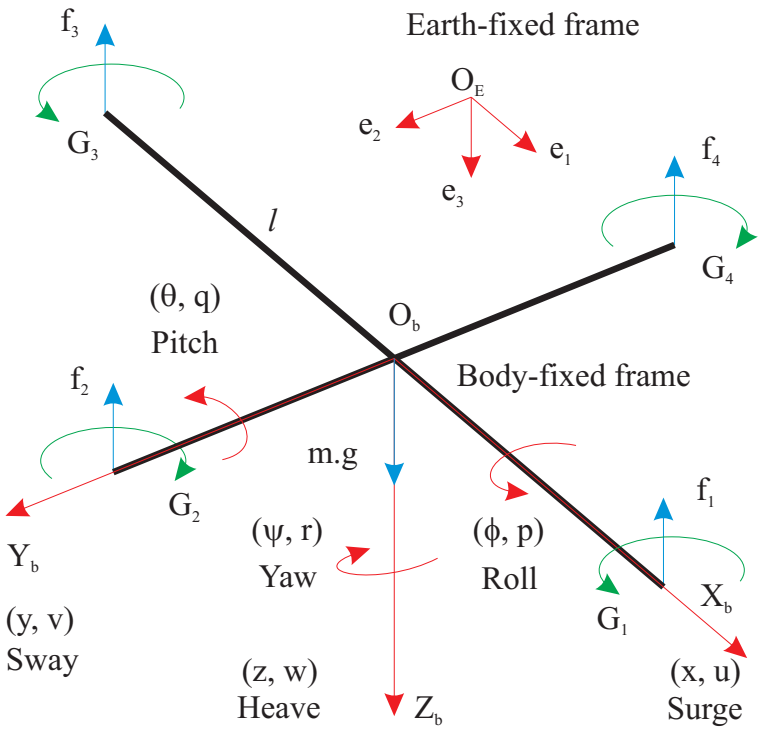

Figure 2.2: Quadrotor parameters.

With Assumption 2.1, the equations of motion of a quadrotor using the Newton-Euler approach are illustrated as follows:

$$\begin{aligned}
\dot{\boldsymbol{p}} &= \boldsymbol{v} \\
\dot{\boldsymbol{v}} &= g\boldsymbol{e}_3 - \tfrac{T}{m}\boldsymbol{R}_\eta^T(\boldsymbol{\eta})\boldsymbol{e}_3 \\
\dot{\boldsymbol{\eta}} &= \boldsymbol{K}_\eta(\boldsymbol{\eta})\boldsymbol{\omega} \\
\boldsymbol{J}\dot{\boldsymbol{\omega}} &= \boldsymbol{\tau} - \boldsymbol{S}(\boldsymbol{\omega})\boldsymbol{J}\boldsymbol{\omega}
\end{aligned} \tag{2.1}$$

where the vector $\boldsymbol{p} = [x\, y\, z]^T$ denotes the displacements of the center of mass and the vector $\boldsymbol{v} = [v_1\, v_2\, v_3]^T$ designates the velocities of the quadrotor coordinated in the earth-fixed frame. The vector $\boldsymbol{\eta} = [\phi\, \theta\, \psi]^T$ denotes the orientation vector with coordinates in the earth-fixed frame. The vector $\boldsymbol{\omega} = [p\, q\, r]^T$ denotes the body angular velocity. The matrices $\boldsymbol{R}_\eta^T(\boldsymbol{\eta})$, $\boldsymbol{K}_\eta(\boldsymbol{\eta})$, $\boldsymbol{J}$ and $\boldsymbol{S}(\boldsymbol{\omega})$ are given by

$$\boldsymbol{R}_\eta^T(\boldsymbol{\eta}) = \begin{bmatrix} C\theta C\psi & -C\phi S\psi + S\phi S\theta C\psi & S\phi S\psi + C\phi S\theta C\psi \\ C\theta S\psi & C\phi C\psi + S\phi S\theta S\psi & -S\phi C\psi + C\phi S\theta S\psi \\ -S\theta & S\phi C\theta & C\phi C\theta \end{bmatrix} \tag{2.2}$$

$$\boldsymbol{K}_\eta(\boldsymbol{\eta}) = \begin{bmatrix} 1 & S\phi T\theta & C\phi T\theta \\ 0 & C\phi & -S\phi \\ 0 & S\phi/C\theta & C\phi/C\theta \end{bmatrix} \tag{2.3}$$

$$\boldsymbol{J} = \begin{bmatrix} I_X & 0 & 0 \\ 0 & I_Y & 0 \\ 0 & 0 & I_Z \end{bmatrix} \tag{2.4}$$

$$\boldsymbol{S}(\boldsymbol{\omega}) = \begin{bmatrix} 0 & -r & q \\ r & 0 & -p \\ -q & p & 0 \end{bmatrix} \tag{2.5}$$

where $\boldsymbol{R}_\eta^T(\boldsymbol{\eta})$ and $\boldsymbol{K}_\eta(\boldsymbol{\eta})$ are the transformation matrices. It can be seen from (2.3) that $\boldsymbol{K}_\eta(\boldsymbol{\eta})$ is singular at $\theta = \pm\frac{\pi}{2}$. $S(\cdot)$, $C(\cdot)$, and $T(\cdot)$ stand for $\sin(\cdot)$, $\cos(\cdot)$, and $\tan(\cdot)$, respectively. $\boldsymbol{S}(\boldsymbol{x})$, a skew-symmetric matrix of the vector $\boldsymbol{x} = [x_1\, x_2\, x_3]^T \in \mathbb{R}^3$, is defined in Definition 2.2. The control vectors T and $\boldsymbol{\tau}$ are given by

$$\begin{aligned} T &= \textstyle\sum_{k=1}^{4} K_t G_k^2 \\ \boldsymbol{\tau} &= \begin{bmatrix} K_t l(G_4^2 - G_2^2) \\ K_t l(G_3^2 - G_1^2) \\ K_d l(-G_1^2 + G_2^2 - G_3^2 + G_4^2) \end{bmatrix} \end{aligned} \tag{2.6}$$

where l is the distance between the center of mass of the quadrotor and the center of a propeller. K_t, K_d are thrust and drag coefficients. G_k is the angular velocity of propeller k, $k = 1, \ldots, 4$. Although attitude describing in Euler angles is easy to visualize, one drawback of this approach is that $\boldsymbol{K}_\eta(\boldsymbol{\eta})$ in (2.3) is singular at $\theta = \pm\frac{\pi}{2}$. Using unit-quaternion approach is a possible solution to overcome this problem. The dynamic model for a quadrotor described by using quaternions is given as follows

$$\begin{aligned}
\dot{\boldsymbol{p}} &= \boldsymbol{v} \\
\dot{\boldsymbol{v}} &= g\boldsymbol{e}_3 - \tfrac{T}{m}\boldsymbol{R}_Q^T(\boldsymbol{Q})\boldsymbol{e}_3 \\
\dot{\boldsymbol{Q}} &= \boldsymbol{K}_Q(\boldsymbol{Q})\boldsymbol{\omega} \\
\boldsymbol{J}\dot{\boldsymbol{\omega}} &= \boldsymbol{\tau} - \boldsymbol{S}(\boldsymbol{\omega})\boldsymbol{J}\boldsymbol{\omega}
\end{aligned} \tag{2.7}$$

where the vector $\boldsymbol{p} = [x\, y\, z]^T$ denotes the displacements of the center of mass and the vector $\boldsymbol{v} = [v_1\, v_2\, v_3]^T$ denotes the velocities of the quadrotor coordinated in the earth-fixed frame. The orientation of the quadrotor is presented by using the four-element unit quaternion $\boldsymbol{Q} = [\eta\, \boldsymbol{q}^T]^T \in \mathbb{Q}$, where $\boldsymbol{q} = [q_1\, q_2\, q_3]^T \in \mathbb{R}^3$ and $\eta \in \mathbb{R}$ satisfy $\eta^2 + \boldsymbol{q}^T\boldsymbol{q} = 1$. $\mathbb{Q}$ is the set of unit-quaternion defined by $\mathbb{Q} = \left\{Q \in \mathbb{R} \times \mathbb{R}^3 | \, \|Q\| = 1\right\}$. The quaternion product between two unit quaternion, $\boldsymbol{Q}_1 = [\eta_1\, \boldsymbol{q}_1^T]^T$ and $\boldsymbol{Q}_2 = [\eta_2\, \boldsymbol{q}_2^T]^T$, is defined by $\boldsymbol{Q}_1 \odot \boldsymbol{Q}_2 = (\eta_1\eta_2 - \boldsymbol{q}_1^T\boldsymbol{q}_2, \eta_1\boldsymbol{q}_2 + \eta_2\boldsymbol{q}_1 + \boldsymbol{S}(\boldsymbol{q}_1)\boldsymbol{q}_2)$. For a more complete description, it can be referred to [Shu93]. m and $\boldsymbol{J} \in \mathbb{R}^{3\times3}$ are the mass and inertia matrix of the quadrotor.

The transformation matrices $\boldsymbol{R}_Q^T(\boldsymbol{Q})$ and $\boldsymbol{K}_Q(\boldsymbol{Q})$ are given by

$$\begin{aligned}
\boldsymbol{R}_Q^T(\boldsymbol{Q}) &= (\eta^2 - \boldsymbol{q}^T\boldsymbol{q})\boldsymbol{I}_{3\times3} + 2\boldsymbol{q}\boldsymbol{q}^T + 2\eta\boldsymbol{S}(\boldsymbol{q}) \\
\boldsymbol{K}_Q(\boldsymbol{Q}) &= \tfrac{1}{2}\begin{bmatrix} -\boldsymbol{q}^T \\ \\ \eta\boldsymbol{I}_{3\times3} + \boldsymbol{S}(\boldsymbol{q}) \end{bmatrix}
\end{aligned} \tag{2.8}$$

Noting that $\boldsymbol{R}_Q^T(\boldsymbol{Q})\boldsymbol{R}_Q(\boldsymbol{Q}) = \boldsymbol{I}_{3\times3}$, $\boldsymbol{K}_Q^T(\boldsymbol{Q})\boldsymbol{K}_Q(\boldsymbol{Q}) = \frac{1}{4}\boldsymbol{I}_{3\times3}$, i.e., the dynamics (2.7) is singular-free. In formation control, there are a number of quadrotors which are cooperated to obtain the formation tasks. Each quadrotor in the group has its own dynamics and can exchange its information with the others. The equations of motion of a quadrotor in the formation can be expanded from the dynamics (2.7) for the quadrotor i as in (2.9). The parameters of quadrotor i are shown in Figure 2.3. In this figure, $O_E e_1 e_2 e_3$ is the earth-fixed frame and $O_{bi} e_{1bi} e_{2bi} e_{3bi}$ is the body-fixed frame whose origin coincides with the center of gravity. As such, equations of motion of the quadrotor i can be described as follows:

$$\begin{aligned}
\dot{\boldsymbol{p}}_i &= \boldsymbol{v}_i \\
\dot{\boldsymbol{v}}_i &= g\boldsymbol{e}_3 - \tfrac{T_i}{m_i}\boldsymbol{R}_Q^T(\boldsymbol{Q}_i)\boldsymbol{e}_3 \\
\dot{\boldsymbol{Q}}_i &= \boldsymbol{K}_Q(\boldsymbol{Q}_i)\boldsymbol{\omega}_i \\
\boldsymbol{J}_i\dot{\boldsymbol{\omega}}_i &= \boldsymbol{\tau}_i - \boldsymbol{S}(\boldsymbol{\omega}_i)\boldsymbol{J}_i\boldsymbol{\omega}_i
\end{aligned} \tag{2.9}$$

where the vector $\boldsymbol{p}_i = [x_i\, y_i\, z_i]^T$ denotes the displacements of the center of mass and the vector $\boldsymbol{v}_i = [v_{1i}\, v_{2i}\, v_{3i}]^T$ denotes the velocities of the quadrotor i coordinated in the earth-fixed frame. The orientation of the quadrotor i is presented by using the four-element unit quaternion $\boldsymbol{Q}_i = [\eta_i\, \boldsymbol{q}_i^T]^T \in \mathbb{Q}$, where $\boldsymbol{q}_i = [q_{1i}\, q_{2i}\, q_{3i}]^T \in \mathbb{R}^3$ and $\eta_i \in \mathbb{R}$ satisfy $\eta_i^2 + \boldsymbol{q}_i^T\boldsymbol{q}_i = 1$. m_i and $\boldsymbol{J}_i \in \mathbb{R}^{3\times3}$

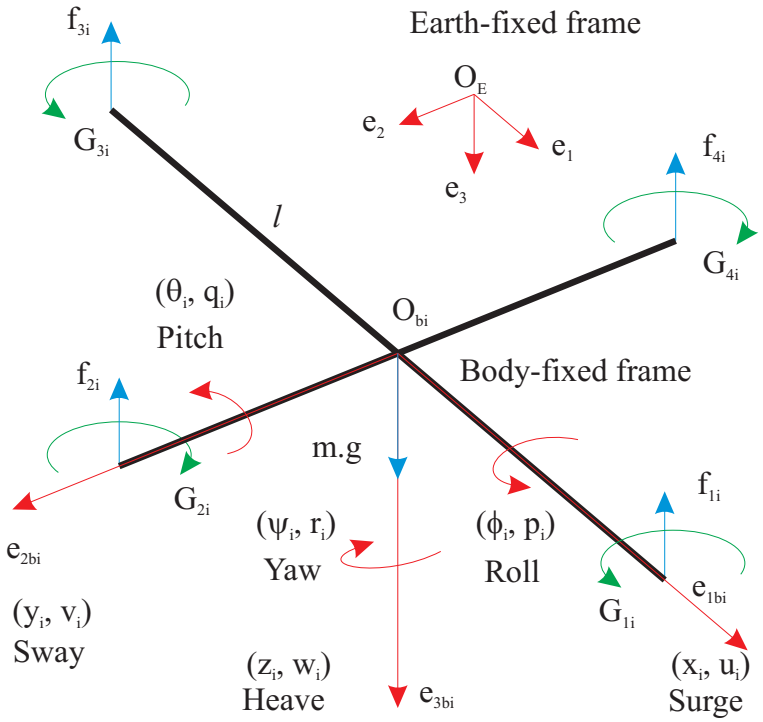

Figure 2.3: Parameters of quadrotor i.

are the mass and inertia matrix of the quadrotor i.

The transformation matrices $\boldsymbol{R}_Q^T(\boldsymbol{Q}_i)$ and $\boldsymbol{K}_Q(\boldsymbol{Q}_i)$ are given by

$$\begin{aligned} \boldsymbol{R}_Q^T(\boldsymbol{Q}_i) &= (\eta_i^2 - \boldsymbol{q}_i^T\boldsymbol{q}_i)\boldsymbol{I}_{3\times 3} + 2\boldsymbol{q}_i\boldsymbol{q}_i^T + 2\eta_i\boldsymbol{S}(\boldsymbol{q}_i) \\ \boldsymbol{K}_Q(\boldsymbol{Q}_i) &= \tfrac{1}{2}\begin{bmatrix} -\boldsymbol{q}_i^T \\ \\ \eta_i\boldsymbol{I}_{3\times 3} + \boldsymbol{S}(\boldsymbol{q}_i) \end{bmatrix} \end{aligned} \tag{2.10}$$

where $\boldsymbol{R}_Q^T(\boldsymbol{Q}_i)\boldsymbol{R}_Q(\boldsymbol{Q}_i) = \boldsymbol{I}_{3\times 3}$, $\boldsymbol{K}_Q^T(\boldsymbol{Q}_i)\boldsymbol{K}_Q(\boldsymbol{Q}_i) = \frac{1}{4}\boldsymbol{I}_{3\times 3}$, i.e., the control vectors T_i and $\boldsymbol{\tau}_i$ are given by

$$\begin{aligned} T_i &= \textstyle\sum_{k=1}^{4} K_{ti}G_{ki}^2 \\ \boldsymbol{\tau}_i &= \begin{bmatrix} K_{ti}l_i(G_{4i}^2 - G_{2i}^2) \\ K_{ti}l_i(G_{3i}^2 - G_{1i}^2) \\ K_{di}l_i(-G_{1i}^2 + G_{2i}^2 - G_{3i}^2 + G_{4i}^2) \end{bmatrix} \end{aligned} \tag{2.11}$$

where l_i is the distance between the center of the quadrotor and the center of a propeller, K_{ti}, K_{di} are thrust and drag coefficients and G_{ki} is the propeller k speed of quadrotor i, $k = 1, \ldots, 4$.

2.2 Skew-Symmetric Matrix

The definition of the skew-symmetric matrix is illustrated as follows

Definition 2.1. *Let $\boldsymbol{x} = [x_1\, x_2\, x_3]^T \in \mathbb{R}^3$ denotes a arbitrary vector. The skew-symmetric matrix $\boldsymbol{S}(\boldsymbol{x}) : \mathbb{R}^3 \to \mathbb{R}^3 \times \mathbb{R}^3$ is given by*

$$\boldsymbol{S}(\boldsymbol{x}) = \begin{bmatrix} 0 & -x_3 & x_2 \\ x_3 & 0 & -x_1 \\ -x_2 & x_1 & 0 \end{bmatrix} \tag{2.12}$$

Some useful properties of this matrix are given as follows

$$\begin{aligned} &\boldsymbol{S}(\boldsymbol{x})\boldsymbol{x} = 0_{3\times 1} \\ &\boldsymbol{S}(\boldsymbol{x})^T = -\boldsymbol{S}(\boldsymbol{x}) \\ &\boldsymbol{S}(\boldsymbol{x})^2 = \boldsymbol{x}\boldsymbol{x}^T - \boldsymbol{x}^T\boldsymbol{x}\boldsymbol{I}_{3\times 3} \end{aligned} \tag{2.13}$$

2.3 Smooth Saturation Functions

A definition of a smooth saturation function to be used in a smooth step function and in control design later is described as follows.

Definition 2.2. *The function $\sigma(x)$ is said to be a smooth saturation function if it possesses the following properties:*

$$\begin{aligned} &\sigma(x) = 0, && \sigma(x)x > 0, && \forall x \in \mathbb{R} - \{0\}, \\ &(x-y)[\sigma(x) - \sigma(y)] \geq 0, && \forall (x,y) \in \mathbb{R}^2, \\ &\sigma(-x) = -\sigma(x), && |\ \sigma(x)\ | \leq 1, && \tfrac{\sigma(x)}{x} \leq 1 \\ &0 \leq \tfrac{\partial \sigma(x)}{\partial x} \leq 1, && \forall x \in \mathbb{R}, \end{aligned} \tag{2.14}$$

Some function satisfying the above properties include $\sigma(x) = tanh(x)$ and $\sigma(x) = \frac{x}{\sqrt{1+x^2}}$. For the vector $\boldsymbol{x} = [x_1, ..., x_n]^T$, we use the notation $\boldsymbol{\sigma(x)} = [\sigma(x_1), ..., \sigma(x_n)]^T$ to denote the smooth saturation function vector of $\boldsymbol{x}$.

2.4 Smooth step function

This section gives a definition of a smooth step function followed by a construction of this function. This function is to be embedded in a pairwise collision avoidance function to avoid discontinuities in the control law in solving the collision avoidance problem.

Definition 2.3. *A scalar function $h(x, a, b)$ is said to be a smooth step function if it is smooth and possesses the following properties:*

$$\begin{aligned} &h(x,a,b) = 0, && \forall x \in (-\infty, a], \\ &h(x,a,b) = 1, && \forall x \in [b, \infty), \\ &0 < h(x,a,b) < 1 && \forall x \in (a, b), \\ &h'(x,a,b) > 0, && \forall x \in (a, b), \end{aligned} \tag{2.15}$$

where $h'(x, a, b) = \frac{\partial h(x,a,b)}{\partial x}$, and a and b are constants such that $a < b$.

Lemma 2.1. *Let the scalar function $h(x, a, b)$ be defined as*

$$h(x,a,b) = \frac{f(\tau)}{f(\tau) + f(1-\tau)}, \quad with\, \tau = \frac{x-a}{b-a}, \tag{2.16}$$

where $f(\tau) = 0$ if $\tau \leq 0$ and $f(\tau) = e^{-\frac{1}{\tau}}$ if $\tau > 0$, with a and b being constants such that $a < b$. Then the function $h(x, a, b)$ is a smooth step function.

Proof. See [Do11]. □

2.5 Attitude and Thrust Extraction

In this section, a new attitude and thrust extraction using the conversion between Euler angles and quaternions is calculated. This algorithm will be employed to develop the controller for a single quadrotor and a formation of quadrotors in the next sections.

Lemma 2.2. *Let $\boldsymbol{F} = \frac{T}{m}\boldsymbol{R}_Q^T(\boldsymbol{Q}_d)\boldsymbol{e}_3 = [F_1\, F_2\, F_3]^T \in \mathbb{R}^3$, ψ_d is a heading angle reference and $\boldsymbol{Q}_d = [\eta_d\, \boldsymbol{q}_d^T]^T$, then the solution for T and $\boldsymbol{Q}_d$ is given by*

$$\begin{aligned} T &= m\,\|\boldsymbol{F}\| \\ \boldsymbol{Q}_d &= \begin{bmatrix} C\frac{\alpha_\phi}{2}C\frac{\alpha_\theta}{2}C\frac{\alpha_\psi}{2} + S\frac{\alpha_\phi}{2}S\frac{\alpha_\theta}{2}S\frac{\alpha_\psi}{2} \\ S\frac{\alpha_\phi}{2}C\frac{\alpha_\theta}{2}C\frac{\alpha_\psi}{2} - C\frac{\alpha_\phi}{2}S\frac{\alpha_\theta}{2}S\frac{\alpha_\psi}{2} \\ C\frac{\alpha_\phi}{2}S\frac{\alpha_\theta}{2}C\frac{\alpha_\psi}{2} + S\frac{\alpha_\phi}{2}C\frac{\alpha_\theta}{2}S\frac{\alpha_\psi}{2} \\ C\frac{\alpha_\phi}{2}C\frac{\alpha_\theta}{2}S\frac{\alpha_\psi}{2} - S\frac{\alpha_\phi}{2}S\frac{\alpha_\theta}{2}C\frac{\alpha_\psi}{2} \end{bmatrix} \end{aligned} \tag{2.17}$$

where $\boldsymbol{F} \neq \boldsymbol{0}$, $\alpha_\psi = \psi_d$, $\alpha_\theta = \arctan\left(\frac{C\alpha_\psi F_1 + S\alpha_\psi F_2}{F_3}\right)$ and $\alpha_\phi = \arcsin\left(\frac{S\alpha_\psi F_1 - C\alpha_\psi F_2}{T}\right)$.
where $S(\cdot)$ and $C(\cdot)$ stand for $\sin(\cdot)$, $\cos(\cdot)$, respectively. $\boldsymbol{\omega}_d$ is the body angular velocity and is calculated as follows

$$\boldsymbol{\omega}_d = \begin{bmatrix} 1 & 0 & -S\alpha_\theta \\ 0 & C\alpha_\phi & S\alpha_\phi C\alpha_\theta \\ 0 & -S\alpha_\phi & C\alpha_\phi C\alpha_\theta \end{bmatrix} \begin{bmatrix} \dot{\alpha}_\phi \\ \dot{\alpha}_\theta \\ \dot{\alpha}_\psi \end{bmatrix} \tag{2.18}$$

Proof. *See Appendix A.1.*

2.6 Projection Operator

To avoid the finite escape time in the adaptive controller, a projection operator is used. The definition of it is shown as

$$\dot{\hat{\theta}} = proj\left(\tau\right) = \begin{cases} \tau & \text{if } Z \leq 0 \text{ or } Z_{\hat{\theta}}\tau \leq 0, \\ 0 & \text{if } Z > 0 \text{ and } Z_{\hat{\theta}}\tau > 0 \end{cases} \tag{2.19}$$

where $Z = \varsigma_m - \hat{\theta}$, $Z_{\hat{\theta}} = \partial Z / \partial \hat{\theta}$, ς_m is a positive constant. Then the projection operator has following properties:

$$\begin{aligned} &|\hat{\theta}| \geq \varsigma_m > 0, \forall t \geq t_0 > 0, \\ &proj(\tau) \text{ is Lipschitz continuous} \\ &|proj(\tau)| \leq |\tau| \end{aligned} \tag{2.20}$$

Proof. *See [KKK95].Appendix A2.*

2.7 Adaptive Backstepping Tracking Controller

The quadrotor dynamics is separated into two individual subsystems after the thrust and attitude extraction algorithm is applied. Each subsystem has a form of a second order system. The following adaptive backstepping tracking controller is developed and applied in the design controller later.

Lemma 2.3. *Consider the following second-order nonlinear system*

$$\begin{aligned} \dot{x}_1 &= x_2 \\ \dot{x}_2 &= \theta_1 u + \theta_2 \varphi(x) \end{aligned} \tag{2.21}$$

where x_1 and x_2 are states, u is the control input, $\theta_1 > 0$ and θ_2 are unknown constant parameters. To globally asymptotically track a reference trajectory x_d with bounded $\dot{x}_d$ and $\ddot{x}_d$, the following control and update laws are used:

$$\begin{aligned} \alpha_2 &= -k_1 x_{1e} + \dot{x}_d \\ u &= \tfrac{-k_2 x_{2e} - x_{1e} - \hat{\theta}_2 \varphi(x) + \dot{\alpha}_2}{\hat{\theta}_1} \\ \dot{\hat{\theta}}_1 &= proj(\gamma_1 x_{2e} u) \\ \dot{\hat{\theta}}_2 &= \gamma_2 x_{2e} \varphi(x) \end{aligned} \tag{2.22}$$

where $x_{1e} = x_1 - x_d$, $x_{2e} = x_2 - \alpha_2$; α_2 is a virtual control of x_2, $\hat{\theta}_1 \geq \varsigma_m > 0$, $\hat{\theta}_1$ and $\hat{\theta}_2$ are update laws of θ_1 and θ_2, respectively. k_1, k_2, and ς_m are positive constants. γ_1 and γ_2 are adaptive gains.

Proof. *See Appendix A.2.*

2.8 Stability Definitions

Through this work, the stability of equilibrium points is concerned. Stability of equilibrium points relates directly with Lyapunov stability. The Lyapunov stability can be referred in [Kha02]. For convenience, some definitions and theorems of stability are represented. An equilibrium point is stable if all solutions starting at nearby points stay nearby; otherwise it is unstable. It is asymptotically stable if all solutions starting at nearby points not only stay nearby but also tend to the equilibrium point as time approaches infinity.
Consider the autonomous system

$$\dot{x} = f(x) \tag{2.23}$$

where $f : D \to \mathbb{R}^n$ is a locally Lipschitz in x on D and $D \subseteq \mathbb{R}^n$ is a domain that contains the origin $x = 0$.

Definition 2.4. *The origin $x = 0$ is the equilibrium of* (2.23) *if*

$$f(0) = 0 \tag{2.24}$$

Definition 2.5. *The equilibrium point $x = 0$ of* (2.23) *is*

- *stable if, for each $\varepsilon > 0$, the is $\delta = \delta(\varepsilon) > 0$ such that*

$$\|x(0)\| < \delta \Rightarrow \|x(t)\| < \varepsilon, \forall t \geq 0 \tag{2.25}$$

- *unstable if it is not stable.*

- *asymptotically stable if it is stable and δ can be chosen such that*

$$\|x(0)\| < \delta \Rightarrow \lim_{t \to \infty} x(t) = 0 \tag{2.26}$$

Definition 2.6. *The equilibrium point $x = 0$ of* (2.23) *is exponentially stable if there exist positive constants c, k, and λ such that*

$$\|x(t)\| \leq \|x(t_0)\| \, e^{-\lambda(t-t_0)}, \forall t \geq t \geq t_0, \forall \, \|x(t_0)\| < c \tag{2.27}$$

Theorem 2.1. *Let $x = 0$ be an equilibrium point for* (2.23) *and $D \subseteq \mathbb{R}^n$ be a domain containing*

$x = 0$. *Let* $V : D \to \mathbb{R}$ *be a continuously differentiable function such that*

$$\begin{aligned} &V(0) = 0 \text{ and } V(x) > 0 \text{ in } D - \{0\} \\ &\dot{V}(x) \leq 0 \text{ in } D \end{aligned} \tag{2.28}$$

Then, $x = 0$ *is stable. Moreover, if*

$$\dot{V}(x) < 0 \text{ in } D - \{0\} \tag{2.29}$$

then $x = 0$ *is asymptotically stable.*

Proof. See [Kha02]. □

Theorem 2.2. *Let* $x = 0$ *be an equilibrium point for* (2.23). *Let* $V : \mathbb{R}^n \to \mathbb{R}$ *be a continuously differentiable function such that*

$$\begin{aligned} &V(0) = 0 \text{ and } V(x) > 0, \forall x \neq 0 \\ &\|x\| \to \inf \Rightarrow V(x) \to \inf \\ &\dot{V}(x) < 0, \forall x \neq 0 \end{aligned} \tag{2.30}$$

then, $x = 0$ *is globally asymptotically stable.*

Proof. See [Kha02]. □

Theorem 2.3. *Let* $x = 0$ *be an equilibrium point for* (2.23). *Let* $V : D \to \mathbb{R}$ *be a continuously differentiable function such that* $V(0) = 0$ *and* $V(x_0) > 0$ *for some* x_0 *with arbitrarily small* $\|x_0\|$. *Let* $B_r = x \in \mathbb{R}^n | \|x\| \leq r$ *denotes a ball of radius* $r > 0$ *and define a set* $U = \{x \in B_r | V(x) > 0\}$, *and suppose that* $\dot{V}(x) > 0$ *in* U. *Then,* $x = 0$ *is unstable.*

Proof. See [Kha02]. □

Lemma 2.4. *(Barbalat's lemma) Consider the function* $\phi : \mathbb{R} \to \mathbb{R}$ *be a uniformly continuous function on* $[0, \infty)$. *Suppose that* $\lim_{t\to\infty} \int_0^t \phi(\tau) d\tau$ *exists and is finite. Then* $\phi(t) \to 0$ *as* $t \to \infty$.

Proof. See [Kha02]. □

CHAPTER

3 Control Design for an underactuated quadrotor

Contents

Quadrotor is one kind of VTOL UAVs for a broad range of applications. Although there are many kinds of quadrotors, it can classify into two classes: underactuated and full-actuated or over-actuated quadrotor. The underactuated quadrotor usually has three to five fixed propellers using as actuators for thrust and stationary whereas the full-actuated or over-actuated quadrotor usually has equal or more than six actuators. With full-actuated and over-actuated quadrotor, it can be directly applied the control design technique to develop the controller for these kinds of quadrotor. For the underactuated quadrotor used in this section has four fixed propellers. The difficulty in motion control of underactuated vehicles mentioned by author [DP09] is that it can not directly applied the full-controller for this kind of vehicles because it totals loss of performance and inability to meet the control objectives in any useful way. It is clear that obtain an efficient attitude control and stabilization schemes is one of the most important tasks. The basic motion tasks for air vehicles can be classified as follows: Point-to-point motion, Path-following, Trajectory-tracking and path-tracking. The point-to-point motion task is a stabilization problem for a (equilibrium) point in the state space. When using a feedback strategy, the point-to-point motion task leads to a state regulation control problem for a point in the state space. In the path-following task, the controller is given a geometric description of the assigned Cartesian path. This information is usually available in a parameterized form expressing the desired motion in terms of a path parameter, which may be in particular the arc length along the path. For this task, time dependence is not relevant because one is concerned only with the geometric displacement between the air vehicle and the path. In the trajectory-tracking and path-tracking tasks, the air vehicle must follow the desired Cartesian path with a specified timing law. Although the reference trajectory/path can be split into a parameterized geometric path and a timing law for the parameter, such separation is not strictly necessary. Often, it is simpler to specify the workspace trajectory as the desired time evolution for the position of some representative point of the air vehicle. The trajectory-tracking and path-tracking problems consist then in the stabilization to zero of the Cartesian errors using all the available control inputs. Attitude control and stabilization for VTOL UAVs has been the focus of many researchers over past years. Although there are a number of successful attitude controllers (refer [WKD91, TM06]), the position control of underactuated VTOL UAVs is more challenge than the attitude control problem because of the lack of global results (see [PSH07, KS98]). In designing position control, the author in [PSH07] used vehicle orientation and thrust as control variables to stabilize the vehicle position and then apply the backstepping method to design control input torque stabilizing the attitudes. Another approach by using the angular velocity instead of the orientation, the author [MDTMC09] employed it as the intermediate control variables. The author in [AT10] uses an extraction algorithm to provide necessary thrust and desired orientation of the aircraft from an intermediate translational force. This algorithm provides nonsingular solutions and has been used to develop the global controllers in many publications. However, this algorithm has a problem of self-rotation around the vertical axis. To deal with this issue, the author [DP13] employs combination of Euler and quaternion method and uses the backstepping technique to design control for a quadrotor in three dimension space. Both authors [AT10, DP13] have proposed a

design system for VTOL UAVs achieving the global stability results.
In this chapter, Two controllers for an underactuated quadrotor are designed. The first controller is described in the Euler angles and the second controller is illustrated in the unit-quaternion. The purpose to design two these controllers is to point out some difficulties in design control for an underactuated system and existed problems. New extraction algorithm using combination of Euler angles and unit-quaternion is developed.

3.1 Trajectory-tracking control of a quadrotor

This section focuses to design control for an underactuated quadrotor following a predefined path which satisfies the Assumption 3.1. The mathematical model is based on Euler angles method and is prepared to develop a new attitude extraction algorithm used for control design later. The proposed controller guarantees that stabilization and tracking errors converge to zero asymptotically. Since the mathematical model of quadrotor is singularity in the second transformation matrix, it is easy to visualize and can avoid this issue with robust design approach. The coordinate transformation calculated in the design controller satisfies the stabilization of the translational dynamics and generates the thrust force and angular reference for design control later. Lyapunov's direct method and backstepping technique are also applied in control design.

3.1.1 Control objective

Before starting the control objective, we make the following assumptions:

Assumption 3.1. *Assume that the reference position trajectory $\boldsymbol{p}_d(t) = [x_d(t)\, y_d(t)\, z_d(t)]^T$ and the reference yaw angle $\psi_d(t)$ are smooth and bounded such that:*

$$\sup_{t\in\mathbb{R}^+} \left\| \boldsymbol{p}_d^{(i)} \right\| \leq \varepsilon_i,\ \sup_{t\in\mathbb{R}^+} \left\| \boldsymbol{\psi}_d^{(j)} \right\| \leq \varepsilon_k \tag{3.1}$$

where ε_i and ε_j are positive constants, $i = 1, ..., 4$, $j = 1, 2$, $k = j + 4$.

For more convenience, the mathematical model of a quadrotor in Euler angles, see Section 2.1, is rewritten as

$$\begin{aligned}
\dot{\boldsymbol{p}} &= \boldsymbol{v} \\
\dot{\boldsymbol{v}} &= g\boldsymbol{e}_3 - \tfrac{T}{m}\boldsymbol{R}_\eta^T(\boldsymbol{\eta})\boldsymbol{e}_3 \\
\dot{\boldsymbol{\eta}} &= \boldsymbol{K}_\eta(\boldsymbol{\eta})\boldsymbol{\omega} \\
\boldsymbol{J}\dot{\boldsymbol{\omega}} &= \boldsymbol{\tau} - \boldsymbol{S}(\boldsymbol{\omega})\boldsymbol{J}\boldsymbol{\omega}
\end{aligned} \tag{3.2}$$

where all symbols in (3.2) are defined as in Section 2.1. Assuming that the predefined path satisfies the Assumptions 3.1, the control objective is to design control inputs, T and $\boldsymbol{\tau}$, such that

the position vector $\boldsymbol{p}(t)$ and the yaw angle $\psi(t)$ of the quadrotor dynamics (3.2) asymptotically track their reference trajectories $\boldsymbol{p}_d(t)$ and heading angular $\psi_d(t)$,

$$\begin{aligned} \lim_{t\to\infty} (\boldsymbol{p}(t) - \boldsymbol{p}_d(t)) = 0 \\ \lim_{t\to\infty} (\psi(t) - \psi_d(t)) = 0 \end{aligned} \tag{3.3}$$

3.1.2 Control Design

In this section we will use backstepping technique [Kha02, KKK95] to design control achieving the Control Objective 3.1.1. The quadrotor dynamics (3.2) can be divided into two subsystems. The first subsystem consists of two first equations for translational dynamics and the second subsystem consists of two last equations for rotational dynamics. The control design includes two steps. In the first step, the control input force for translational dynamics tracking the predefined path is obtained. Unlike the standard application of backstepping method applied for design control for an underactuated quadrotor, after the first step, a total force T satisfying the control objective and a rotational reference $\boldsymbol{\eta}_d$ are generated. In the next step, the rotational reference $\boldsymbol{\eta}_d$ are employed to design the control torque input $\boldsymbol{\tau}$ to achieve the Control objective 3.1.1.

Step 1

In this step, the translational dynamics of (3.2) is considered. We will design a virtual control of $\boldsymbol{v}$ to force $\boldsymbol{p}(t)$ to globally asymptotically track its reference trajectory $\boldsymbol{p}_d(t)$. As such, we define the tracking errors as follows:

$$\begin{aligned} \boldsymbol{p}_e &= \boldsymbol{p} - \boldsymbol{p}_d, \\ \boldsymbol{v}_e &= \boldsymbol{v} - \boldsymbol{\alpha}_v \end{aligned} \tag{3.4}$$

where $\boldsymbol{\alpha}_v$ is a virtual control of $\boldsymbol{v}$. Substituting (3.4) into the first equation of (3.2) results in

$$\dot{\boldsymbol{p}}_e = \boldsymbol{v}_e + \boldsymbol{\alpha}_v - \dot{\boldsymbol{p}}_d, \tag{3.5}$$

To design the virtual control $\boldsymbol{\alpha}_v$, we consider the following Lyapunov function candidate

$$V_1 = \tfrac{1}{2}\boldsymbol{p}_e^T\boldsymbol{p}_e, \tag{3.6}$$

which is positive definite and radially unbounded in $\boldsymbol{p}_e$. Differentiating both sides of (3.6) along the solutions of (3.5) gives

$$\dot{V}_1 = \boldsymbol{p}_e^T\left(\boldsymbol{v}_e + \boldsymbol{\alpha}_v - \dot{\boldsymbol{p}}_d\right), \tag{3.7}$$

which suggest that we choose the virtual control $\boldsymbol{\alpha}_v$ as follows

$$\boldsymbol{\alpha}_v = -k_1\boldsymbol{p}_e + \dot{\boldsymbol{p}}_d, \tag{3.8}$$

where k_1 is a positive constant. Then the time derivative of V_1 becomes

$$\dot{V}_1 = -k_1 \boldsymbol{p}_e^T \boldsymbol{p}_e + \boldsymbol{p}_e^T \boldsymbol{v}_e, \tag{3.9}$$

To prepare for the next step, we calculate $\dot{\boldsymbol{v}}$ by differentiating both sides of the second equation of (3.4) along the solutions of (3.2) and (3.8) to obtain

$$\dot{\boldsymbol{v}}_e = g\boldsymbol{e}_3 - \boldsymbol{F} - \dot{\boldsymbol{\alpha}}_v, \tag{3.10}$$

where $\boldsymbol{F} = \frac{T}{m}\boldsymbol{R}_\eta^T(\boldsymbol{\eta})\boldsymbol{e}_3$ is an intermediate control input force for the translational dynamics. Unlike the standard backstepping method, for the next step, the stabilization of the orientation in the rotational dynamics is controlled by a virtual control of $\boldsymbol{\eta}$. In this section, we design the intermediate control input $\boldsymbol{F}$ such that the tracking error, $\boldsymbol{v}_e$ globally asymptotically converges to zero. After that the control input T and the orientation reference are generated. To design the intermediate control input $\boldsymbol{F}$, consider the following Lyapunov candidate

$$\boldsymbol{V}_2 = V_1 + \tfrac{1}{2}\boldsymbol{v}_e^T \boldsymbol{v}_e, \tag{3.11}$$

Its time derivative is given by

$$\dot{\boldsymbol{V}}_2 = -k_1 \boldsymbol{p}_e^T \boldsymbol{p}_e + \boldsymbol{v}_e^T \left(g\boldsymbol{e}_3 - \boldsymbol{F} - \dot{\boldsymbol{\alpha}}_v + \boldsymbol{p}_e\right), \tag{3.12}$$

which suggests that we choose

$$\boldsymbol{F} = k_2 \boldsymbol{v}_e + g\boldsymbol{e}_3 - \dot{\boldsymbol{\alpha}}_v + \boldsymbol{p}_e, \tag{3.13}$$

where k_2 is a positive constant. Then the derivative of Lyapunov candidate of V_2 is

$$\dot{\boldsymbol{V}}_2 = -k_1 \boldsymbol{p}_e^T \boldsymbol{p}_e - k_2 \boldsymbol{v}_e^T \boldsymbol{v}_e, \tag{3.14}$$

To generate the input force T and the rotation reference $\boldsymbol{\alpha}_\eta$, we assume that the transformation matrix satisfies the control objective for the heading angle ψ_d then the intermediate control input $\boldsymbol{F}$ can be expressed as follows:

$$T\boldsymbol{e}_3 = m\boldsymbol{R}_\eta(\boldsymbol{\alpha}_\eta)\boldsymbol{F} \tag{3.15}$$

Since ${\boldsymbol{R}_\eta}^T(\boldsymbol{\alpha}_\eta)\boldsymbol{R}_\eta(\boldsymbol{\alpha}_\eta) = \boldsymbol{I}_{3\times 3}$, equation (3.15) yields

$$T = m\sqrt{\boldsymbol{F}^T\boldsymbol{F}} \tag{3.16}$$

On the other hand, we expand the term $\boldsymbol{R}_\eta(\boldsymbol{\alpha}_\eta)\boldsymbol{F}$ in (3.15) by using $\boldsymbol{e}_3 = [0\,0\,1]^T$ to obtain $\boldsymbol{\alpha}_\eta$.

$$\begin{aligned} C\alpha_\theta C\alpha_\psi F_1 + C\alpha_\theta S\alpha_\psi F_2 - S\alpha_\theta F_3 &= 0 \\ \left[-C\alpha_\phi S\alpha_\psi + S\alpha_\phi S\alpha_\theta C\alpha_\psi\right] F_1 + \left[C\alpha_\phi C\alpha_\psi\right. & \\ \left. + S\alpha_\phi S\alpha_\theta S\alpha_\psi\right] F_2 + S\alpha_\phi C\alpha_\theta F_3 &= 0 \\ \left[S\alpha_\phi S\alpha_\psi + C\alpha_\phi S\alpha_\theta C\alpha_\psi\right] F_1 + \left[-S\alpha_\phi C\alpha_\psi\right. & \\ \left. + C\alpha_\phi S\alpha_\theta S\alpha_\psi\right] F_2 + C\alpha_\phi C\alpha_\theta F_3 &= T \end{aligned} \tag{3.17}$$

We choose $\alpha_\psi = \psi_d$ and calculate α_ϕ and α_θ depending on it. From the first equation of (3.17) we have

$$\alpha_\theta = \arctan\left(\frac{C\alpha_\psi F_1 + S\alpha_\psi F_2}{F_3}\right) \tag{3.18}$$

Moreover, by multiplying the second equation of (3.17) with $-cos(\alpha_\phi)$ and the third equation of (3.17) with $sin(\alpha_\phi)$ then adding them together, we obtain

$$\alpha_\phi = \arcsin\left(\frac{S\alpha_\psi F_1 - C\alpha_\psi F_2}{T}\right) \tag{3.19}$$

Step 2

After first step, we obtain the input control force T in (3.16) and the rotation reference $\boldsymbol{\alpha}_\eta = [\alpha_\phi\,\alpha_\theta\,\alpha_\psi]^T$ where $\alpha_\psi = \psi_d$; α_ϕ and α_θ are expressed by (3.19) and (3.18). In the second step, we first define the tracking errors for the rotational dynamics as follows

$$\begin{aligned} \boldsymbol{\eta}_e &= \boldsymbol{\eta} - \boldsymbol{\alpha}_\eta, \\ \boldsymbol{\omega}_e &= \boldsymbol{\omega} - \boldsymbol{\alpha}_\omega \end{aligned} \tag{3.20}$$

where $\boldsymbol{\alpha}_\omega$ is a virtual control of $\boldsymbol{\omega}$. Substituting (3.20) into the third equation of (3.2) results in

$$\dot{\boldsymbol{\eta}}_e = \boldsymbol{K}_\eta(\boldsymbol{\eta})(\boldsymbol{\omega}_e + \boldsymbol{\alpha}_\omega) - \dot{\boldsymbol{\alpha}}_\eta, \tag{3.21}$$

To design the virtual control $\boldsymbol{\alpha}_\omega$, we consider the following Lyapunov function candidate

$$V_3 = \tfrac{1}{2}\boldsymbol{\eta}_e^T\boldsymbol{\eta}_e, \tag{3.22}$$

Differentiating both sides of (3.22) along the solutions of (3.20) gives

$$\dot{V}_3 = \boldsymbol{\eta}_e^T\left(\boldsymbol{K}_\eta(\boldsymbol{\eta})(\boldsymbol{\omega}_e + \boldsymbol{\alpha}_\omega) - \dot{\boldsymbol{\alpha}}_\eta\right), \tag{3.23}$$

which suggest that we choose the virtual control $\boldsymbol{\alpha}_\omega$ as follows

$$\boldsymbol{\alpha}_\omega = \boldsymbol{K}_\eta^{-1}(\boldsymbol{\eta})\left(-k_3\boldsymbol{\eta}_e + \dot{\boldsymbol{\alpha}}_\eta\right), \tag{3.24}$$

where k_3 is a positive constant. Substituting (3.24) into (3.23) gives

$$\dot{V}_3 = -k_3 \boldsymbol{\eta}_e^T \boldsymbol{\eta}_e + \boldsymbol{\eta}_e^T \boldsymbol{K}_\eta(\boldsymbol{\eta}) \boldsymbol{\omega}_e, \tag{3.25}$$

To design the control input torque $\boldsymbol{\tau}$ to stabilize $\boldsymbol{\omega}_e$ at the origin, differentiating both sides of (3.20) along solutions of (3.24) and (3.2) yields

$$\dot{\boldsymbol{\omega}}_e = \boldsymbol{J}^{-1}\boldsymbol{\tau} - \boldsymbol{J}^{-1}\boldsymbol{S}(\boldsymbol{\omega})\boldsymbol{J}\boldsymbol{\omega} - \dot{\boldsymbol{\alpha}}_\omega, \tag{3.26}$$

Consider the following Lyapunov function

$$V_4 = V_3 + \tfrac{1}{2}\boldsymbol{\omega}_e^T \boldsymbol{\omega}_e, \tag{3.27}$$

Its time derivative gives

$$\dot{V}_4 = -k_3 \boldsymbol{\eta}_e^T \boldsymbol{\eta}_e + \boldsymbol{\omega}_e^T \left(\boldsymbol{J}^{-1}\boldsymbol{\tau} - \boldsymbol{J}^{-1}\boldsymbol{S}(\boldsymbol{\omega})\boldsymbol{J}\boldsymbol{\omega} - \dot{\boldsymbol{\alpha}}_\omega + \boldsymbol{K}_\eta(\boldsymbol{\eta})\boldsymbol{\eta}_e \right), \tag{3.28}$$

which suggests that we choose the control input torque $\boldsymbol{\tau}$ as

$$\boldsymbol{\tau} = \boldsymbol{J}\left(-k_4 \boldsymbol{\omega}_e + \boldsymbol{J}^{-1}\boldsymbol{S}(\boldsymbol{\omega})\boldsymbol{J}\boldsymbol{\omega} + \dot{\boldsymbol{\alpha}}_\omega - \boldsymbol{K}_\eta(\boldsymbol{\eta})\boldsymbol{\eta}_e \right), \tag{3.29}$$

where k_4 is a positive constant. Then the derivative of Lyapunov candidate of V_4 is

$$\dot{\boldsymbol{V}}_4 = -k_3 \boldsymbol{\eta}_e^T \boldsymbol{\eta}_e - k_4 \boldsymbol{\omega}_e^T \boldsymbol{\omega}_e, \tag{3.30}$$

Substituting control and virtual control from (3.8), (3.13), (3.24) and (3.29) into (3.5), (3.10), (3.21) and (3.26), yields the closed loop system

$$\begin{aligned} \dot{\boldsymbol{p}}_e &= -k_1 \boldsymbol{p}_e + \boldsymbol{v}_e, \\ \dot{\boldsymbol{v}}_e &= -k_2 \boldsymbol{v}_e - \boldsymbol{p}_e, \\ \dot{\boldsymbol{\eta}}_e &= -k_3 \boldsymbol{\eta}_e + \boldsymbol{K}_\eta(\boldsymbol{\eta})\boldsymbol{\omega}_e, \\ \dot{\boldsymbol{\omega}}_e &= -k_4 \boldsymbol{\omega}_e - \boldsymbol{K}_\eta(\boldsymbol{\eta})\boldsymbol{\eta}_e, \end{aligned} \tag{3.31}$$

The control design has been completed. We summarize the results in the following theorem.

Theorem 3.1. *Under Assumption 3.1, the control inputs consisting of* (3.16) *and* (3.29) *for the quadrotor achieve the Control Objective 3.1.1. The position $\boldsymbol{p}(t)$ and yaw angle $\psi(t)$ of the quadrotor asymptotically track the reference trajectories $\boldsymbol{p}_d(t)$ and $\psi_d(t)$; $\lim_{t\to\infty}(\boldsymbol{p}(t) - \boldsymbol{p}_d(t)) = 0$, $\lim_{t\to\infty}(\psi(t) - \psi_d(t)) = 0$ and the closed loop system* (3.31) *is forward complete.*

Proof. *See Appendix B.1.*

3.1.3 Simulation Results

In this section, we illustrate the effectiveness of the proposed controller through a numerical simulation. The quadrotor parameters for the simulation are taken from [EInE12] as follows: m=1 kg, g = 9.81 $kg\,m^2$, $l = 0.15m$, $I_X = 15.67 \times 10^{-3}\,kg\,m^2$, $I_Y = 15.67 \times 10^{-3}\,kg\,m^2$; $I_Z = 28.34\times10^{-3}\,kg\,m^2$, $K_t = 192.32\times10^{-7}Ns^2$, $K_d = 4.003\times10^{-7}Nms^2$. The initial conditions are taken as

$$\boldsymbol{p} = [0\,0\,0]^T; \boldsymbol{v} = [0\,0\,0]^T; \boldsymbol{\eta} = [0\,0\,0]^T; \boldsymbol{\omega} = [0\,0\,0]^T \tag{3.32}$$

The reference trajectories are taken as

$$s = t, \boldsymbol{p}_d = [2.5sin(2s)\ 2.5cos(s)\ 5]^T, \psi_d = t \tag{3.33}$$

This reference path satisfies Assumption 3.1. The control gains are chosen as follows: $k_1 = 2$, $k_2 = 3$, $k_3 = 1$ and $k_4 = 1$.

The simulation results are plotted as follows: the reference and real position trajectories are plotted in Figure 3.1. The position tracking errors and attitude tracking errors are plotted in Figure 3.2 and Figure 3.3. It can be seen from these figures that all tracking errors asymptotically converge to zero. The control inputs, T and $\boldsymbol{\tau}$ are illustrated in Figure 3.6

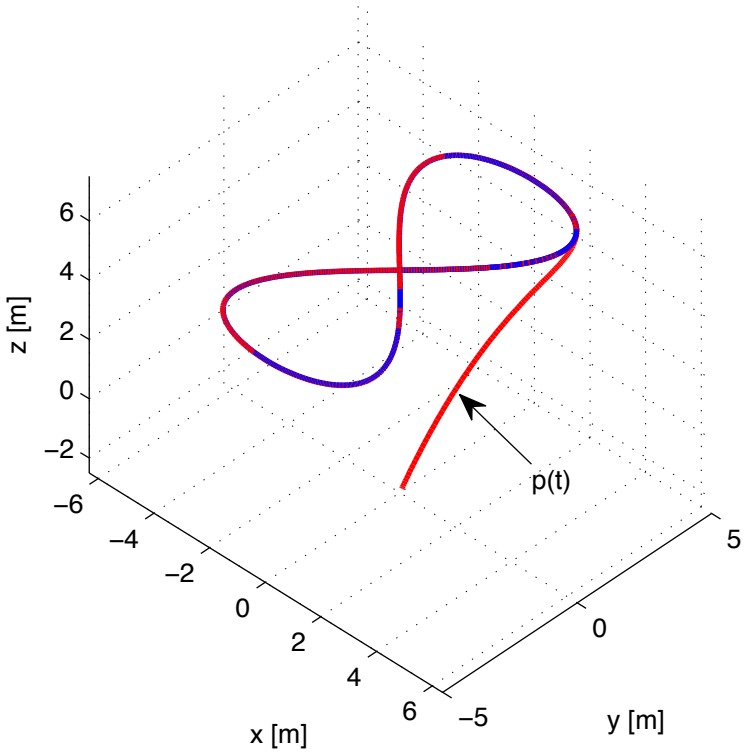

Figure 3.1: Reference and real position trajectories $\boldsymbol{p}_d$ and $\boldsymbol{p}$.

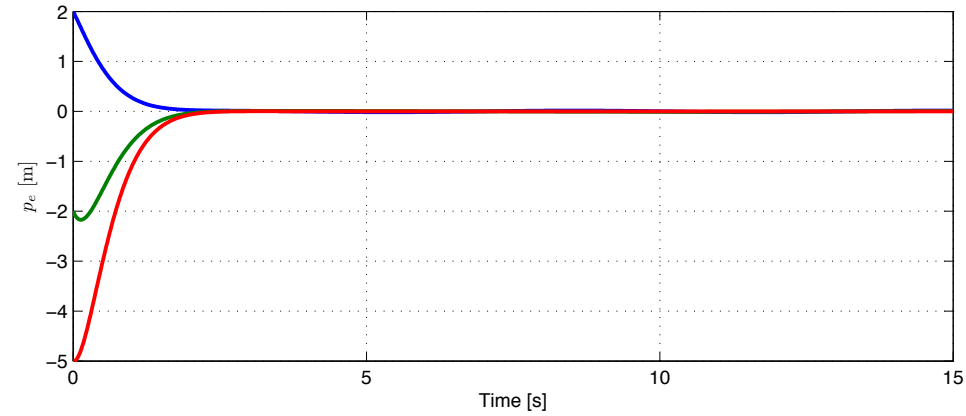

Figure 3.2: Position tracking errors.

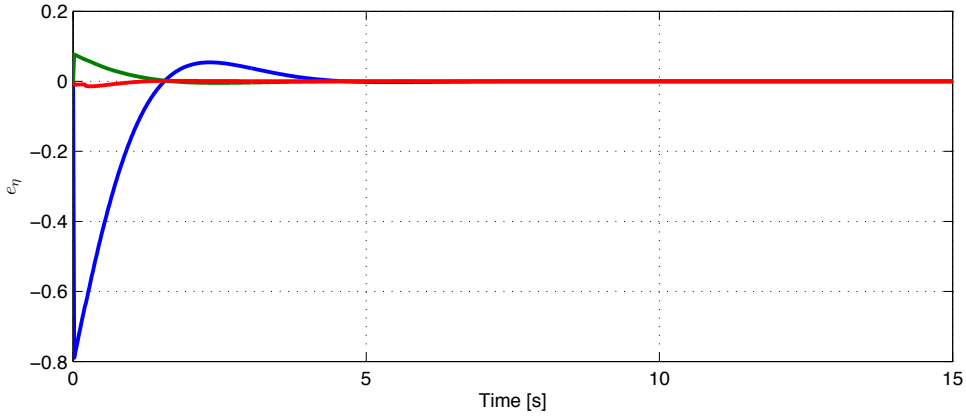

Figure 3.3: Attitude tracking errors.

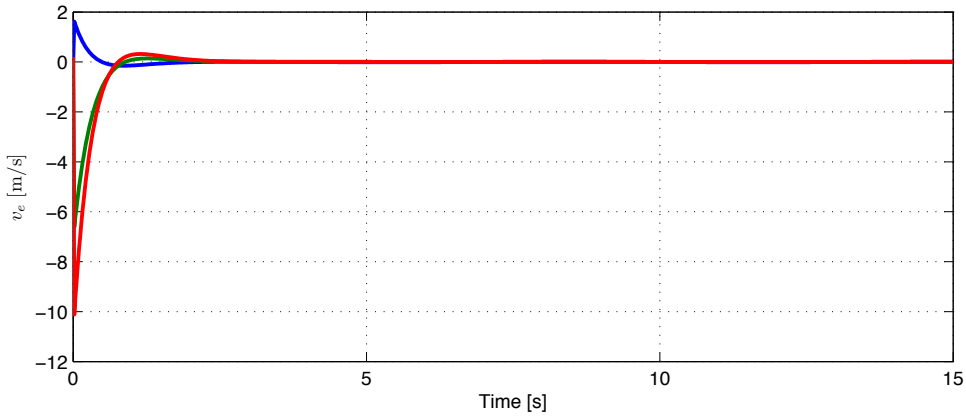

Figure 3.4: Linear velocity tracking errors.

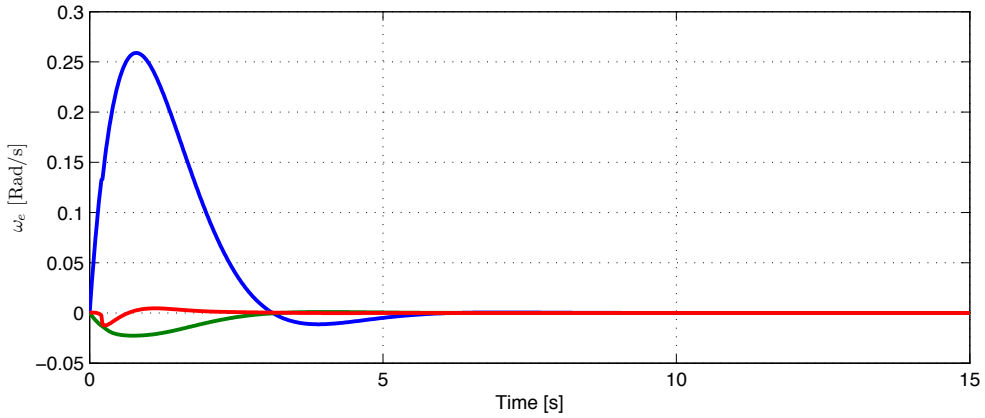

Figure 3.5: Angular velocity tracking errors.

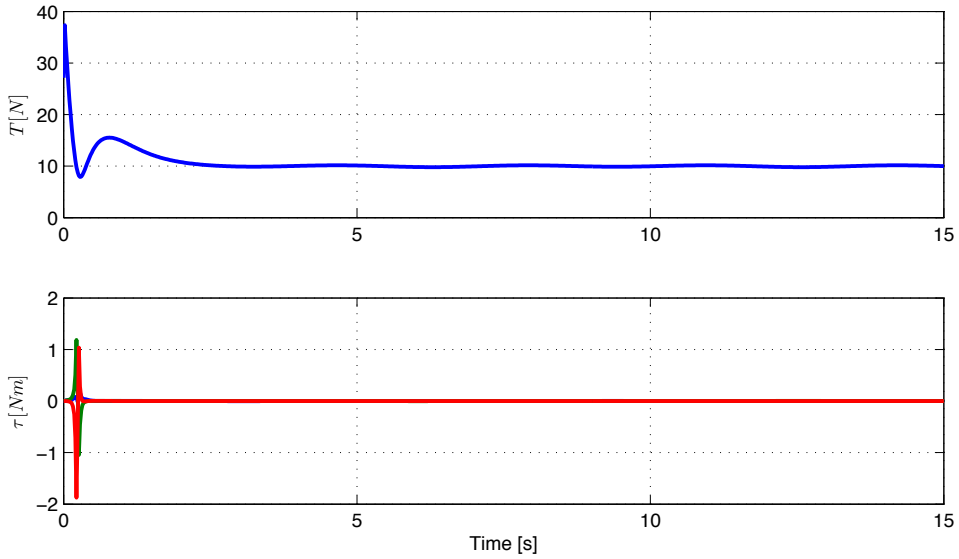

Figure 3.6: Thrust and torques.

3.1.4 Conclusion

A controller for an underactuated quadrotor asymptotically tracking a predefined path has been presented. The quadrotor dynamics is divided into two subsystems, translational and rotational subsystem. The tracking errors between the real and reference path in the translational subsystem were achieved by the intermediate control input. This intermediate control input was used to calculate and generate the input force and the rotation reference. After this step, the second subsystem was stabilized directly by application of backstepping method. Although the quadrotor dynamics only describes in the simplest case where the disturbance of environment and the change of quadrotor parameters are not considered, the separation in quadrotor dynamics is a

based approach for employing and developing new controllers in next sections. The simulation results demonstrated the effectiveness of the proposed controller.

3.2 Path-following control of a quadrotor

In this section, we focus to design control for an underactuated quadrotor following a predefined path which satisfies the Assumption 3.1 under the effect of changing quadrotor parameters and disturbance of environment. The proposed controller guarantees that stabilization and tracking errors converge to zero asymptotically from any initial values. In comparison with the preceding section, this section deal with the singularity issue in the transformation matrix by expanding the model of quadrotor from the Euler angles form to the unit-quaternion form. Moreover, the disturbances of changing environment and unknown parameters of an underactuated quadrotor are also considered. The developed controller is based on the coordinate transformations which employ the combination of Euler angles and unit quaternion via the attitude extraction algorithm which generates force and unit quaternion reference for design control later, Lyapunov's direct method, and adaptive backstepping technique [KKK95].

3.2.1 Control objective

For more convenience, the mathematical model of a quadrotor, see Section 2.1, is recaptured and expanded as

$$\begin{aligned}
\dot{\boldsymbol{p}} &= \boldsymbol{v} \\
\dot{\boldsymbol{v}} &= g\boldsymbol{e}_3 - \boldsymbol{J}_1^{-1} T \boldsymbol{R}_Q^T(\boldsymbol{Q})\boldsymbol{e}_3 + \boldsymbol{d}_v \\
\dot{\boldsymbol{Q}} &= \boldsymbol{K}(\boldsymbol{Q})\boldsymbol{\omega} \\
\dot{\boldsymbol{\omega}} &= \boldsymbol{J}_2^{-1}\boldsymbol{\tau} - \boldsymbol{J}_2^{-1}\boldsymbol{S}(\boldsymbol{\omega})\boldsymbol{J}_2\boldsymbol{\omega} + \boldsymbol{d}_\omega
\end{aligned} \tag{3.34}$$

where $\boldsymbol{d}_v \in \mathbb{R}^3$ and $\boldsymbol{d}_\omega \in \mathbb{R}^3$ are unknown disturbance matrices, $\boldsymbol{J}_1$ and $\boldsymbol{J}_2 \in \mathbb{R}^{3\times 3}$ are unknown mass and inertial matrices, all the other symbols in (3.34) are defined as in Section 2.1.

To solve the path-tracking problem, assuming that the predefined path satisfies the Assumptions 3.1 , the control objective is to design control inputs, T and $\boldsymbol{\tau}$, such that the position vector $\boldsymbol{p}(t)$ and the yaw angle $\psi(t)$ of the quadrotor dynamics (3.34) globally track their reference trajectories $\boldsymbol{p}_d(t)$ and heading angular $\psi_d(t)$ under the effect of unknown parameters and disturbance,

$$\begin{aligned}
\lim_{t\to\infty} \left(\boldsymbol{p}(t) - \boldsymbol{p}_d(t)\right) &= 0 \\
\lim_{t\to\infty} \left(\psi(t) - \psi_d(t)\right) &= 0
\end{aligned} \tag{3.35}$$

3.2.2 Control Design

In this section we will use adaptive backstepping technique [KKK95] to design control and develop a new extraction algorithm for a quadrotor. Like in the previous section, the quadrotor dynamics (3.34) is separated into two subsystems. The first subsystem contains two first equations for translational dynamics and the second subsystem consists two last equations for rotational dynamics. In the first step, the adaptive backstepping technique evolved in the Section 2.3 is applied to obtain the control input force for translational dynamics tracking the predefined path. After this step, a new extraction algorithm using some conversions between Euler angles and unit-quaternion to reject the self-rotation of quadrotor around its vertical axis to generate a total force T and a unit-quaternion reference Q_d which can be employed as the reference for the second subsystem is applied. The attitude extraction algorithm is shown in Figure 3.7. In the next step, the torque $\boldsymbol{\tau}$ to force $\boldsymbol{Q} \rightarrow \boldsymbol{Q}_d$ is designed.

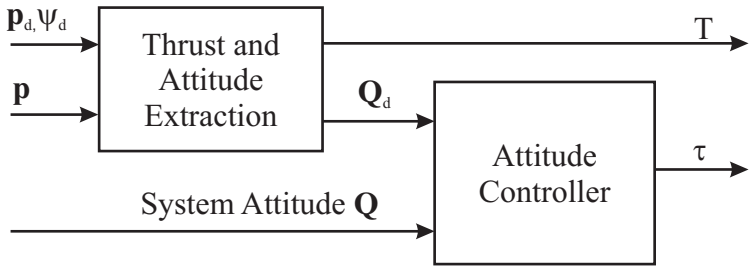

Figure 3.7: Attitude Extraction Algorithm.

Step 1

In this step, the translational dynamics of (3.2) is considered. We will design a virtual control of $\boldsymbol{v}$ to force $\boldsymbol{p}(t)$ to globally asymptotically track its reference trajectory $\boldsymbol{p}_d(t)$. As such, we define the tracking errors as follows:

$$\begin{aligned} \boldsymbol{p}_e &= \boldsymbol{p} - \boldsymbol{p}_d, \\ \boldsymbol{v}_e &= \boldsymbol{v} - \boldsymbol{\alpha}_v, \end{aligned} \tag{3.36}$$

where $\boldsymbol{\alpha}_v$ is a virtual control of $\boldsymbol{v}$. differentiating both sides of (3.36) and using the first subsystem, the error dynamics are expressed as

$$\begin{aligned} \dot{\boldsymbol{p}}_e &= \boldsymbol{v}_e + \boldsymbol{\alpha}_v - \dot{\boldsymbol{p}}_d, \\ \dot{\boldsymbol{v}}_e &= g\boldsymbol{e}_3 - \boldsymbol{J}_1^{-1}\boldsymbol{F} + \boldsymbol{d}_v - \dot{\boldsymbol{\alpha}}_v \end{aligned} \tag{3.37}$$

where $\boldsymbol{F}$ is an intermediate control input. It can be seen from (3.37) that it has the form of (2.21) in which $\boldsymbol{J}_1$ and $\boldsymbol{d}_v$ are unknown parameters. We can use the results of Lemma 2.3 to design the control and update laws for the tracking errors (3.37) as

$$\begin{aligned}
\boldsymbol{\alpha}_v &= -k_1\boldsymbol{p}_e + \dot{\boldsymbol{p}}_d \\
\boldsymbol{F} &= \hat{\boldsymbol{J}}_{\boldsymbol{1}}(k_2\boldsymbol{v}_e + \boldsymbol{p}_e - \dot{\boldsymbol{\alpha}}_v + g\boldsymbol{e}_3 + \hat{\boldsymbol{d}}_v) \\
\dot{\hat{\boldsymbol{J}}}_1 &= (\hat{\boldsymbol{J}}_1^T)^{-1} proj(\gamma_{v1}\boldsymbol{v}_e^T\hat{\boldsymbol{J}}_1\boldsymbol{F}) \\
\dot{\hat{\boldsymbol{d}}}_v &= \gamma_{v2}\boldsymbol{v}_e
\end{aligned} \tag{3.38}$$

Noting that $\boldsymbol{F} = T\boldsymbol{R}_Q^T(\boldsymbol{Q})\boldsymbol{e}_3$ and it can be expressed in the Euler angles form as $\boldsymbol{F} = T\boldsymbol{R}_\eta^T(\boldsymbol{\eta})\boldsymbol{e}_3$. Differing from standard backstepping application that the errors of $\boldsymbol{\eta}$ would be controlled by a virtual control of $\boldsymbol{\eta}$, we assume that the control input $\boldsymbol{F}$ forces the quadrotor tracking the predefined path and heading angle ψ_d in ideal case. We define an orientation vector $\boldsymbol{\alpha}_Q = [\alpha_\phi\, \alpha_\theta\, \alpha_\psi]^T$ in the earth-fixed frame and $\boldsymbol{R}_\eta^T(\boldsymbol{\alpha}_Q)$ is the transformation matrix (A.3) such that $\boldsymbol{R}_\eta^T(\boldsymbol{\alpha}_Q) = \boldsymbol{R}_Q^T(\boldsymbol{Q}_d)$ where the combination of the transformation matrix $\boldsymbol{R}_Q^T(\boldsymbol{Q}_d)$ and thrust force T stabilizes the tracking error (3.37) at the origin. The α_ϕ, α_θ and α_ψ are the roll, pitch and yaw angles, respectively. Applying Lemma 2.3 for the tracking error (3.37), we obtain the thrust T and the reference unit-quaternion vector as follows:

$$\begin{aligned}
T &= \|\boldsymbol{F}\| \\
\boldsymbol{Q}_d &= \begin{bmatrix}
C\frac{\alpha_\phi}{2}C\frac{\alpha_\theta}{2}C\frac{\alpha_\psi}{2} + S\frac{\alpha_\phi}{2}S\frac{\alpha_\theta}{2}S\frac{\alpha_\psi}{2} \\
S\frac{\alpha_\phi}{2}C\frac{\alpha_\theta}{2}C\frac{\alpha_\psi}{2} - C\frac{\alpha_\phi}{2}S\frac{\alpha_\theta}{2}S\frac{\alpha_\psi}{2} \\
C\frac{\alpha_\phi}{2}S\frac{\alpha_\theta}{2}C\frac{\alpha_\psi}{2} + S\frac{\alpha_\phi}{2}C\frac{\alpha_\theta}{2}S\frac{\alpha_\psi}{2} \\
C\frac{\alpha_\phi}{2}C\frac{\alpha_\theta}{2}S\frac{\alpha_\psi}{2} - S\frac{\alpha_\phi}{2}S\frac{\alpha_\theta}{2}C\frac{\alpha_\psi}{2}
\end{bmatrix}
\end{aligned} \tag{3.39}$$

where

$$\begin{aligned}
\alpha_\psi &= \psi_d, \\
\alpha_\theta &= \arctan\left(\frac{C\alpha_\psi F_1 + S\alpha_\psi F_2}{F_3}\right), \\
\alpha_\phi &= \arcsin\left(\frac{S\alpha_\psi F_1 - C\alpha_\psi F_2}{T}\right),
\end{aligned} \tag{3.40}$$

The desired angular velocity is calculated as follows

$$\boldsymbol{\omega}_d = \begin{bmatrix}
1 & 0 & -S\alpha_\theta \\
0 & C\alpha_\phi & S\alpha_\phi C\alpha_\theta \\
0 & -S\alpha_\phi & C\alpha_\phi C\alpha_\theta
\end{bmatrix}\begin{bmatrix}
\dot{\alpha}_\phi \\ \dot{\alpha}_\theta \\ \dot{\alpha}_\psi
\end{bmatrix} \tag{3.41}$$

where $\boldsymbol{\omega}_d$ is the body angular velocity; $S(\cdot)$ and $C(\cdot)$ stand for $\sin(\cdot)$, $\cos(\cdot)$, respectively.

Step 2

In this step, the torque input, $\boldsymbol{\tau}$, will be designed. The unit-quaternion vector $\boldsymbol{Q}_d$ is used as the

reference. We first define the following tracking errors

$$\begin{aligned} \boldsymbol{Q}_e &= \boldsymbol{Q}_d^{-1} \odot \boldsymbol{Q}, \\ \boldsymbol{\omega}_e &= \boldsymbol{\omega} - \boldsymbol{\alpha}_\omega, \end{aligned} \tag{3.42}$$

where $\boldsymbol{\alpha}_\omega$ is a virtual control of $\boldsymbol{\omega}$; $\boldsymbol{Q}_e = [\eta_e \, \boldsymbol{q}_e^T]^T$ and $\boldsymbol{\omega}_e$ are attitude tracking and angular velocity error vector, respectively.

Differentiating both sides of (3.42) yields

$$\begin{aligned} \dot{\boldsymbol{q}}_e &= \boldsymbol{G}(\boldsymbol{\omega}_e + \boldsymbol{\alpha}_\omega - \boldsymbol{\omega}_d) \\ \dot{\boldsymbol{\omega}}_e &= \boldsymbol{J}_2^{-1}\boldsymbol{\tau} - \boldsymbol{J}_2^{-1}\boldsymbol{S}(\boldsymbol{\omega})\boldsymbol{J}_2\boldsymbol{\omega} + \boldsymbol{d}_\omega - \dot{\boldsymbol{\alpha}}_\omega \end{aligned} \tag{3.43}$$

where $\boldsymbol{G} = \frac{1}{2}\left(\eta_e \boldsymbol{I}_{3\times 3} + \boldsymbol{S}(\boldsymbol{q}_e)\right)$ and $\boldsymbol{\omega}_d$ can be obtained by using equation (3.41). Using Lemma 2.3 for the tracking error (3.43), the following update laws and controls are employed:

$$\begin{aligned} \boldsymbol{\alpha}_\omega &= -k_3 \boldsymbol{G}^T \boldsymbol{q}_e + \boldsymbol{\omega}_d \\ \boldsymbol{\tau} &= \hat{\boldsymbol{J}}_{\boldsymbol{2}}(-k_4\boldsymbol{\omega}_e - \boldsymbol{G}\boldsymbol{q}_e + \dot{\boldsymbol{\alpha}}_\omega + \boldsymbol{S}(\boldsymbol{\omega})\boldsymbol{\omega} - \hat{\boldsymbol{d}}_\omega) \\ \dot{\hat{\boldsymbol{J}}}_2 &= (\hat{\boldsymbol{J}}_2^T)^{-1} proj(\gamma_{\omega 1}(\boldsymbol{q}_e^T \hat{\boldsymbol{J}}_2 \boldsymbol{\tau}) \\ \dot{\hat{\boldsymbol{d}}}_\omega &= \gamma_{\omega 2}\boldsymbol{\omega}_e \end{aligned} \tag{3.44}$$

From the above control design, we have the following closed loop system:

$$\begin{aligned} \dot{\boldsymbol{p}}_e &= -k_1 \boldsymbol{p}_e + \boldsymbol{v}_e \\ \dot{\boldsymbol{v}}_e &= -k_2 \boldsymbol{v}_e - \boldsymbol{p}_e - \tilde{\boldsymbol{J}}_1^{-1}\boldsymbol{F}_d + \tilde{\boldsymbol{d}}_v \\ \dot{\boldsymbol{q}}_e &= -k_3 \boldsymbol{G}\boldsymbol{G}^T \boldsymbol{q}_e + \boldsymbol{G}\boldsymbol{\omega}_e \\ \dot{\boldsymbol{\omega}}_e &= -k_4 \boldsymbol{\omega}_e - \boldsymbol{G}\boldsymbol{q}_e + \tilde{\boldsymbol{J}}_2^{-1}\boldsymbol{\tau} + \tilde{\boldsymbol{d}}_\omega \\ \dot{\tilde{\boldsymbol{J}}}_1 &= -(\tilde{\boldsymbol{J}}_1^T)^{-1} proj(\gamma_{v1}(\boldsymbol{v}_e^T \tilde{\boldsymbol{J}}_1 \boldsymbol{F}_d) \\ \dot{\tilde{\boldsymbol{d}}}_v &= -\gamma_{v2}\boldsymbol{v}_e \\ \dot{\tilde{\boldsymbol{J}}}_2 &= -(\tilde{\boldsymbol{J}}_2^T)^{-1} proj(\gamma_{\omega 1}(\boldsymbol{q}_e^T \tilde{\boldsymbol{J}}_2 \boldsymbol{\tau}) \\ \dot{\tilde{\boldsymbol{d}}}_\omega &= -\gamma_{\omega 2}\boldsymbol{\omega}_e \end{aligned} \tag{3.45}$$

The control design has been completed. We summarize the results in the following theorem.

Theorem 3.2. *Under Assumption in the section 3.2.1, the control and update laws consisting of* (3.38) *and* (3.44) *for the quadrotor achieve the Control Objective 3.2.1. The position $\boldsymbol{p}(t)$ and yaw angle $\psi(t)$ of the quadrotor globally asymptotically track the reference trajectories $\boldsymbol{p}_d(t)$ and $\psi_d(t)$; $\lim_{t\to\infty}(\boldsymbol{p}(t) - \boldsymbol{p}_d(t)) = 0$, $\lim_{t\to\infty}(\psi(t) - \psi_d(t)) = 0$ and the closed loop system* (3.45) *is forward complete.*

Proof. *See Appendix B.2.*

3.2.3 Simulation Results

In this section, we illustrate the effectiveness of the proposed controller through a numerical simulation. The quadrotor parameters for the simulation are taken from [EInE12] as follows: m=1 kg, g = 9.81 $kg\,m^2$, $l = 0.15m$, $I_X = 15.67 \times 10^{-3}\,kg\,m^2$, $I_Y = 15.67 \times 10^{-3}\,kg\,m^2$; $I_Z = 28.34\times10^{-3}\,kg\,m^2$, $K_t = 192.32\times10^{-7}Ns^2$, $K_d = 4.003\times10^{-7}Nms^2$. The initial conditions are taken as

$$\boldsymbol{p} = [0\,0\,0]^T; \boldsymbol{v} = [0\,0\,0]^T; \boldsymbol{Q}_i = [1\,0\,0\,0]^T; \boldsymbol{\omega} = [0\,0\,0]^T \tag{3.46}$$

The reference trajectory are taken as

$$s = 0.5t, \boldsymbol{p}_d = [2.5sin(0.5s)\ 2.5cos(0.5s)\ 2]^T, \psi_d = 0.5t \tag{3.47}$$

This reference satisfies assumption (3.1). The control gains are chosen as follows: $k_1 = 1$, $k_2 = 2$, $k_3 = 5$ and $k_4 = 2$. The unknown parameters are taken as follows: $\boldsymbol{d}_v = [.5+.2*sin(rand); 1+0.2*cos(rand); 1.5+.2*sin(rand)]$, $\boldsymbol{d}_\omega = [0.3+0.1*rand; 0.5+0.1*rand; 0.7+0.1*rand]$, and after 10s $J_1 = 2J_1$. With these unknown parameters, the quadrotor used in simulation is affected by uncertain case and external disturbance.

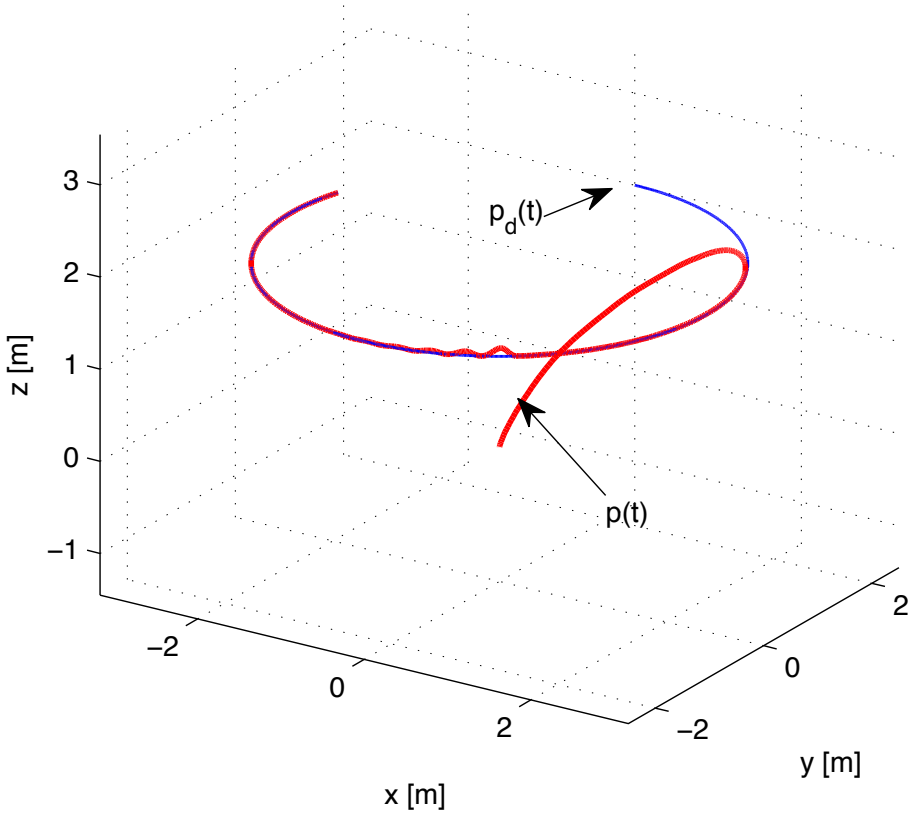

Figure 3.8: Reference and real position trajectories $\boldsymbol{p}_d$ and $\boldsymbol{p}$.

The simulation results are plotted as follows: the reference and real position trajectories are plotted in Figure 3.8. The position tracking errors and attitude tracking errors are plotted in Figure 3.9 and Figure 3.10. It can be seen from these figures that all tracking errors globally asymptotically converge to zero. Unknown parameters are shown in Figure 3.12, 3.14 and 3.15. Unlike the observer design approach that all the observers reach to the real values, the estimates of disturbance and uncertainty via control update laws are combined with the energy function to eliminate the tracking errors. The control inputs, T and τ are illustrated in Figure 3.16

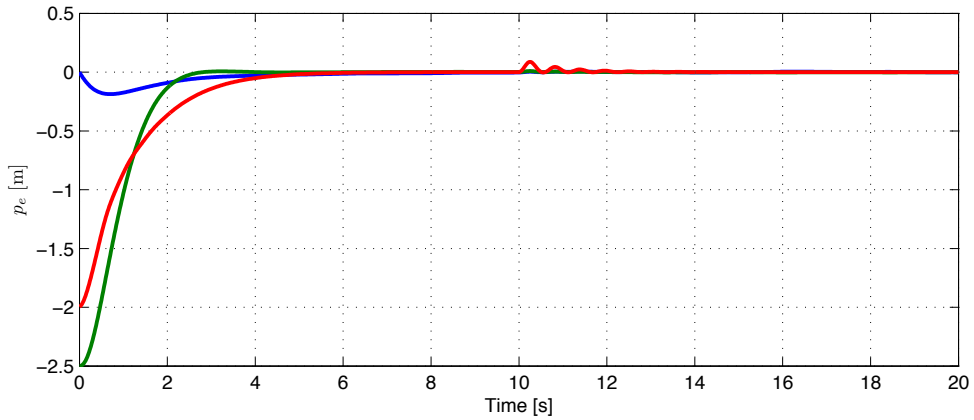

Figure 3.9: Position tracking errors.

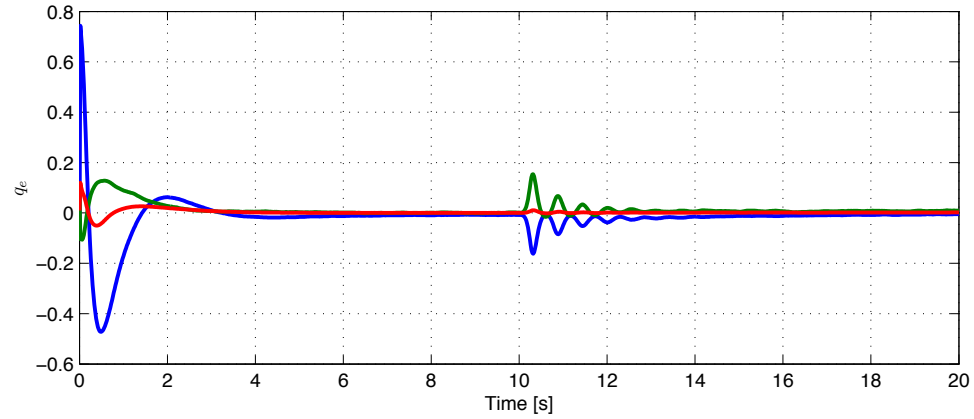

Figure 3.10: Attitude tracking errors.

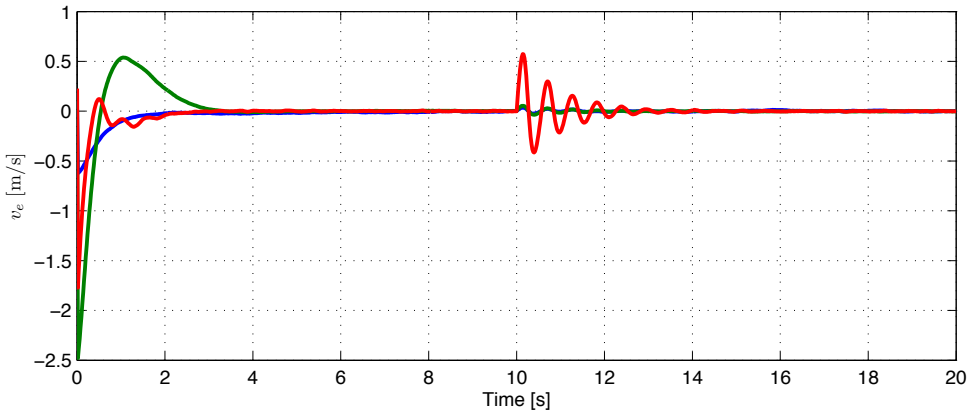

Figure 3.11: Linear velocity tracking errors.

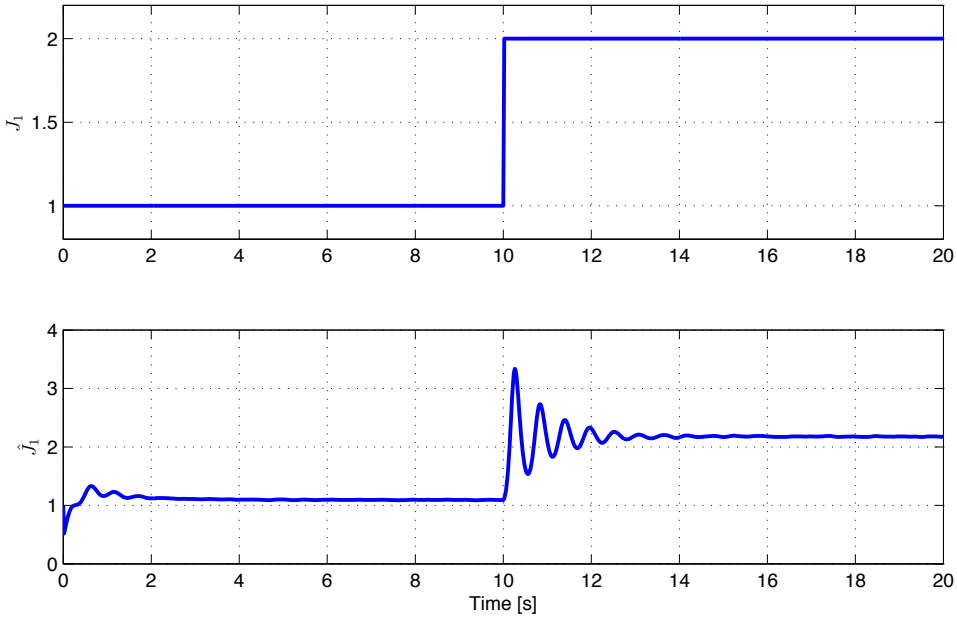

Figure 3.12: Unknown parameters $\boldsymbol{J}_1$ and $\hat{\boldsymbol{J}}_1$.

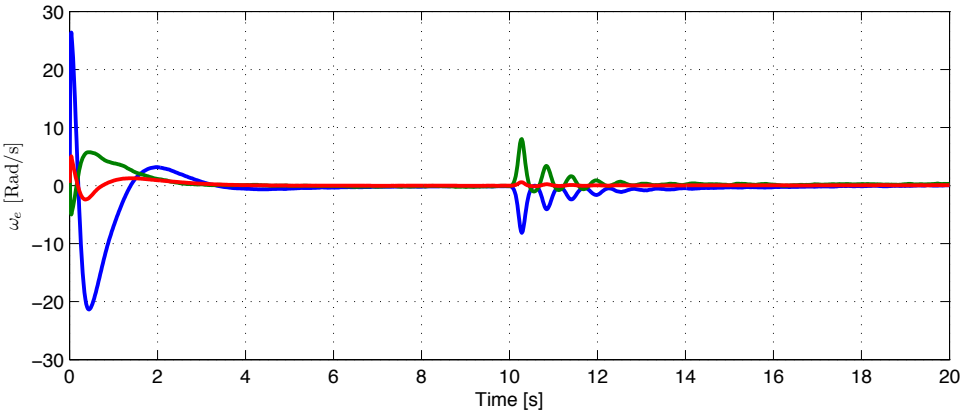

Figure 3.13: Angular velocity tracking errors.

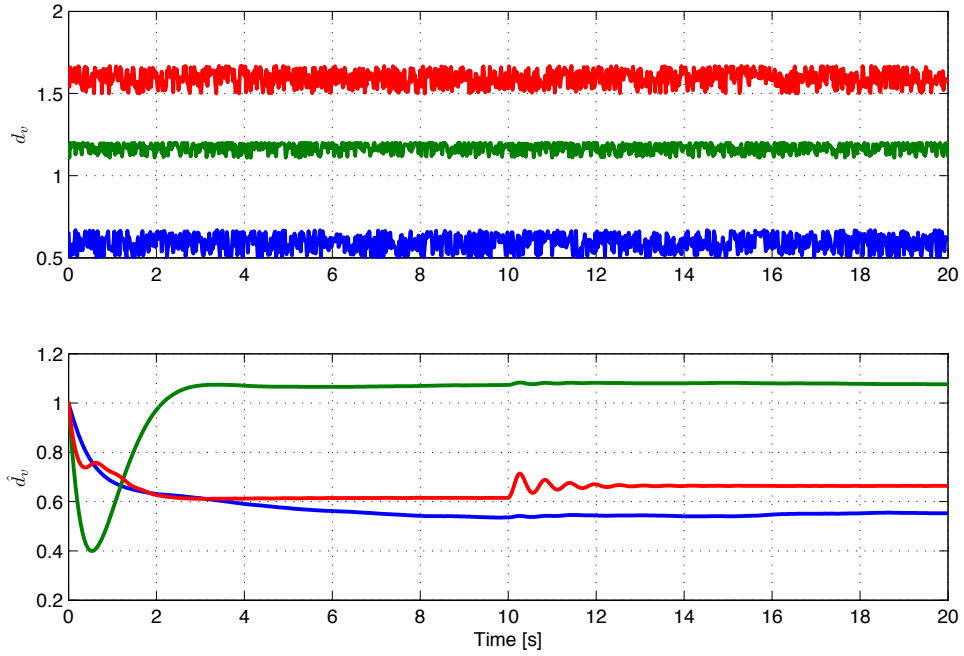

Figure 3.14: Unknown parameters $\boldsymbol{d}_v$ and $\hat{\boldsymbol{d}}_v$.

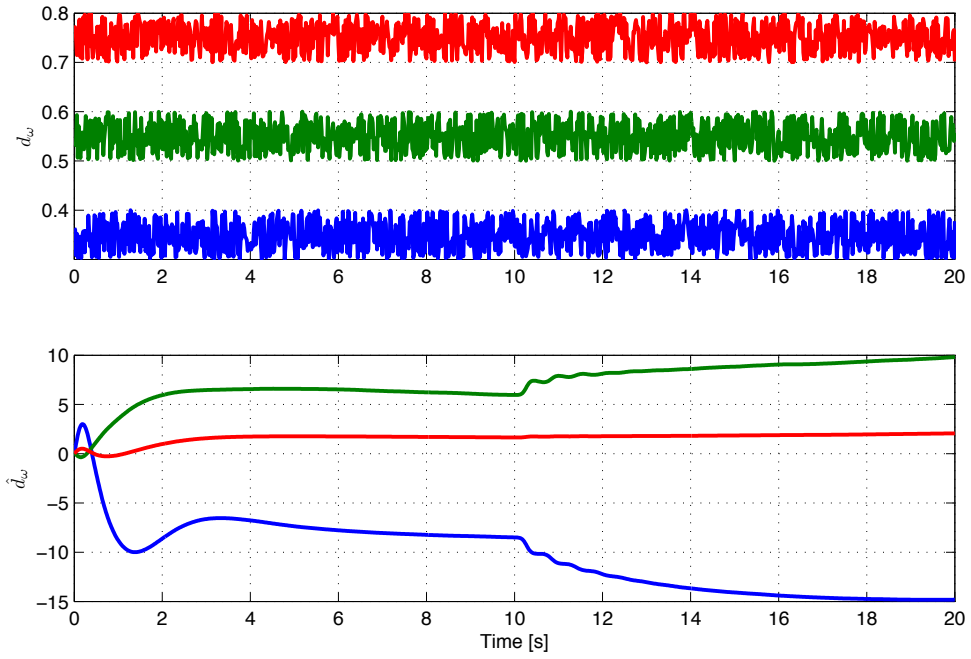

Figure 3.15: Unknown parameters $\boldsymbol{d}_\omega$ and $\hat{\boldsymbol{d}}_\omega$.

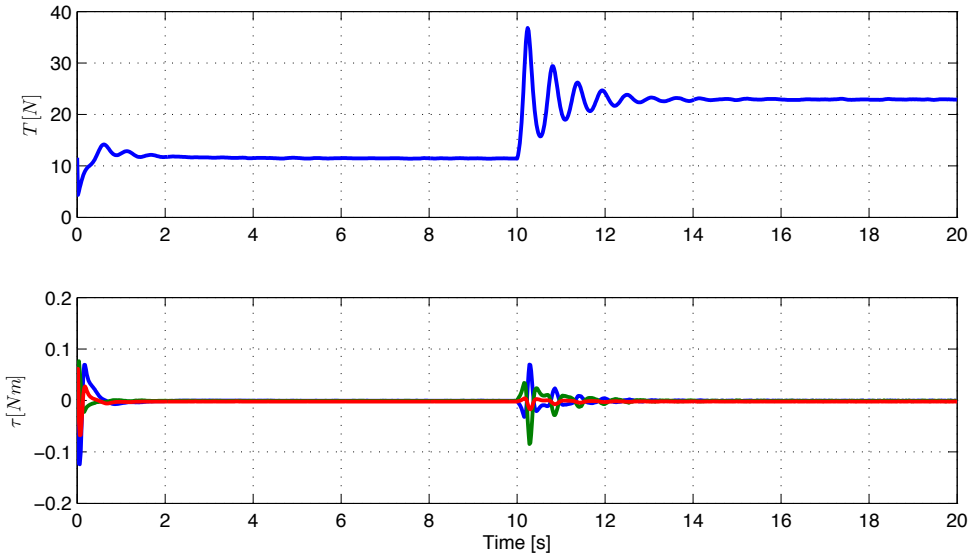

Figure 3.16: Thrust and torques.

3.2.4 Conclusion

A global controller for tracking a predefined path was presented. By using combination of Euler and unit-quaternion model, the singularity in the quadrotor dynamics and self-rotation of the quadrotor are rejected. Uncertainty and external disturbances are solved by employing adaptive backstepping method in which they are estimated as unknown parameters. The simulation results demonstrated that the the proposed controller works well with changing of internal and external disturbances.

3.3 Conclusion

Two controllers for an underactuated quadrotor have been developed. In the first controller, a transformation coordinate is calculated from that a thrust force to stabilize the translational subsystem is generated. Moreover, the orientation for the rotational subsystem used as a reference is also created. However, it has the singularity in describing the quadrotor dynamics in the Euler angles. To overcome this problems, the quadrotor dynamics describing in unit-quaternion is used in the second controller. Furthermore, a new extraction algorithm, using conversion between Euler angles and quaternions to generate the total force thrust to stabilize the translational subsystem and to create the unit-quaternion reference which ideally tracks the heading angle reference, is constructed. This new extraction algorithm is used to develop the controllers for formation of quadrotors in the next chapter.

CHAPTER

4

Fomation control design for a group of quadrotors

Contents

The ability to maintain the position of a group of autonomous vehicles relative to each other or relative to a reference is referred to as formation control. The study of formation control is motivated by the advantages achieved by using a formation of vehicles, instead of a single vehicle. It can be seen that a formation of vehicles each with a variety of sensors offers the opportunity for increased sensor coverage when compared to a single mobile sensor or multiple stationary sensors. The common unmanned vehicles would be a variety of kinds of vehicles from on the ground, in the water to in the space. Each kind of environments has its own dynamic modeling that would be concerned when designing control for these vehicles. The control design for formation of vehicles can be centralized or decentralized. Centralized control uses a main station that plan tasks for agents in formation to perform. This can be advantageous because it has all information receiving from network so that the optimal tasks can be centralized and generated to achieve a global objective. However, centralized control requires more power of computation and multi-directional information flow. In contrast, a decentralized control requires local information exchange between agents to achieve the control objective goal. Comparing with centralized control, the multi-directional information flow is separated to the agents in the decentralized control. However, there usually exists delay in exchange information between agents. Several coordination control approaches have been considered in the literature such as leader-follower [AT13, BMF$^+$11, BM02, EBOA04], behavior-based [BLH01, BSZX12], virtual structure [CMSW11, BLH01, AT09], Geometric formation based on graph theory [ZK12], on flocking [BVV11], and on swam aggregation [PAR05, HC08].
In this chapter, all the quadrotor dynamics is described in unit-quaternion form. The extraction algorithm developed in the previous chapter is applied to design control for formation of quadrotors. After an obstacle avoidance function is defined and constructed, the formation control in five sections.

4.1 Obstacle avoidance functions

The collision avoidance approach can be divided into: 1) Global path planning, 2) Local collision avoidance and 3) Combining both global and local collision avoidance. Global path planning method usually attempts to find optimal paths to the target and check other vehicle's dynamic constraints when the environment (such as free-obstacle, static-obstacle and dynamic environment) is known in advance. Local collision avoidance usually deals with the static and dynamic obstacles in its sensing range to evade from them and keep following the global target. It can be seen that when solving collision problem, depending on the environment, the collision problem can be split into three different problem layers. Collision avoiding 1) in the free-obstacle environment, 2) in the static-obstacle environment and 3) in the dynamic environment. To solve this problem, the parameters of location or distance from the obstacles to the vehicle, size and movement speed of obstacles relative with the vehicle position need to be determined. However, the location, size, kinetic and dynamics parameters of the vehicle also affect to the ability to handle the collision problems. In particle, these values can be provided by sensors installed

on/out of vehicles such as GPS, RADAR, Laser units, IMU,... These values used as reference data for control design can be directly taken from these data or combined with other algorithms to increase the precise reference data. An example for this can be referred [CLH+05] in which the distance from other vehicles and obstacles can be determined through the SLAM algorithms.

Many collision avoidance approaches such as Geometric approach, Grid-based approach and Artificial potential field approach. In the geometric approach, one of the straightforward approach is based in a simple geometric space to solve the collision problem among vehicles. There are some approaches in this area such as point of closest approach [POT08], collision cone approach [Muj09], and Dubins paths [STWZ10]. With the point of closed approach, based on current vehicle speed, bearing and its future way-point, the miss distance vector between vehicles is created. When the actual distance is less than the desired distance, both vehicles take a avoiding action by turning along the miss distance vector in positive and negative direction to extend the space between them. With collision cone approach, a circle around obstacles and other vehicles are placed and two tangent lines from the center of vehicle to these circles form the collision cone. If the path of vehicle in these cones, an avoiding algorithm based on the velocity and bearing of vehicle is made to evade these obstacles. Geometric approach has simple and direct approach for solving collision problem. However, when the number of vehicles increase, it need a lot of time to calculate for path planning and to check again and recalculate for possible conflicts with other vehicles in its sense. In the grid-based approach, graph search algorithms for collision-free path planning, based on grid approach and usually searching an optimal trajectory between initial and goal target, are deployed in two steps: A map of the environment showing all possible ability for vehicle without collision is generated and a trajectory for vehicle with a minimized cost function, typically with the shortest distant path, with dynamic constraints or with the most economic issue, is deployed. Some popular technique examples for this approach are A* search algorithm [TDY09] and probabilistic sampling based planners such as [CLH+05]. This approach usually archives global and local result for path planning [LaV06] and can be applied for 2D and 3D environment. In the artificial potential field approach, the potential function is usually based on electric potential and applied for real time robot control. It can be classified into: Artificial potential field (APF) methods and artificial intelligence (AI) methods. Many existed AI methods relative to path planning based on artificial intelligence tools such as fuzzy, neural network, genetic algorithm, evolutionary algorithm [RKPC02]. These methods are connected with optimal algorithms for the best global path planning and relative to complex calculation and time consuming. Motivating from the first public for avoiding collision in [Kha85] , some other potential field approaches are illustrated by using artificial potential field in [LF01], artificial force field, total field [SH03]. With these approaches, the path will be generated safely and optimal when combining with AI approaches.

A plenty of collision avoidance approaches solving the global and local problem in path planning are reviewed in which some main methods mentioned above. It seems that probabilistic approach and potential field are can be applied for real robots when resolving collision problem. It can be also seen that the collision avoidance is directly related to local problems, the

distance from the position of the robot to the obstacle, the kinetic and the dynamic parameters of the robot. There have been many theoretical models presented path planning for dealing with obstacles and determine the trajectory that robot can be followed, but the problem is how to measure the value of the distance from the obstacle to the robot in simulation. In particle, some common sensors used in robotics and control as mentioned above provide the desired value for control design.

The collision avoidance function used in this chapter is one kind of potential functions. The definition of this function is described in the subsection 4.1.1.

4.1.1 Pairwise Collision Avoidance Functions

This section gives a definition of the pairwise collision avoidance function. This function will be embedded in a potential function for the formation control design later.

Definition 4.1. *Let β_{ij} with $(i,j) \in \mathbb{N}$ and $i \neq j$ be a scalar function of α_{ij}, which is defined in* (4.3)*. The function β_{ij} is said to be a pairwise collision function if it possesses the following properties:*

$$\begin{aligned}
&(1) \quad \beta_{ij} = 0, \quad {\beta'}_{ij} = 0, \quad {\beta''}_{ij} = 0, \quad \forall \alpha_{ij} \in [\alpha^*_{ij}, \infty), \\
&(2) \quad \beta_{ij} > 0, \quad \forall \alpha_{ij} \in (0, \alpha^*_{ij}), \quad {\beta'}_{ij} < 0, \quad \forall \alpha_{ij} \in \mathbb{R}, \\
&(3) \quad \lim_{\alpha_{ij} \to 0} \beta_{ij} = \infty, \quad \lim_{\alpha_{ij} \to 0} {\beta'}_{ij} = -\infty, \quad \lim_{\alpha_{ij} \to 0} {\beta''}_{ij} = -\infty, \\
&(4) \quad \beta_{ij} \textit{ is smooth}, \quad \forall \alpha_{ij} \in (0, \infty),
\end{aligned} \tag{4.1}$$

where ${\beta'}_{ij} = \frac{\partial \beta_{ij}}{\partial \alpha_{ij}}$, ${\beta''}_{ij} = \frac{\partial^2 \beta_{ij}}{\partial \alpha_{ij}^2}$, and α^*_{ij} is a strictly positive constant satisfying the following condition:

$$\alpha^*_{ij} \leq \alpha^R_{ij} \tag{4.2}$$

Remark 4.1. *Property (1) implies that the function β_{ij} is zero when the quadrotors i and j are at their desired locations or adequately far away from each other since the constant α^*_{ij} satisfies the condition* (4.2)*. Property (2) implies that the function β_{ij} is positive definite when the quadrotors i and j are sufficiently close to each other. Property (3) means that the function β_{ij} is equal to infinity when a collision between quadrotor i and j occurs. Property (4) allows us to use control design and stability analysis methods for continuous systems. Using the smooth function given in Definition 2.14, we can find many functions that satisfy all the properties listed in* (4.1)*. The function β_{ij} is defined in* (4.3)*.*

$$\beta_{ij} = \frac{1 - h(\alpha_{ij}, a_{ij}, b_{ij})}{\alpha_{ij}} \tag{4.3}$$

where $h(\alpha_{ij}, a_{ij}, b_{ij})$ is a smooth step function defined in Definition 2.3. The positive constants a_{ij} and b_{ij} satisfy the following condition:

$$0 < a_{ij} < b_{ij} \leq \alpha^*_{ij} \tag{4.4}$$

It can be directly verified that the function β_{ij} given in (4.3) *possesses all the properties listed in* (4.1).

4.2 Controller 1 - Global formation tracking control

In this section, we focus to design control for a group of quadrotor following predefined paths which satisfies the Assumption 4.2. The proposed controller guarantees that stabilization and tracking errors converge to zero asymptotically from any initial values. The developed controller is based on the coordinate transformations which employ the combination of Newton-Euler and unit quaternion via the attitude extraction algorithm which has been presented in the preview chapter. The Lyapunov's direct method, and backstepping technique [KKK95] are also used to design for the formation controller.

4.2.1 Control objective

The quadrotor dynamics i, described in Section 2.1, is rewritten as follows

$$\begin{aligned}
\dot{\boldsymbol{p}}_i &= \boldsymbol{v}_i \\
\dot{\boldsymbol{v}}_i &= g\boldsymbol{e}_3 - \tfrac{T_i}{m_i}\boldsymbol{R}_Q^T(\boldsymbol{Q}_i)\boldsymbol{e}_3 \\
\dot{\boldsymbol{Q}}_i &= \boldsymbol{K}_Q(\boldsymbol{Q}_i)\boldsymbol{\omega}_i \\
\boldsymbol{J}_i\dot{\boldsymbol{\omega}}_i &= \boldsymbol{\tau}_i - \boldsymbol{S}(\boldsymbol{\omega}_i)\boldsymbol{J}_i\boldsymbol{\omega}_i
\end{aligned} \tag{4.5}$$

where $i \in \mathbb{N}$, $\mathbb{N}$ is the set of all quadrotors in the group. All other symbols are defined in the Section 2.1.
It can be seen from Figure 4.1, each quadrotor in the formation needs its reference trajectory to track. The reference trajectory can be predefined or obtained from measurement data. Furthermore, each quadrotor needs to communicate with other quadrotors in the group to perform its cooperative mission. Thus, before starting the formation control objective we impose the following assumption on the reference trajectories, communication and initial conditions between the quadrotor in the group:

Assumption 4.1.

1. *The quadrotor i has a physical safety ball, which is centered at the point $\boldsymbol{p}_i$ and has a radius α_i^S, and has a communication ball, which is centered at the point $\boldsymbol{p}_i$ and has a radius α_i^R, see Figure 4.1. Let us define*

$$\begin{aligned}
\boldsymbol{p}_{ij} &= \boldsymbol{p}_i - \boldsymbol{p}_j \\
\boldsymbol{v}_{ij} &= \boldsymbol{v}_i - \boldsymbol{v}_j \\
\boldsymbol{\alpha}_{ij} &= \boldsymbol{p}_{ij}^T\boldsymbol{p}_{ij}
\end{aligned} \tag{4.6}$$

Then the distance between quadrotor i and quadrotor j, α_{ij}, is such that

$$\boldsymbol{\alpha}_{ij} > (\alpha_i^S + \alpha_j^S) \tag{4.7}$$

for all $i, j \in \mathbb{N}$, $i \neq j$

2. *The quadrotor i and j can communicate with each other and exchange their states, if they satisfy the following condition:*

$$\alpha_{ij} \leq min(\alpha_i^R, \alpha_j^R) \tag{4.8}$$

3. *Let $\boldsymbol{p}_{od}$ is a based point on the predefined trajectory and the desired formation structure be formed by the vectors $\boldsymbol{l}_i$, $i \in \mathbb{N}$, coordinated at $\boldsymbol{p}_{od}$. The desired velocity vector $\dot{\boldsymbol{l}}_i$ is bounded in norm, and specifies a desired change of the desired formation shape. The design of $\dot{\boldsymbol{l}}_i$ depends on a specific application.*

4. *the quadrotor i and j can measure their relative position if they are in their communication region. In the dynamical environment, it also assumes that the minimum distance from quadrotor i to obstacles can be measured.*

5. *At the initial time $t_0 \geq 0$. all the quadrotors in the group are sufficiently far away from each other in the sense that there are no collision between all the quadrotors.*

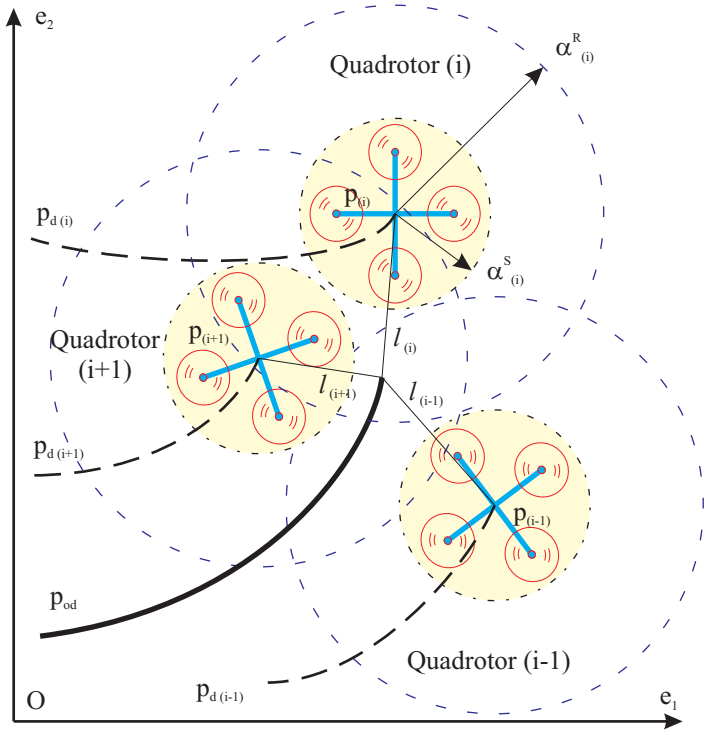

Figure 4.1: Formation parameters.

Remark 4.2. *Item 2) specifies the way each quadrotor communicating with other quadrotors in the group with in its communication range. In Figure 4.1, the quadrotor i and $(i+1)$ are communicating with each other since the points $\boldsymbol{p}_i$ and $\boldsymbol{p}_{(i+1)}$ are in the communication areas of the quadrotors i and $(i+1)$, respectively. In other hand, the quadrotor $(i-1)$ is not in the communication region. The conditions* (4.7) *and* (4.8) *imply that there are no collision between all the quadrotors and that all the quadrotors are communicating with each other.*

Assumption 4.2.

1. *The reference position trajectory $\boldsymbol{p}_{di}(t) = [x_{di}(t)\, y_{di}(t)\, z_{di}(t)]^T$ and the heading angle ψ_{id} for the quadrotor i to track satisfies the following condition:*

$$\begin{aligned} &\|p_{dij}\| \geq \varepsilon_{ij}, \\ &\left\|\boldsymbol{p}_{di}^{(k)}\right\| \leq \varepsilon_{kd}, \\ &\left\|\psi_{di}^{(k)}\right\| \leq \delta_{kd}, \end{aligned} \tag{4.9}$$

   for all $(i,j) \in \mathbb{N}, i \neq j$ where $p_{dij} = p_{di} - p_{dj}$, ε_{ij} is a strictly positive constant. ε_{kd} and δ_{kd}, $k = 1, \ldots, 4$, are nonnegative constants.

2. *Each quadrotor starts at a different location and do not have any collision among all the quadrotors. Specially, there exist strictly positive constants ε_{ij} and $\alpha_{ij}^S = (\alpha_i^S + \alpha_j^S)$ such that for all $(i,j) \in \mathbb{N}, i \neq j$, the following conditions holds:*

$$\begin{aligned} &\|p_{ij}(t_0)\| \geq \varepsilon_{ij}, \\ &\alpha_{ij}(t_0) \geq \alpha_{ij}^S \end{aligned} \tag{4.10}$$

Remark 4.3. *In the Assumption 4.2, property 1) specifies possible reference trajectory $\boldsymbol{p}_{di}$ for the quadrotor i in the group to track since it has to satisfy the condition* (4.9)*. Property 2) implies that at the initial time, there are no collision between all the quadrotors.*

Control Objective 4.1. *Under the Assumption 4.2, for each quadrotor i design the control inputs T_i and $\boldsymbol{\tau}_i$ such that the position vector $\boldsymbol{p}_i(t)$ of the quadrotor i track their reference trajectories $\boldsymbol{p}_{di}(t)$ while avoid collision with all the other quadrotors. Specifically, we design the control inputs T_i and $\boldsymbol{\tau}_i$ such that*

$$\begin{aligned} &\lim_{t\to\infty} (\boldsymbol{p}_i(t) - \boldsymbol{p}_{di}(t)) = 0, \\ &\lim_{t\to\infty} (\psi_i(t) - \psi_{di}(t)) = 0 \\ &\|\boldsymbol{p}_i - \boldsymbol{p}_j\| \geq \alpha_{ij}^S \end{aligned} \tag{4.11}$$

For all $(i,j) \in \mathbb{N}, i \neq j$ and $t \geq t_0 \geq 0$, the control design needs to keep all other states of the quadrotor dynamics bounded for all initial conditions and there are no collision between all the quadrotors.

4.2.2 Formation control design

In this section we will use the pairwise collision avoidance function (4.3) and the new attitude extraction algorithm to design control for a formation of quadrotors. Similarly in the previous section, the quadrotor dynamics i (4.5) is separated into two subsystems. The first subsystem contains two first equations for translational dynamics and the second subsystem consists two last equations for rotational dynamics. In the first step, the intermediate control input for the translational dynamics tracking the predefined path is designed. After this step, the new extraction algorithm using some conversions between Euler angles and unit-quaternion to reject the self-rotation of quadrotor around its vertical axis to generate a total force T_i and a unit-quaternion reference Q_{di} which can be employed as the reference for the second subsystem is applied. The attitude extraction algorithm is shown in Figure 3.7. In the next step, the torque $\boldsymbol{\tau}_i$ to force $\boldsymbol{Q}_i \to \boldsymbol{Q}_{di}$ is designed.

Step 1

In this step, the translational dynamics of (4.5) is considered. We will design a virtual control of $\boldsymbol{v}_i$ to force $\boldsymbol{p}_i(t)$ to globally asymptotically track its reference trajectory $\boldsymbol{p}_{di}(t)$. As such, we define the tracking errors as follows:

$$\begin{aligned} \boldsymbol{p}_{ei} &= \boldsymbol{p}_i - \boldsymbol{p}_{di}, \\ \boldsymbol{v}_{ei} &= \boldsymbol{v}_i - \boldsymbol{\alpha}_{vi}, \end{aligned} \tag{4.12}$$

where $\boldsymbol{\alpha}_{vi}$ is a virtual control of $\boldsymbol{v}_i$. Differentiating both sides of (4.12) and using the first subsystem, the error dynamics are expressed as

$$\begin{aligned} \dot{\boldsymbol{p}}_{ei} &= \boldsymbol{v}_{ei} + \boldsymbol{\alpha}_{vi} - \dot{\boldsymbol{p}}_{di}, \\ \dot{\boldsymbol{v}}_{ei} &= g\boldsymbol{e}_3 - \boldsymbol{F} - \dot{\boldsymbol{\alpha}}_{vi} \end{aligned} \tag{4.13}$$

where $\boldsymbol{F}_i$ is an intermediate control input and $\boldsymbol{F}_i = \frac{T_i}{m_i}\boldsymbol{R}_Q^T(\boldsymbol{Q}_i)\boldsymbol{e}_3$

In order to design the intermediate control input $\boldsymbol{F}_i$ for quadrotor i that achieves the Formation control objective 4.1, we consider the following potential function:

$$V_1 = \frac{1}{2}\sum_{i=1}^{N}\left[\boldsymbol{p}_{ei}{}^T\boldsymbol{p}_{ei} + \sum_{J\in\mathbb{N}_i}\beta_{ij}\right] \tag{4.14}$$

where $\mathbb{N}_i$ is the set containing all the quadrotors except for the quadrotor i, β_{ij} is taken from (4.3) where α_{ij} is calculated from (4.6).

Differentiating both sides of (4.14) gives

$$\begin{aligned}\dot{V}_1 &= \sum_{i=1}^{N}\left[\boldsymbol{p}_{ei}{}^T\dot{\boldsymbol{p}}_{ei} + \sum_{j\in\mathbb{N}_i}\beta'_{\text{ij}}\dot{\alpha}_{\text{ij}}\right] \\ &= \sum_{i=1}^{N}\left[\boldsymbol{p}_{ei}{}^T\dot{\boldsymbol{p}}_{ei} + \sum_{j\in\mathbb{N}_i}\beta'_{ij}\boldsymbol{p}_{ij}{}^T\dot{\boldsymbol{p}}_{ij}\right]\end{aligned} \tag{4.15}$$

Noting that $\dot{\boldsymbol{p}}_{ij} = (\dot{\boldsymbol{p}}_i - \dot{\boldsymbol{p}}_{di}) - (\dot{\boldsymbol{p}}_j - \dot{\boldsymbol{p}}_{dj}) = \boldsymbol{v}_{ei} - \boldsymbol{v}_{ej}$, we can write (4.15) as follows

$$\begin{aligned}\dot{V}_1 &= \sum_{i=1}^{N}(\boldsymbol{p}_{ei}{}^T + \sum_{j\in\mathbb{N}_i}\beta'_{ij}\boldsymbol{p}_{ij}{}^T)(\boldsymbol{v}_{ei} + \boldsymbol{\alpha}_{vi} - \dot{\boldsymbol{p}}_{di}) \\ &= \sum_{i=1}^{N}\boldsymbol{\Omega}_i{}^T(\boldsymbol{v}_{ei} + \boldsymbol{\alpha}_{vi} - \dot{\boldsymbol{p}}_{di})\end{aligned} \tag{4.16}$$

where

$$\boldsymbol{\Omega}_i = \boldsymbol{p}_{ei} + \sum_{j\in\mathbb{N}_i}\beta'_{ij}\boldsymbol{p}_{ij} \tag{4.17}$$

The equation (4.16) suggests that we choose

$$\boldsymbol{\alpha}_{vi} = -k_1\boldsymbol{\Omega}_i + \dot{\boldsymbol{p}}_{di} \tag{4.18}$$

To design the intermediate control input $\boldsymbol{F}_i$, considering the following Lyapunov function

$$V_2 = V_1 + \frac{1}{2}\sum_{i=1}^{N}\boldsymbol{v}_{ei}{}^T\boldsymbol{v}_{ei} \tag{4.19}$$

Differentiating both sides of (4.19) gives

$$\dot{V}_2 = \sum_{i=1}^{N}\left[-k_1\boldsymbol{\Omega}_i{}^T\boldsymbol{\Omega}_i + \boldsymbol{v}_{ei}{}^T(ge_3 - \boldsymbol{F}_i - \dot{\boldsymbol{\alpha}}_{vi} + \boldsymbol{\Omega}_i)\right] \tag{4.20}$$

which suggests that we choose:

$$\boldsymbol{F}_i = k_2\boldsymbol{v}_{\boldsymbol{ei}} + ge_3 - \dot{\boldsymbol{\alpha}}_{vi} + \boldsymbol{\Omega}_i \tag{4.21}$$

We assume that the control input $\boldsymbol{F}_i$ forces the quadrotor i tracking the predefined path and heading angle ψ_{di} in ideal case. Applying Lemma 2.3 for the intermediate control input (4.21),

we obtain the thrust T_i and the reference unit-quaternion vector $\boldsymbol{Q}_{di}$ as follows:

$$
\begin{aligned}
T_i &= \|\boldsymbol{F}_i\| \\
\boldsymbol{Q}_{di} &= \begin{bmatrix} C\frac{\alpha_{\phi i}}{2}C\frac{\alpha_{\theta i}}{2}C\frac{\alpha_{\psi i}}{2} + S\frac{\alpha_{\phi i}}{2}S\frac{\alpha_{\theta i}}{2}S\frac{\alpha_{\psi i}}{2} \\ S\frac{\alpha_{\phi i}}{2}C\frac{\alpha_{\theta i}}{2}C\frac{\alpha_{\psi i}}{2} - C\frac{\alpha_{\phi i}}{2}S\frac{\alpha_{\theta i}}{2}S\frac{\alpha_{\psi i}}{2} \\ C\frac{\alpha_{\phi i}}{2}S\frac{\alpha_{\theta i}}{2}C\frac{\alpha_{\psi i}}{2} + S\frac{\alpha_{\phi i}}{2}C\frac{\alpha_{\theta i}}{2}S\frac{\alpha_{\psi i}}{2} \\ C\frac{\alpha_{\phi i}}{2}C\frac{\alpha_{\theta i}}{2}S\frac{\alpha_{\psi i}}{2} - S\frac{\alpha_{\phi i}}{2}S\frac{\alpha_{\theta i}}{2}C\frac{\alpha_{\psi i}}{2} \end{bmatrix}
\end{aligned}
\tag{4.22}
$$

where

$$
\begin{aligned}
\alpha_{\psi i} &= \psi_{di}, \\
\alpha_{\theta i} &= \arctan\left(\frac{C\alpha_{\psi i}F_{i1} + S\alpha_{\psi i}F_{i2}}{F_{i3}}\right), \\
\alpha_{\phi i} &= \arcsin\left(\frac{S\alpha_{\psi i}F_{i1} - C\alpha_{\psi i}F_{i2}}{T_i}\right),
\end{aligned}
\tag{4.23}
$$

The reference angular velocity of quadrotor i is calculated as follows

$$
\boldsymbol{\omega}_{di} = \begin{bmatrix} 1 & 0 & -S\alpha_{\theta i} \\ 0 & C\alpha_{\phi i} & S\alpha_{\phi i}C\alpha_{\theta i} \\ 0 & -S\alpha_{\phi i} & C\alpha_{\phi i}C\alpha_{\theta i} \end{bmatrix} \begin{bmatrix} \dot{\alpha}_{\phi i} \\ \dot{\alpha}_{\theta i} \\ \dot{\alpha}_{\psi i} \end{bmatrix}
\tag{4.24}
$$

where $\boldsymbol{\omega}_{di}$ is the body reference angular velocity; $S(\cdot)$ and $C(\cdot)$ stand for $\sin(\cdot)$, $\cos(\cdot)$, respectively.

Step 2

In this step, the torque input $\boldsymbol{\tau}_i$ will be designed. The unit-quaternion vector $\boldsymbol{Q}_{di}$ is used as the reference. We first define the following tracking errors

$$
\begin{aligned}
\boldsymbol{Q}_{ei} &= \boldsymbol{Q}_{di}^{-1} \odot \boldsymbol{Q}_i, \\
\boldsymbol{\omega}_{ei} &= \boldsymbol{\omega}_i - \boldsymbol{\alpha}_{\omega i}
\end{aligned}
\tag{4.25}
$$

where $\boldsymbol{\alpha}_{\omega i}$ is a virtual control of ω_i. $\boldsymbol{Q}_{ei} = [\eta_{ei}\, \boldsymbol{q}_{ei}^T]^T$ and $\boldsymbol{\omega}_{ei}$ are attitude tracking and angular velocity error vector, respectively.

Differentiating both sides of (4.25) yields

$$
\begin{aligned}
\dot{\boldsymbol{q}}_{ei} &= \boldsymbol{G}_i(\boldsymbol{\omega}_{ei} + \boldsymbol{\alpha}_{\omega i} - \boldsymbol{\omega}_{di}) \\
\dot{\boldsymbol{\omega}}_{ei} &= \boldsymbol{J}_i^{-1}\left(\boldsymbol{\tau}_i - \boldsymbol{S}(\boldsymbol{\omega}_i)\boldsymbol{J}_i\boldsymbol{\omega}_i\right) - \dot{\boldsymbol{\alpha}}_{\omega i}
\end{aligned}
\tag{4.26}
$$

where $\boldsymbol{G}_i = \frac{1}{2}\left(\eta_{ei}\boldsymbol{I}_{3\times 3} + \boldsymbol{S}(\boldsymbol{q}_{ei})\right)$ and $\boldsymbol{\omega}_{di}$ can be obtained by using equation (4.24).

To obtain the control input $\boldsymbol{\tau}_i$, we consider the following Lyapunov function:

$$V_3 = \sum_{i=1}^{N} \frac{1}{2} \boldsymbol{q}_{ei}^T \boldsymbol{q}_{ei} \tag{4.27}$$

The time derivative of V_3 along solutions (4.26) is given by

$$\dot{V}_3 = \sum_{i=1}^{N} \boldsymbol{q}_{ei}^T \boldsymbol{G}_i (\boldsymbol{\omega}_{ei} + \boldsymbol{\alpha}_{\omega i} - \boldsymbol{\omega}_{di}) \tag{4.28}$$

which suggests that we choose

$$\boldsymbol{\alpha}_{\omega i} = -k_3 \boldsymbol{G}_i^T \boldsymbol{q}_{ei} + \boldsymbol{\omega}_{di} \tag{4.29}$$

To design the control input torque, $\boldsymbol{\tau}_i$, considering the following Lyapunov candidate

$$V_4 = V_3 + \sum_{i=1}^{N} \boldsymbol{\omega}_{ei}^T \boldsymbol{\omega}_{ei} \tag{4.30}$$

The time derivative of (4.30) is given

$$\dot{V}_4 = \sum_{i=1}^{N} \left(-k_3 \boldsymbol{q}_{ei}^T \boldsymbol{G}_i \boldsymbol{G}_i^T \boldsymbol{q}_{ei} + \boldsymbol{\omega}_{ei}^T (\boldsymbol{J}_i^{-1} (\boldsymbol{\tau}_i - \boldsymbol{S}(\boldsymbol{\omega}_i) \boldsymbol{J}_i \boldsymbol{\omega}_i) - \dot{\boldsymbol{\alpha}}_{\omega i} + \boldsymbol{G}_i \boldsymbol{q}_{ei}) \right) \tag{4.31}$$

which suggests that we choose the control input torque as follows

$$\boldsymbol{\tau}_i = \boldsymbol{J}_i (-k_4 \boldsymbol{\omega}_{ei} + \dot{\boldsymbol{\alpha}}_{\omega i} - \boldsymbol{G}_i \boldsymbol{q}_{ei}) + \boldsymbol{S}(\boldsymbol{\omega}_i) \boldsymbol{J}_i \boldsymbol{\omega}_i \tag{4.32}$$

Substituting control and virtual control from (4.18), (4.21), (4.29) and (4.32) into (4.13), and (4.25), we have the following closed loop system:

$$\begin{aligned} \dot{\boldsymbol{p}}_{ei} &= \boldsymbol{v}_{ei} - k_1 \boldsymbol{\Omega}_i \\ \dot{\boldsymbol{v}}_{ei} &= -k_2 \boldsymbol{v}_{ei} - \boldsymbol{\Omega}_{\boldsymbol{i}} \\ \dot{\boldsymbol{q}}_{ei} &= \boldsymbol{G}_i (-k_3 \boldsymbol{G}_i^T \boldsymbol{q}_{ei} + \boldsymbol{\omega}_{ei}) \\ \dot{\boldsymbol{\omega}}_{ei} &= -k_4 \boldsymbol{\omega}_{ei} - \boldsymbol{G}_i \boldsymbol{q}_{ei} \end{aligned} \tag{4.33}$$

The control design has been completed. We summarize the results in the following theorem.

Theorem 4.1. *Under Assumption 4.2, the formation control laws consisting of* (4.21) *and* (4.32) *for the quadrotor i achieve the Formation Control Objective 4.1, there is no collision between all the quadrotors, the position $\boldsymbol{p}_i$ and heading angle ψ_i of quadrotor i globally asymptotically track their*

reference trajectories $\boldsymbol{p}_{di}$ *and* ψ_{di}*,*

$$\begin{aligned} &\lim_{t\to\infty}(\boldsymbol{p}_i(t)-\boldsymbol{p}_{di}(t))=0,\\ &\lim_{t\to\infty}(\psi_i(t)-\psi_{di}(t))=0\\ &\|\boldsymbol{p}_i-\boldsymbol{p}_j\|\geq\alpha_{ij}^S \end{aligned} \tag{4.34}$$

and the closed loop system (4.33) *is forward complete.*

Proof. *See Appendix B.3.*

4.2.3 Simulation results

In this section, we illustrate the effectiveness of the proposed formation control design through a numerical simulation on a group of $N = 12$ identical quadrotors. The quadrotor parameters for the simulation are taken from [EInE12] as following: m_i=0.35 kg, g = 9.81 $kg\,m^2$, $l_i = 0.15m$, $I_{X_i} = 15.67 \times 10^{-3}\,kg\,m^2$, $I_{Y_i} = 15.67 \times 10^{-3}\,kg\,m^2$; $I_{Z_i} = 28.34 \times 10^{-3}\,kg\,m^2$, $K_{ti} = 192.32 \times 10^{-7}Ns^2$, $K_{di} = 4.003 \times 10^{-7}Nms^2$.
The initial conditions are taken as

$$\begin{aligned} &\boldsymbol{p}_i(0)=[R_1*j \quad R_1*k \quad 0]^T;\boldsymbol{v}_i(0)=[0\,0\,0]^T\\ &\boldsymbol{Q}_i(0)=[1\,0\,0\,0]^T;\boldsymbol{\omega}_i(0)=[0\,0\,0]^T \end{aligned} \tag{4.35}$$

where $R_1 = 1.5m$, j and k combine such that at the first time, all quadrotors are distributed on land in a rectangle form with 3 rows and 4 columns. The initial distance between quadrotors are satisfied (4.10).
For the stabilization, the reference points are taken as

$$\begin{aligned} &\boldsymbol{L}_{di}=[R_0 sin((i-1)2pi/N)\ R_0 cos((i-1)2pi/N)\ 0]^T,\\ &\boldsymbol{p}_{0d}=[5\ 5\ 10]^T,\\ &\boldsymbol{p}_{di}=\boldsymbol{p}_0+\boldsymbol{L}_{di},\\ &\psi_{di}=0, \end{aligned} \tag{4.36}$$

and for the path-tracking, the reference trajectories are chosen as

$$\begin{aligned} &\boldsymbol{L}_{di}=[R_0 sin((i-1)2pi/N)\ R_0 cos((i-1)2pi/N)\ 0]^T,\\ &s=0.5*t,\\ &\boldsymbol{p}_{0d}=[3*sin(0.5*s)\ 3*cos(0.5*s)\ 5+s]^T,\\ &\boldsymbol{p}_{di}=\boldsymbol{p}_0+\boldsymbol{L}_{di},\\ &\psi_{di}=0.5*t, \end{aligned} \tag{4.37}$$

with $R_0 = 5m$. The purpose of choosing the initial (4.36) is to illustrate both collision avoidance and reference tracking capacities of the proposed formation controller. With the above initial reference, all quadrotors are distributed on a circle shape at the goal point or tracking a helix path $\boldsymbol{p}_0$ and satisfy conditions (4.9) and (4.10).
The control gains are chosen as $|a_{ij}| = 0.4m$, $|b_{ij}| = 5m$, $k_1 = 1$, $k_2 = 2$, $k_3 = 5$ and $k_4 = 2$. Simulation results are plotted in two cases, formation formed at the goal point, Figure. 4.2, and at a predefined path, Figure. 4.10. To illustrate the effectiveness of collision avoidance function and formation controller, the minimum distances among quadrotors and position errors are shown in Figure. 4.7 and Figure. 4.15. Noting that the minimum distances among quadrotors satisfy that there are no collisions among any quadrotors,in which the minimum distances among quadrotors are always larger than 0.3m (safe area α_{ij}^S). and all the tracking errors converge to the origin are shown in the Figure 4.3, 4.4, 4.5, and 4.11, 4.12, 4.13. Torque and force applied for quadrotor 1 are demonstrated in Figure 4.14 and Figure 4.14.
Case 1: All the quadrotors in the formation is distributed at the goal point in a circle shape.

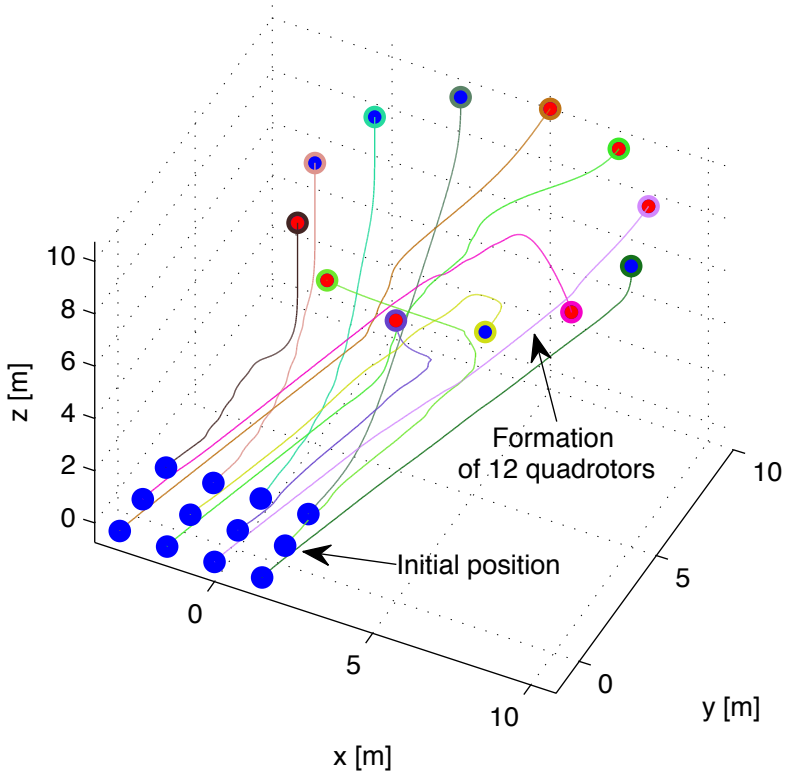

Figure 4.2: Formation of 12 quadrotors.

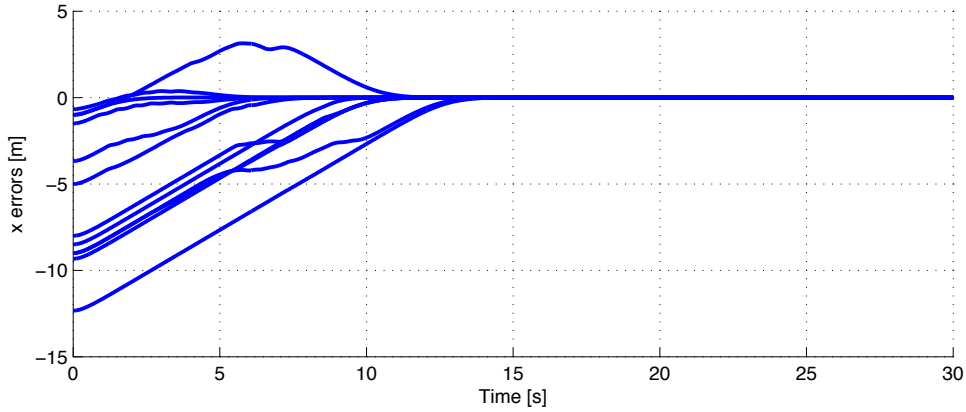

Figure 4.3: x tracking errors.

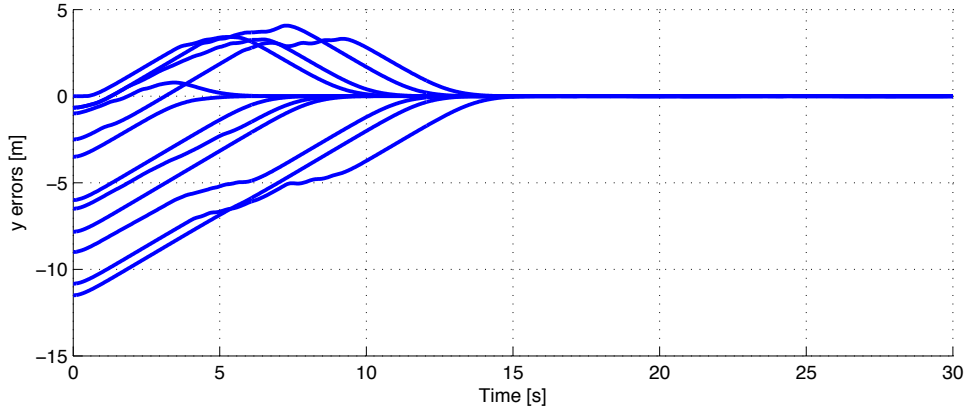

Figure 4.4: y tracking errors.

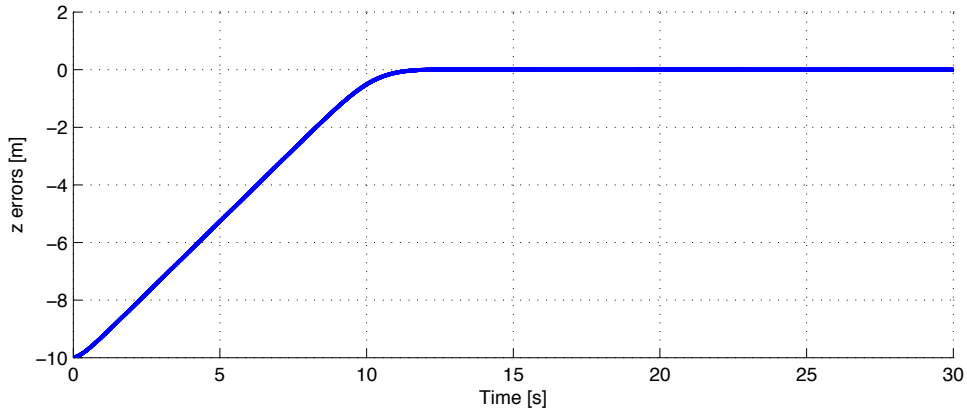

Figure 4.5: z tracking errors.

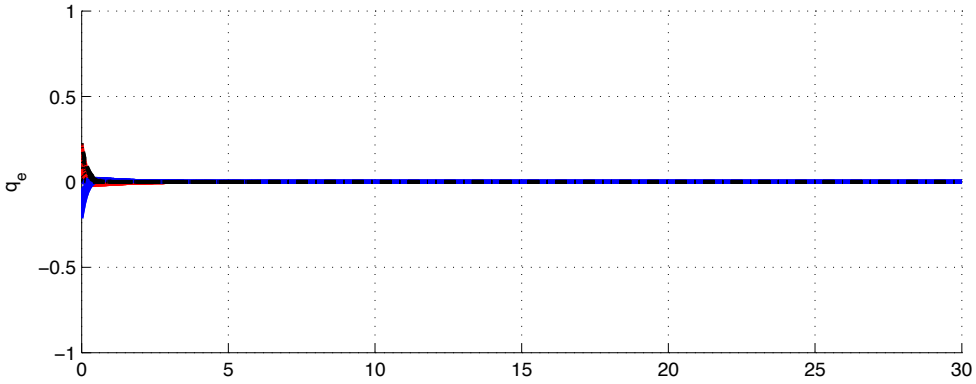

Figure 4.6: Attitude tracking errors.

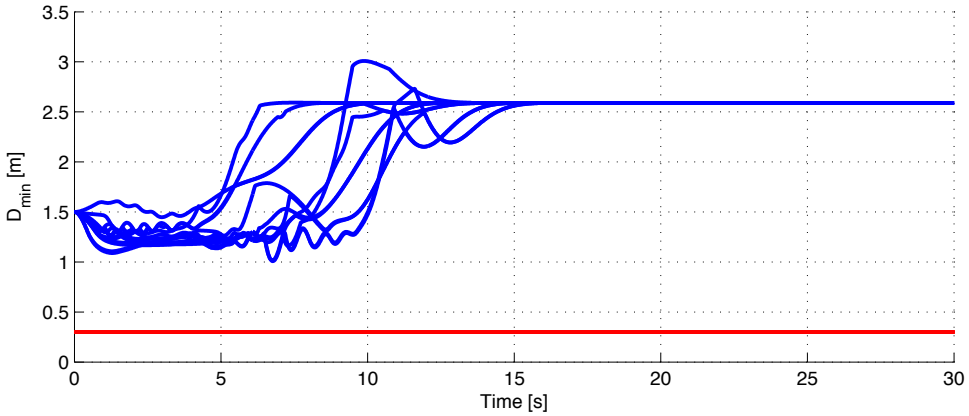

Figure 4.7: The minimum distance among quadrotors.

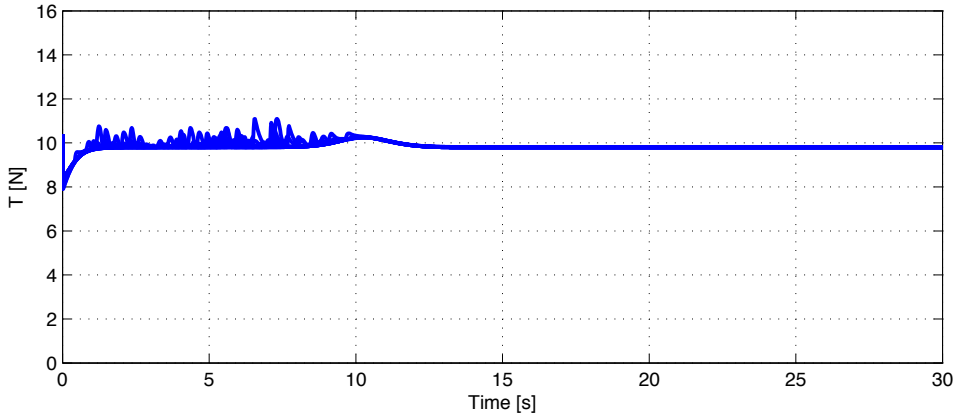

Figure 4.8: Force of 12 quadrotors.

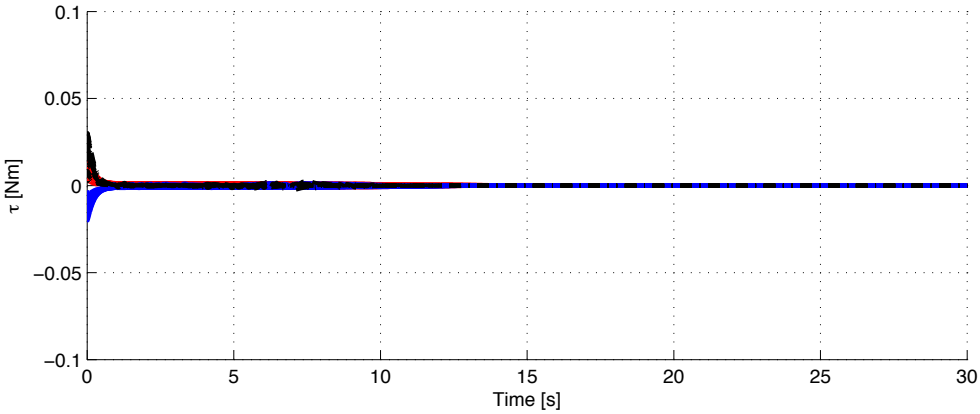

Figure 4.9: Torque of 12 quadrotors.

Case 2: All the quadrotors in the formation is distributed in a circle shape while tracking a predefined helix path.

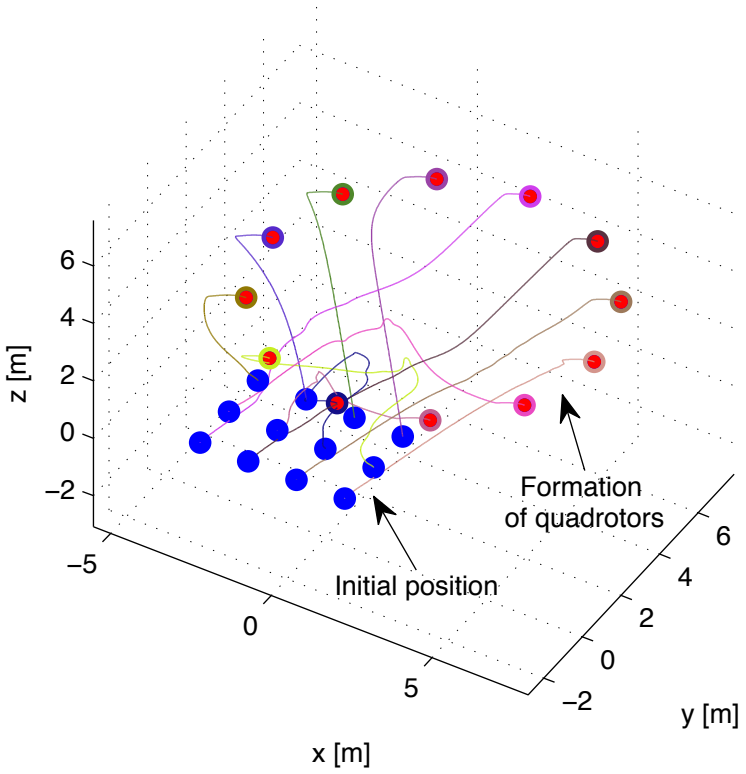

Figure 4.10: The formation of 12 quadrotors.

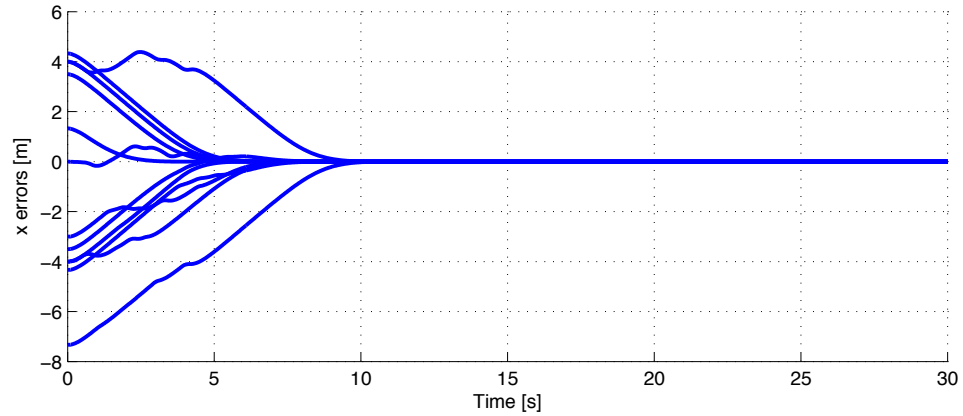

Figure 4.11: x tracking errors.

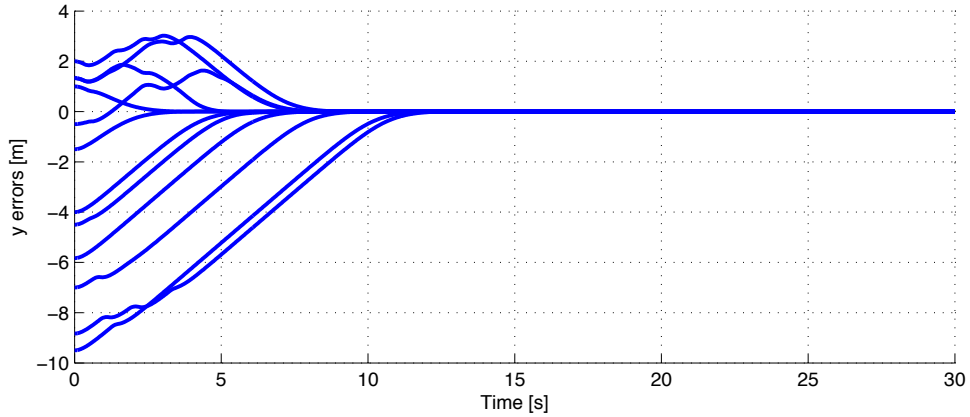

Figure 4.12: y tracking errors.

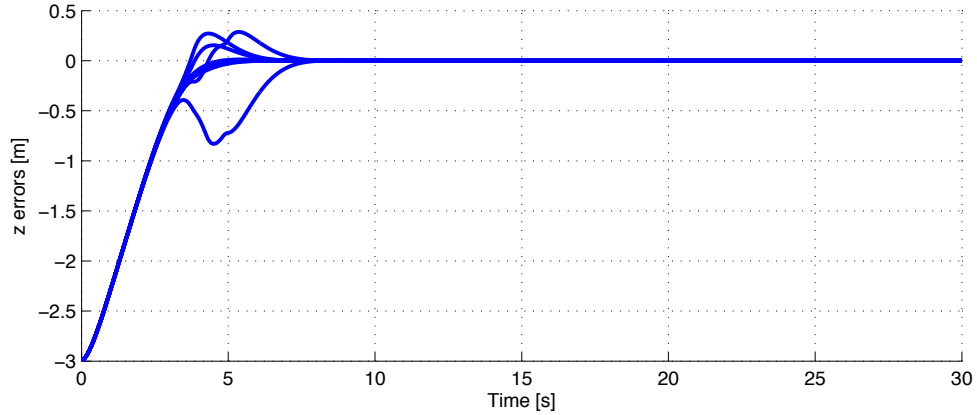

Figure 4.13: z tracking errors.

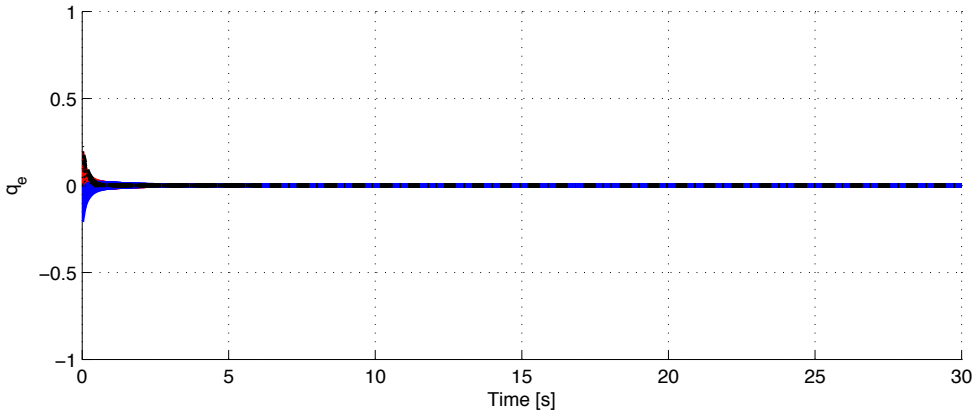

Figure 4.14: Attitude tracking errors.

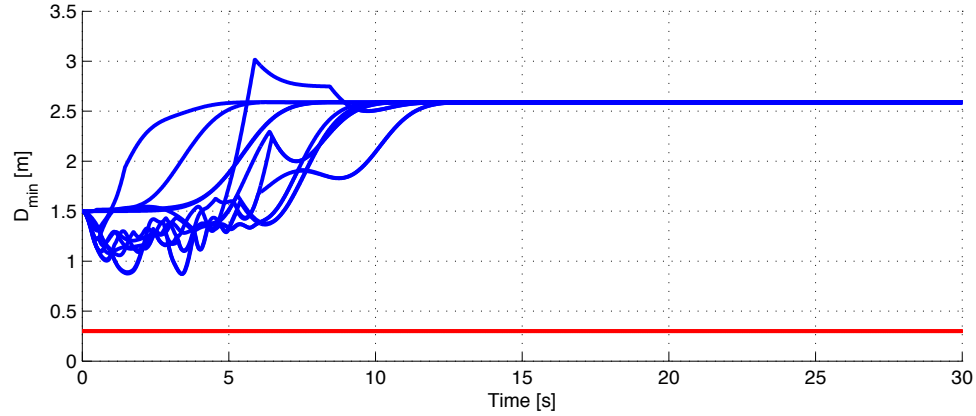

Figure 4.15: The minimum distance among quadrotors.

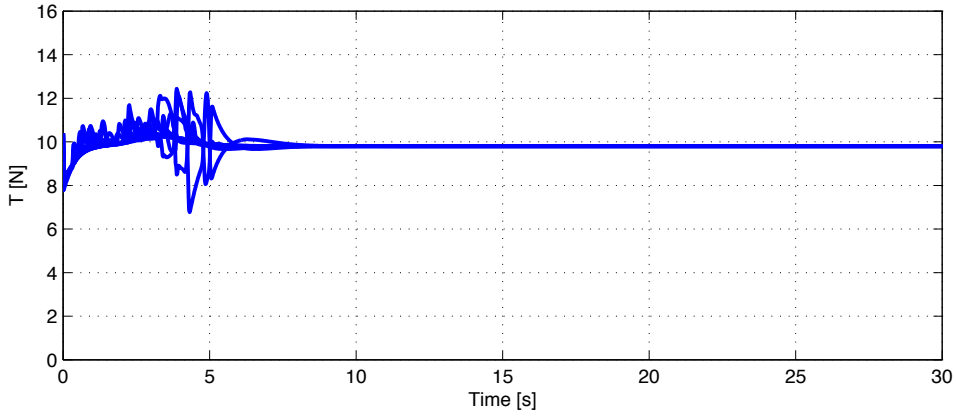

Figure 4.16: Force of 12 quadrotors.

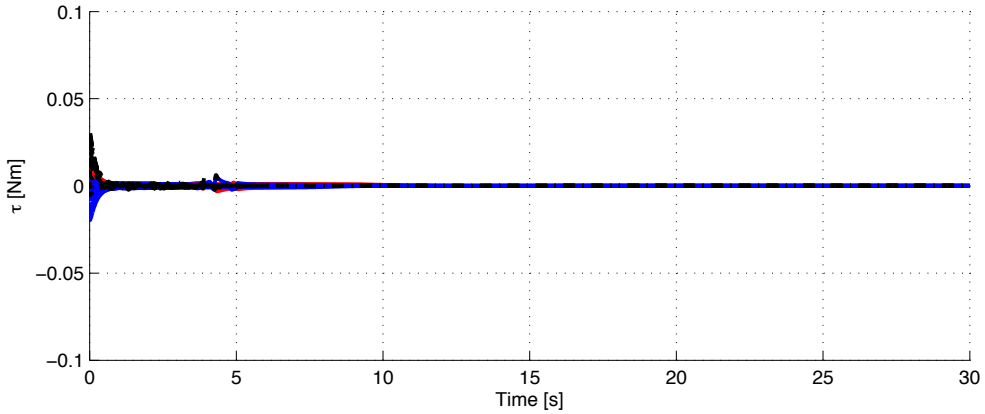

Figure 4.17: Torque of 12 quadrotors.

4.2.4 Conclusion

A distributed formation controllers for a group of underactuated quadrotors in three dimensional space has been presented. The controllers guaranteed no collision among any quadrotors and satisfied all properties of the formation control objective. The design procedure is based on the attitude extraction algorithm for the desired orientation which is satisfied to be singularity-free under the input control conditions. The simulation results illustrated the effectiveness of the proposed controllers.

4.3 Controller 2 - linear velocity and disturbance observer

In this section the controller is developed and solved by focusing on the formation problem with assuming that the dynamics of quadrotor has disturbances from environment and the linear velocity is not measured. After the control objective is proposed, the observers for linear velocity and disturbance are designed. The control design is illustrated in Section 4.3.3.

4.3.1 Control objective

The dynamics of quadrotor is written as in (4.38)

$$\begin{aligned}
\dot{\boldsymbol{p}}_i &= \boldsymbol{v}_i \\
\dot{\boldsymbol{v}}_i &= g\boldsymbol{e}_3 - \tfrac{T_i}{m_i}\boldsymbol{R}_Q^T(\boldsymbol{Q}_i)\boldsymbol{e}_3 + \boldsymbol{d}_{vi} \\
\dot{\boldsymbol{Q}}_i &= \boldsymbol{K}_Q(\boldsymbol{Q}_i)\boldsymbol{\omega}_i \\
\boldsymbol{J}_i\dot{\boldsymbol{\omega}}_i &= \boldsymbol{\tau}_i - \boldsymbol{S}(\boldsymbol{\omega}_i)\boldsymbol{J}_i\boldsymbol{\omega}_i + \boldsymbol{d}_{\omega i}
\end{aligned} \tag{4.38}$$

where $i \in \mathbb{N}$, $\mathbb{N}$ is the set of all quadrotors in the group. $\boldsymbol{d}_v$ and $\boldsymbol{d}_\omega$ are unknown disturbances. All the other symbols are defined in the Section 2.1.

Before starting the formation control objective we impose the following assumption on the reference trajectories, communication and initial conditions between the quadrotor in the group.

Assumption 4.3.

1. *The reference position trajectory $\boldsymbol{p}_{di}(t) = [x_{di}(t)\, y_{di}(t)\, z_{di}(t)]^T$ and the heading angle ψ_{di} for the quadrotor i to track satisfies the following conditions:*

$$\begin{aligned} &\|p_{dij}\| \geq \varepsilon_{ij}, \\ &\left\|\boldsymbol{p}_{di}^{(k)}\right\| \leq \varepsilon_{kd}, \\ &\left\|\psi_{di}^{(k)}\right\| \leq \delta_{kd}, \end{aligned} \tag{4.39}$$

   for all $(i,j) \in \mathbb{N}, i \neq j$ where $p_{dij} = p_{di} - p_{dj}$, ε_{ij} is a strictly positive constant. ε_{kd}, $k = 1, \ldots, 4$, are nonnegative constants.

2. *The quadrotor i and j can communicate with each other and exchange their states, if satisfy the following condition:*

$$\alpha_{ij} \leq \alpha_{ij}^R \tag{4.40}$$

   where α_{ij}^R is a strictly positive constant.

3. *Let us define*

$$\begin{aligned} \hat{\boldsymbol{p}}_{ij} &= \hat{\boldsymbol{p}}_i - \hat{\boldsymbol{p}}_j \\ \boldsymbol{\alpha}_{ij} &= \tfrac{1}{2}\hat{\boldsymbol{p}}_{ij}^T \hat{\boldsymbol{p}}_{ij} \end{aligned} \tag{4.41}$$

   Each quadrotor starts at a different location and do not have any collision among them. Specially, there exist strictly positive constants ε_{ij} and α_{ij}^S such that for all $(i,j) \in \mathbb{N}, i \neq j$, the following conditions hold:

$$\begin{aligned} &\|p_{ij}(t_0)\| \geq \varepsilon_{ij}, \\ &\alpha_{ij}(t_0) \geq \alpha_{ij}^S \end{aligned} \tag{4.42}$$

Remark 4.4. *In the Assumption 4.3, property (1) specifies possible reference trajectory $\boldsymbol{p}_{di}$ for the quadrotor i in the group to track since it has to satisfy the condition* (4.39)*, property (2) implies that we need to design a distributed formation control system since the condition* (4.40) *indicates that when $\alpha_{ij} \geq \alpha_{ij}^R$ the quadrotor i and j do not communicate with each other, and property (3) implies that the designed controllers for the formation guarantee collision avoidance among the quadrotors.*

Control Objective 4.2. *Under the Assumption 4.3, for each quadrotor i design the control inputs T_i and $\boldsymbol{\tau}_i$ such that the position vector $\boldsymbol{p}_i(t)$ of the quadrotor i track their reference trajectories $\boldsymbol{p}_{di}(t)$ under the effect of environment disturbance while avoid collision with all other quadrotor.*

Specifically, we design the control inputs T_i and $\boldsymbol{\tau}_i$ such that

$$\begin{aligned} &\lim_{t\to\infty}(\boldsymbol{p}_i(t)-\boldsymbol{p}_{di}(t))=0,\\ &\lim_{t\to\infty}(\psi_i(t)-\psi_{di}(t))=0\\ &\|\boldsymbol{p}_i-\boldsymbol{p}_j\|\geq\alpha_{ij}^S \end{aligned} \tag{4.43}$$

For all $(i,j)\in\mathbb{N}, i\neq j$ and $t\geq t_0\geq 0$, the control design needs to keep all other states of the quadrotor dynamics bounded for all initial conditions.

4.3.2 Observer design

With the assumption that the linear velocity and environment disturbance are unmeasured. Before designing control for a formation of quadrotor, we first design observers to estimate the linear velocity and environment disturbance then we use these estimated values to design the formation controller later.

4.3.2.1 Linear Velocity Observer

Consider the first subsystem

$$\begin{aligned} \dot{\boldsymbol{p}}_i&=\boldsymbol{v}_i\\ \dot{\boldsymbol{v}}_i&=g\boldsymbol{e}_3-\tfrac{T_i}{m_i}\boldsymbol{R}_Q^T(\boldsymbol{Q}_i)\boldsymbol{e}_3+\boldsymbol{d}_{vi} \end{aligned} \tag{4.44}$$

The following observer:

$$\begin{aligned} \dot{\hat{\boldsymbol{p}}}_i&=\hat{\boldsymbol{v}}_2\\ \hat{\boldsymbol{v}}_i&=\boldsymbol{\xi}_i+k_2(\boldsymbol{p}_i-\hat{\boldsymbol{p}}_i)\\ \dot{\boldsymbol{\xi}}_i&=g\boldsymbol{e}_3-\tfrac{T_i}{m_i}\boldsymbol{R}_Q^T(\boldsymbol{Q}_i)\boldsymbol{e}_3+\boldsymbol{d}_{vi}+k_1(\boldsymbol{p}_i-\hat{\boldsymbol{p}}_i) \end{aligned} \tag{4.45}$$

guarantees that the observer errors $\tilde{\boldsymbol{p}}_i$ and $\tilde{\boldsymbol{v}}_i$ of (4.45) semi-globally converges to the origin. where $\hat{\boldsymbol{p}}_i$ and $\hat{\boldsymbol{v}}_i$ denote estimates of $\boldsymbol{p}_i$ and $\boldsymbol{v}_i$, respectively, k_1 and k_2 are positive constants.

Proof. *We define the following observer errors:*

$$\begin{aligned} \tilde{\boldsymbol{p}}_i&=\boldsymbol{p}_i-\hat{\boldsymbol{p}}_i\\ \tilde{\boldsymbol{v}}_i&=\boldsymbol{v}_i-\hat{\boldsymbol{v}}_i \end{aligned} \tag{4.46}$$

Differentiating both sides of (4.46) *along the solutions of* (4.44) *and* (4.45) *yields*

$$\begin{aligned} \dot{\tilde{\boldsymbol{p}}}_i&=\tilde{\boldsymbol{v}}_i\\ \dot{\tilde{\boldsymbol{v}}}_i&=-k_1\tilde{\boldsymbol{p}}_i-k_2\tilde{\boldsymbol{v}}_i \end{aligned} \tag{4.47}$$

Consider the following Lyapunov function

$$V_{ov} = \tfrac{1}{2}\tilde{\boldsymbol{p}}_i^T\tilde{\boldsymbol{p}}_i + \tfrac{1}{2}\tilde{\boldsymbol{v}}_i^T\tilde{\boldsymbol{v}}_i \tag{4.48}$$

Differentiating both sides of (4.48) *yields*

$$\dot{V}_{ov} = \tilde{\boldsymbol{p}}_i^T\tilde{\boldsymbol{v}}_i + \tilde{\boldsymbol{v}}_i^T(-k_1\tilde{\boldsymbol{p}}_i - k_2\tilde{\boldsymbol{v}}_i) \tag{4.49}$$

If $k_1 = 1$ *then* (4.49) *can be rewritten as*

$$\dot{V}_{ov} = -k_2\tilde{\boldsymbol{v}}_i^T\tilde{\boldsymbol{v}}_i \leq 0 \tag{4.50}$$

By using LaSalle's invariance principle, It can be seen that the observer errors of (4.47)*asymptotically stable at the origin.*

4.3.2.2 Disturbance Observer

We rewrite the dynamics system (4.38) in the following form

$$\begin{aligned}\dot{\boldsymbol{x}}_{1i} &= \boldsymbol{F}_{1i}(\boldsymbol{x}_{1i}, \boldsymbol{x}_{2i}) \\ \dot{\boldsymbol{x}}_{2i} &= \boldsymbol{F}_{2i}(\boldsymbol{x}_{1i}, \boldsymbol{x}_{2i}, \boldsymbol{u}_i) + \boldsymbol{G}_{2i}(x_{1i})\boldsymbol{d}_i\end{aligned} \tag{4.51}$$

where $\boldsymbol{x}_{1i} = [\boldsymbol{p}_i \quad \boldsymbol{Q}_i]^T$, $\boldsymbol{x}_{2i} = [\boldsymbol{v}_i \quad \boldsymbol{\omega}_i]^T$, $\boldsymbol{F}_{1i}(\boldsymbol{x}_{1i}, \boldsymbol{x}_{2i}) = [\boldsymbol{v}_i \quad \boldsymbol{K}_Q(\boldsymbol{Q}_i)\boldsymbol{\omega}_i]^T$; $\boldsymbol{F}_{2i}(\boldsymbol{x}_{1i}, \boldsymbol{x}_{2i}, u_i) = [g\boldsymbol{e}_3 - \frac{T_i}{m_i}\boldsymbol{R}_Q^T(\boldsymbol{Q}_i)\boldsymbol{e}_3 \quad \boldsymbol{J}_i^{-1}(\boldsymbol{\tau}_i - \boldsymbol{S}(\boldsymbol{\omega}_i)\boldsymbol{J}_i\boldsymbol{\omega}_i)]^T$; $\boldsymbol{G}_{2i}(\boldsymbol{x}_{1i}) = [1 \quad 0; 0 \quad 1]$ is an invertible matrix; $\boldsymbol{d}_i = [\boldsymbol{d}_{vi} \quad \boldsymbol{d}_{\omega i}]$ is a vector of unknown disturbance. We assume that there exists a nonnegative constant C_d such that $\dot{\boldsymbol{d}}_i \leq C_d$. Now we want to design a disturbance observer, $\hat{\boldsymbol{d}}_i$, that estimates $\boldsymbol{d}_i$ sufficiently accurately.
The disturbance observer is given in the following lemma.

Lemma 4.1.

$$\begin{aligned}\hat{\boldsymbol{d}}_i &= \boldsymbol{z}_i + \boldsymbol{K}_{0i}\boldsymbol{G}_{2i}^{-1}(\boldsymbol{x}_{1i})\boldsymbol{x}_{2i} \\ \dot{\boldsymbol{z}}_i &= -\boldsymbol{K}_{0i}\boldsymbol{z}_i - \boldsymbol{K}_{0i}[\dot{\boldsymbol{G}}_{2i}^{-1}(\boldsymbol{x}_{1i})\boldsymbol{x}_{2i} + \boldsymbol{G}_{2i}^{-1}(\boldsymbol{x}_{1i})\boldsymbol{F}_{2i}(\boldsymbol{x}_{1i}, \boldsymbol{x}_{2i}, \boldsymbol{u}_i) + \boldsymbol{K}_{0i}\boldsymbol{G}_{2i}^{-1}(\boldsymbol{x}_{1i})\boldsymbol{x}_{2i}]\end{aligned} \tag{4.52}$$

where $\boldsymbol{K}_{0i}$ *is a positive definite symmetric matrix. The disturbance observer* (4.52) *guarantees that the disturbance observer error* $\tilde{\boldsymbol{d}}_i(t) = \boldsymbol{d}_i(t) - \hat{\boldsymbol{d}}_i(t)$ *exponentially converges to a ball centered at the origin. The radius of this ball can be made arbitrarily small by adjusting the matrix* $\boldsymbol{K}_{0i}$*. In the case where the disturbance vector* $\boldsymbol{d}_i(t)$ *is constant, the disturbance observer error* $\tilde{\boldsymbol{d}}_i(t)$ *exponentially converges to zero.*

Proof. *See Appendix A.2*

4.3.3 Formation control design

The dynamics system (4.38) is rewritten as follows

$$\begin{aligned}
\dot{\hat{\boldsymbol{p}}}_i &= \hat{\boldsymbol{v}}_i \\
\dot{\hat{\boldsymbol{v}}}_i &= g\boldsymbol{e}_3 - \tfrac{T_i}{m_i}\boldsymbol{R}_Q^T(\boldsymbol{Q}_i)\boldsymbol{e}_3 + \hat{\boldsymbol{d}}_{vi} + \tilde{\boldsymbol{d}}_{vi} + k_2\tilde{\boldsymbol{v}}_i + k_1\tilde{\boldsymbol{p}}_i \\
\dot{\boldsymbol{Q}}_i &= \boldsymbol{K}_Q(\boldsymbol{Q}_i)\boldsymbol{\omega}_i \\
\boldsymbol{J}_i\dot{\boldsymbol{\omega}}_i &= \boldsymbol{\tau}_i - \boldsymbol{S}(\boldsymbol{\omega}_i)\boldsymbol{J}_i\boldsymbol{\omega}_i + \hat{\boldsymbol{d}}_{\omega i} + \tilde{\boldsymbol{d}}_{\omega i}
\end{aligned} \tag{4.53}$$

Similarly in the previous section, the quadrotor dynamics i (4.53) is separated into two subsystems. The first subsystem contains two first equations for translational dynamics and the second subsystem consists two last equations for rotational dynamics. For convenience, the control design process is re-illustrated. In the first step, the intermediate control input for the translational dynamics tracking the predefined path is designed. After this step, the new extraction algorithm using some conversions between Euler angles and unit-quaternion to reject the self-rotation of quadrotor around its vertical axis to generate a total force T_i and a unit-quaternion reference Q_{di} which can be employed as the reference for the second subsystem is applied. In the next step, the torque $\boldsymbol{\tau}_i$ to force $\boldsymbol{Q}_i \to \boldsymbol{Q}_{di}$ is designed.

Step 1

In this step, the translational dynamics of (4.53) is considered. We will design a virtual control of $\boldsymbol{v}_i$ to force $\boldsymbol{p}_i(t)$ to globally asymptotically track its reference trajectory $\boldsymbol{p}_{di}(t)$. As such, we define the tracking errors as follows:

$$\begin{aligned}
\boldsymbol{p}_{ei} &= \hat{\boldsymbol{p}}_i - \boldsymbol{p}_{di}, \\
\boldsymbol{v}_{ei} &= \hat{\boldsymbol{v}}_i - \boldsymbol{\alpha}_{vi},
\end{aligned} \tag{4.54}$$

where $\boldsymbol{\alpha}_{vi}$ is a virtual control of $\hat{\boldsymbol{v}}_i$. differentiating both sides of (4.54) and using the first subsystem, the error dynamics are expressed as

$$\begin{aligned}
\dot{\boldsymbol{p}}_{ei} &= \boldsymbol{v}_{ei} + \boldsymbol{\alpha}_{vi} - \dot{\boldsymbol{p}}_{di}, \\
\dot{\boldsymbol{v}}_{ei} &= g\boldsymbol{e}_3 - \boldsymbol{F} + \hat{\boldsymbol{d}}_{vi} + \tilde{\boldsymbol{d}}_{vi} + k_2\tilde{\boldsymbol{v}}_i + k_1\tilde{\boldsymbol{p}}_i - \dot{\boldsymbol{\alpha}}_{vi}
\end{aligned} \tag{4.55}$$

where $\boldsymbol{F}_i$ is an intermediate control input and $\boldsymbol{F}_i = \frac{T_i}{m_i}\boldsymbol{R}_Q^T(\boldsymbol{Q}_{di})\boldsymbol{e}_3$ is illustrated in the ideal case where $\boldsymbol{Q}_{di}$ is obtained via Lemma 2.3.

In order to design the intermediate control input $\boldsymbol{F}_i$ for quadrotor i that achieves the Formation control objective 4.2, we consider the following potential function:

$$V_1 = \frac{1}{2}\sum_{i=1}^{N}\left[\boldsymbol{p}_{ei}{}^T\boldsymbol{p}_{ei} + \sum_{J\in\mathbb{N}_i}\beta_{ij}\right] \tag{4.56}$$

where $\mathbb{N}_i$ is the set containing all the quadrotors except for the quadrotor i, β_{ij} is taken from (4.3) where α_{ij} is calculated from (4.41).

Differentiating both sides of (4.56) gives

$$\begin{aligned} \dot{V}_1 &= \sum_{i=1}^{N} \left[\boldsymbol{p}_{ei}{}^T \dot{\boldsymbol{p}}_{ei} + \sum_{j \in \mathbb{N}_i} \beta'_{\text{ij}} \dot{\alpha}_{\text{ij}} \right] \\ &= \sum_{i=1}^{N} \left[\boldsymbol{p}_{ei}{}^T \dot{\boldsymbol{p}}_{ei} + \sum_{j \in \mathbb{N}_i} \beta'_{ij} \hat{\boldsymbol{p}}_{ij}^T \dot{\hat{\boldsymbol{p}}}_{ij} \right] \end{aligned} \tag{4.57}$$

Noting that $\dot{\hat{\boldsymbol{p}}}_{ij} = (\dot{\hat{\boldsymbol{p}}}_i - \dot{\boldsymbol{p}}_{di}) - (\dot{\hat{\boldsymbol{p}}}_j - \dot{\boldsymbol{p}}_{dj}) = \boldsymbol{v}_{ei} - \boldsymbol{v}_{ej}$, we can write (4.57) as follows

$$\begin{aligned} \dot{V}_1 &= \sum_{i=1}^{N} (\boldsymbol{p}_{ei}{}^T + \sum_{j \in \mathbb{N}_i} \beta'_{ij} \hat{\boldsymbol{p}}_{ij}^T)(\boldsymbol{v}_{ei} + \boldsymbol{\alpha}_{vi} - \dot{\boldsymbol{p}}_{di}) \\ &= \sum_{i=1}^{N} \boldsymbol{\Omega}_i{}^T (\boldsymbol{v}_{ei} + \boldsymbol{\alpha}_{vi} - \dot{\boldsymbol{p}}_{di}) \end{aligned} \tag{4.58}$$

where

$$\boldsymbol{\Omega}_i = \boldsymbol{p}_{ei} + \sum_{j \in \mathbb{N}_i} \beta'_{ij} \hat{\boldsymbol{p}}_{ij} \tag{4.59}$$

The equation (4.58) suggests that we choose

$$\boldsymbol{\alpha}_{vi} = -k_1 \boldsymbol{\Omega}_i + \dot{\boldsymbol{p}}_{di} \tag{4.60}$$

To design the intermediate control input $\boldsymbol{F}_i$, considering the following Lyapunov function

$$V_2 = V_1 + \frac{1}{2} \sum_{i=1}^{N} \boldsymbol{v}_{ei}{}^T \boldsymbol{v}_{ei} \tag{4.61}$$

Differentiating both sides of (4.61) gives

$$\begin{aligned} \dot{V}_2 &= \sum_{i=1}^{N} \left[-k_1 \boldsymbol{\Omega}_i{}^T \boldsymbol{\Omega}_i + \boldsymbol{v}_{ei}{}^T (g e_3 - \boldsymbol{F}_i - \dot{\boldsymbol{\alpha}}_{vi} + \boldsymbol{\Omega}_i + \hat{\boldsymbol{d}}_{vi} + \tilde{\boldsymbol{d}}_{vi} + k_2 \tilde{\boldsymbol{v}}_i + k_1 \tilde{\boldsymbol{p}}_i) \right] \\ &= \sum_{i=1}^{N} \left[-k_1 \boldsymbol{\Omega}_i{}^T \boldsymbol{\Omega}_i + \boldsymbol{v}_{ei}{}^T (g e_3 - \boldsymbol{F}_i - \dot{\boldsymbol{\alpha}}_{vi} + \boldsymbol{\Omega}_i + \hat{\boldsymbol{d}}_{vi}) + \boldsymbol{v}_{ei}{}^T (\tilde{\boldsymbol{d}}_{vi} + k_2 \tilde{\boldsymbol{v}}_i + k_1 \tilde{\boldsymbol{p}}_i) \right] \end{aligned} \tag{4.62}$$

which suggests that we choose:

$$\boldsymbol{F}_i = k_2 \boldsymbol{v_{ei}} + g e_3 - \dot{\boldsymbol{\alpha}}_{vi} + \boldsymbol{\Omega}_i + \hat{\boldsymbol{d}}_{vi} \tag{4.63}$$

We assume that the control input $\boldsymbol{F}_i$ forces the quadrotor i tracking the predefined path and heading angle ψ_{di} in ideal case. Applying Lemma 2.3 for the intermediate control input (4.63), we obtain the thrust T_i and the reference unit-quaternion vector $\boldsymbol{Q}_{di}$ as follows:

$$T_i = \|\boldsymbol{F}_i\|$$

$$\boldsymbol{Q}_{di} = \begin{bmatrix} C\frac{\alpha_{\phi i}}{2}C\frac{\alpha_{\theta i}}{2}C\frac{\alpha_{\psi i}}{2} + S\frac{\alpha_{\phi i}}{2}S\frac{\alpha_{\theta i}}{2}S\frac{\alpha_{\psi i}}{2} \\ S\frac{\alpha_{\phi i}}{2}C\frac{\alpha_{\theta i}}{2}C\frac{\alpha_{\psi i}}{2} - C\frac{\alpha_{\phi i}}{2}S\frac{\alpha_{\theta i}}{2}S\frac{\alpha_{\psi i}}{2} \\ C\frac{\alpha_{\phi i}}{2}S\frac{\alpha_{\theta i}}{2}C\frac{\alpha_{\psi i}}{2} + S\frac{\alpha_{\phi i}}{2}C\frac{\alpha_{\theta i}}{2}S\frac{\alpha_{\psi i}}{2} \\ C\frac{\alpha_{\phi i}}{2}C\frac{\alpha_{\theta i}}{2}S\frac{\alpha_{\psi i}}{2} - S\frac{\alpha_{\phi i}}{2}S\frac{\alpha_{\theta i}}{2}C\frac{\alpha_{\psi i}}{2} \end{bmatrix} \tag{4.64}$$

where

$$\begin{aligned} \alpha_{\psi i} &= \psi_{di}, \\ \alpha_{\theta i} &= \arctan\left(\frac{C\alpha_{\psi i}F_{i1} + S\alpha_{\psi i}F_{i2}}{F_{i3}}\right), \\ \alpha_{\phi i} &= \arcsin\left(\frac{S\alpha_{\psi i}F_{i1} - C\alpha_{\psi i}F_{i2}}{T_i}\right), \end{aligned} \tag{4.65}$$

The reference angular velocity of quadrotor i is calculated as follows

$$\boldsymbol{\omega}_{di} = \begin{bmatrix} 1 & 0 & -S\alpha_{\theta i} \\ 0 & C\alpha_{\phi i} & S\alpha_{\phi i}C\alpha_{\theta i} \\ 0 & -S\alpha_{\phi i} & C\alpha_{\phi i}C\alpha_{\theta i} \end{bmatrix} \begin{bmatrix} \dot{\alpha}_{\phi i} \\ \dot{\alpha}_{\theta i} \\ \dot{\alpha}_{\psi i} \end{bmatrix} \tag{4.66}$$

where $\boldsymbol{\omega}_{di}$ is the body reference angular velocity; $S(\cdot)$ and $C(\cdot)$ stand for $\sin(\cdot)$, $\cos(\cdot)$, respectively.

Step 2

In this step, the torque input, $\boldsymbol{\tau}_i$, will be designed. The unit-quaternion vector $\boldsymbol{Q}_{di}$ is used as the reference. We first define the following tracking errors

$$\begin{aligned} \boldsymbol{Q}_{ei} &= \boldsymbol{Q}_{di}^{-1} \odot \boldsymbol{Q}_i, \\ \boldsymbol{\omega}_{ei} &= \boldsymbol{\omega}_i - \boldsymbol{\alpha}_{\omega i} \end{aligned} \tag{4.67}$$

where $\boldsymbol{\alpha}_{\omega i}$ is a virtual control of ω_i. $\boldsymbol{Q}_{ei} = [\eta_{ei}\, \boldsymbol{q}_{ei}^T]^T$ and $\boldsymbol{\omega}_{ei}$ are attitude tracking and angular velocity error vector, respectively.

Differentiating both sides of (4.67) yields

$$\begin{aligned} \dot{\boldsymbol{q}}_{ei} &= \boldsymbol{G}_i(\boldsymbol{\omega}_{ei} + \boldsymbol{\alpha}_{\omega i} - \boldsymbol{\omega}_{di}) \\ \dot{\boldsymbol{\omega}}_{ei} &= \boldsymbol{J}_i^{-1}\left(\boldsymbol{\tau}_i - \boldsymbol{S}(\boldsymbol{\omega}_i)\boldsymbol{J}_i\boldsymbol{\omega}_i + \hat{\boldsymbol{d}}_{\omega i} + \tilde{\boldsymbol{d}}_{\omega i}\right) - \dot{\boldsymbol{\alpha}}_{\omega i} \end{aligned} \tag{4.68}$$

where $\boldsymbol{G}_i = \frac{1}{2}\left(\eta_{ei}\boldsymbol{I}_{3\times 3} + \boldsymbol{S}(\boldsymbol{q}_{ei})\right)$ and $\boldsymbol{\omega}_{di}$ can be obtained by using equation (4.66).

To obtain the control input $\boldsymbol{\tau}_i$, we consider the following Lyapunov function:

$$V_3 = \sum_{i=1}^{N} \frac{1}{2}\boldsymbol{q}_{ei}^T\boldsymbol{q}_{ei} \tag{4.69}$$

The time derivative of V_3 along solutions (4.68) is given by

$$\dot{V}_3 = \sum_{i=1}^{N} \boldsymbol{q}_{ei}^T \boldsymbol{G}_i(\boldsymbol{\omega}_{ei} + \boldsymbol{\alpha}_{\omega i} - \boldsymbol{\omega}_{di}) \tag{4.70}$$

which suggests that we choose

$$\boldsymbol{\alpha}_{\omega i} = -k_3 \boldsymbol{G}_i^T \boldsymbol{q}_{ei} + \boldsymbol{\omega}_{di} \tag{4.71}$$

To design the control input torque, $\boldsymbol{\tau}_i$, considering the following Lyapunov candidate

$$V_4 = V_3 + \sum_{i=1}^{N} \boldsymbol{\omega}_{ei}^T \boldsymbol{\omega}_{ei} \tag{4.72}$$

The time derivative of (4.72) is given

$$\begin{aligned} \dot{V}_4 &= \sum_{i=1}^{N} \left[-k_3 \boldsymbol{q}_{ei}^T \boldsymbol{G}_i \boldsymbol{G}_i^T \boldsymbol{q}_{ei} \right] \\ &+ \sum_{i=1}^{N} \left[\boldsymbol{\omega}_{ei}^T \left(\boldsymbol{J}_i^{-1} \left(\boldsymbol{\tau}_i - \boldsymbol{S}(\boldsymbol{\omega}_i) \boldsymbol{J}_i \boldsymbol{\omega}_i + \hat{\boldsymbol{d}}_{\omega i} + \tilde{\boldsymbol{d}}_{\omega i} \right) - \dot{\boldsymbol{\alpha}}_{\omega i} + \boldsymbol{G}_i \boldsymbol{q}_{ei} \right) \right] \\ &= \sum_{i=1}^{N} \left[-k_3 \boldsymbol{q}_{ei}^T \boldsymbol{G}_i \boldsymbol{G}_i^T \boldsymbol{q}_{ei} \right] \\ &+ \sum_{i=1}^{N} \left[\boldsymbol{\omega}_{ei}^T \left(\boldsymbol{J}_i^{-1} \left(\boldsymbol{\tau}_i - \boldsymbol{S}(\boldsymbol{\omega}_i) \boldsymbol{J}_i \boldsymbol{\omega}_i + \hat{\boldsymbol{d}}_{\omega i} \right) - \dot{\boldsymbol{\alpha}}_{\omega i} + \boldsymbol{G}_i \boldsymbol{q}_{ei} \right) + \boldsymbol{\omega}_{ei}^T \boldsymbol{J}_i^{-1} \tilde{\boldsymbol{d}}_{\omega i} \right] \end{aligned} \tag{4.73}$$

which suggests that we choose the control input torque as follows

$$\boldsymbol{\tau}_i = \boldsymbol{J}_i(-k_4 \boldsymbol{\omega}_{ei} + \dot{\boldsymbol{\alpha}}_{\omega i} - \boldsymbol{G}_i \boldsymbol{q}_{ei}) + \boldsymbol{S}(\boldsymbol{\omega}_i) \boldsymbol{J}_i \boldsymbol{\omega}_i - \hat{\boldsymbol{d}}_{\omega i} \tag{4.74}$$

Substituting control and virtual control from (4.60), (4.63), (4.71) and (4.74) into (4.55), and (4.68), we have the following closed loop system:

$$\begin{aligned} \dot{\boldsymbol{p}}_{ei} &= \boldsymbol{v}_{ei} - k_1 \boldsymbol{\Omega}_i \\ \dot{\boldsymbol{v}}_{ei} &= -k_2 \boldsymbol{v}_{ei} - \boldsymbol{\Omega_i} + \tilde{\boldsymbol{d}}_{vi} + k_2 \tilde{\boldsymbol{v}}_i + k_1 \tilde{\boldsymbol{p}}_i \\ \dot{\boldsymbol{q}}_{ei} &= \boldsymbol{G}_i(-k_3 \boldsymbol{G}_i^T \boldsymbol{q}_{ei} + \boldsymbol{\omega}_{ei}) \\ \dot{\boldsymbol{\omega}}_{ei} &= -k_4 \boldsymbol{\omega}_{ei} - \boldsymbol{G}_i \boldsymbol{q}_{ei} + \boldsymbol{J}_i^{-1} \tilde{\boldsymbol{d}}_{\omega i} \end{aligned} \tag{4.75}$$

The control design has been completed. We summarize the results in the following theorem.

Theorem 4.2. *Under Assumption 4.3, the formation control laws consisting of* (4.63) *and* (4.74) *for the quadrotor i achieve the Formation Control Objective 4.2, there is no collision between all the quadrotors, the position $\boldsymbol{p}_i$ and heading angle ψ_i of quadrotor i globally asymptotically track their*

reference trajectories $\boldsymbol{p}_{di}$ *and* ψ_{di}*,*

$$\begin{aligned}
&\lim_{t\to\infty}(\boldsymbol{p}_i(t)-\boldsymbol{p}_{di}(t))=0,\\
&\lim_{t\to\infty}(\psi_i(t)-\psi_{di}(t))=0\\
&\|\boldsymbol{p}_i-\boldsymbol{p}_j\|\geq\alpha_{ij}^S
\end{aligned} \tag{4.76}$$

and the closed loop system (4.75) *is forward complete.*

Proof. *See Appendix B.4.*

4.3.4 Simulation results

In this section, we illustrate the effectiveness of the proposed formation control design through a numerical simulation on a group of $N=9$ identical quadrotors. The quadrotor parameters for the simulation are taken from [EInE12] as following: m_i=0.35 kg, g = 9.81 $kg\,m^2$, $l_i=0.15m$, $I_{X_i}=15.67\times10^{-3}\,kg\,m^2$, $I_{Y_i}=15.67\times10^{-3}\,kg\,m^2$; $I_{Z_i}=28.34\times10^{-3}\,kg\,m^2$, $K_{ti}=192.32\times10^{-7}Ns^2$, $K_{di}=4.003\times10^{-7}Nms^2$.
The initial conditions are taken as

$$\begin{aligned}
&\boldsymbol{p}_i(0)=[R_1*j\quad R_1*k\quad 0]^T;\boldsymbol{v}_i(0)=[0\,0\,0]^T\\
&\boldsymbol{Q}_i(0)=[1\,0\,0\,0]^T;\boldsymbol{\omega}_i(0)=[0\,0\,0]^T
\end{aligned} \tag{4.77}$$

where $R_1=1.5m$, j and k combine such that at the first time, all quadrotors are distributed on land in a rectangle form with 3 rows and 3 columns. The initial distance between quadrotors are satisfied (4.42).
For the path-tracking, the reference trajectories are chosen as

$$\begin{aligned}
&\boldsymbol{L}_{di}=[R_f sin((i-1)2pi/N)\ R_0 cos((i-1)2pi/N)\ 0]^T,\\
&s=0.5*t,\\
&\boldsymbol{p}_{0d}=[s\ 3*sin(0.5*s)\ 3]^T,\\
&\boldsymbol{p}_{di}=\boldsymbol{p}_0+\boldsymbol{L}_{di},\\
&\psi_{di}=0.5*t,
\end{aligned} \tag{4.78}$$

with $R_0=5m$, $R_f=3m$. The purpose of choosing the initial (4.36) is to illustrate both collision avoidance and reference tracking capacities of the proposed formation controller. With the above initial reference, all quadrotors are distributed on a ellipse shape and tracking a sine path $\boldsymbol{p}_0$. These initial reference satisfies conditions (4.39) and (4.42).
The control gains are chosen as $|a_{ij}|=0.4m$, $|b_{ij}|=5m$, $k_1=1$, $k_2=2$, $k_3=5$ and $k_4=2$. Simulation results are plotted in two cases, where the disturbances are chosen as follows

Case 1:

$$\begin{aligned} \boldsymbol{d}_{vi} &= [.5 + .2sin(s); 1 + 0.2cos(2s); 1.5 + .2sin(3s)]^T; \\ \boldsymbol{d}_{\omega i} &= [.1 + .2sin(.5s); .3 + 0.2cos(s); 1.5 + .2sin(2.5s)]^T; \end{aligned} \tag{4.79}$$

Case 2:

$$\begin{aligned} \boldsymbol{d}_{vi} &= [.5 + .2sin(s + rand); 1 + 0.2cos(2s + rand); 1.5 + .2sin(3s + rand)]^T; \\ \boldsymbol{d}_{\omega i} &= [.1 + .2sin(.5s + rand); .3 + 0.2cos(s + rand); 1.5 + .2sin(2.5s + rand)]^T; \end{aligned} \tag{4.80}$$

The observers of quadrotor 1 for linear velocity and disturbances are plotted on the Figure. 4.28, Figure. 4.39, Figure. 4.26, Figure. 4.37, Figure. 4.27 and Figure. 4.38. It can be seen from these figures that all the observers converge to the real values. The formation results are shown on the Figure. 4.18 and the Figure. 4.29. From the Figure. 4.23 and the Figure. 4.34, there are no collisions between all the quadrotors. The tracking errors in both two cases are convergent to the origin as shown in the Figure 4.19, 4.20, 4.21, and 4.30, 4.31, 4.32. Torque and force applied for quadrotor 1 are demonstrated in Figure 4.22 and Figure 4.33.

Case 1: All the quadrotors in the formation is distributed in an ellipse shape while tracking a sine path. The disturbance of translational and rotational subsystem is chosen as in (4.79)

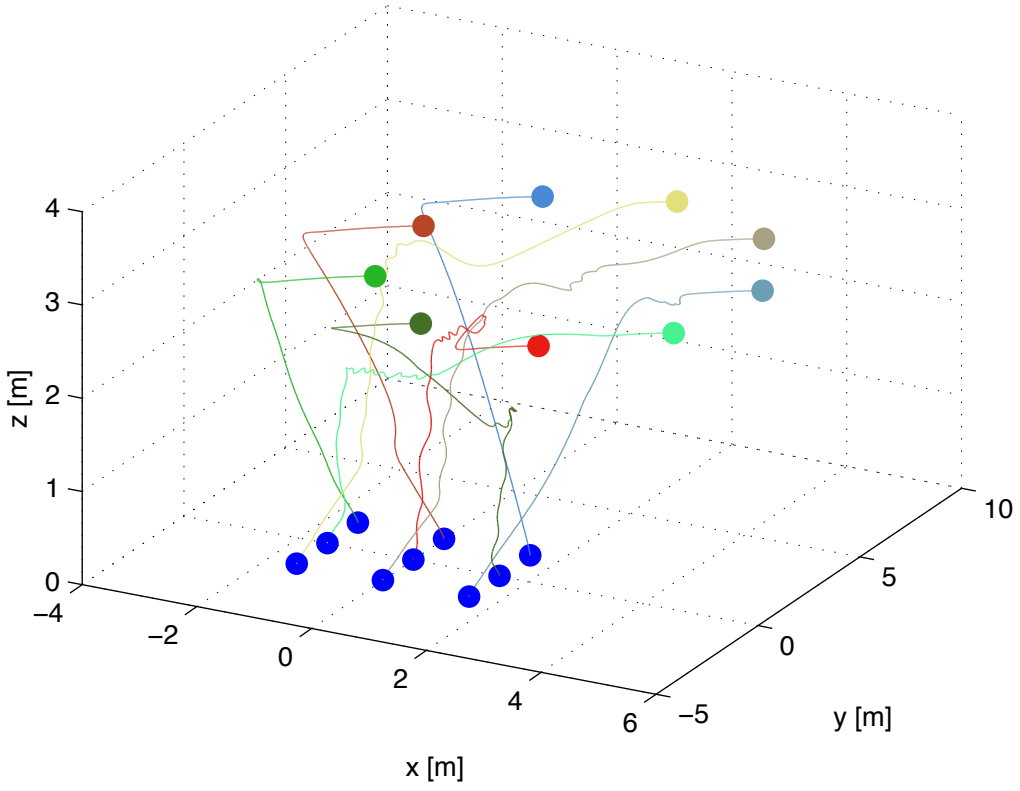

Figure 4.18: The formation of 9 quadrotors.

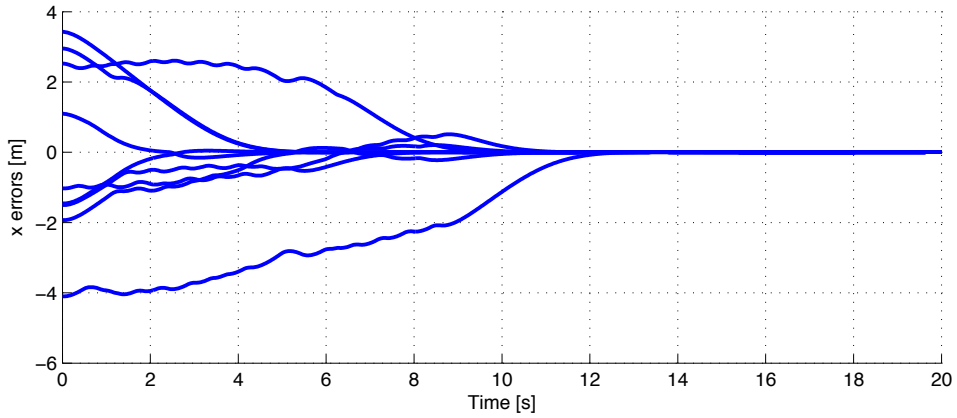

Figure 4.19: x tracking errors.

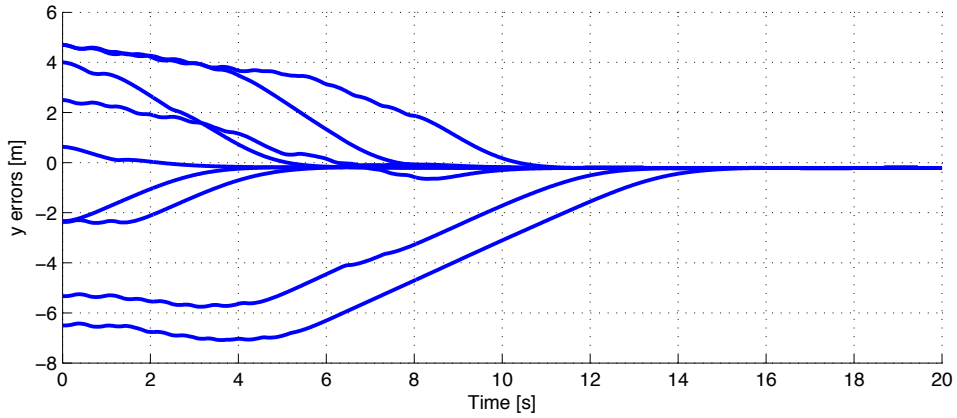

Figure 4.20: y tracking errors.

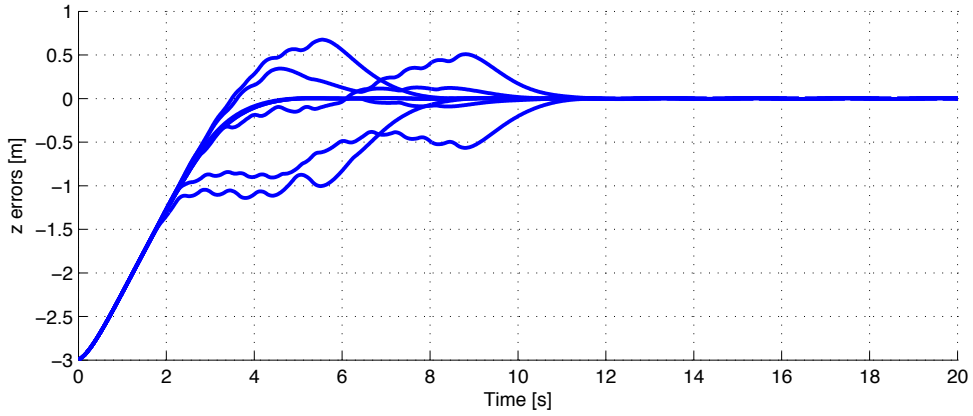

Figure 4.21: z tracking errors.

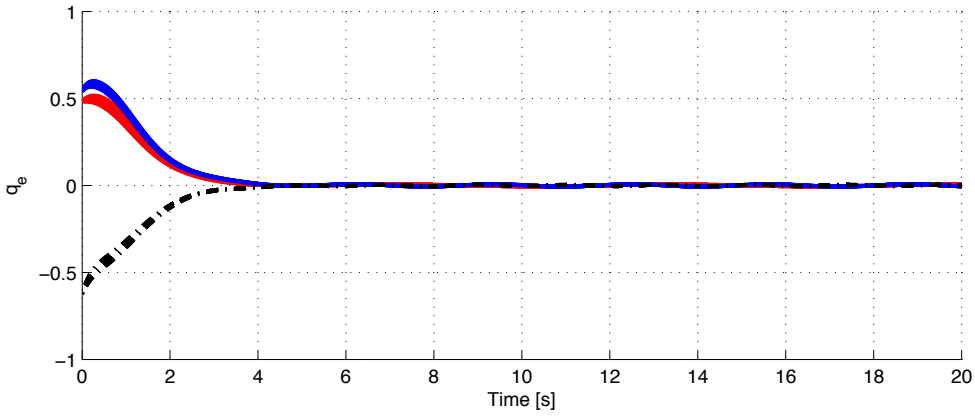

Figure 4.22: Attitude tracking errors.

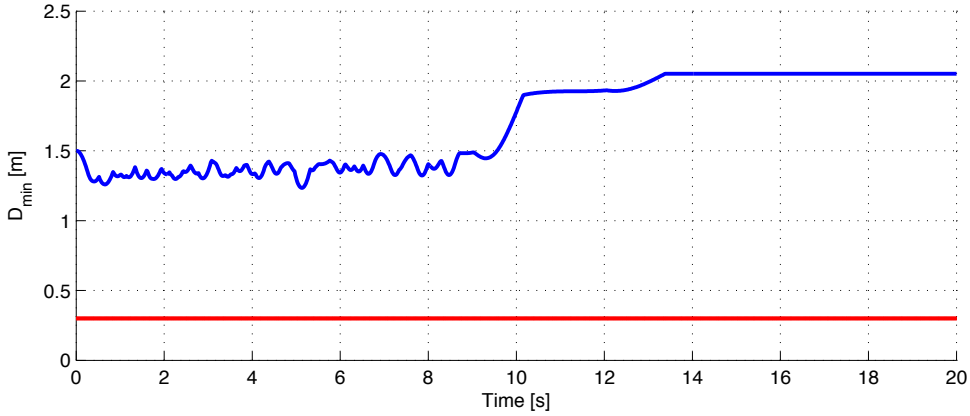

Figure 4.23: The minimum distance among quadrotors.

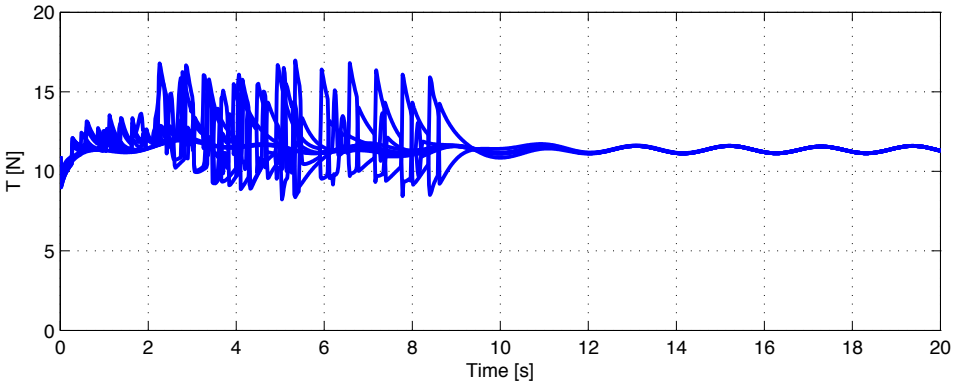

Figure 4.24: Thrust force of 9 quadrotors.

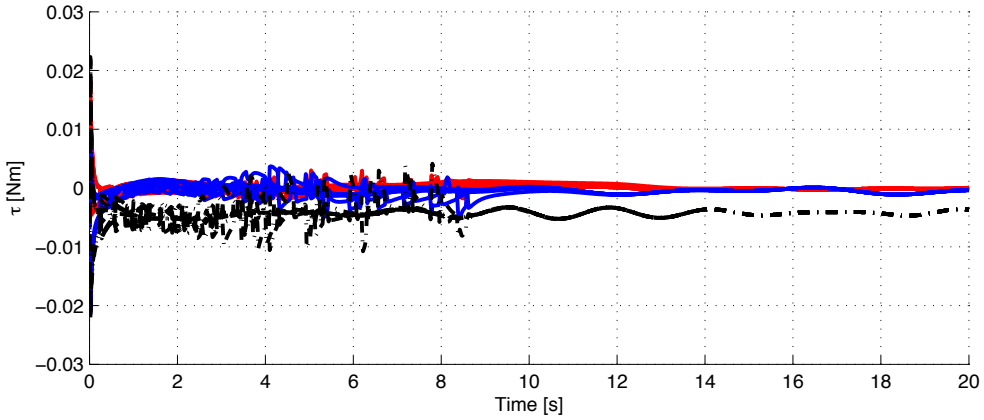

Figure 4.25: Torque of 9 quadrotors.

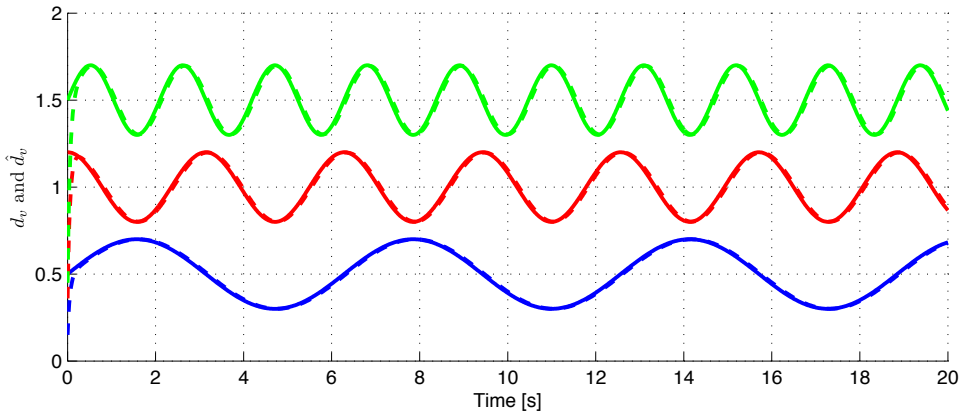

Figure 4.26: Disturbances and estimations of $\boldsymbol{d}_v$ of the quadrotor 1

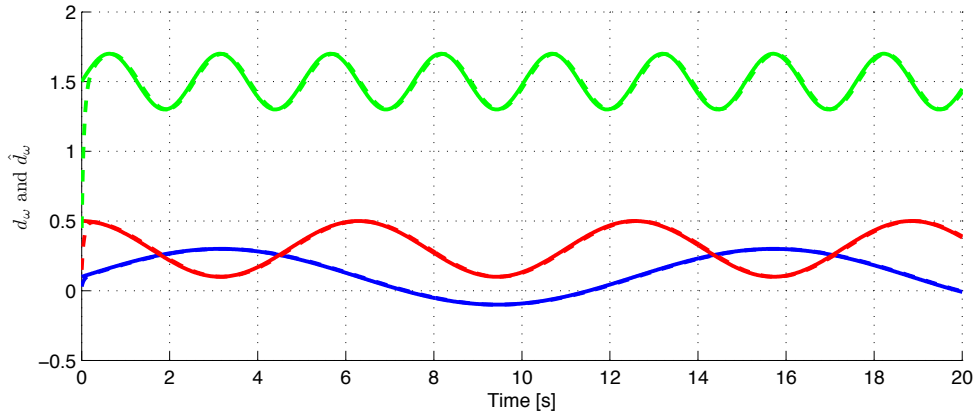

Figure 4.27: Disturbances and estimations of $\boldsymbol{d}_o$ of the quadrotor 1

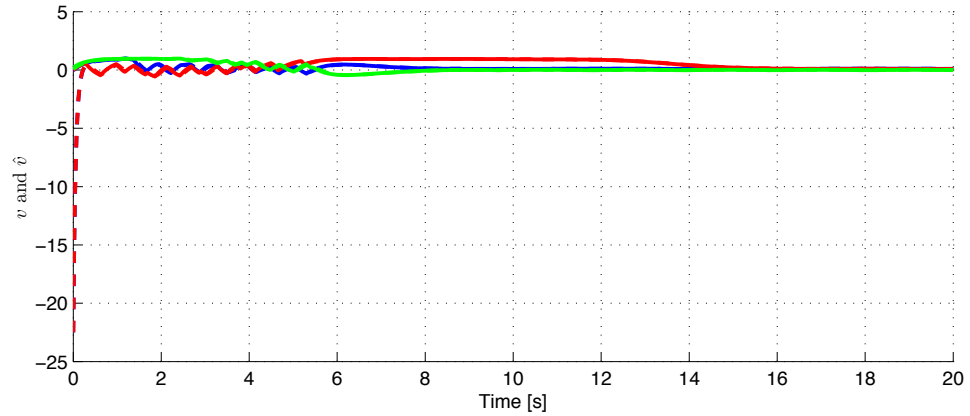

Figure 4.28: Velocities and estimations of the quadrotor 1

Case 2: All the quadrotors in the formation is distributed in an ellipse shape while tracking a sine path. The disturbance with random signal on translational and rotational subsystem is chosen as in (4.80)

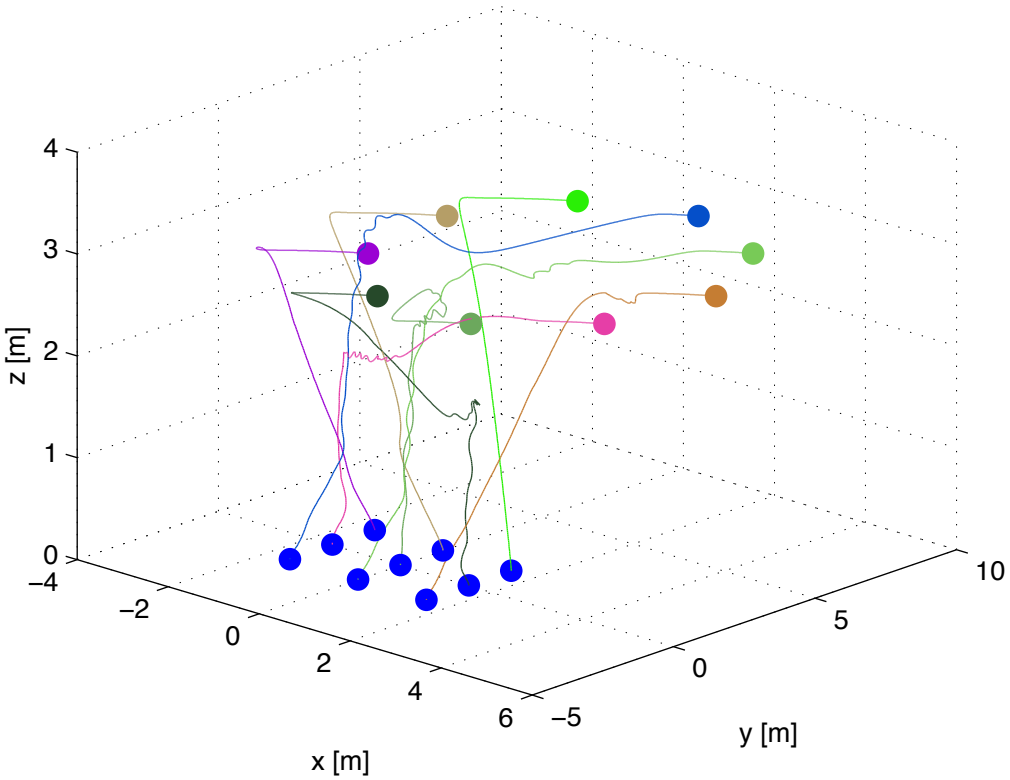

Figure 4.29: The formation of 9 quadrotors.

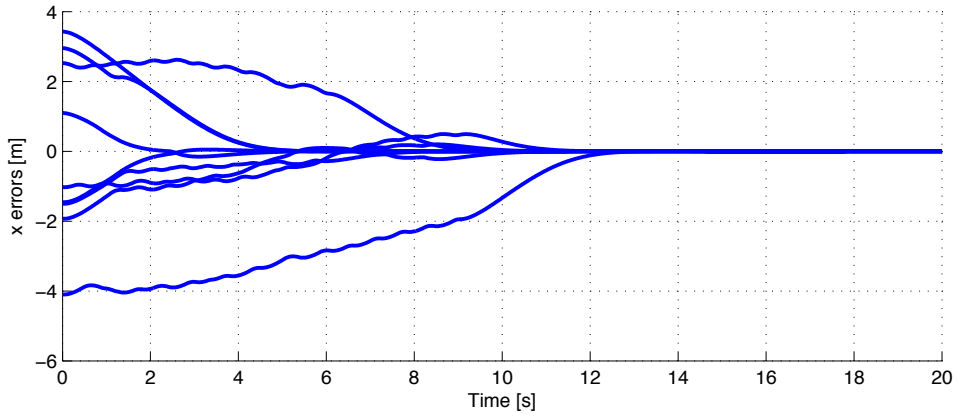

Figure 4.30: x tracking errors.

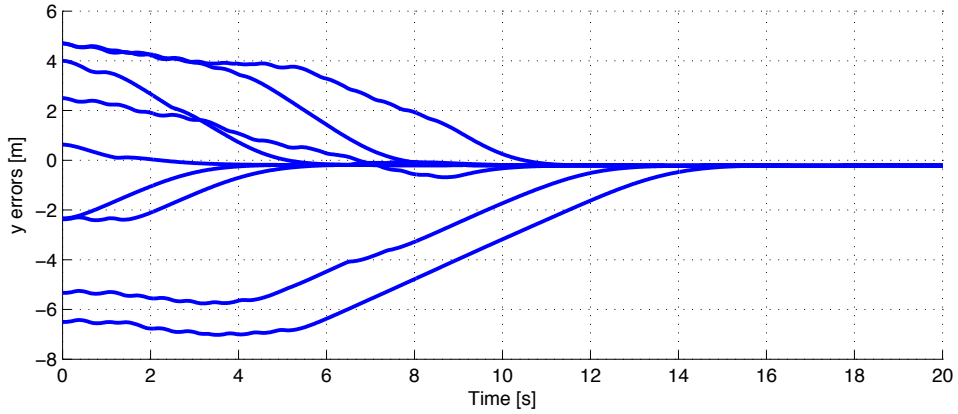

Figure 4.31: y tracking errors.

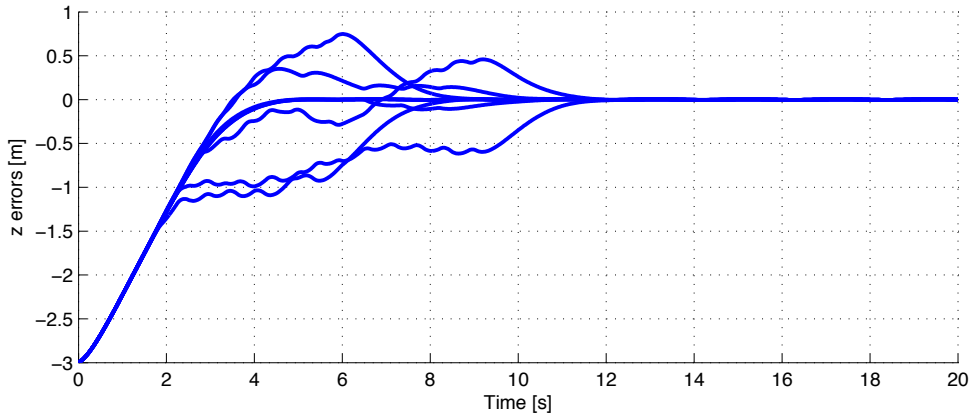

Figure 4.32: z tracking errors.

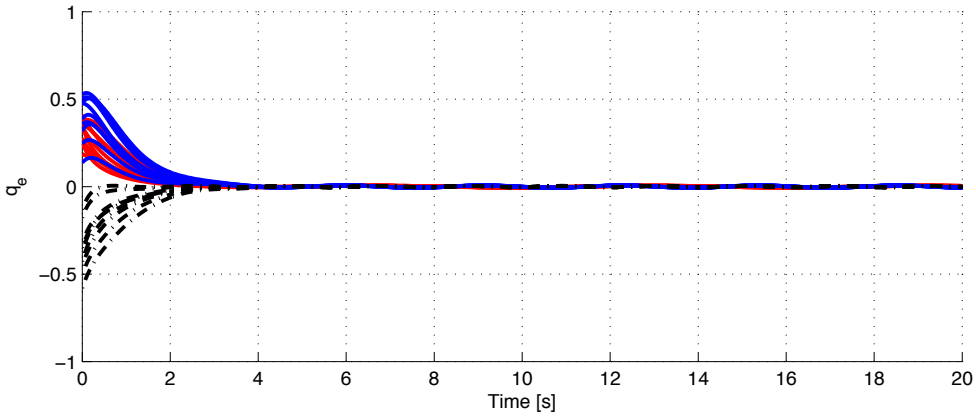

Figure 4.33: Attitude tracking errors.

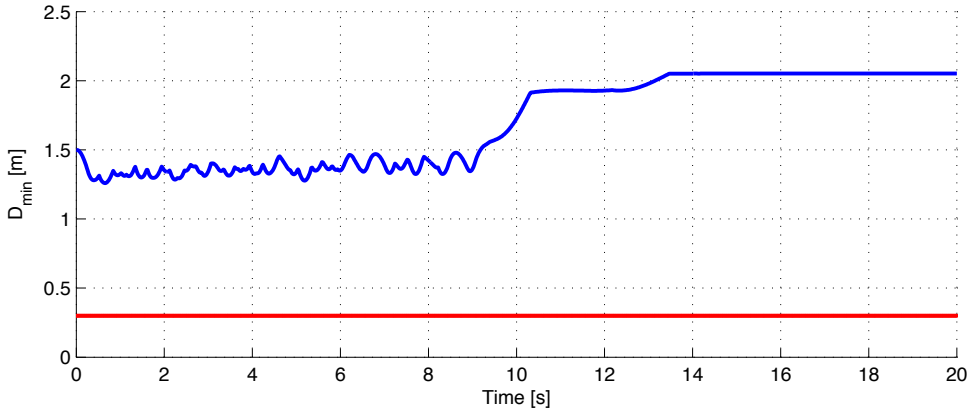

Figure 4.34: The minimum distance among quadrotors.

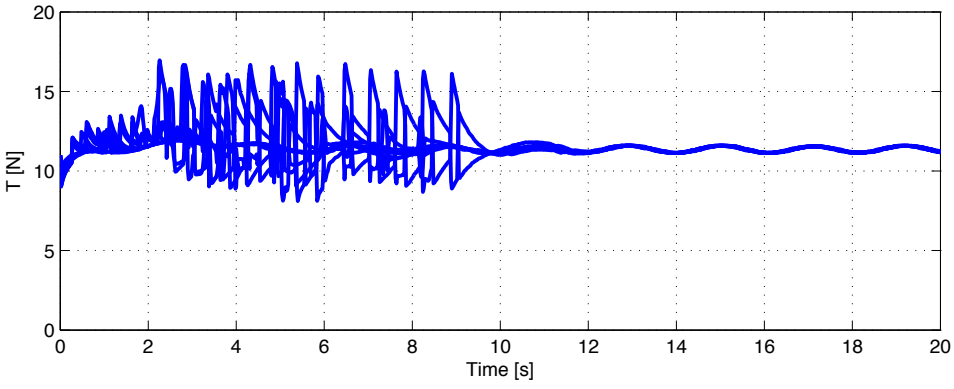

Figure 4.35: Thrust force of 9 quadrotors.

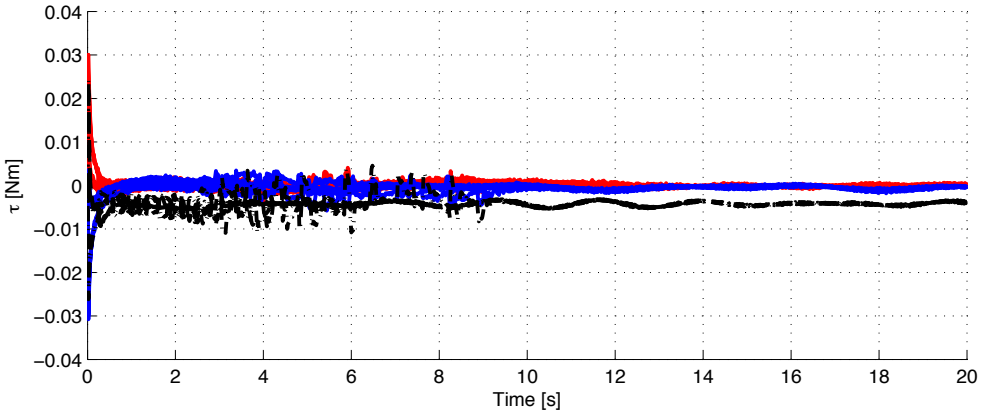

Figure 4.36: Torque of 9 quadrotors.

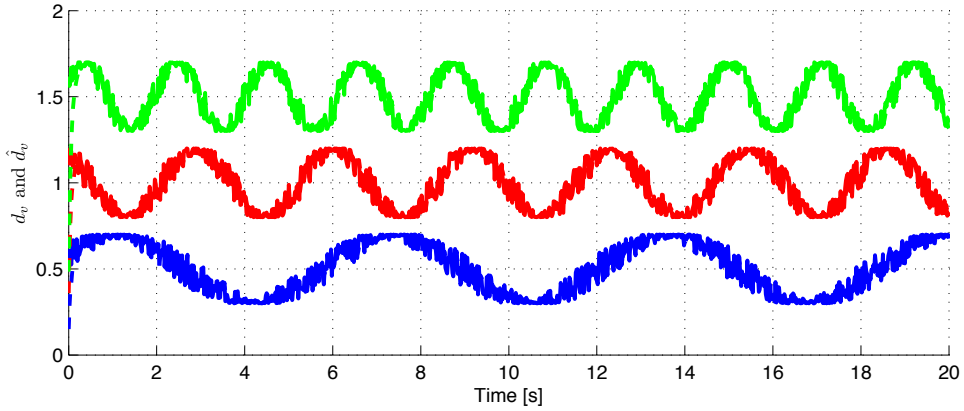

Figure 4.37: Disturbances and estimations of $\boldsymbol{d}_v$ of the quadrotor 1

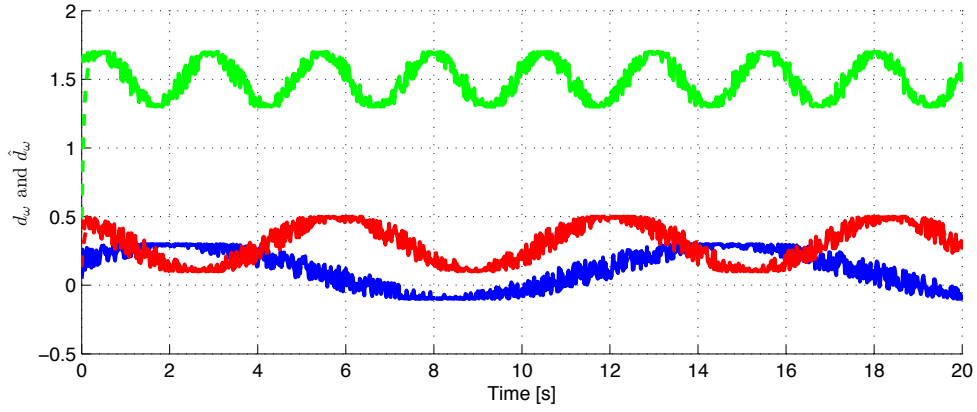

Figure 4.38: Disturbances and estimations of $\boldsymbol{d}_o$ of the quadrotor 1

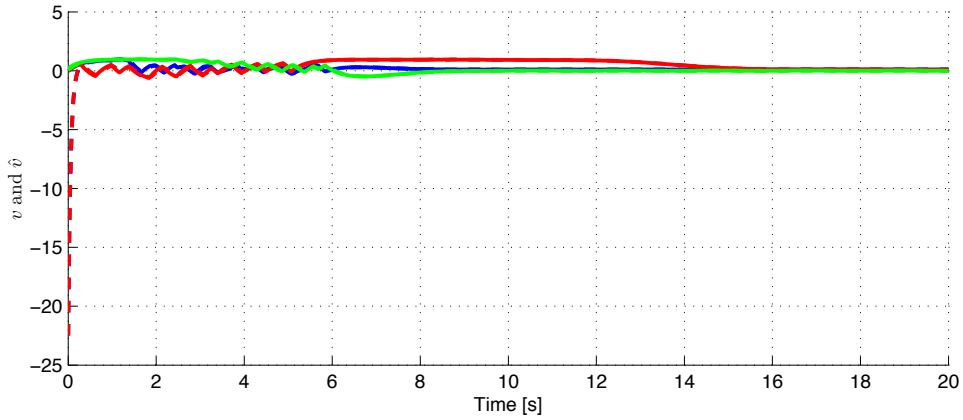

Figure 4.39: Velocities and estimations of the quadrotor 1

4.3.5 Conclusion

A distributed formation controllers for a group of underactuated quadrotors in three dimensional space under the assumption that the linear velocity and disturbance are unmeasured was presented. As proving via simulations, all the observer errors of linear velocity and disturbance were converged to the zero and the formation controller guaranteed no collision between all the quadrotors and satisfied all properties of the formation control objective. The simulation results shown that the proposed controller worked well with the disturbance of environment.

4.4 Controller 3 - Adaptive control

In this section the controller is developed and solved by focusing on the formation problem with assuming that the dynamics of quadrotor has disturbances from environment and the mass and inertia matrix are unknown. The controller developed in this section is based on the adaptive backstepping technique [KKK95].

4.4.1 Control objective

The dynamics of quadrotor is written as in (4.81)

$$\begin{aligned}
\dot{\boldsymbol{p}}_i &= \boldsymbol{v}_i \\
\dot{\boldsymbol{v}}_i &= g\boldsymbol{e}_3 - \tfrac{T_i}{m_i}\boldsymbol{R}_Q^T(\boldsymbol{Q}_i)\boldsymbol{e}_3 + \boldsymbol{d}_{vi} \\
\dot{\boldsymbol{Q}}_i &= \boldsymbol{K}_Q(\boldsymbol{Q}_i)\boldsymbol{\omega}_i \\
\dot{\boldsymbol{\omega}}_i &= \boldsymbol{J}_i^{-1}\boldsymbol{\tau}_i - \boldsymbol{J}_i^{-1}\boldsymbol{S}(\boldsymbol{\omega}_i)\boldsymbol{J}_i\boldsymbol{\omega}_i + \boldsymbol{d}_{\omega i}
\end{aligned} \tag{4.81}$$

where $i \in \mathbb{N}$, $\mathbb{N}$ is the set of all quadrotors in the group. $\boldsymbol{d}_{vi} \in \mathbb{R}^3$ and $\boldsymbol{d}_{\omega i} \in \mathbb{R}^3$ are unknown disturbance matrices, m_i and $\boldsymbol{J}_i \in \mathbb{R}^{3\times3}$ are unknown mass and inertial matrices, all the other

symbols in (4.81) are defined as in Section 2.1.
Before starting the formation control objective we impose the following assumption on the reference trajectories, communication and initial conditions between the quadrotor in the group.

Assumption 4.4.

1. *The reference position trajectory $\boldsymbol{p}_{di}(t) = [x_{di}(t)\, y_{di}(t)\, z_{di}(t)]^T$ and the heading angle ψ_{di} for the quadrotor i to track satisfy the following conditions:*

$$\begin{aligned} &\|p_{dij}\| \geq \varepsilon_{ij}, \\ &\left\|\boldsymbol{p}_{di}^{(k)}\right\| \leq \varepsilon_{kd}, \\ &\left\|\psi_{di}^{(k)}\right\| \leq \delta_{kd}, \end{aligned} \tag{4.82}$$

   for all $(i,j) \in \mathbb{N}, i \neq j$ where $p_{dij} = p_{di} - p_{dj}$, ε_{ij} is a strictly positive constant. ε_{kd}, $k = 1, \ldots, 4$, are nonnegative constants.

2. *The quadrotor i and j can communicate with each other and exchange their states, if satisfy the following condition:*

$$\alpha_{ij} \leq \alpha_{ij}^R \tag{4.83}$$

   where α_{ij}^R is a strictly positive constant.

3. *Let us define*

$$\begin{aligned} \boldsymbol{p}_{ij} &= \boldsymbol{p}_i - \boldsymbol{p}_j \\ \boldsymbol{\alpha}_{ij} &= \tfrac{1}{2}\boldsymbol{p}_{ij}^T \boldsymbol{p}_{ij} \end{aligned} \tag{4.84}$$

   Each quadrotor starts at a different location and do not have any collision among them. Specially, there exist strictly positive constants ε_{ij} and α_{ij}^S such that for all $(i,j) \in \mathbb{N}, i \neq j$, the following conditions holds:

$$\begin{aligned} &\|p_{ij}(t_0)\| \geq \varepsilon_{ij}, \\ &\alpha_{ij}(t_0) \geq \alpha_{ij}^S \end{aligned} \tag{4.85}$$

Control Objective 4.3. *Under the Assumption 4.4, for each quadrotor i design the control inputs T_i and $\boldsymbol{\tau}_i$ such that the position vector $\boldsymbol{p}_i(t)$ of the quadrotor i track their reference trajectories $\boldsymbol{p}_{di}(t)$ while avoid collision with all other quadrotor with assuming that environment disturbance, mass and inertia matrix are unknown. Specifically, we design the control inputs T_i and $\boldsymbol{\tau}_i$ such that*

$$\begin{aligned} &\lim_{t\to\infty} (\boldsymbol{p}_i(t) - \boldsymbol{p}_{di}(t)) = 0, \\ &\lim_{t\to\infty} (\psi_i(t) - \psi_{di}(t)) = 0 \\ &\|\boldsymbol{p}_i - \boldsymbol{p}_j\| \geq \alpha_{ij}^S \end{aligned} \tag{4.86}$$

For all $(i,j) \in \mathbb{N}, i \neq j$ and $t \geq t_0 \geq 0$, the control design needs to keep all other states of the quadrotor dynamics bounded for all initial conditions.

4.4.2 Control Design

In this section we will use adaptive backstepping technique [KKK95] to design control for a formation of quadrotor satisfying the control objective 4.3. Similarly in the previous section, the dynamics of quadrotor i (4.81) is separated into two subsystems. The first subsystem contains two first equations for translational dynamics and the second subsystem consists two last equations for rotational dynamics. In the first step, the adaptive backstepping technique evolved in the Section 2.3 is applied to obtain the intermediate control input force for translational dynamics asymptotically tracking the predefined path. Using the extraction algorithm, the total force T_i and a unit-quaternion reference Q_{di} are generated. The attitude extraction algorithm is shown in Figure 4.40. In the next step, the torque $\boldsymbol{\tau}$ to force $\boldsymbol{Q} \to \boldsymbol{Q}_d$ is designed.

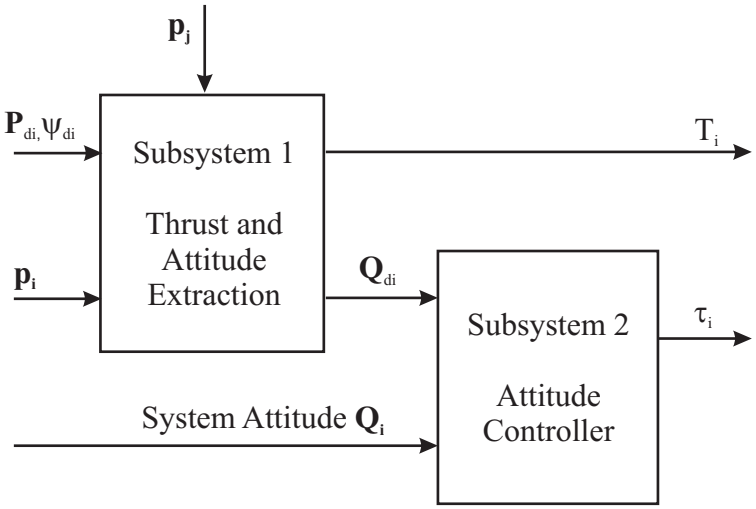

Figure 4.40: Attitude Extraction Algorithm.

Step 1

In this step, the translational dynamics of (4.81) is considered. We will design a virtual control of $\boldsymbol{v}_i$ to force $\boldsymbol{p}_i(t)$ to globally asymptotically track its reference trajectory $\boldsymbol{p}_{di}(t)$. As such, we define the tracking errors as follows:

$$\begin{aligned} \boldsymbol{p}_{ei} &= \boldsymbol{p}_i - \boldsymbol{p}_{di}, \\ \boldsymbol{v}_{ei} &= \boldsymbol{v}_i - \boldsymbol{\alpha}_{vi}, \end{aligned} \tag{4.87}$$

where $\boldsymbol{\alpha}_{vi}$ is a virtual control of $\boldsymbol{v}_i$.

Differentiating both sides of (4.87) and using the first subsystem, the error dynamics are expressed as

$$\begin{aligned} \dot{\boldsymbol{p}}_{ei} &= \boldsymbol{v}_{ei} + \boldsymbol{\alpha}_{vi} - \dot{\boldsymbol{p}}_{di}, \\ \dot{\boldsymbol{v}}_{ei} &= g\boldsymbol{e}_3 - J_{1i}\boldsymbol{F}_i + \boldsymbol{d}_{vi} - \dot{\boldsymbol{\alpha}}_{vi} \end{aligned} \tag{4.88}$$

where $\boldsymbol{F}_i$ is an intermediate control input and $\boldsymbol{F}_i = T_i \boldsymbol{R}_Q^T(\boldsymbol{Q}_{di})e_3$ is illustrated in the ideal case

where $\boldsymbol{Q}_{di}$ is obtained via Lemma 2.3.

In order to design the intermediate control input $\boldsymbol{F}_i$ for quadrotor i which achieves the Formation control objective 4.3, we consider the following potential function:

$$V_1 = \frac{1}{2}\sum_{i=1}^{N}\left[\boldsymbol{p}_{ei}{}^T\boldsymbol{p}_{ei} + \sum_{J\in\mathbb{N}_i}\beta_{ij}\right] \tag{4.89}$$

where $\mathbb{N}_i$ is the set containing all the quadrotors except for the quadrotor i, β_{ij} is taken from (4.3) where α_{ij} is calculated from (4.84).

Differentiating both sides of (4.89) gives

$$\begin{aligned}\dot{V}_1 &= \sum_{i=1}^{N}\left[\boldsymbol{p}_{ei}{}^T\dot{\boldsymbol{p}}_{ei} + \sum_{j\in\mathbb{N}_i}\beta'_{\text{ij}}\dot{\alpha}_{\text{ij}}\right] \\ &= \sum_{i=1}^{N}\left[\boldsymbol{p}_{ei}{}^T\dot{\boldsymbol{p}}_{ei} + \sum_{j\in\mathbb{N}_i}\beta'_{ij}\boldsymbol{p}_{ij}{}^T\dot{\boldsymbol{p}}_{ij}\right]\end{aligned} \tag{4.90}$$

Noting that $\dot{\boldsymbol{p}}_{ij} = (\dot{\boldsymbol{p}}_i - \dot{\boldsymbol{p}}_{di}) - (\dot{\boldsymbol{p}}_j - \dot{\boldsymbol{p}}_{dj}) = \boldsymbol{v}_{ei} - \boldsymbol{v}_{ej}$, we can write (4.90) as follows

$$\begin{aligned}\dot{V}_1 &= \sum_{i=1}^{N}(\boldsymbol{p}_{ei}{}^T + \sum_{j\in\mathbb{N}_i}\beta'_{ij}\boldsymbol{p}_{ij}{}^T)(\boldsymbol{v}_{ei} + \boldsymbol{\alpha}_{vi} - \dot{\boldsymbol{p}}_{di}) \\ &= \sum_{i=1}^{N}\boldsymbol{\Omega}_i{}^T(\boldsymbol{v}_{ei} + \boldsymbol{\alpha}_{vi} - \dot{\boldsymbol{p}}_{di})\end{aligned} \tag{4.91}$$

where

$$\boldsymbol{\Omega}_i = \boldsymbol{p}_{ei} + \sum_{j\in\mathbb{N}_i}\beta'_{ij}\boldsymbol{p}_{ij} \tag{4.92}$$

The equation (4.91) suggests that we choose

$$\boldsymbol{\alpha}_{vi} = -k_1\boldsymbol{\Omega}_i + \dot{\boldsymbol{p}}_{di} \tag{4.93}$$

To design the intermediate control input $\boldsymbol{F}_i$, considering the following Lyapunov function

$$V_2 = V_1 + \frac{1}{2}\sum_{i=1}^{N}\boldsymbol{v}_{ei}{}^T\boldsymbol{v}_{ei} \tag{4.94}$$

Differentiating both sides of (4.94) gives

$$\begin{aligned}\dot{V}_2 &= \sum_{i=1}^{N}\left[-k_1\boldsymbol{\Omega}_i{}^T\boldsymbol{\Omega}_i + \boldsymbol{v}_{ei}{}^T(ge_3 - J_{1i}\boldsymbol{F}_i - \dot{\boldsymbol{\alpha}}_{vi} + \boldsymbol{\Omega}_i + \boldsymbol{d}_{vi})\right] \\ &= \sum_{i=1}^{N}\left[-k_1\boldsymbol{\Omega}_i{}^T\boldsymbol{\Omega}_i + \boldsymbol{v}_{ei}{}^T(ge_3 - \hat{J}_{1i}\boldsymbol{F}_i - \dot{\boldsymbol{\alpha}}_{vi} + \boldsymbol{\Omega}_i + \hat{\boldsymbol{d}}_{vi}) + \boldsymbol{v}_{ei}{}^T(-\tilde{J}_{1i}\boldsymbol{F}_i + \tilde{\boldsymbol{d}}_{vi})\right]\end{aligned} \tag{4.95}$$

which suggests that we choose:

$$\boldsymbol{F}_i = (k_2 \boldsymbol{v_{ei}} + g e_3 - \dot{\boldsymbol{\alpha}}_{vi} + \boldsymbol{\Omega}_i + \hat{\boldsymbol{d}}_{vi})/\hat{J}_{1i} \tag{4.96}$$

where $\hat{J}_{1i}$ and $\hat{\boldsymbol{d}}_{vi}$ are estimations of J_{1i} and $\boldsymbol{d}_{vi}$, respectively. The update laws for these estimations and are chosen as follows

$$\begin{aligned} \dot{\hat{J}}_{1i} &= proj(\gamma_{1v} \boldsymbol{v}_{ei}^T \boldsymbol{F}_i) \\ \dot{\hat{\boldsymbol{d}}}_{vi} &= \gamma_{2v} \boldsymbol{v}_{ei} \end{aligned} \tag{4.97}$$

We assume that the intermediate control input $\boldsymbol{F}_i$ forces the quadrotor i tracking the predefined path and heading angle ψ_{di} in ideal case. Applying Lemma 2.3 for the intermediate control input (4.63), we obtain the thrust T_i and the reference unit-quaternion vector $\boldsymbol{Q}_{di}$ as follows:

$$\begin{aligned} T_i &= \|\boldsymbol{F}_i\| \\ \boldsymbol{Q}_{di} &= \begin{bmatrix} C\frac{\alpha_{\phi i}}{2} C\frac{\alpha_{\theta i}}{2} C\frac{\alpha_{\psi i}}{2} + S\frac{\alpha_{\phi i}}{2} S\frac{\alpha_{\theta i}}{2} S\frac{\alpha_{\psi i}}{2} \\ S\frac{\alpha_{\phi i}}{2} C\frac{\alpha_{\theta i}}{2} C\frac{\alpha_{\psi i}}{2} - C\frac{\alpha_{\phi i}}{2} S\frac{\alpha_{\theta i}}{2} S\frac{\alpha_{\psi i}}{2} \\ C\frac{\alpha_{\phi i}}{2} S\frac{\alpha_{\theta i}}{2} C\frac{\alpha_{\psi i}}{2} + S\frac{\alpha_{\phi i}}{2} C\frac{\alpha_{\theta i}}{2} S\frac{\alpha_{\psi i}}{2} \\ C\frac{\alpha_{\phi i}}{2} C\frac{\alpha_{\theta i}}{2} S\frac{\alpha_{\psi i}}{2} - S\frac{\alpha_{\phi i}}{2} S\frac{\alpha_{\theta i}}{2} C\frac{\alpha_{\psi i}}{2} \end{bmatrix} \end{aligned} \tag{4.98}$$

where

$$\begin{aligned} \alpha_{\psi i} &= \psi_{di}, \\ \alpha_{\theta i} &= \arctan\left(\frac{C\alpha_{\psi i} F_{i1} + S\alpha_{\psi i} F_{i2}}{F_{i3}}\right), \\ \alpha_{\phi i} &= \arcsin\left(\frac{S\alpha_{\psi i} F_{i1} - C\alpha_{\psi i} F_{i2}}{T_i}\right), \end{aligned} \tag{4.99}$$

The reference angular velocity of quadrotor i is calculated as follows

$$\boldsymbol{\omega}_{di} = \begin{bmatrix} 1 & 0 & -S\alpha_{\theta i} \\ 0 & C\alpha_{\phi i} & S\alpha_{\phi i} C\alpha_{\theta i} \\ 0 & -S\alpha_{\phi i} & C\alpha_{\phi i} C\alpha_{\theta i} \end{bmatrix} \begin{bmatrix} \dot{\alpha}_{\phi i} \\ \dot{\alpha}_{\theta i} \\ \dot{\alpha}_{\psi i} \end{bmatrix} \tag{4.100}$$

where $\boldsymbol{\omega}_{di}$ is the body reference angular velocity; $S(\cdot)$ and $C(\cdot)$ stand for $\sin(\cdot)$, $\cos(\cdot)$, respectively.

Step 2

In this step, the unit-quaternion vector $\boldsymbol{Q}_{di}$ obtained from (4.98) is used as the reference for designing the torque input $\boldsymbol{\tau}_i$.

$$\begin{aligned} \boldsymbol{Q}_{ei} &= \boldsymbol{Q}_{di}^{-1} \odot \boldsymbol{Q}_i, \\ \boldsymbol{\omega}_{ei} &= \boldsymbol{\omega}_i - \boldsymbol{\alpha}_{\omega i} \end{aligned} \tag{4.101}$$

where $\boldsymbol{\alpha}_{\omega i}$ is a virtual control of ω_i. $\boldsymbol{Q}_{ei} = [\eta_{ei}\, \boldsymbol{q}_{ei}^T]^T$ and $\boldsymbol{\omega}_{ei}$ are attitude tracking and angular

velocity error vector, respectively.
Differentiating both sides of (4.101) yields

$$\begin{aligned}\dot{\boldsymbol{q}}_{ei} &= \boldsymbol{G}_i(\boldsymbol{\omega}_{ei} + \boldsymbol{\alpha}_{\omega i} - \boldsymbol{\omega}_{di}) \\ \dot{\boldsymbol{\omega}}_{ei} &= \boldsymbol{J}_i^{-1}\boldsymbol{\tau}_i - \boldsymbol{J}_i^{-1}\boldsymbol{S}(\boldsymbol{\omega}_i)\boldsymbol{J}_i\boldsymbol{\omega}_i + \boldsymbol{d}_{\omega i} - \dot{\boldsymbol{\alpha}}_{\omega i}\end{aligned} \tag{4.102}$$

where $\boldsymbol{G}_i = \frac{1}{2}\left(\eta_{ei}\boldsymbol{I}_{3\times 3} + \boldsymbol{S}(\boldsymbol{q}_{ei})\right)$ and $\boldsymbol{\omega}_{di}$ can be obtained by using equation (4.100).
To obtain the control input $\boldsymbol{\tau}_i$, we consider the following Lyapunov function:

$$V_3 = \sum_{i=1}^{N} \frac{1}{2}\boldsymbol{q}_{ei}^T\boldsymbol{q}_{ei} \tag{4.103}$$

The time derivative of V_3 along solutions (4.102) is given by

$$\dot{V}_3 = \sum_{i=1}^{N} \boldsymbol{q}_{ei}^T\boldsymbol{G}_i(\boldsymbol{\omega}_{ei} + \boldsymbol{\alpha}_{\omega i} - \boldsymbol{\omega}_{di}) \tag{4.104}$$

which suggests that we choose

$$\boldsymbol{\alpha}_{\omega i} = -k_3\boldsymbol{G}_i^T\boldsymbol{q}_{ei} + \boldsymbol{\omega}_{di} \tag{4.105}$$

To design the control input torque, $\boldsymbol{\tau}_i$, considering the following Lyapunov candidate

$$V_4 = V_3 + \sum_{i=1}^{N} \boldsymbol{\omega}_{ei}^T\boldsymbol{\omega}_{ei} \tag{4.106}$$

The time derivative of (4.106) is given

$$\begin{aligned}\dot{V}_4 &= \sum_{i=1}^{N}\left[-k_3\boldsymbol{q}_{ei}^T\boldsymbol{G}_i\boldsymbol{G}_i^T\boldsymbol{q}_{ei}\right] \\ &\quad + \sum_{i=1}^{N}\left[\boldsymbol{\omega}_{ei}^T\left(\boldsymbol{J}_i^{-1}\boldsymbol{\tau}_i - \boldsymbol{J}_i^{-1}\boldsymbol{S}(\boldsymbol{\omega}_i)\boldsymbol{J}_i\boldsymbol{\omega}_i + \boldsymbol{d}_{\omega i} - \dot{\boldsymbol{\alpha}}_{\omega i} + \boldsymbol{G}_i\boldsymbol{q}_{ei}\right)\right] \\ &= \sum_{i=1}^{N}\left[-k_3\boldsymbol{q}_{ei}^T\boldsymbol{G}_i\boldsymbol{G}_i^T\boldsymbol{q}_{ei}\right] \\ &\quad + \sum_{i=1}^{N}\left[\boldsymbol{\omega}_{ei}^T\left(\hat{\boldsymbol{J}}_i^{-1}\boldsymbol{\tau}_i - \boldsymbol{J}_i^{-1}\boldsymbol{S}(\boldsymbol{\omega}_i)\boldsymbol{J}_i\boldsymbol{\omega}_i + \hat{\boldsymbol{d}}_{\omega i} - \dot{\boldsymbol{\alpha}}_{\omega i} + \boldsymbol{G}_i\boldsymbol{q}_{ei}\right)\right] \\ &\quad + \sum_{i=1}^{N}\left[\boldsymbol{\omega}_{ei}^T\left(\tilde{\boldsymbol{J}}_i^{-1}\boldsymbol{\tau}_i + \tilde{\boldsymbol{d}}_{\omega i}\right)\right]\end{aligned} \tag{4.107}$$

which suggests that we choose the control input torque as follows

$$\boldsymbol{\tau}_i = \hat{\boldsymbol{J}}_i\left(-k_4\boldsymbol{\omega}_{ei} + \dot{\boldsymbol{\alpha}}_{\omega i} - \boldsymbol{G}_i\boldsymbol{q}_{ei}) + \boldsymbol{J}_i^{-1}\boldsymbol{S}(\boldsymbol{\omega}_i\boldsymbol{J}_i\boldsymbol{\omega}_i - \hat{\boldsymbol{d}}_{\omega i}\right) \tag{4.108}$$

where $\hat{\boldsymbol{J}}_i$ and $\hat{\boldsymbol{d}}_{\omega i}$ are estimations of $\boldsymbol{J}_i$ and $\boldsymbol{d}_{\omega i}$, respectively. The update laws for these estima-

tions and are chosen as follows

$$\begin{aligned}\dot{\hat{\boldsymbol{J}}}_i^{-1} &= proj(\hat{\boldsymbol{J}}_i(\gamma_{1\omega}\boldsymbol{\omega}_{ei}^T\boldsymbol{F}_i))\\ \dot{\hat{\boldsymbol{d}}}_{\omega i} &= \gamma_{2\omega}\boldsymbol{\omega}_{ei}\end{aligned} \tag{4.109}$$

Substituting update laws, controls and virtual controls from (4.93), (4.96), (4.97), (4.105) (4.109) and (4.108) into (4.88), and (4.102), we have the following closed loop system:

$$\begin{aligned}\dot{\boldsymbol{p}}_{ei} &= \boldsymbol{v}_{ei} - k_1\boldsymbol{\Omega}_i\\ \dot{\boldsymbol{v}}_{ei} &= -k_2\boldsymbol{v}_{ei} - \boldsymbol{\Omega_i} - \tilde{J}_{1i}\boldsymbol{F}_i + \tilde{\boldsymbol{d}}_{vi}\\ \dot{\boldsymbol{q}}_{ei} &= \boldsymbol{G}_i(-k_3\boldsymbol{G}_i^T\boldsymbol{q}_{ei} + \boldsymbol{\omega}_{ei})\\ \dot{\boldsymbol{\omega}}_{ei} &= -k_4\boldsymbol{\omega}_{ei} - \boldsymbol{G}_i\boldsymbol{q}_{ei} + \tilde{\boldsymbol{J}}_i^{-1}\tilde{\boldsymbol{\tau}}_i + \tilde{\boldsymbol{d}}_{\omega i}\\ \dot{\tilde{J}}_{1i} &= -\dot{\hat{J}}_{1i} = -proj(\gamma_{1v}\boldsymbol{v}_{ei}^T\boldsymbol{F}_i)\\ \dot{\tilde{\boldsymbol{d}}}_{vi} &= -\dot{\hat{\boldsymbol{d}}}_{vi} = -\gamma_{2v}\boldsymbol{v}_{ei}\\ \dot{\tilde{\boldsymbol{J}}}_i^{-1} &= -\dot{\hat{\boldsymbol{J}}}_i^{-1} = -proj(\hat{\boldsymbol{J}}_i(\gamma_{1\omega}\boldsymbol{\omega}_{ei}^T\boldsymbol{F}_i))\\ \dot{\tilde{\boldsymbol{d}}}_{\omega i} &= -\dot{\hat{\boldsymbol{d}}}_{\omega i} = -\gamma_{2\omega}\boldsymbol{\omega}_{ei}\end{aligned} \tag{4.110}$$

The control design has been completed. We summarize the results in the following theorem.

Theorem 4.3. *Under Assumption 4.4, the formation control and update laws consisting of* (4.96)*,* (4.97)*,* (4.109) *and* (4.108) *for the quadrotor i achieve the Formation Control Objective 4.3, there is no collision between all the quadrotors, the position $\boldsymbol{p}_i$ and heading angle ψ_i of quadrotor i globally asymptotically track their reference trajectories $\boldsymbol{p}_{di}$ and ψ_{di},*

$$\begin{aligned}&\lim_{t\to\infty}(\boldsymbol{p}_i(t) - \boldsymbol{p}_{di}(t)) = 0,\\ &\lim_{t\to\infty}(\psi_i(t) - \psi_{di}(t)) = 0\\ &\|\boldsymbol{p}_i - \boldsymbol{p}_j\| \geq \alpha_{ij}^S\end{aligned} \tag{4.111}$$

and the closed loop system (4.110) *is forward complete.*

Proof. *See Appendix B.5.*

4.4.3 Simulation Results

In this section, we illustrate the effectiveness of the proposed formation control design through a numerical simulation on a group of $N = 3$ identical quadrotors. The parameters of quadrotor i for the simulation are taken from [EInE12] as following: m_i=0.35 kg, g = 9.81 $kg\,m^2$, $l_i = 0.15m$, $I_{X_i} = 15.67 \times 10^{-3}\,kg\,m^2$, $I_{Y_i} = 15.67 \times 10^{-3}\,kg\,m^2$; $I_{Z_i} = 28.34 \times 10^{-3}\,kg\,m^2$, $K_{ti} = 192.32 \times 10^{-7}Ns^2$, $K_{di} = 4.003 \times 10^{-7}Nms^2$.

The initial conditions are taken as

$$\begin{aligned}&\boldsymbol{p}_i(0) = [R_1 * j \quad R_1 * k \quad 0]^T; \boldsymbol{v}_i(0) = [0\,0\,0]^T\\&\boldsymbol{Q}_i(0) = [1\,0\,0\,0]^T; \boldsymbol{\omega}_i(0) = [0\,0\,0]^T\end{aligned} \tag{4.112}$$

where $R_1 = 1.5m$, j and k combine such that at the first time, all quadrotors are distributed on land in a rectangle form with 1 row and 3 columns. The initial distance between quadrotors are satisfied (4.85).
For the path-tracking, the reference trajectories are chosen as

$$\begin{aligned}&\boldsymbol{L}_{di} = [R_f sin((i-1)2pi/N)\ R_0 cos((i-1)2pi/N)\ 0]^T,\\&s = 0.5 * t,\\&\boldsymbol{p}_{0d} = [s\ 3 * sin(0.5 * s)\ 3]^T,\\&\boldsymbol{p}_{di} = \boldsymbol{p}_{0d} + \boldsymbol{L}_{di},\\&\psi_{di} = 0.5 * t,\end{aligned} \tag{4.113}$$

with $R_0 = 5m$, $R_f = 3m$. The purpose of choosing the initial (4.113) is to illustrate both collision avoidance and reference tracking capacities of the proposed formation controller. With the above initial reference, all quadrotors are distributed on a ellipse shape and tracking a sine path $\boldsymbol{p}_{di}$. These initial reference satisfies conditions (4.82) and (4.85).
The control gains are chosen as $|a_{ij}| = 0.4m$, $|b_{ij}| = 5m$, $k_1 = 1$, $k_2 = 2$, $k_3 = 5$ and $k_4 = 2$. Simulation results are plotted in two cases, where the disturbances are chosen as follows
Case 1:

$$\begin{aligned}&m_i = m_{01} + sin(0.5 * s)\\&\boldsymbol{J}_i = \boldsymbol{J}_{0i}(1 + sin(0.5 * s))\\&\boldsymbol{d}_{vi} = [.5 + .2sin(s); 1 + 0.2cos(2s); 1.5 + .2sin(3s)]^T;\\&\boldsymbol{d}_{\omega i} = [.1 + .2sin(.5s); .3 + 0.2cos(s); 1.5 + .2sin(2.5s)]^T;\end{aligned} \tag{4.114}$$

Case 2:

$$\begin{aligned}&m_i = m_{01} + sin(0.5 * s)\\&\boldsymbol{J}_i = \boldsymbol{J}_{0i}(1 + sin(0.5 * s))\\&\boldsymbol{d}_{vi} = [.5 + .2sin(s + rand); 1 + 0.2cos(2s + rand); 1.5 + .2sin(3s + rand)]^T;\\&\boldsymbol{d}_{\omega i} = [.1 + .2sin(.5s + rand); .3 + 0.2cos(s + rand); 1.5 + .2sin(2.5s + rand)]^T;\end{aligned} \tag{4.115}$$

The estimations of unknown parameters for quadrotor 1 are plotted on the Figure. 4.51, Figure. 4.62, Figure. 4.49, Figure. 4.60, Figure. 4.50 and Figure. 4.61. Unlike previous section that all the estimation parameters converge to the real values, in this section, all the estimation values are generated such that they eliminate the errors in the energy functions. The forma-

tion results are shown on the Figure. 4.41 and the Figure. 4.52. From the Figure. 4.46 and the Figure. 4.57, it can be seen that there are no collision among all the quadrotors. The tracking errors in both two cases are converged to the origin as shown in the Figure 4.42, 4.43, 4.44, for case 1 and 4.53, 4.54, 4.55 for case 2. Torque and thrust force are demonstrated in Figure 4.47, 4.48, 4.58 and 4.59.

Case 1: Formation of three quadrotors distributed on a circle shape while tracking a sine path is simulated. The disturbance on translational and rotational subsystem is chosen as in (4.114)

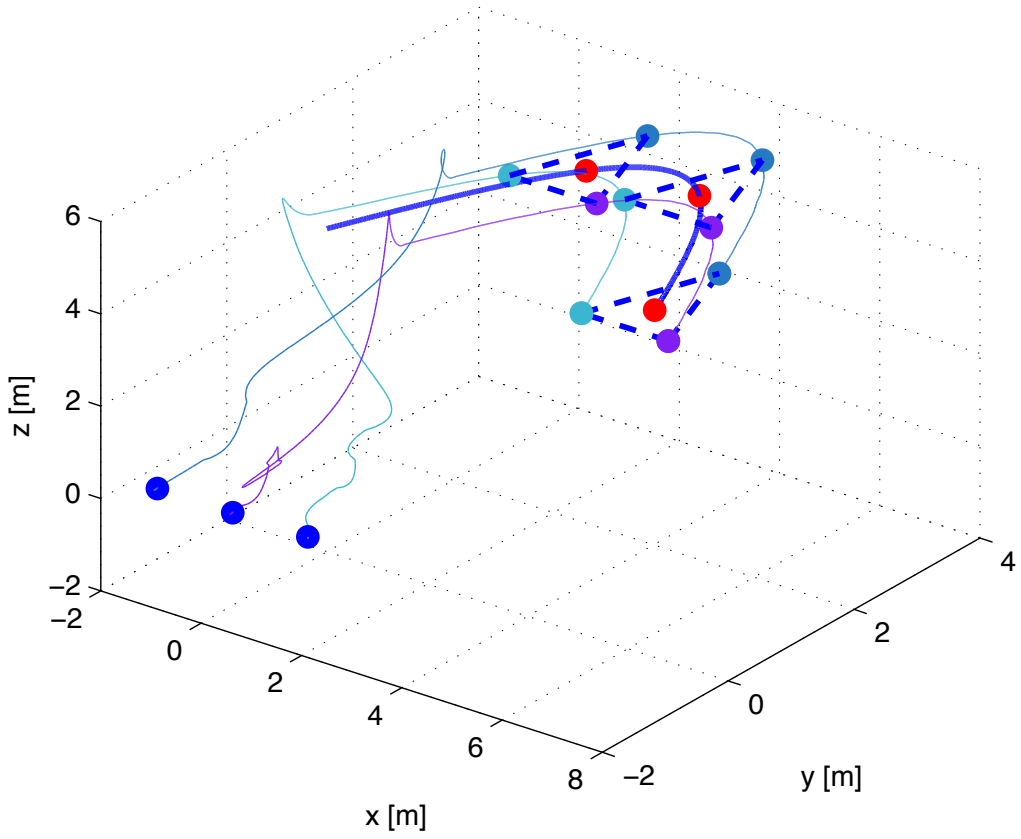

Figure 4.41: The formation of three quadrotors.

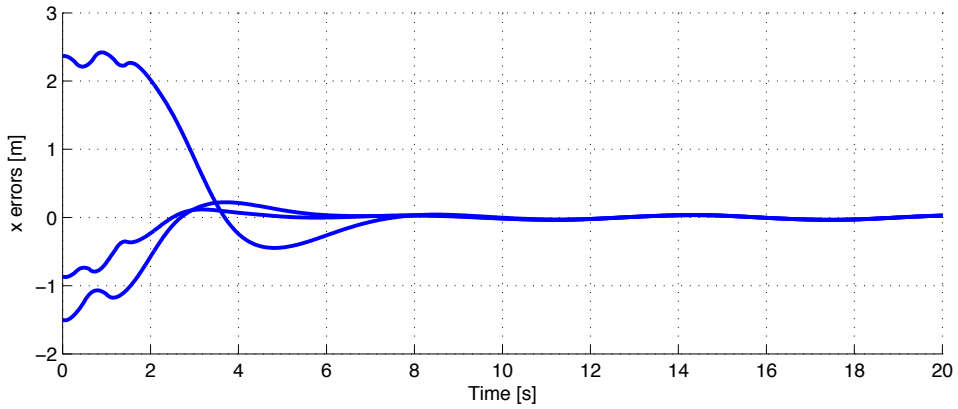

Figure 4.42: x tracking errors.

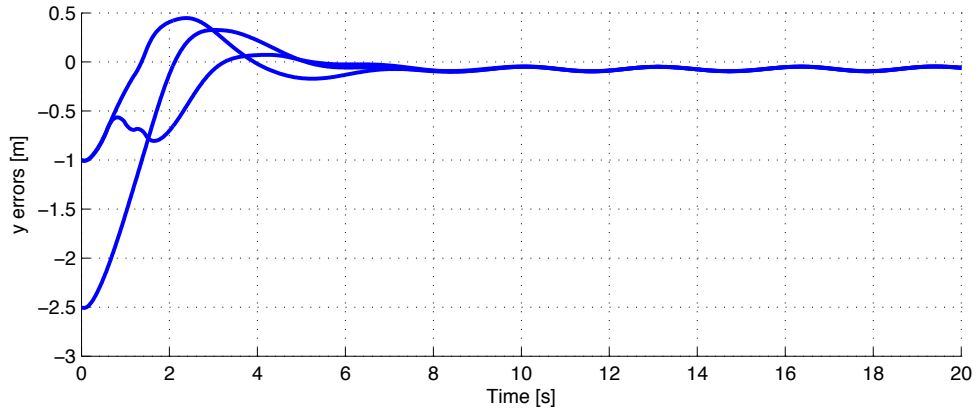

Figure 4.43: y tracking errors.

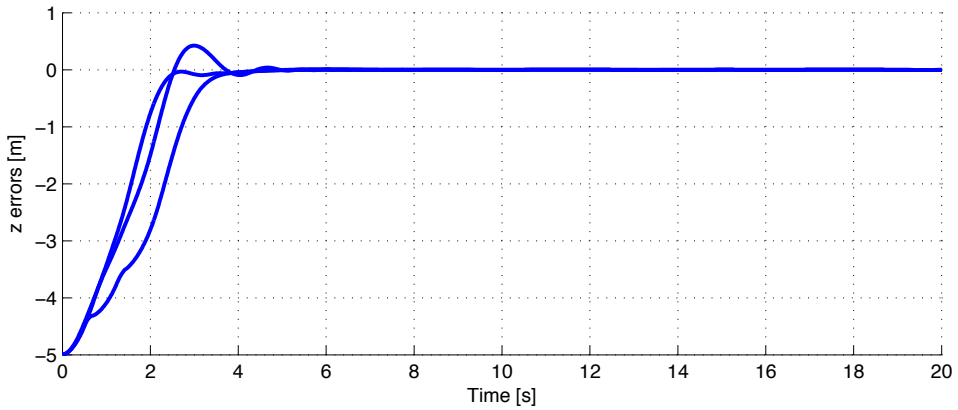

Figure 4.44: z tracking errors.

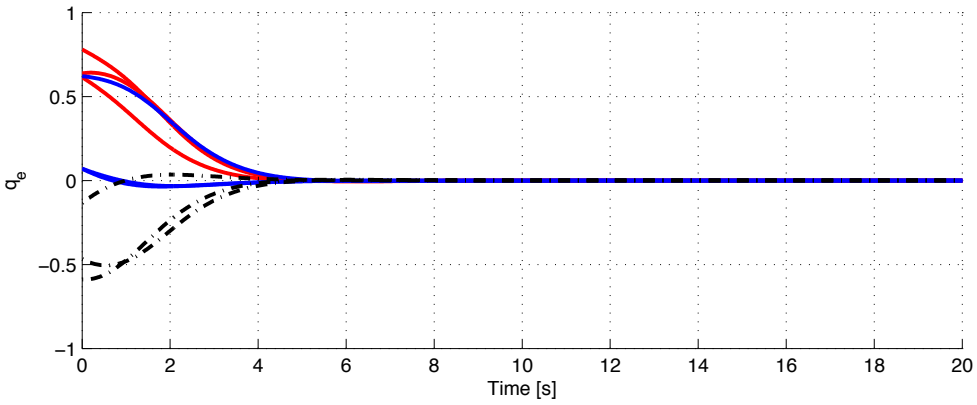

Figure 4.45: Attitude tracking errors.

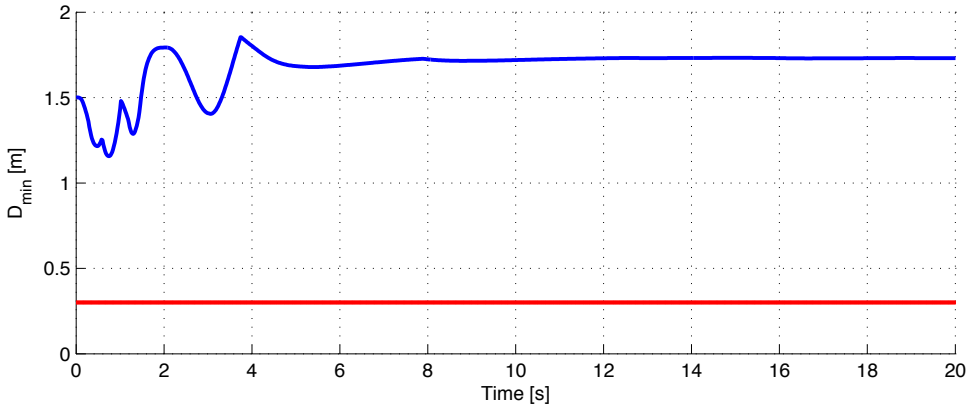

Figure 4.46: The minimum distance among quadrotors.

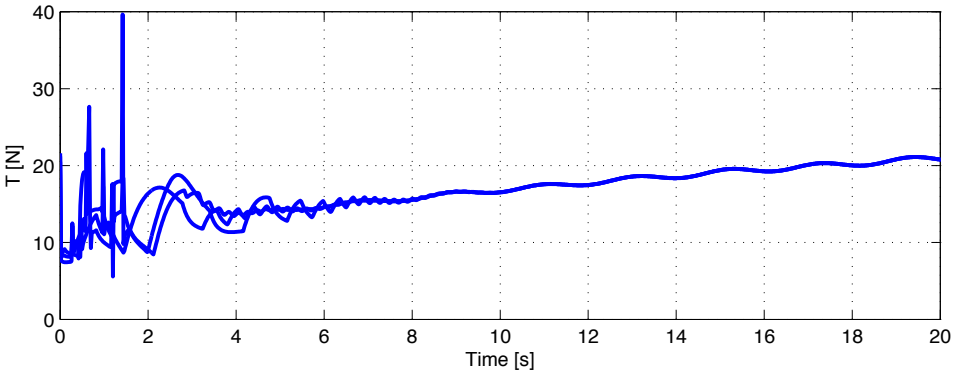

Figure 4.47: Force of three quadrotors.

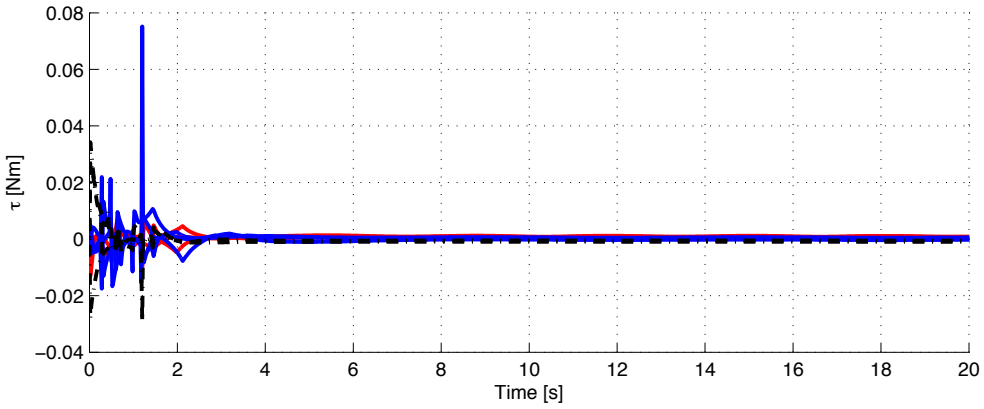

Figure 4.48: Torque of three quadrotors.

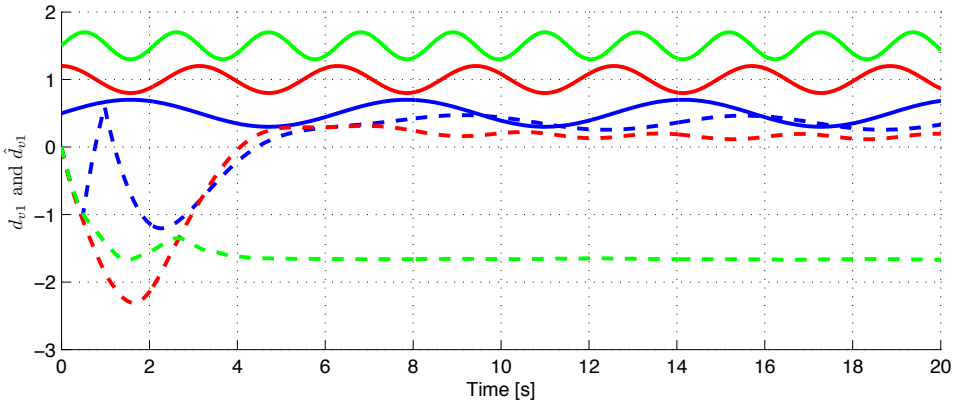

Figure 4.49: Disturbances and estimations of $\boldsymbol{d}_v$ of the quadrotor 1

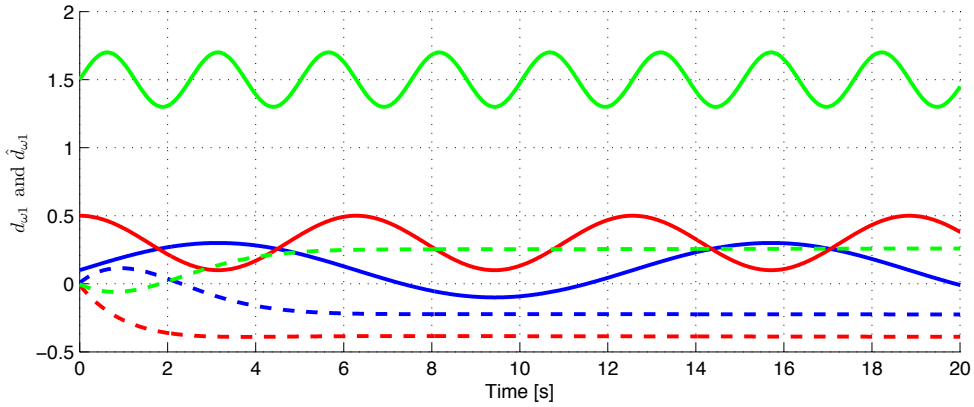

Figure 4.50: Disturbances and estimations of $\boldsymbol{d}_o$ of the quadrotor 1

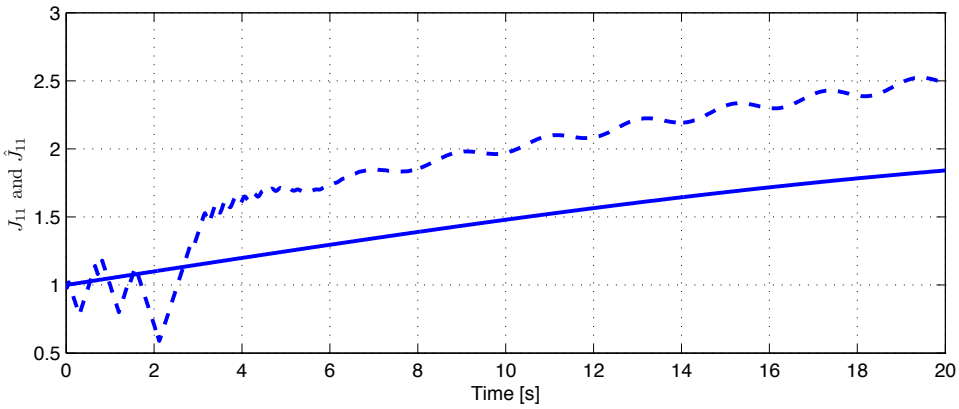

Figure 4.51: Uncertainty and estimation of mass of the quadrotor 1

Case 2: Formation of three quadrotors distributed on a circle shape while tracking a sine path is simulated. The disturbance with random signal acting on translational and rotational subsystem is chosen as in (4.115)

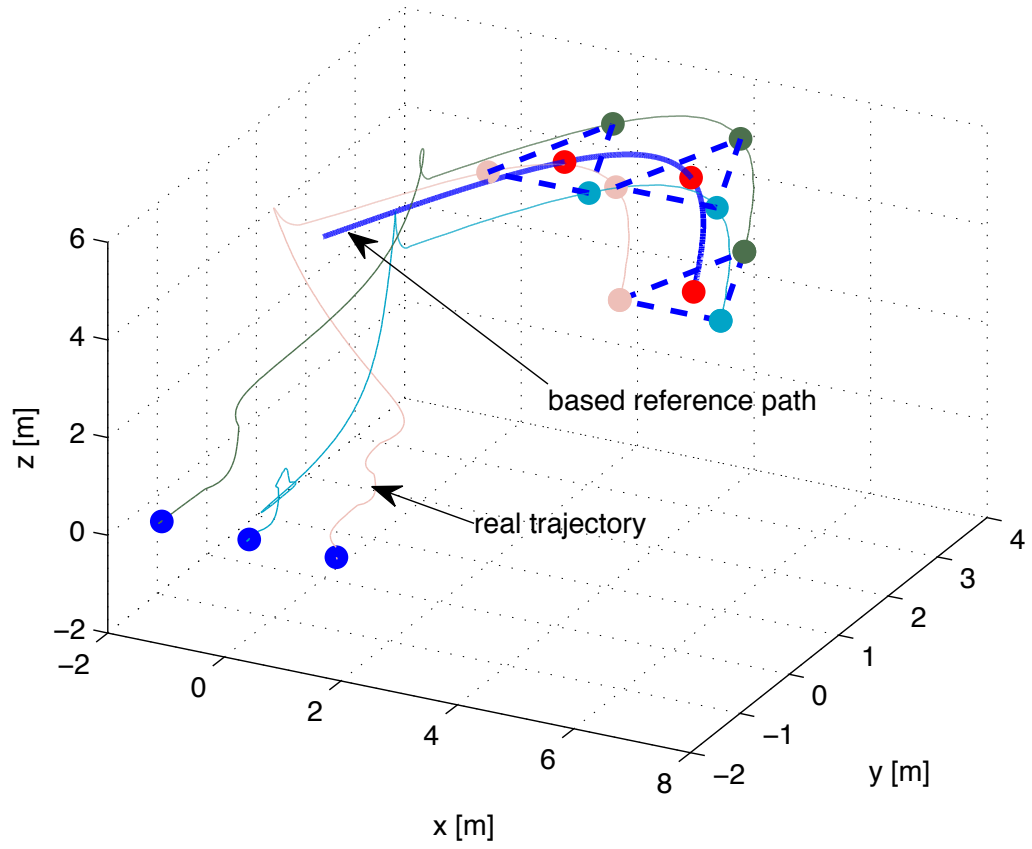

Figure 4.52: The formation of three quadrotors.

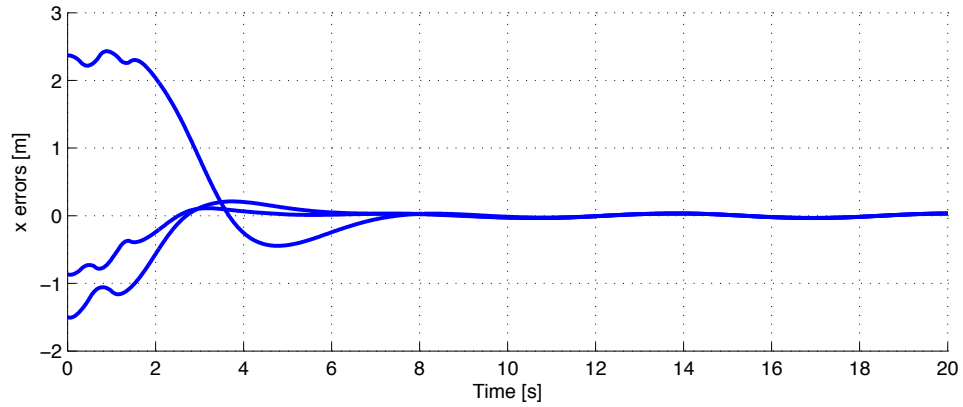

Figure 4.53: x tracking errors.

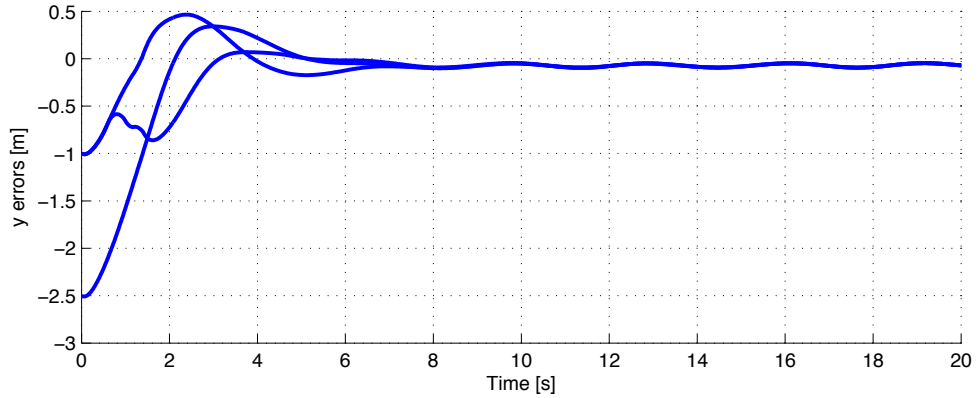

Figure 4.54: y tracking errors.

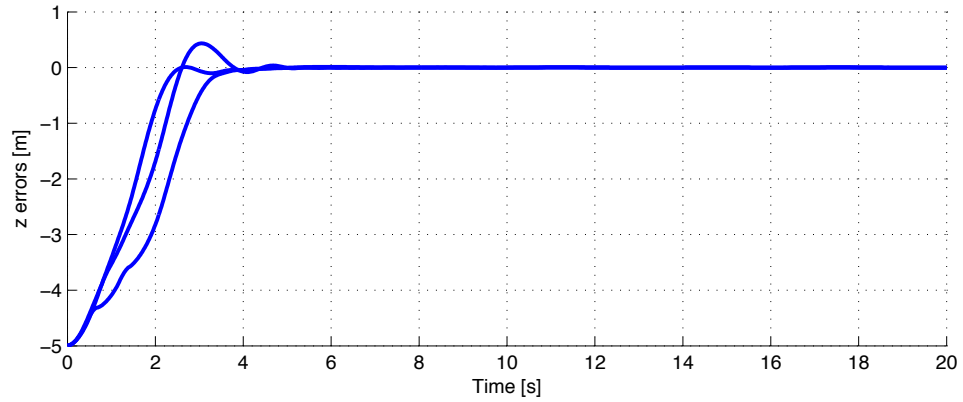

Figure 4.55: z tracking errors.

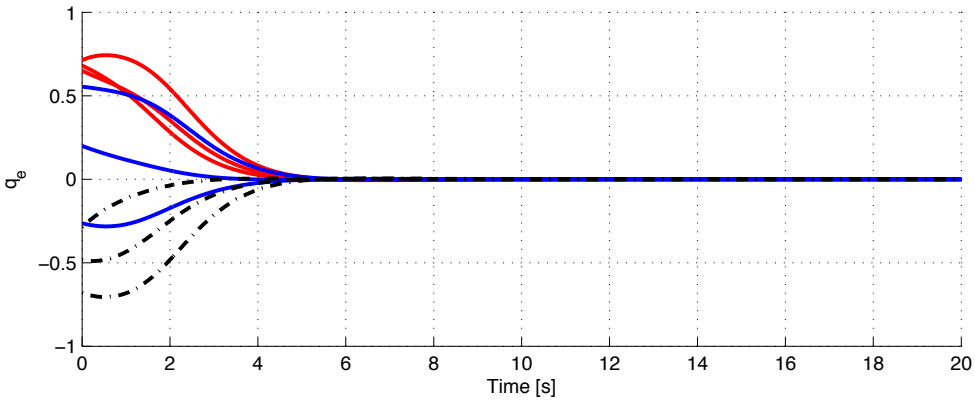

Figure 4.56: Attitude tracking errors.

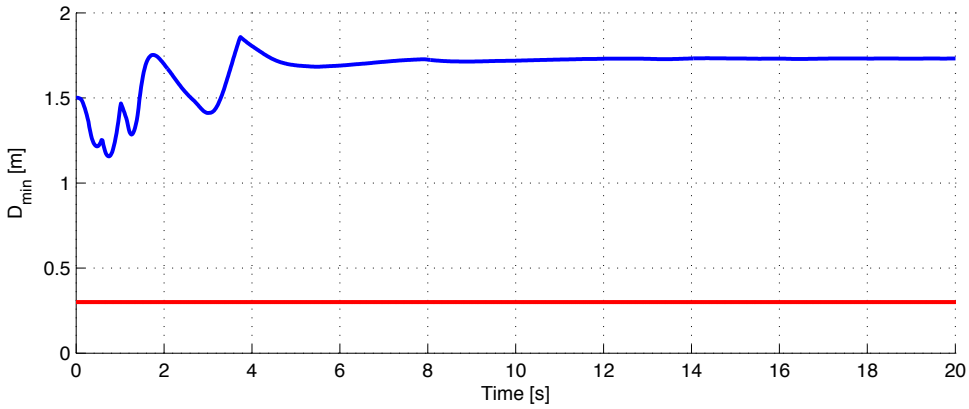

Figure 4.57: The minimum distance among quadrotors.

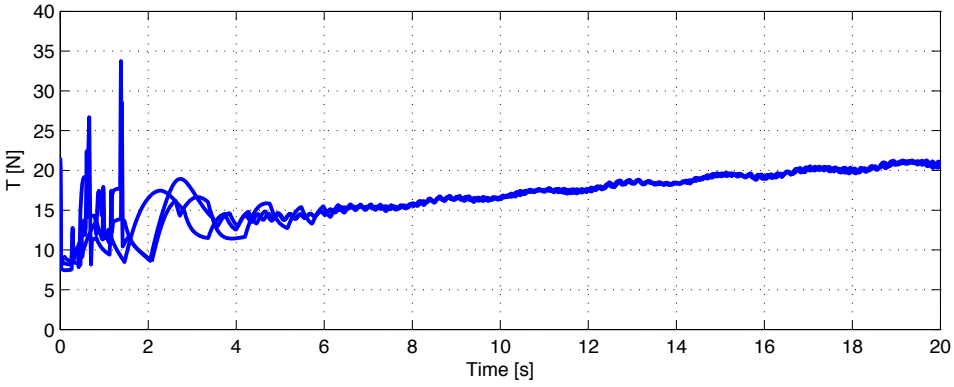

Figure 4.58: Thrust force of three quadrotors.

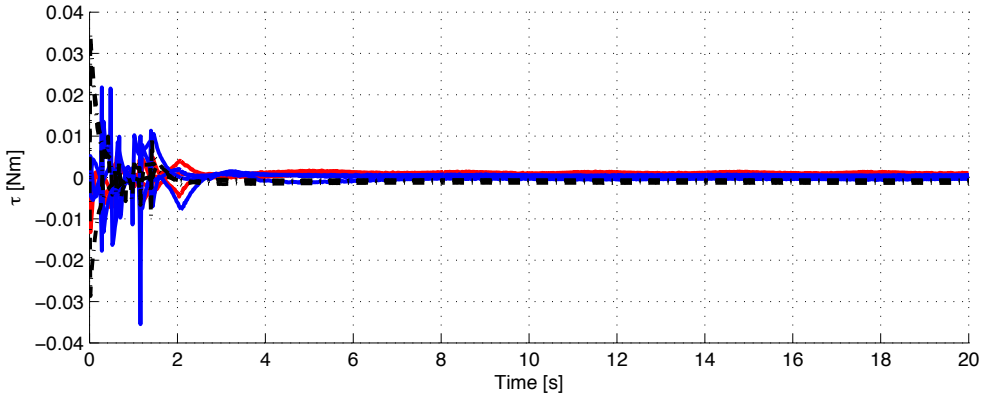

Figure 4.59: Torque of three quadrotors.

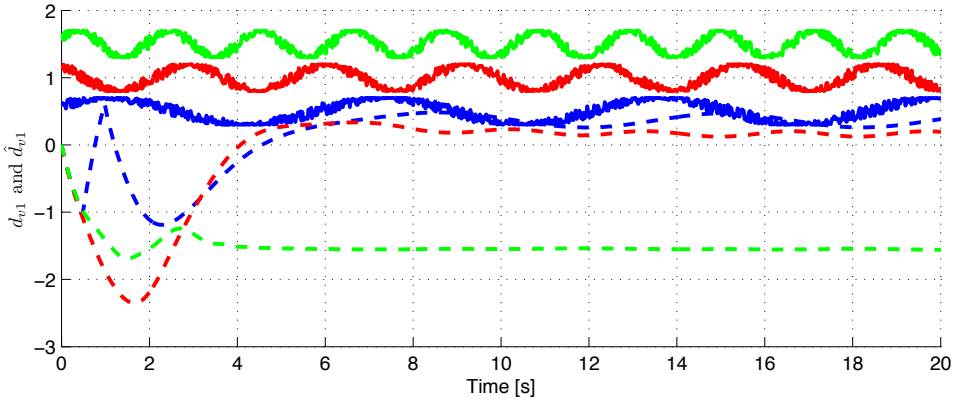

Figure 4.60: Disturbances and estimations of $\boldsymbol{d}_v$ of the quadrotor 1

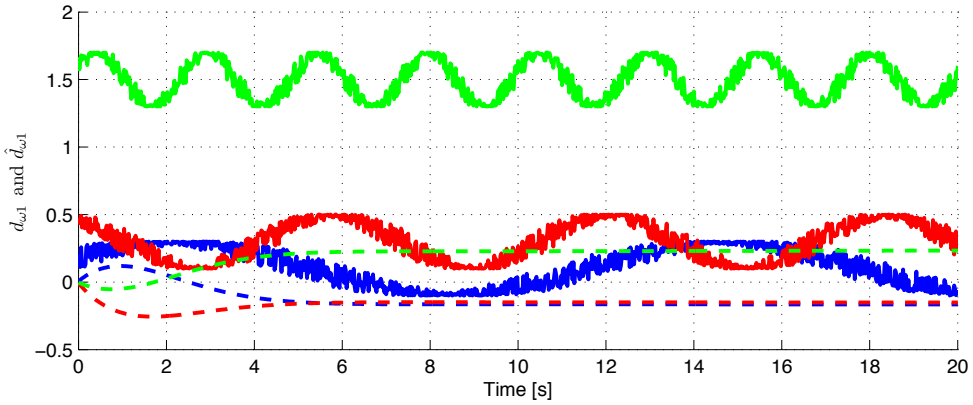

Figure 4.61: Disturbances and estimations of $\boldsymbol{d}_o$ of the quadrotor 1

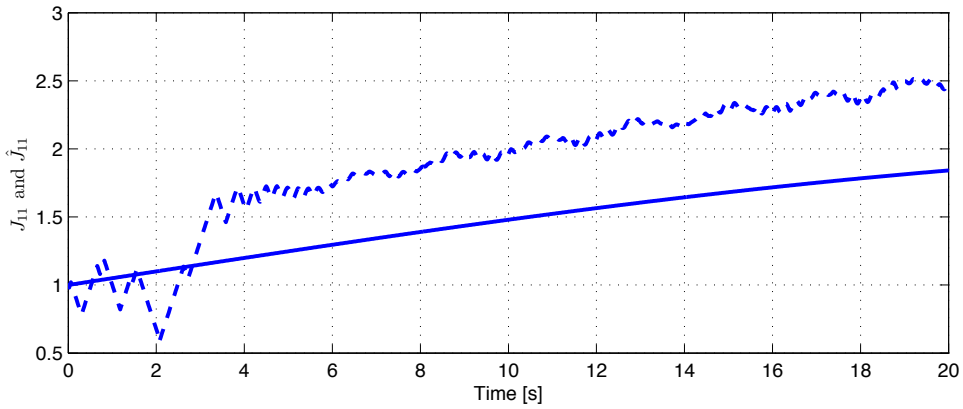

Figure 4.62: Uncertainty and estimation of mass of the quadrotor 1

4.4.4 Conclusion

An adaptive formation controller was presented. Uncertainty and external disturbances are estimated by employing adaptive backstepping method. The simulation results demonstrated that the proposed controller works well with changing of unknown parameters and external disturbances. The total force for each quadrotor is still high and the formation is not rotative during tracking the reference path. These problems are going to concern in the next section.

4.5 Controller 4 - Leader-follower with limited sensing

In this section, a leader-follower formation controller is developed. Assuming that the dynamics of quadrotor has disturbances from environment and the mass and inertia matrix are unknown. Moreover, only quadrotor in the sensing range can exchange their information. The problems in the previous section, the rotation of formation along the predefined path is also concerned.

4.5.1 Control objective

The dynamics of quadrotor is written as in (4.116)

$$\begin{aligned}
\dot{\boldsymbol{p}}_{ij} &= \boldsymbol{v}_{ij} \\
\dot{\boldsymbol{v}}_{ij} &= g\boldsymbol{e}_3 - \tfrac{T_{ij}}{m_{ij}}\boldsymbol{R}_Q^T(\boldsymbol{Q}_{ij})e_3 + \boldsymbol{d}_{vij} \\
\dot{\boldsymbol{Q}}_{ij} &= \boldsymbol{K}_Q(\boldsymbol{Q}_{ij})\boldsymbol{\omega}_{ij} \\
\dot{\boldsymbol{\omega}}_{ij} &= \boldsymbol{J}_{ij}^{-1}\boldsymbol{\tau}_{ij} - \boldsymbol{J}_{ij}^{-1}\boldsymbol{S}(\boldsymbol{\omega}_{ij})\boldsymbol{J}_{ij}\boldsymbol{\omega}_{ij} + \boldsymbol{d}_{\omega ij}
\end{aligned} \tag{4.116}$$

where $ij \in \mathbb{N}$, $\mathbb{N}$ is the set of all quadrotors in the group. $\boldsymbol{d}_{vij} \in \mathbb{R}^3$ and $\boldsymbol{d}_{\omega ij} \in \mathbb{R}^3$ are unknown disturbance matrices, m_{ij} and $\boldsymbol{J}_{ij} \in \mathbb{R}^{3\times 3}$ are unknown mass and inertial matrices, all the other symbols in (4.116) are defined as in Section 2.1.

Before starting the formation control objective we impose the following assumption on the reference trajectories, communication and initial conditions between the quadrotor in the group

Assumption 4.5.

1. *Let us define the formation of a group of quadrotors and the initial position of the leader quadrotor as follows*

$$\begin{aligned} \boldsymbol{L}_{LdLi} &= [x_{LdLi}\, y_{LdLi}\, z_{LdLi}]^T \\ \boldsymbol{p}_{Li}(t) &= [x_{i1}(t)\, y_{i1}(t)\, z_{i1}(t)]^T \end{aligned} \tag{4.117}$$

   where $\boldsymbol{L}_{Ldi}$ defines the formation shape of the leader quadrotors and $\boldsymbol{p}_{Li}$ is position vector of the leader quadrotors and it is defined as the first quadrotor in each group. The follower dynamics then is defined as follows

$$\begin{aligned} \boldsymbol{L}_{F\_Ldij} &= [x_{F\_Ldij}\, y_{F\_Ldij}\, z_{F\_Ldij}]^T \\ \boldsymbol{p}_{F\_Lij}(t) &= [x_{F\_Lij}(t)\, y_{F\_Lij}(t)\, z_{F\_Lij}(t)]^T \end{aligned} \tag{4.118}$$

   where $\boldsymbol{L}_{F\_Ldij}$ defines the formation shape of the follower quadrotors and $\boldsymbol{p}_{F\_Lij}(t)$ is position vector of follower quadrotors in the $\boldsymbol{p}_{Li}$ group.

2. *The reference position trajectory $\boldsymbol{p}_d(t) = [x_d(t)\, y_d(t)\, z_d(t)]^T$ and the heading angle ψ_d are the based path for the leader quadrotors to track satisfying the assumption 4.4. The other initial values satisfy that there is no collision and all the quadrotors are in the sensing range.*

3. *Let us define*

$$\begin{aligned} \boldsymbol{p}_{ijmn} &= \boldsymbol{p}_{ij} - \boldsymbol{p}_{mn} \\ \boldsymbol{\alpha}_{ijmn} &= \tfrac{1}{2}\boldsymbol{p}_{ijmn}^T \boldsymbol{p}_{ijmn} \end{aligned} \tag{4.119}$$

   where $ij \in \mathbb{N}_{mn}$, $\mathbb{N}_{mn}$ is the set of all quadrotors in the sensing range except the quadrotor ij.

   To avoid collision and keep all the quadrotors in the sensing range, the collision avoidance function is chosen as follows

$$\beta_{ijmn} = k_\beta \frac{1 - h(\alpha_{ijmn}, \alpha^S_{ijmn}, \alpha^S_{ijmn} + \delta) + h(\alpha_{ijmn}, \alpha^R_{ijmn} - \delta, \alpha^R_{ijmn})}{\alpha_{ijmn}} \tag{4.120}$$

where δ is a positive constant defined the working zone of the obstacle avoidance function.

Remark 4.5. *In the Assumption 4.5, property (1) is the definition for formation shape of the leaders and followers. Property (2) implies that at the initial time, there is no collision between all the quadrotors and the reference path smooth for tracking. Property (3) illustrates a definition of an obstacle avoidance which guarantees capacity of communication and no collision among the quadrotors.*

Control Objective 4.4. *Under the Assumption 4.5, first we design control input T_{Li} and τ_{Li} such that the Leader quadrotor vector $\boldsymbol{p}_{Li}(t)$ globally track the reference trajectory $\boldsymbol{p}_{Ldi}(t) = \boldsymbol{p}_d + \boldsymbol{L}_{LdLi}$.*

Then for each quadrotor in the group, design control for the followers to track their references formed by vector $\boldsymbol{p}_{F\_Ldij}(t) = \boldsymbol{p}_{Li} + \boldsymbol{L}_{F\_Ldij}$*. In more detail, For each quadrotor* F_Lij*, design the control inputs* T_{F_Lij} *and* $\boldsymbol{\tau}_{F\_Lij}$ *such that the position vector* $\boldsymbol{p}_{F\_Lij}(t)$ *of the follower quadrotor* F_Lij *track their reference trajectories* $\boldsymbol{p}_{F\_Ldij}(t)$ *while avoid collision with all other quadrotors and keep them in the sensing range. The environment disturbance, mass and inertia matrix are unknown. Specifically, we design the control inputs* T_{Li}*,* $\boldsymbol{\tau}_{Li}$*,* T_{F_Lij} *and* $\boldsymbol{\tau}_{F\_Lij}$ *such that*

$$\begin{aligned}
&\lim_{t\to\infty} \left(\boldsymbol{p}_{Li}(t) - \boldsymbol{p}_{Ldi}(t)\right) = 0,\\
&\lim_{t\to\infty} \left(\psi_{Li}(t) - \psi_{di}(t)\right) = 0\\
&\lim_{t\to\infty} \left(\boldsymbol{p}_{F_Lij}(t) - \boldsymbol{p}_{F_Ldij}(t)\right) = 0,\\
&\lim_{t\to\infty} \left(\psi_{F_Lij}(t) - \psi_{Li}(t)\right) = 0\\
&\|\boldsymbol{p}_{ij} - \boldsymbol{p}_{mn}\| \geq \alpha^S_{ijmn}
\end{aligned} \tag{4.121}$$

For all $ij \in \mathbb{N}, ij \neq mn$ *and* $t \geq t_0 \geq 0$*, the control design needs to keep all other states of the quadrotor dynamics bounded for all initial conditions.*

4.5.2 Control Design

In this section we will use adaptive backstepping technique [KKK95] to design control for a formation of quadrotor satisfying the control objective 4.4. In first step, the controller for the leader quadrotor track the predefined path is designed. After that the reference formation of followers is formed then the control inputs T_{Li}, $\boldsymbol{\tau}_{Li}$, T_{F_Lij} and $\boldsymbol{\tau}_{F\_Lij}$ are constructed.

Step 1

In this step, the control inputs to force the leader quadrotors tracking their references are designed. The control design process is similar in the previous section. For convenience, the details of these steps are represented. Two groups, leaders and followers, are concerned. First the translational dynamics of (4.116) is considered. We will design a virtual control of $\boldsymbol{v}_{Li}$ to force $\boldsymbol{p}_{Li}(t)$ to globally asymptotically track its reference trajectory $\boldsymbol{p}_{Ldi}(t)$, and design a virtual control of $\boldsymbol{v}_{F\_Lij}$ to force $\boldsymbol{p}_{F\_Lij}(t)$ to globally asymptotically track its reference trajectory $\boldsymbol{p}_{F\_Ldij}(t)$ As such, we define the tracking errors as follows:

$$\begin{aligned}
\boldsymbol{p}_{eLi} &= \boldsymbol{p}_{Li} - \boldsymbol{p}_{Ldi},\\
\boldsymbol{v}_{eLi} &= \boldsymbol{v}_{Li} - \boldsymbol{\alpha}_{vLi},\\
\boldsymbol{p}_{eF_Lij} &= \boldsymbol{p}_{F_Lij} - \boldsymbol{p}_{F_Ldij},\\
\boldsymbol{v}_{eF_Lij} &= \boldsymbol{v}_{F_Lij} - \boldsymbol{\alpha}_{vF_Lij},
\end{aligned} \tag{4.122}$$

where $\boldsymbol{\alpha}_{vLi}$ is a virtual control of leader velocity $\boldsymbol{v}_{Li}$ and $\boldsymbol{\alpha}_{vF\_Lij}$ is a virtual control of follower velocity $\boldsymbol{v}_{F\_Lij}$.

Differentiating both sides of (4.122) and using the first subsystem of (4.116), the error dynamics

are expressed as

$$\begin{aligned}
\dot{\boldsymbol{p}}_{eLi} &= \boldsymbol{v}_{eLi} + \boldsymbol{\alpha}_{vLi} - \dot{\boldsymbol{p}}_{Ldi}, \\
\dot{\boldsymbol{v}}_{eLi} &= g\boldsymbol{e}_3 - J_{1Li}\boldsymbol{F}_{Li} + \boldsymbol{d}_{vLi} - \dot{\boldsymbol{\alpha}}_{vLi} \\
\dot{\boldsymbol{p}}_{F_Lij} &= \boldsymbol{v}_{eF_Lij} + \boldsymbol{\alpha}_{vF_Lij} - \dot{\boldsymbol{p}}_{F_Lij}, \\
\dot{\boldsymbol{v}}_{eF_Lij} &= g\boldsymbol{e}_3 - J_{1F_Lij}\boldsymbol{F}_{F_Lij} + \boldsymbol{d}_{vF_Lij} - \dot{\boldsymbol{\alpha}}_{vF_Lij}
\end{aligned} \tag{4.123}$$

where $\boldsymbol{F}_{Li}$ is an intermediate control input of the leader Li and $\boldsymbol{F}_{Li} = T_{Li}\boldsymbol{R}_Q^T(\boldsymbol{Q}_{Ldi})\boldsymbol{e}_3$ is illustrated in the ideal case where $\boldsymbol{Q}_{di}$ is obtained via Lemma 2.3. Similarly, $\boldsymbol{F}_{F\_Lij}$ is an intermediate control input of the follower F_Lij where $\boldsymbol{F}_{F\_Lij} = T_{F\_Lij}\boldsymbol{R}_Q^T(\boldsymbol{Q}_{F\_Ldij})\boldsymbol{e}_3$ and $\boldsymbol{Q}_{F\_Ldij}$ is also obtained via Lemma 2.3.

In order to design the intermediate control input $\boldsymbol{F}_{Li}$ for the leader quadrotor Li and the intermediate control input $\boldsymbol{F}_{F\_Lij}$ for the follower quadrotor F_Lij achieving the Formation control objective 4.4, we consider the following potential function:

$$V_{1a} = \frac{1}{2}\sum_{i=1}^{NL}\sum_{j=1}^{NF(i)}\left[\boldsymbol{p}_{eLi}^T\boldsymbol{p}_{eLi} + \sum_{ij\in\mathbb{N}_{ij}}\beta_{ijmn}\right] \tag{4.124}$$

where $\mathbb{N}_{ij}$ is the set containing all the quadrotors in the sensing range except for the quadrotor ij, NL is number of leaders, and $NF(i)$ is number of followers in the group i. β_{ijmn} is taken from (4.120) where α_{ijmn} is calculated from (4.119).

Differentiating both sides of (4.124) gives

$$\begin{aligned}
\dot{V}_{1a} &= \sum_{i=1}^{NL}\sum_{j=1}^{NF(i)}\left[\boldsymbol{p}_{eLi}^T\dot{\boldsymbol{p}}_{eLi} + \sum_{ij\in\mathbb{N}_{ij}}\beta'_{\text{ijmn}}\dot{\alpha}_{\text{ijmn}}\right] \\
&= \sum_{i=1}^{NL}\sum_{j=1}^{NF(i)}\left[\boldsymbol{p}_{eLi}^T\dot{\boldsymbol{p}}_{eLi} + \sum_{ij\in\mathbb{N}_{ij}}\beta'_{ijmn}\boldsymbol{p}_{ijmn}^T\dot{\boldsymbol{p}}_{ijmn}\right]
\end{aligned} \tag{4.125}$$

Noting that $\dot{\boldsymbol{p}}_{ijmn} = (\dot{\boldsymbol{p}}_{ij} - \dot{\boldsymbol{p}}_{Ldij}) - (\dot{\boldsymbol{p}}_{mn} - \dot{\boldsymbol{p}}_{Ldmn}) = \boldsymbol{v}_{eLij} - \boldsymbol{v}_{eLmn}$, we can write (4.125) as follows

$$\begin{aligned}
\dot{V}_{1a} &= \sum_{i=1}^{NL}\sum_{j=1}^{NF(i)}(\boldsymbol{p}_{eLi}^T + \sum_{ij\in\mathbb{N}_{ij}}\beta'_{ijmn}\boldsymbol{p}_{ijmn}^T)(\boldsymbol{v}_{eLi} + \boldsymbol{\alpha}_{vLi} - \dot{\boldsymbol{p}}_{Ldi}) \\
&= \sum_{i=1}^{NL}\sum_{j=1}^{NF(i)}\boldsymbol{\Omega}_{Li}^T(\boldsymbol{v}_{eLi} + \boldsymbol{\alpha}_{vLi} - \dot{\boldsymbol{p}}_{Ldi})
\end{aligned} \tag{4.126}$$

where

$$\boldsymbol{\Omega}_{Li} = \boldsymbol{p}_{eLi} + \sum_{ij\in\mathbb{N}_{ij}}\beta'_{ijmn}\boldsymbol{p}_{ijmn} \tag{4.127}$$

The equation (4.126) suggests that we choose

$$\boldsymbol{\alpha}_{vLi} = -k_1\boldsymbol{\Omega}_{Li} + \dot{\boldsymbol{p}}_{Ldi} \tag{4.128}$$

To design the intermediate control input $\boldsymbol{F}_{Li}$, considering the following Lyapunov function

$$V_{2a} = V_{1a} + \frac{1}{2}\sum_{i=1}^{NL}\sum_{j=1}^{NF(i)} {\boldsymbol{v}_{ei}}^T \boldsymbol{v}_{ei} \tag{4.129}$$

Differentiating both sides of (4.129) gives

$$\begin{aligned}
\dot{V}_{2a} &= \sum_{i=1}^{NL}\sum_{j=1}^{NF(i)} \left[-k_1 \boldsymbol{\Omega}_{Li}^T \boldsymbol{\Omega}_{Li} + \boldsymbol{v}_{ei}^T (ge_3 - J_{1Li}\boldsymbol{F}_{Li} - \dot{\boldsymbol{\alpha}}_{vLi} + \boldsymbol{\Omega}_{Li} + \boldsymbol{d}_{vLi})\right] \\
&= \sum_{i=1}^{NL}\sum_{j=1}^{NF(i)} \left[-k_1 \boldsymbol{\Omega}_{Li}^T \boldsymbol{\Omega}_{Li} + {\boldsymbol{v}_{eLi}}^T (ge_3 - \hat{J}_{1Li}\boldsymbol{F}_{Li} - \dot{\boldsymbol{\alpha}}_{vLi} + \boldsymbol{\Omega}_{Li} + \hat{\boldsymbol{d}}_{vLi})\right] \\
&\quad + \sum_{i=1}^{NL}\sum_{j=1}^{NF(i)} \left[\boldsymbol{v}_{eLi}^T (-\tilde{J}_{1Li}\boldsymbol{F}_{Li} + \tilde{\boldsymbol{d}}_{vLi})\right]
\end{aligned} \tag{4.130}$$

which suggests that we choose:

$$\boldsymbol{F}_{Li} = (k_2 \boldsymbol{v}_{\boldsymbol{eLi}} + ge_3 - \dot{\boldsymbol{\alpha}}_{vLi} + \boldsymbol{\Omega}_{Li} + \hat{\boldsymbol{d}}_{vLi})/\hat{J}_{1Li} \tag{4.131}$$

where $\hat{J}_{1Li}$ and $\hat{\boldsymbol{d}}_{vLi}$ are estimations of J_{1Li} and $\boldsymbol{d}_{vLi}$, respectively. The update laws for these estimations and are chosen as follows

$$\begin{aligned}
\dot{\hat{J}}_{1Li} &= proj(\gamma_{1v} \boldsymbol{v}_{eLi}^T \boldsymbol{F}_{Li}) \\
\dot{\hat{\boldsymbol{d}}}_{vLi} &= \gamma_{2v} \boldsymbol{v}_{eLi}
\end{aligned} \tag{4.132}$$

For the follower group, the design process is similar as above. The intermediate control force $\boldsymbol{F}_{F\_Lij}$ is constructed by considering the following Lyapunov function

$$V_{1b} = \frac{1}{2}\sum_{i=1}^{NL}\sum_{j=1}^{NF(i)} \left[\boldsymbol{p}_{eF\_Lij}^T \boldsymbol{p}_{eF\_Lij} + \sum_{ij\in\mathbb{N}_{ij}} \beta_{ijmn}\right] \tag{4.133}$$

Differentiating both sides of (4.133) gives

$$\begin{aligned}
\dot{V}_{1b} &= \sum_{i=1}^{NL}\sum_{j=1}^{NF(i)} \left[\boldsymbol{p}_{eF_Lij}^T \dot{\boldsymbol{p}}_{eF_Lij} + \sum_{ij\in\mathbb{N}_{ij}} \beta'_{\text{ijmn}} \dot{\alpha}_{\text{ijmn}}\right] \\
&= \sum_{i=1}^{NL}\sum_{j=1}^{NF(i)} \left[\boldsymbol{p}_{eF_Lij}^T \dot{\boldsymbol{p}}_{eF_Lij} + \sum_{ij\in\mathbb{N}_{ij}} \beta'_{ijmn} \boldsymbol{p}_{ijmn}^T \dot{\boldsymbol{p}}_{ijmn}\right]
\end{aligned} \tag{4.134}$$

Noting that $\dot{\boldsymbol{p}}_{ijmn} = (\dot{\boldsymbol{p}}_{ij} - \dot{\boldsymbol{p}}_{F\_Ldij}) - (\dot{\boldsymbol{p}}_{mn} - \dot{\boldsymbol{p}}_{F\_Ldmn}) = \boldsymbol{v}_{eF\_Lij} - \boldsymbol{v}_{eF\_Lmn}$, we can write

(4.134) as follows

$$\begin{aligned}\dot{V}_{1b} &= \sum_{i=1}^{NL}\sum_{j=1}^{NF(i)}(\boldsymbol{p}_{eF\_Lij}^T + \sum_{ij\in\mathbb{N}_{ij}}\beta'_{ijmn}\boldsymbol{p}_{ijmn}^T)(\boldsymbol{v}_{eF\_Lij} + \boldsymbol{\alpha}_{vF\_Lij} - \dot{\boldsymbol{p}}_{F\_Ldij}) \\ &= \sum_{i=1}^{NL}\sum_{j=1}^{NF(i)}\boldsymbol{\Omega}_{F\_Lij}^T(\boldsymbol{v}_{eF\_Lij} + \boldsymbol{\alpha}_{vF\_Lij} - \dot{\boldsymbol{p}}_{F\_Ldij})\end{aligned} \tag{4.135}$$

where

$$\boldsymbol{\Omega}_{F\_Lij} = \boldsymbol{p}_{eF\_Lij} + \sum_{ij\in\mathbb{N}_{ij}}\beta'_{ijmn}\boldsymbol{p}_{ijmn} \tag{4.136}$$

The equation (4.135) suggests that we choose

$$\boldsymbol{\alpha}_{vF\_Lij} = -k_1\boldsymbol{\Omega}_{F\_Lij} + \dot{\boldsymbol{p}}_{F\_Ldi} \tag{4.137}$$

To design the intermediate control input $\boldsymbol{F}_{F\_Lij}$, considering the following Lyapunov function

$$V_{2b} = V_{1b} + \frac{1}{2}\sum_{i=1}^{NL}\sum_{j=1}^{NF(i)}\boldsymbol{v}_{eF\_Lij}{}^T\boldsymbol{v}_{eF\_Lij} \tag{4.138}$$

Differentiating both sides of (4.138) gives

$$\begin{aligned}\dot{V}_{2b} &= \sum_{i=1}^{NL}\sum_{j=1}^{NF(i)}\Big[-k_1\boldsymbol{\Omega}_{F\_Lij}^T\boldsymbol{\Omega}_{F\_Lij} + \boldsymbol{v}_{eF\_Lij}^T(ge_3 - J_{1F\_Lij}\boldsymbol{F}_{F\_Lij} - \dot{\boldsymbol{\alpha}}_{vF\_Lij} + \boldsymbol{\Omega}_{F\_Lij} + \boldsymbol{d}_{vF\_Lij})\Big] \\ &= \sum_{i=1}^{NL}\sum_{j=1}^{NF(i)}\Big[-k_1\boldsymbol{\Omega}_{F\_Lij}^T\boldsymbol{\Omega}_{F\_Lij} + \boldsymbol{v}_{eF\_Lij}{}^T(ge_3 - \hat{J}_{1F\_Lij}\boldsymbol{F}_{F\_Lij} - \dot{\boldsymbol{\alpha}}_{vF\_Lij} + \boldsymbol{\Omega}_{F\_Lij} + \hat{\boldsymbol{d}}_{vF\_Lij})\Big] \\ &\quad + \sum_{i=1}^{NL}\sum_{j=1}^{NF(i)}\Big[\boldsymbol{v}_{eF\_Lij}^T(-\tilde{J}_{1F\_Lij}\boldsymbol{F}_{F\_Lij} + \tilde{\boldsymbol{d}}_{vF\_Lij})\Big]\end{aligned} \tag{4.139}$$

which suggests that we choose:

$$\boldsymbol{F}_{F\_Lij} = (k_2\boldsymbol{v}_{\boldsymbol{eF\_Lij}} + ge_3 - \dot{\boldsymbol{\alpha}}_{vF\_Lij} + \boldsymbol{\Omega}_{F\_Lij} + \hat{\boldsymbol{d}}_{vF\_Lij})/\hat{J}_{1F\_Lij} \tag{4.140}$$

where $\hat{J}_{1F\_Lij}$ and $\hat{\boldsymbol{d}}_{vF\_Lij}$ are estimations of J_{1F_Lij} and $\boldsymbol{d}_{vF\_Lij}$, respectively. The update laws for these estimations and are chosen as follows

$$\begin{aligned}\dot{\hat{J}}_{1F\_Lij} &= proj(\gamma_{1v}\boldsymbol{v}_{eF\_Lij}^T\boldsymbol{F}_{F\_Lij}) \\ \dot{\hat{\boldsymbol{d}}}_{vF\_Lij} &= \gamma_{2v}\boldsymbol{v}_{eF\_Lij}\end{aligned} \tag{4.141}$$

We assume that the intermediate control input $\boldsymbol{F}_{Li}$ forces the leader quadrotor Li tracking the predefined path $\boldsymbol{p}_{Ldi}$ and heading angle ψ_{di} is in the ideal case where the heading angle error is equal zero. Similarly, the intermediate control input $\boldsymbol{F}_{F\_Lij}$ forces the follower quadrotor F_Lij tracking the leader position $\boldsymbol{p}_{F\_Ldij}$ and heading angle ψ_{Ldi} is also having no error with

the heading tracking. Applying Lemma 2.3 for these intermediate control inputs, we obtain the thrust T_{Fi}, $\boldsymbol{Q}_{Ldi}$, T_{F_Lij} and $\boldsymbol{Q}_{F\_Ldij}$ as follows:

$$
\begin{aligned}
T_{Li} &= \|\boldsymbol{F}_{Li}\| \\
\boldsymbol{Q}_{Ldi} &= \begin{bmatrix} C\frac{\alpha_{\phi Li}}{2}C\frac{\alpha_{\theta Li}}{2}C\frac{\alpha_{\psi Li}}{2} + S\frac{\alpha_{\phi Li}}{2}S\frac{\alpha_{\theta Li}}{2}S\frac{\alpha_{\psi Li}}{2} \\ S\frac{\alpha_{\phi Li}}{2}C\frac{\alpha_{\theta Li}}{2}C\frac{\alpha_{\psi Li}}{2} - C\frac{\alpha_{\phi Li}}{2}S\frac{\alpha_{\theta Li}}{2}S\frac{\alpha_{\psi Li}}{2} \\ C\frac{\alpha_{\phi Li}}{2}S\frac{\alpha_{\theta Li}}{2}C\frac{\alpha_{\psi Li}}{2} + S\frac{\alpha_{\phi Li}}{2}C\frac{\alpha_{\theta Li}}{2}S\frac{\alpha_{\psi Li}}{2} \\ C\frac{\alpha_{\phi Li}}{2}C\frac{\alpha_{\theta Li}}{2}S\frac{\alpha_{\psi Li}}{2} - S\frac{\alpha_{\phi Li}}{2}S\frac{\alpha_{\theta Li}}{2}C\frac{\alpha_{\psi Li}}{2} \end{bmatrix}
\end{aligned}
\tag{4.142}
$$

where

$$
\begin{aligned}
\alpha_{\psi Li} &= \psi_d, \\
\alpha_{\theta Li} &= \arctan\left(\frac{C\alpha_{\psi Li}F_{Li1}+S\alpha_{\psi Li}F_{Li2}}{F_{Li3}}\right), \\
\alpha_{\phi Li} &= \arcsin\left(\frac{S\alpha_{\psi Li}F_{Li1}-C\alpha_{\psi Li}F_{Li2}}{T_{Li}}\right),
\end{aligned}
\tag{4.143}
$$

The reference angular velocity of quadrotor Li is calculated as follows

$$
\boldsymbol{\omega}_{Ldi} = \begin{bmatrix} 1 & 0 & -S\alpha_{\theta Li} \\ 0 & C\alpha_{\phi Li} & S\alpha_{\phi Li}C\alpha_{\theta Li} \\ 0 & -S\alpha_{\phi Li} & C\alpha_{\phi Li}C\alpha_{\theta Li} \end{bmatrix} \begin{bmatrix} \dot{\alpha}_{\phi Li} \\ \dot{\alpha}_{\theta Li} \\ \dot{\alpha}_{\psi Li} \end{bmatrix}
\tag{4.144}
$$

where $\boldsymbol{\omega}_{Ldi}$ is the body reference angular velocity; $S(\cdot)$ and $C(\cdot)$ stand for $\sin(\cdot)$, $\cos(\cdot)$, respectively.

$$
\begin{aligned}
T_{F\_Lij} &= \left\|\boldsymbol{F}_{F\_Lij}\right\| \\
\boldsymbol{Q}_{F\_Ldi} &= \begin{bmatrix} C\frac{\alpha_{\phi F\_Lij}}{2}C\frac{\alpha_{\theta F\_Lij}}{2}C\frac{\alpha_{\psi F\_Lij}}{2} + S\frac{\alpha_{\phi F\_Lij}}{2}S\frac{\alpha_{\theta F\_Lij}}{2}S\frac{\alpha_{\psi F\_Lij}}{2} \\ S\frac{\alpha_{\phi F\_Lij}}{2}C\frac{\alpha_{\theta F\_Lij}}{2}C\frac{\alpha_{\psi F\_Lij}}{2} - C\frac{\alpha_{\phi F\_Lij}}{2}S\frac{\alpha_{\theta F\_Lij}}{2}S\frac{\alpha_{\psi F\_Lij}}{2} \\ C\frac{\alpha_{\phi F\_Lij}}{2}S\frac{\alpha_{\theta F\_Lij}}{2}C\frac{\alpha_{\psi F\_Lij}}{2} + S\frac{\alpha_{\phi F\_Lij}}{2}C\frac{\alpha_{\theta F\_Lij}}{2}S\frac{\alpha_{\psi F\_Lij}}{2} \\ C\frac{\alpha_{\phi F\_Lij}}{2}C\frac{\alpha_{\theta F\_Lij}}{2}S\frac{\alpha_{\psi F\_Lij}}{2} - S\frac{\alpha_{\phi F\_Lij}}{2}S\frac{\alpha_{\theta F\_Lij}}{2}C\frac{\alpha_{\psi F\_Lij}}{2} \end{bmatrix}
\end{aligned}
\tag{4.145}
$$

where

$$
\begin{aligned}
\alpha_{\psi F\_Lij} &= \psi_d, \\
\alpha_{\theta F\_Lij} &= \arctan\left(\frac{C\alpha_{\psi F\_Lij}F_{F\_Lij1}+S\alpha_{\psi F\_Lij}F_{F\_Lij2}}{F_{F\_Lij3}}\right), \\
\alpha_{\phi F\_Lij} &= \arcsin\left(\frac{S\alpha_{\psi F\_Lij}F_{F\_Lij1}-C\alpha_{\psi F\_Lij}F_{F\_Lij2}}{T_{F\_Lij}}\right),
\end{aligned}
\tag{4.146}
$$

The reference angular velocity of quadrotor F_Lij is calculated as follows

$$\boldsymbol{\omega}_{F\_Ldi} = \begin{bmatrix} 1 & 0 & -S\alpha_{\theta F\_Lij} \\ 0 & C\alpha_{\phi F\_Lij} & S\alpha_{\phi F\_Lij} C\alpha_{\theta F\_Lij} \\ 0 & -S\alpha_{\phi F\_Lij} & C\alpha_{\phi F\_Lij} C\alpha_{\theta F\_Lij} \end{bmatrix} \begin{bmatrix} \dot{\alpha}_{\phi F\_Lij} \\ \dot{\alpha}_{\theta F\_Lij} \\ \dot{\alpha}_{\psi F\_Lij} \end{bmatrix} \tag{4.147}$$

where $\boldsymbol{\omega}_{F\_Ldi}$ is the body reference angular velocity; $S(\cdot)$ and $C(\cdot)$ stand for $\sin(\cdot)$, $\cos(\cdot)$, respectively.

Step 2

In this step, The unit-quaternion vector $\boldsymbol{Q}_{Ldi}$ and $\boldsymbol{Q}_{F\_Ldij}$ obtained from (4.142) and (4.145) are used as the references for designing the torque inputs, $\boldsymbol{\tau}_{Li}$ and $\boldsymbol{\tau}_{F\_Lij}$. We define the tracking errors as follows

$$\begin{aligned} \boldsymbol{Q}_{eLi} &= \boldsymbol{Q}_{Ldi}^{-1} \odot \boldsymbol{Q}_{Li}, \\ \boldsymbol{\omega}_{eLi} &= \boldsymbol{\omega}_{Li} - \boldsymbol{\alpha}_{\omega Li} \\ \boldsymbol{Q}_{eF\_Lij} &= \boldsymbol{Q}_{F\_Ldij}^{-1} \odot \boldsymbol{Q}_{F\_Lij}, \\ \boldsymbol{\omega}_{eF\_Lij} &= \boldsymbol{\omega}_{F\_Lij} - \boldsymbol{\alpha}_{\omega F\_Lij} \end{aligned} \tag{4.148}$$

where $\boldsymbol{\alpha}_{\omega Li}$ is a virtual control of ω_{Li} and $\boldsymbol{\alpha}_{\omega F\_Lij}$ is a virtual control of ω_{F_Lij}. $\boldsymbol{Q}_{eLi} = [\eta_{eLi}\, \boldsymbol{q}_{eLi}^T]^T$, $\boldsymbol{\omega}_{eLi}$, $\boldsymbol{Q}_{eF\_Lij} = [\eta_{eF\_Lij}\, \boldsymbol{q}_{eF\_Lij}^T]^T$ and $\boldsymbol{\omega}_{eF\_Lij}$ are attitude tracking and angular velocity error vectors, respectively.

Differentiating both sides of (4.148) yields

$$\begin{aligned} \dot{\boldsymbol{q}}_{eLi} &= \boldsymbol{G}_{Li}(\boldsymbol{\omega}_{eLi} + \boldsymbol{\alpha}_{\omega Li} - \boldsymbol{\omega}_{Ldi}) \\ \dot{\boldsymbol{\omega}}_{eLi} &= \boldsymbol{J}_{Li}^{-1}\boldsymbol{\tau}_{Li} - \boldsymbol{J}_{Li}^{-1}\boldsymbol{S}(\boldsymbol{\omega}_{Li})\boldsymbol{J}_{Li}\boldsymbol{\omega}_{Li} + \boldsymbol{d}_{\omega Li} - \dot{\boldsymbol{\alpha}}_{\omega Li} \\ \dot{\boldsymbol{q}}_{eF\_Lij} &= \boldsymbol{G}_{F\_Lij}(\boldsymbol{\omega}_{eF\_Lij} + \boldsymbol{\alpha}_{\omega F\_Lij} - \boldsymbol{\omega}_{Ldi}) \\ \dot{\boldsymbol{\omega}}_{eF\_Lij} &= \boldsymbol{J}_{F\_Lij}^{-1}\boldsymbol{\tau}_{F\_Lij} - \boldsymbol{J}_{F\_Lij}^{-1}\boldsymbol{S}(\boldsymbol{\omega}_{F\_Lij})\boldsymbol{J}_{F\_Lij}\boldsymbol{\omega}_{F\_Lij} + \boldsymbol{d}_{\omega F\_Lij} - \dot{\boldsymbol{\alpha}}_{\omega F\_Lij} \end{aligned} \tag{4.149}$$

where $\boldsymbol{G}_{Li} = \frac{1}{2}\left(\eta_{eLi}\boldsymbol{I}_{3\times 3} + \boldsymbol{S}(\boldsymbol{q}_{eLi})\right)$ and $\boldsymbol{\omega}_{Ldi}$ can be obtained by using equation (4.144). $\boldsymbol{G}_{F\_Lij} = \frac{1}{2}\left(\eta_{eF\_Lij}\boldsymbol{I}_{3\times 3} + \boldsymbol{S}(\boldsymbol{q}_{eF\_Lij})\right)$ and $\boldsymbol{\omega}_{F\_Ldij}$ can be obtained by using equation (4.147).

To obtain the control input $\boldsymbol{\tau}_{Li}$ and $\boldsymbol{\tau}_{F\_Lij}$, we consider the following Lyapunov function:

$$V_3 = \sum_{i=1}^{NL}\sum_{j=1}^{NF(i)}\left[\frac{1}{2}\boldsymbol{q}_{eLi}^T\boldsymbol{q}_{eLi} + \frac{1}{2}\boldsymbol{q}_{eF\_Lij}^T\boldsymbol{q}_{eF\_Lij}\right] \tag{4.150}$$

The time derivative of V_3 along solutions (4.149) is given by

$$\begin{aligned}\dot{V}_3 &= \sum_{i=1}^{NL}\sum_{j=1}^{NF(i)} \boldsymbol{q}_{eLi}^T \boldsymbol{G}_{Li}(\boldsymbol{\omega}_{eLi} + \boldsymbol{\alpha}_{\omega Li} - \boldsymbol{\omega}_{Ldi}) \\ &\quad + \sum_{i=1}^{NL}\sum_{j=1}^{NF(i)} \boldsymbol{q}_{eF\_Lij}^T \boldsymbol{G}_{F\_Lij}(\boldsymbol{\omega}_{eF\_Lij} + \boldsymbol{\alpha}_{\omega F\_Lij} - \boldsymbol{\omega}_{F\_Ldij})\end{aligned} \tag{4.151}$$

which suggests that we choose

$$\begin{aligned}\boldsymbol{\alpha}_{\omega Li} &= -k_3 \boldsymbol{G}_{Li}^T \boldsymbol{q}_{eLi} + \boldsymbol{\omega}_{Ldi} \\ \boldsymbol{\alpha}_{\omega F\_Lij} &= -k_3 \boldsymbol{G}_{F\_Lij}^T \boldsymbol{q}_{eF\_Lij} + \boldsymbol{\omega}_{F\_Ldi}\end{aligned} \tag{4.152}$$

To design the control input torque, $\boldsymbol{\tau}_{Li}$ and $\boldsymbol{\tau}_{F\_Lij}$, considering the following Lyapunov candidate

$$V_4 = V_3 + \sum_{i=1}^{NL}\sum_{j=1}^{NF(i)} \left[\boldsymbol{\omega}_{eLi}^T \boldsymbol{\omega}_{eLi} + \boldsymbol{\omega}_{eF\_Lij}^T \boldsymbol{\omega}_{eF\_Lij}\right] \tag{4.153}$$

The time derivative of (4.153) is given

$$\begin{aligned}\dot{V}_4 &= \sum_{i=1}^{NL}\sum_{j=1}^{NF(i)} \left[-k_3 \boldsymbol{q}_{eLi}^T \boldsymbol{G}_{Li} \boldsymbol{G}_{Li}^T \boldsymbol{q}_{eLi} - k_3 \boldsymbol{q}_{eF\_Lij}^T \boldsymbol{G}_{F\_Lij} \boldsymbol{G}_{F\_Lij}^T \boldsymbol{q}_{eF\_Lij}\right] \\ &\quad + \sum_{i=1}^{NL}\sum_{j=1}^{NF(i)} \left[\boldsymbol{\omega}_{eLi}^T \left(\boldsymbol{J}_{Li}^{-1}\boldsymbol{\tau}_{Li} - \boldsymbol{J}_{Li}^{-1}\boldsymbol{S}(\boldsymbol{\omega}_{Li})\boldsymbol{J}_{Li}\boldsymbol{\omega}_{Li} + \boldsymbol{d}_{\omega Li} - \dot{\boldsymbol{\alpha}}_{\omega Li} + \boldsymbol{G}_{Li}\boldsymbol{q}_{eLi}\right)\right] \\ &\quad + \sum_{i=1}^{NL}\sum_{j=1}^{NF(i)} \left[\boldsymbol{\omega}_{eF\_Lij}^T \left(\boldsymbol{J}_{F\_Lij}^{-1}\boldsymbol{\tau}_{F\_Lij} - \boldsymbol{J}_{F\_Lij}^{-1}\boldsymbol{S}(\boldsymbol{\omega}_{F\_Lij})\boldsymbol{J}_{F\_Lij}\boldsymbol{\omega}_{F\_Lij}\right)\right] \\ &\quad + \sum_{i=1}^{NL}\sum_{j=1}^{NF(i)} \left[\boldsymbol{\omega}_{eF\_Lij}^T \left(\boldsymbol{d}_{\omega F\_Lij} - \dot{\boldsymbol{\alpha}}_{\omega F\_Lij} + \boldsymbol{G}_{F\_Lij}\boldsymbol{q}_{eF\_Lij}\right)\right] \\ &= \sum_{i=1}^{NL}\sum_{j=1}^{NF(i)} \left[-k_3 \boldsymbol{q}_{eLi}^T \boldsymbol{G}_{Li} \boldsymbol{G}_{Li}^T \boldsymbol{q}_{eLi} - k_3 \boldsymbol{q}_{eF\_Lij}^T \boldsymbol{G}_{F\_Lij} \boldsymbol{G}_{F\_Lij}^T \boldsymbol{q}_{eF\_Lij}\right] \\ &\quad + \sum_{i=1}^{NL}\sum_{j=1}^{NF(i)} \left[\boldsymbol{\omega}_{eLi}^T \left(\hat{\boldsymbol{J}}_{Li}^{-1}\boldsymbol{\tau}_{Li} - \boldsymbol{J}_{Li}^{-1}\boldsymbol{S}(\boldsymbol{\omega}_{Li})\boldsymbol{J}_{Li}\boldsymbol{\omega}_{Li} + \hat{\boldsymbol{d}}_{\omega Li} - \dot{\boldsymbol{\alpha}}_{\omega Li} + \boldsymbol{G}_{Li}\boldsymbol{q}_{eLi}\right)\right] \\ &\quad + \sum_{i=1}^{NL}\sum_{j=1}^{NF(i)} \left[\boldsymbol{\omega}_{eLi}^T \left(\tilde{\boldsymbol{J}}_{Li}^{-1}\boldsymbol{\tau}_{Li} + \tilde{\boldsymbol{d}}_{\omega Li}\right)\right] \\ &\quad + \sum_{i=1}^{NL}\sum_{j=1}^{NF(i)} \left[\boldsymbol{\omega}_{eF\_Lij}^T \left(\hat{\boldsymbol{J}}_{F\_Lij}^{-1}\boldsymbol{\tau}_{F\_Lij} - \boldsymbol{J}_{F\_Lij}^{-1}\boldsymbol{S}(\boldsymbol{\omega}_{F\_Lij})\boldsymbol{J}_{F\_Lij}\boldsymbol{\omega}_{F\_Lij}\right)\right] \\ &\quad + \sum_{i=1}^{NL}\sum_{j=1}^{NF(i)} \left[\boldsymbol{\omega}_{eF\_Lij}^T \left(\hat{\boldsymbol{d}}_{\omega F\_Lij} - \dot{\boldsymbol{\alpha}}_{\omega F\_Lij} + \boldsymbol{G}_{F\_Lij}\boldsymbol{q}_{eF\_Lij}\right)\right] \\ &\quad + \sum_{i=1}^{NL}\sum_{j=1}^{NF(i)} \left[\boldsymbol{\omega}_{eF\_Lij}^T \left(\tilde{\boldsymbol{J}}_{F\_Lij}^{-1}\boldsymbol{\tau}_{F\_Lij} + \tilde{\boldsymbol{d}}_{\omega F\_Lij}\right)\right]\end{aligned} \tag{4.154}$$

which suggests that we choose the control input torques as follows

$$\begin{aligned}\boldsymbol{\tau}_{Li} &= \hat{\boldsymbol{J}}_{Li}\left(-k_4\boldsymbol{\omega}_{eLi}+\dot{\boldsymbol{\alpha}}_{\omega Li}-\boldsymbol{G}_{Li}\boldsymbol{q}_{eLi}+\boldsymbol{J}_{Li}^{-1}\boldsymbol{S}(\boldsymbol{\omega}_{Li})\boldsymbol{J}_{Li}\boldsymbol{\omega}_{Li}-\hat{\boldsymbol{d}}_{\omega Li}\right)\\ \boldsymbol{\tau}_{F\_Lij} &= \hat{\boldsymbol{J}}_{F\_Lij}\left(-k_4\boldsymbol{\omega}_{eF\_Lij}+\dot{\boldsymbol{\alpha}}_{\omega F\_Lij}-\boldsymbol{G}_{F\_Lij}\boldsymbol{q}_{eF\_Lij}\right)\\ &\quad+\hat{\boldsymbol{J}}_{F\_Lij}\left(\boldsymbol{J}_{F\_Lij}^{-1}\boldsymbol{S}(\boldsymbol{\omega}_{F\_Lij})\boldsymbol{J}_{F\_Lij}\boldsymbol{\omega}_{F\_Lij}-\hat{\boldsymbol{d}}_{\omega F\_Lij}\right)\end{aligned} \tag{4.155}$$

where $\hat{\boldsymbol{J}}_{Li}$, $\hat{\boldsymbol{d}}_{\omega Li}$, $\hat{\boldsymbol{J}}_{F\_Lij}$, and $\hat{\boldsymbol{d}}_{\omega F\_Lij}$ are estimations of $\boldsymbol{J}_{Li}$, $\boldsymbol{d}_{\omega Li}$, $\boldsymbol{J}_{F\_Lij}$, and $\boldsymbol{d}_{\omega F\_Lij}$, respectively. The update laws for these estimations are chosen as follows

$$\begin{aligned}\dot{\hat{\boldsymbol{J}}}_{Li}^{-1} &= proj(\hat{\boldsymbol{J}}_{Li}(\gamma_{1\omega}\boldsymbol{\omega}_{eLi}^T\boldsymbol{F}_{Li}))\\ \dot{\hat{\boldsymbol{d}}}_{\omega Li} &= \gamma_{2\omega}\boldsymbol{\omega}_{eLi}\\ \dot{\hat{\boldsymbol{J}}}_{F\_Lij}^{-1} &= proj(\hat{\boldsymbol{J}}_{F\_Lij}(\gamma_{1\omega}\boldsymbol{\omega}_{eF\_Lij}^T\boldsymbol{F}_{F\_Lij}))\\ \dot{\hat{\boldsymbol{d}}}_{\omega F\_Lij} &= \gamma_{2\omega}\boldsymbol{\omega}_{eF\_Lij}\end{aligned} \tag{4.156}$$

Substituting update laws, controls and virtual controls from (4.128), (4.131), (4.132), (4.152) (4.156) and (4.155) into (4.123), and (4.149), we have the following closed loop system:

$$\begin{aligned}\dot{\boldsymbol{p}}_{eLi} &= \boldsymbol{v}_{eLi}-k_1\boldsymbol{\Omega}_{Li}\\ \dot{\boldsymbol{v}}_{eLi} &= -k_2\boldsymbol{v}_{eLi}-\boldsymbol{\Omega}_{\boldsymbol{Li}}-\tilde{J}_{1Li}\boldsymbol{F}_{Li}+\tilde{\boldsymbol{d}}_{vLi}\\ \dot{\boldsymbol{q}}_{eLi} &= \boldsymbol{G}_{Li}(-k_3\boldsymbol{G}_{Li}^T\boldsymbol{q}_{eLi}+\boldsymbol{\omega}_{eLi})\\ \dot{\boldsymbol{\omega}}_{eLi} &= -k_4\boldsymbol{\omega}_{eLi}-\boldsymbol{G}_{Li}\boldsymbol{q}_{eLi}+\tilde{\boldsymbol{J}}_{Li}^{-1}\tilde{\boldsymbol{\tau}}_{Li}+\tilde{\boldsymbol{d}}_{\omega Li}\\ \dot{\tilde{J}}_{1Li} &= -\dot{\hat{J}}_{1Li}=-proj(\gamma_{1v}\boldsymbol{v}_{eLi}^T\boldsymbol{F}_{Li})\\ \dot{\tilde{\boldsymbol{d}}}_{vLi} &= -\dot{\hat{\boldsymbol{d}}}_{vLi}=-\gamma_{2v}\boldsymbol{v}_{eLi}\\ \dot{\tilde{\boldsymbol{J}}}_{Li}^{-1} &= -\dot{\hat{\boldsymbol{J}}}_{Li}^{-1}=-proj(\hat{\boldsymbol{J}}_{Li}(\gamma_{1\omega}\boldsymbol{\omega}_{eLi}^T\boldsymbol{F}_{Li}))\\ \dot{\tilde{\boldsymbol{d}}}_{\omega Li} &= -\dot{\hat{\boldsymbol{d}}}_{\omega Li}=-\gamma_{2\omega}\boldsymbol{\omega}_{eLi}\\ \dot{\boldsymbol{p}}_{eF\_Lij} &= \boldsymbol{v}_{eF\_Lij}-k_1\boldsymbol{\Omega}_{F\_Lij}\\ \dot{\boldsymbol{v}}_{eF\_Lij} &= -k_2\boldsymbol{v}_{eF\_Lij}-\boldsymbol{\Omega}_{\boldsymbol{F\_Lij}}-\tilde{J}_{1F\_Lij}\boldsymbol{F}_{F\_Lij}+\tilde{\boldsymbol{d}}_{vF\_Lij}\\ \dot{\boldsymbol{q}}_{eF\_Lij} &= \boldsymbol{G}_{F\_Lij}(-k_3\boldsymbol{G}_{F\_Lij}^T\boldsymbol{q}_{eF\_Lij}+\boldsymbol{\omega}_{eF\_Lij})\\ \dot{\boldsymbol{\omega}}_{eF\_Lij} &= -k_4\boldsymbol{\omega}_{eF\_Lij}-\boldsymbol{G}_{F\_Lij}\boldsymbol{q}_{eF\_Lij}+\tilde{\boldsymbol{J}}_{F\_Lij}^{-1}\tilde{\boldsymbol{\tau}}_{F\_Lij}+\tilde{\boldsymbol{d}}_{\omega F\_Lij}\\ \dot{\tilde{J}}_{1F\_Lij} &= -\dot{\hat{J}}_{1F\_Lij}=-proj(\gamma_{1v}\boldsymbol{v}_{eF\_Lij}^T\boldsymbol{F}_{F\_Lij})\\ \dot{\tilde{\boldsymbol{d}}}_{vF\_Lij} &= -\dot{\hat{\boldsymbol{d}}}_{vF\_Lij}=-\gamma_{2v}\boldsymbol{v}_{eF\_Lij}\\ \dot{\tilde{\boldsymbol{J}}}_{F\_Lij}^{-1} &= -\dot{\hat{\boldsymbol{J}}}_{F\_Lij}^{-1}=-proj(\hat{\boldsymbol{J}}_{F\_Lij}(\gamma_{1\omega}\boldsymbol{\omega}_{eF\_Lij}^T\boldsymbol{F}_{F\_Lij}))\\ \dot{\tilde{\boldsymbol{d}}}_{\omega F\_Lij} &= -\dot{\hat{\boldsymbol{d}}}_{\omega F\_Lij}=-\gamma_{2\omega}\boldsymbol{\omega}_{eLi}\end{aligned} \tag{4.157}$$

The control design has been completed. We summarize the results in the following theorem.

Theorem 4.4. *Under Assumption 4.5, the formation control and update laws consisting of* (4.131), (4.132), (4.156) *and* (4.155) *for the quadrotor i achieve the Formation Control Objective 4.4, there*

is no collision between all the quadrotors, the position $\boldsymbol{p}_{Li}$, heading angle ψ_{Li} of the leader quadrotor Li, the position $\boldsymbol{p}_{F\_Lij}$ and heading angle ψ_{F_Lij} of the follower quadrotor F_Lij globally asymptotically track their reference trajectories $\boldsymbol{p}_{Ldi}$, ψ_{Ldi}, $\boldsymbol{p}_{F\_Ldij}$, and ψ_{F_Ldij}, respectively.

$$\begin{aligned}
&\lim_{t\to\infty}(\boldsymbol{p}_{Li}(t)-\boldsymbol{p}_{Ldi}(t))=0,\\
&\lim_{t\to\infty}(\psi_{Li}(t)-\psi_{di}(t))=0\\
&\lim_{t\to\infty}\big(\boldsymbol{p}_{F_Lij}(t)-\boldsymbol{p}_{F_Ldij}(t)\big)=0,\\
&\lim_{t\to\infty}\big(\psi_{F_Lij}(t)-\psi_{Li}(t)\big)=0\\
&\|\boldsymbol{p}_{ij}-\boldsymbol{p}_{mn}\|\geq\alpha^{S}_{ijmn}
\end{aligned} \tag{4.158}$$

and the closed loop system (4.157) *is forward complete.*

Proof. *See Appendix B.6.*

4.5.3 Simulation Results

In this section, we illustrate the effectiveness of the proposed formation control design through a numerical simulation. The parameters of quadrotor ij for the simulation are taken from [EInE12] as following: m_ij=0.35 kg, g = 9.81 $kg\,m^2$, $l_{ij}=0.15m$, $I_{X_{ij}}=15.67\times10^{-3}\,kg\,m^2$, $I_{Y_{ij}}=15.67\times10^{-3}\,kg\,m^2$; $I_{Z_{ij}}=28.34\times10^{-3}\,kg\,m^2$, $K_{tij}=192.32\times10^{-7}Ns^2$, $K_{dij}=4.003\times10^{-7}Nms^2$.

The initial conditions are taken as

$$\begin{aligned}
&\boldsymbol{p}_{ij}(0)=[(i-1)*R_1\quad(j-1)*R_1\quad 0]^T;\boldsymbol{v}_i(0)=[0\,0\,0]^T\\
&\boldsymbol{Q}_i(0)=[1\,0\,0\,0]^T;\boldsymbol{\omega}_i(0)=[0\,0\,0]^T
\end{aligned} \tag{4.159}$$

where $R_1=1.5m$, at the first time, all quadrotors are distributed on land in column. The initial distance between quadrotors are satisfied (4.120).

The simulation is taken in two cases. The first case illustrates a formation control for a leader and 12 followers and the second case presents a formation of multiple leaders and followers. The disturbances in the first case is chosen as

$$\begin{aligned}
&m_i=m_{01}+sin(0.5*s)\\
&\boldsymbol{J}_i=\boldsymbol{J}_{0i}(1+sin(0.5*s))\\
&\boldsymbol{d}_{vi}=[.5+.2sin(s);1+0.2cos(2s);1.5+.2sin(3s)]^T;\\
&\boldsymbol{d}_{\omega i}=[.1+.2sin(.5s);.3+0.2cos(s);1.5+.2sin(2.5s)]^T;
\end{aligned} \tag{4.160}$$

In the first case, $NL=1$, $NF1=13$, the reference path and formation of the leader and follower

are chosen as follows

$$\begin{aligned}
&\boldsymbol{L}_{LdLi} = [0\ 0\ 0]^T,\\
&\boldsymbol{L}_{F_Ldij} = [Rf.sin((j-1).2.pi/(NF(i)))\ R0.cos((j-1).2.pi/(NF(i)))\ 0.5.(i-1)]^T,\\
&s = 0.5.t,\\
&\boldsymbol{p}_d = [10.cos(0.1.s)\ 10.sin(0.1.s)\ 5]^T,\\
&\psi_d = 0.1.t,
\end{aligned} \tag{4.161}$$

with $R_0 = 1.5m$, $R_f = 1m$. With these initial values, all the quadrotor is distributed on an ellipse shape. The leader quadrotor track the predefined path $\boldsymbol{p}_d$ and there are no collision among quadrotors at the initial time. These initial reference satisfies assumption 4.5.

In the second case, $NL = 4$, $NF = [4\,5\,6\,7]^T$, the reference path and formation of the leader and follower are chosen as follows

$$\begin{aligned}
&\boldsymbol{L}_{LdLi} = [RL0.sin((i-1).2.pi/(NL))\ RL0.cos((i-1).2.pi/(NL))\ 0];^T,\\
&\boldsymbol{L}_{F_Ld1j} = [Rf.sin((j-1).2.pi/(NF(1)-1))\ R0.cos((j-1).2.pi/(NF(1)-1))\ 0.5.(1-1)]^T,\\
&\boldsymbol{L}_{F_Ld2j} = [0\ R0.sin((2-1).2.pi/(NF(2)-1))\ R0.cos((j-1).2.pi/(NF(2)-1)) + R0]^T,\\
&\boldsymbol{L}_{F_Ld3j} = [Rf.sin((j-1).2.pi/(NF(3)-1))\ R0.cos((j-1).2.pi/(NF(3)-1))\ 0.5.(i-1)]^T,\\
&\boldsymbol{L}_{F_Ld4j} = [Rf.sin((j-1).2.pi/(NF(4)-1))\ R0.cos((j-1).2.pi/(NF(4)-1))\ 0]^T,\\
&s = 0.5.t,\\
&\boldsymbol{p}_d = [10.cos(0.1.s)\ 10.sin(0.1.s)\ 5]^T,\\
&\psi_d = 0.1.t,
\end{aligned} \tag{4.162}$$

with $R_0 = 1.5m$, $R_f = 1m$, $RL0 = 5m$. With these initial values, the formation of the leaders are distributed on a circle shape with radius $RL0$. The formation shape of the followers are listed as follows: group 1: an ellipse, group 2: a circle on yoz plane, group 3 and 4: an ellipse. These initial reference satisfies condition (4.120).

The control gains are chosen as $|a_{ij}| = 0.4m$, $|b_{ij}| = 10m$, $\delta = 1m$, $k_1 = 3$, $k_2 = 2$, $k_3 = 1$ and $k_4 = 1$. The disturbance for the second case is chosen as follows

$$\begin{aligned}
&m_i = m_{01} + sin(0.5 * s)\\
&\boldsymbol{J}_i = \boldsymbol{J}_{0i}(1 + sin(0.5 * s))\\
&\boldsymbol{d}_{vi} = [.5 + .2sin(s + rand); 1 + 0.2cos(2s + rand); 1.5 + .2sin(3s + rand)]^T;\\
&\boldsymbol{d}_{\omega i} = [.1 + .2sin(.5s + rand); .3 + 0.2cos(s + rand); 1.5 + .2sin(2.5s + rand)]^T;
\end{aligned} \tag{4.163}$$

The estimations of unknown parameters for quadrotor 1.1 are plotted on the Figure 4.75, Figure 4.88, Figure 4.73, Figure 4.86, Figure 4.74 and Figure 4.87. The formation results are shown on the Figure 4.63 and the Figure 4.76. From the Figure 4.68 and the Figure 4.81, one can see that there are no collision between all the quadrotors. The tracking errors in both two cases are convergent to the origin as shown in the Figure 4.64, 4.65, 4.66, 4.69, 4.70, and 4.77, 4.78, 4.79 4.82, 4.83. Torque and thrust force are illustrated in Figure 4.67 and Figure 4.80.

Case 1: Formation of a leader quadrotor and 12 follower quadrotors distributed on an ellipse shape while tracking a circle trajectory.

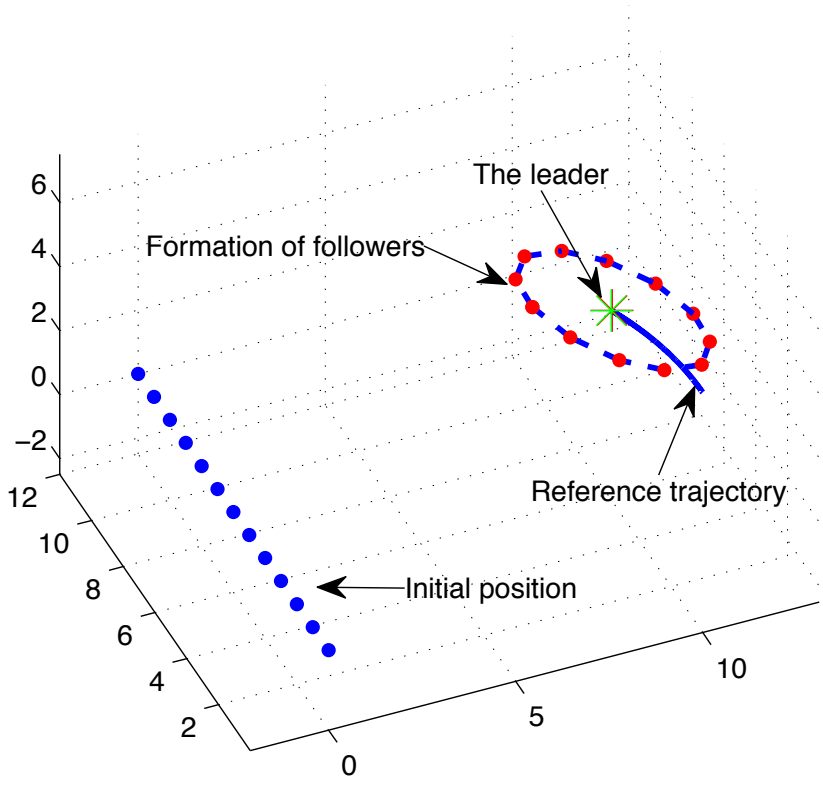

Figure 4.63: The formation of a leader and 12 followere quadrotors.

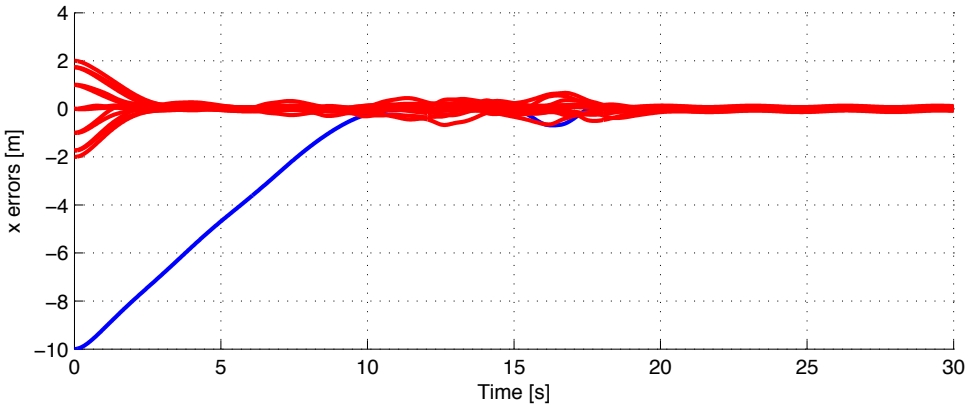

Figure 4.64: Position tracking errors on x axis.

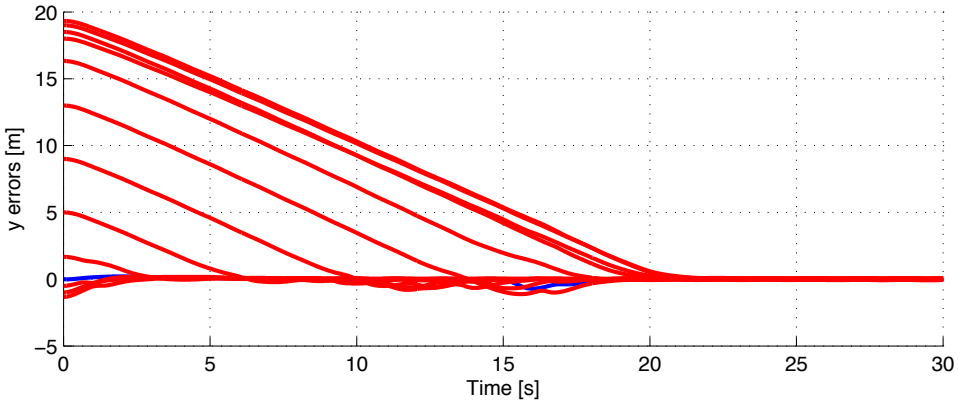

Figure 4.65: Position tracking errors on y axis.

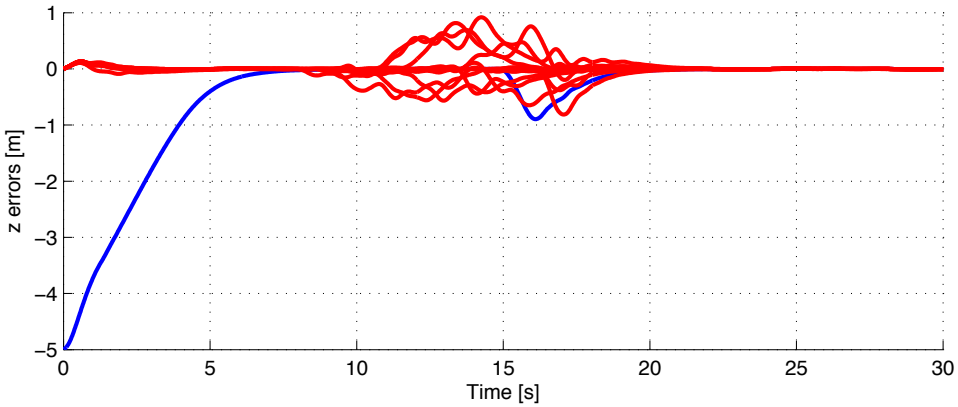

Figure 4.66: Position tracking errors on z axis.

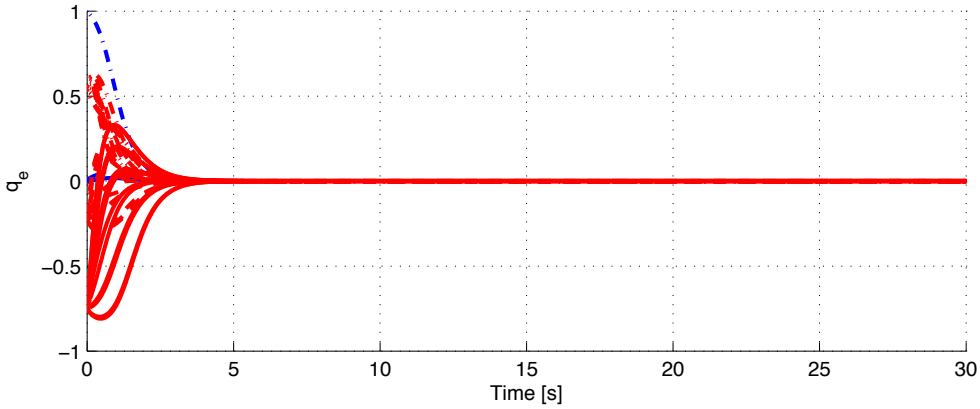

Figure 4.67: Attitude tracking errors.

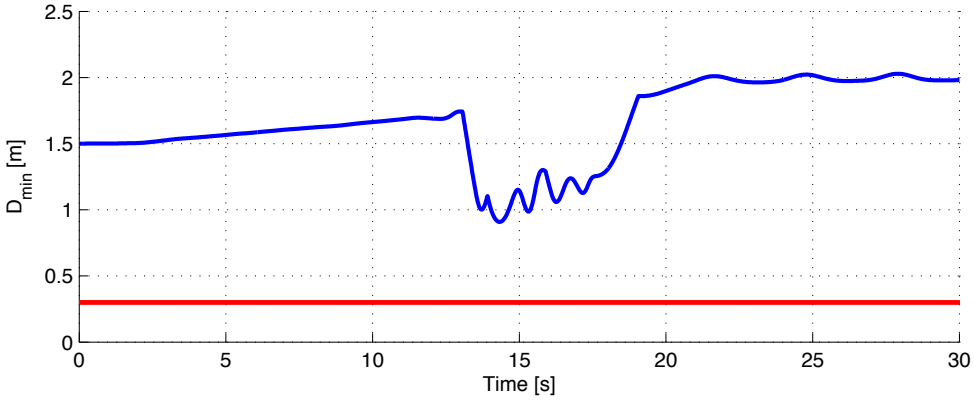

Figure 4.68: The minimum distance among quadrotors.

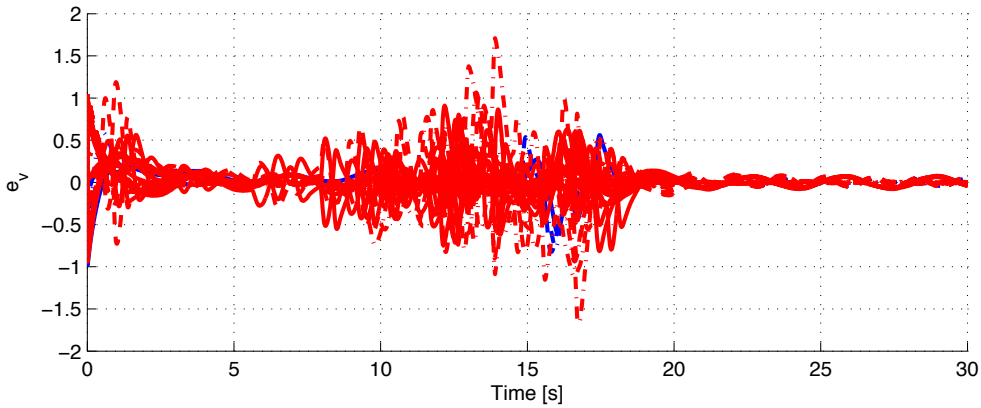

Figure 4.69: Linear velocity tracking errors.

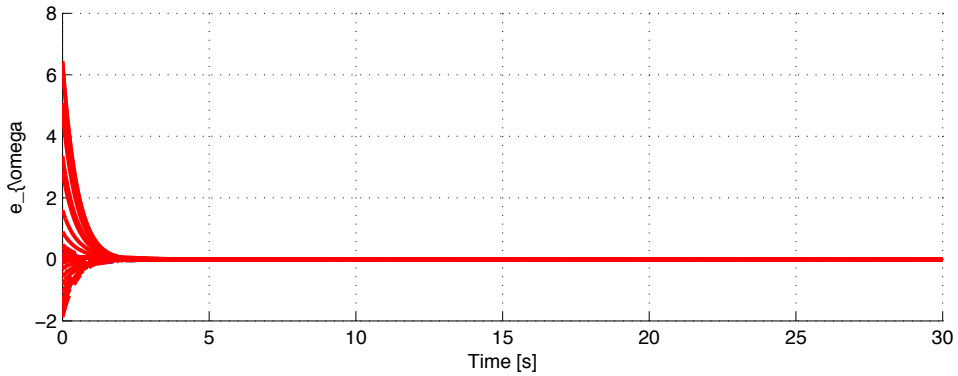

Figure 4.70: Angular velocity tracking errors.

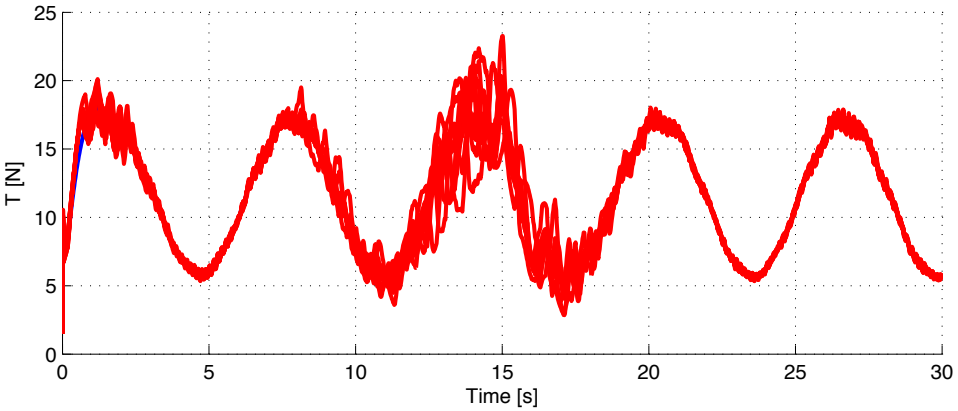

Figure 4.71: Thrust forces of the leader and followers.

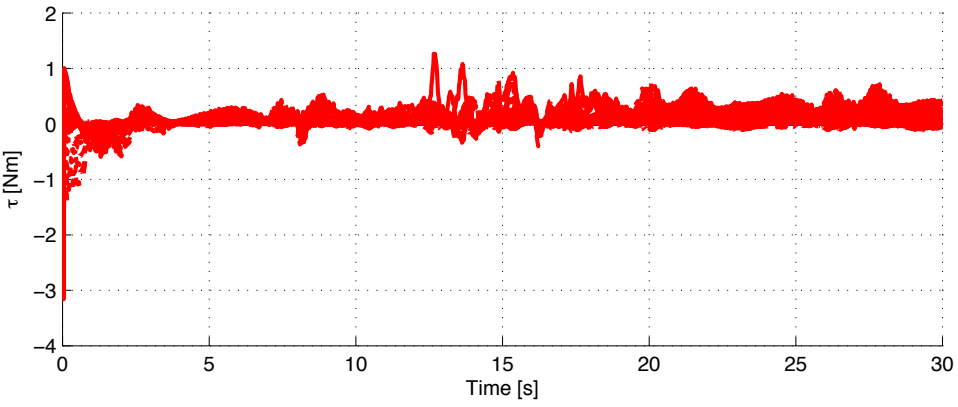

Figure 4.72: Torques of the leader and followers.

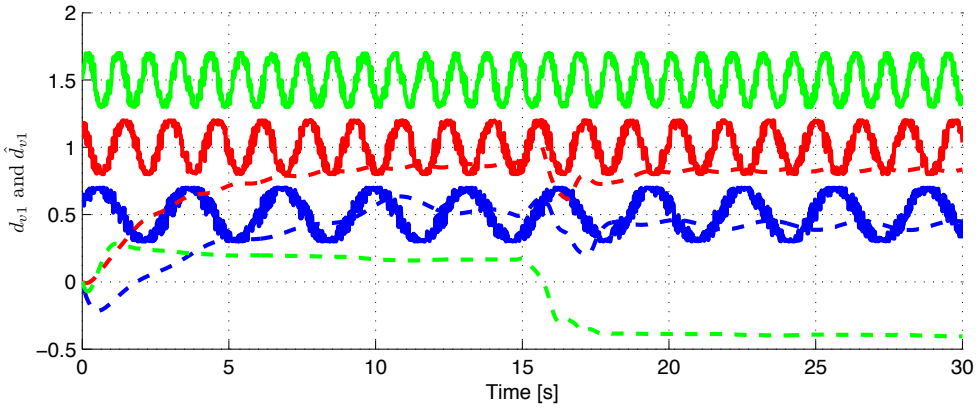

Figure 4.73: Disturbances and estimations of $\boldsymbol{d}_v$ of the leader quadrotor 1

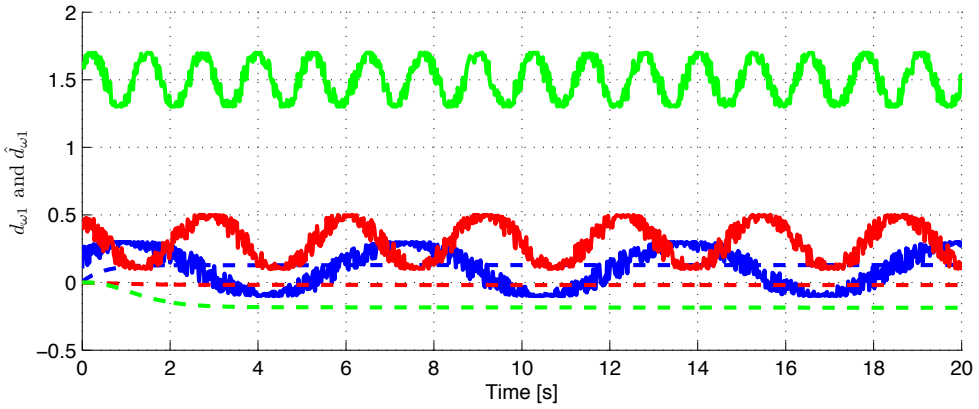

Figure 4.74: Disturbances and estimations of $\boldsymbol{d}_o$ of the leader quadrotor 1

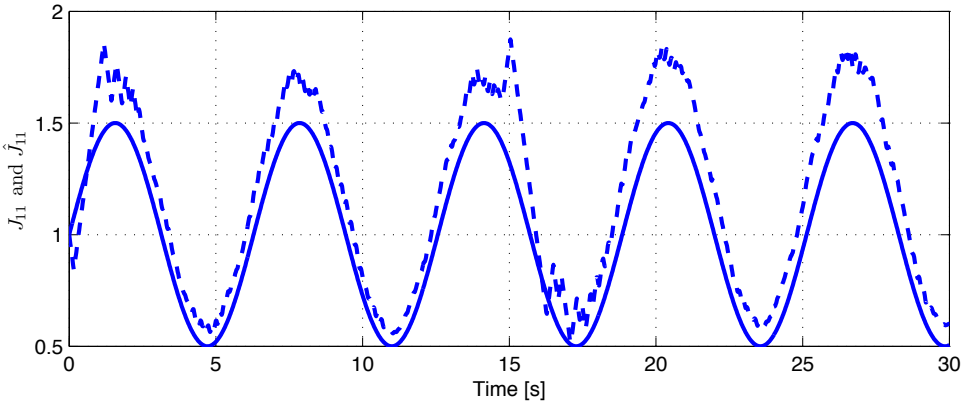

Figure 4.75: Uncertainty and estimation of mass of the leader quadrotor 1

Case 2: Leader follower formation of multiple leaders and followers where the leader formation distributes on a circle shape and track a circle trajectory.

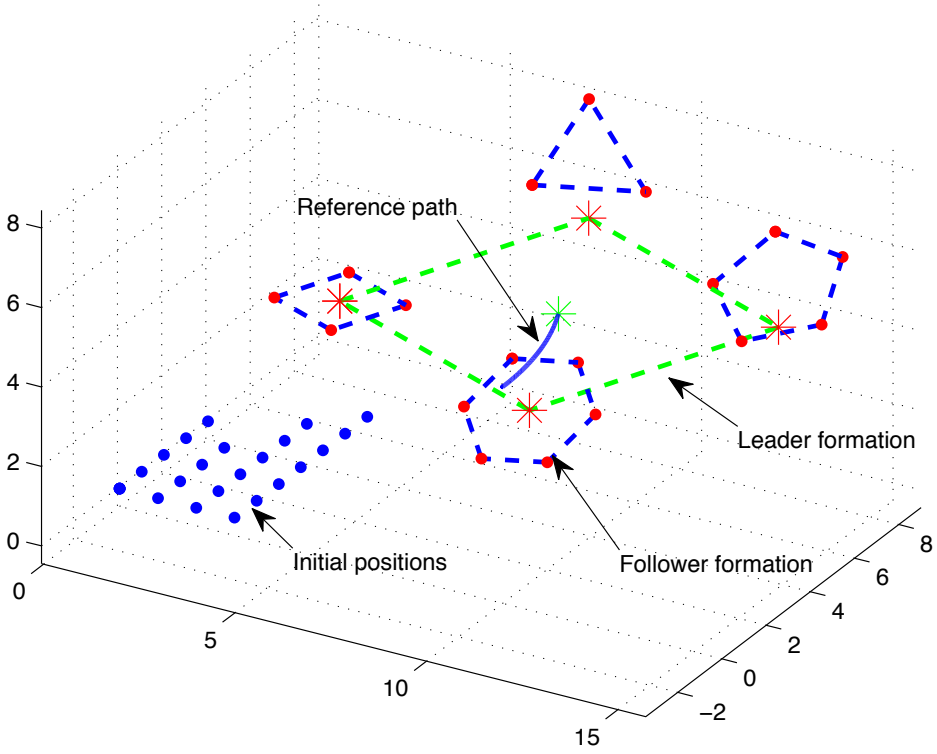

Figure 4.76: The formation of leader and follower quadrotors.

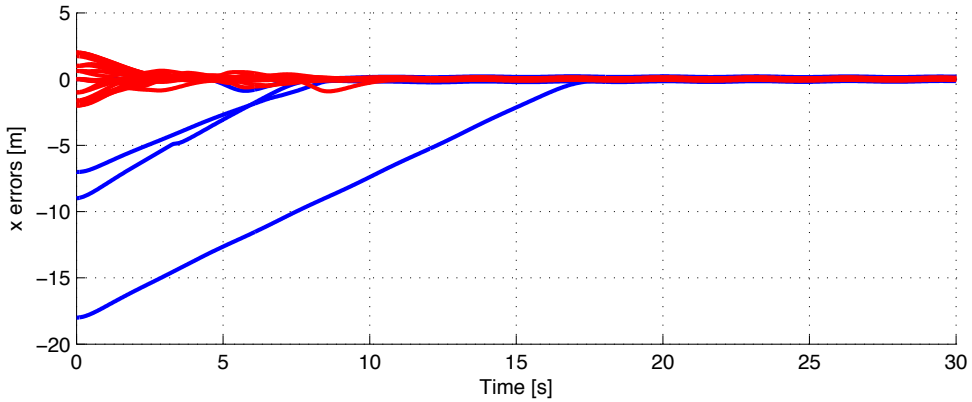

Figure 4.77: Position tracking errors on x axis.

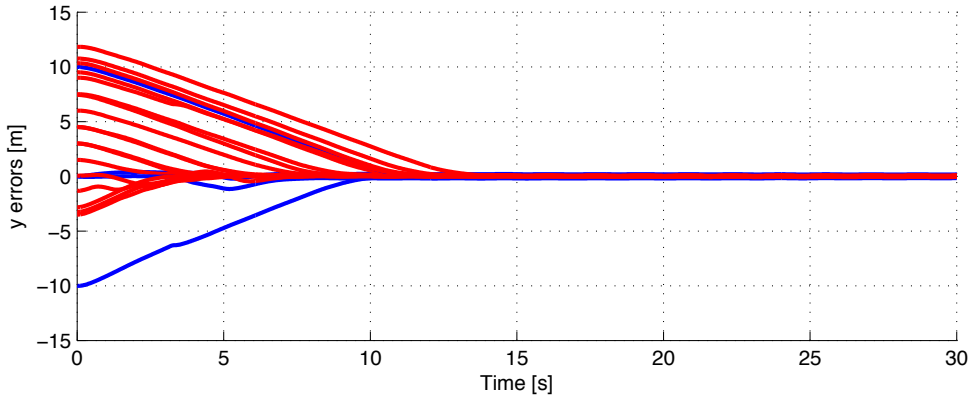

Figure 4.78: Position tracking errors on y axis.

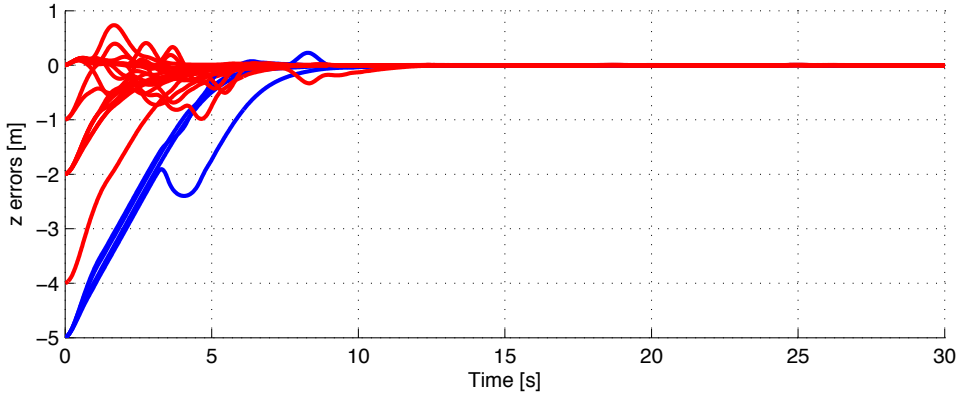

Figure 4.79: Position tracking errors on z axis.

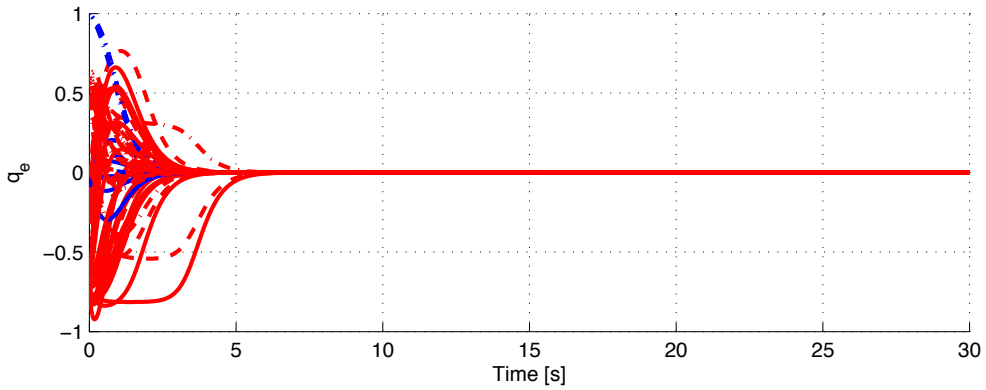

Figure 4.80: Attitude tracking errors.

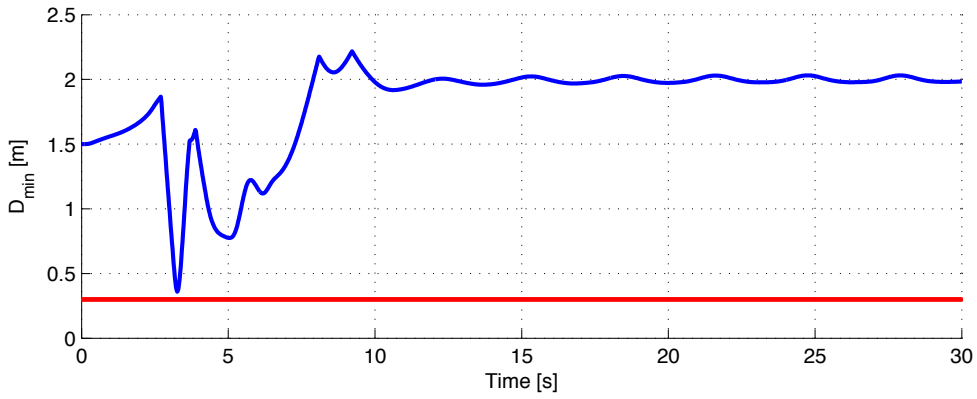

Figure 4.81: The minimum distance among quadrotors.

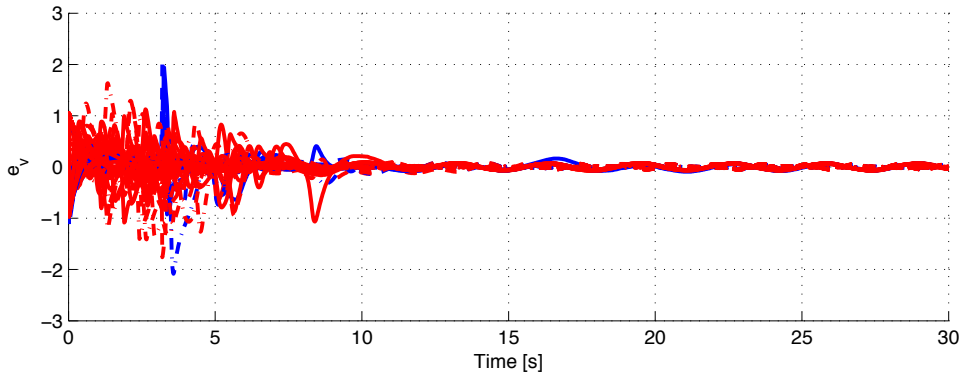

Figure 4.82: Linear velocity tracking errors.

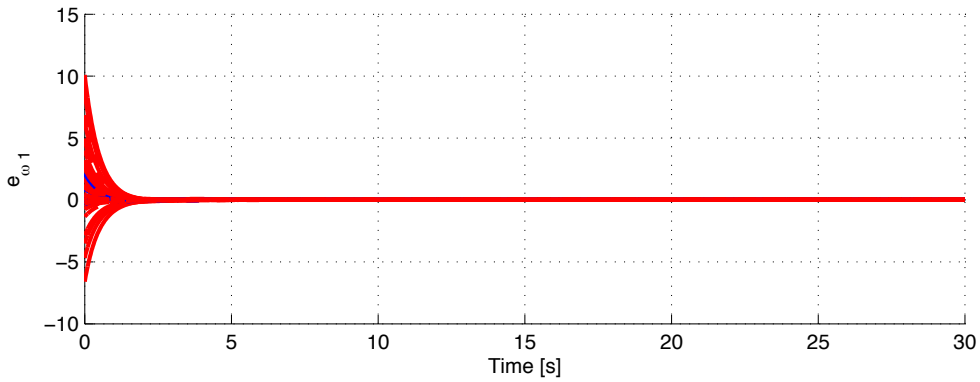

Figure 4.83: Angular velocity tracking errors.

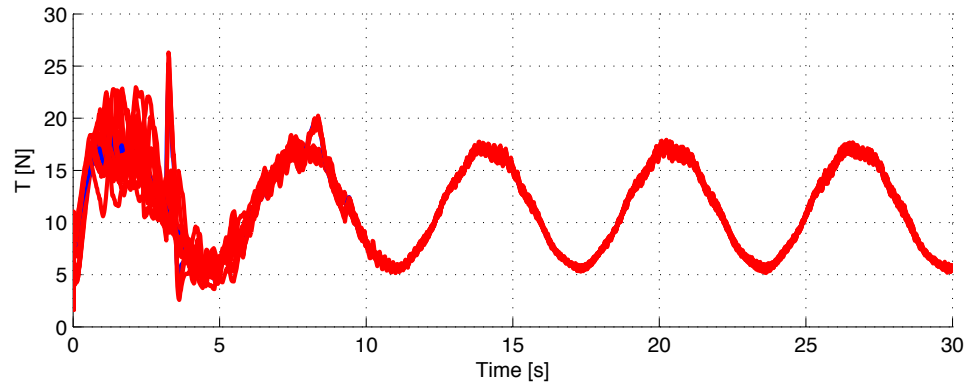

Figure 4.84: Thrust forces of leaders and followers.

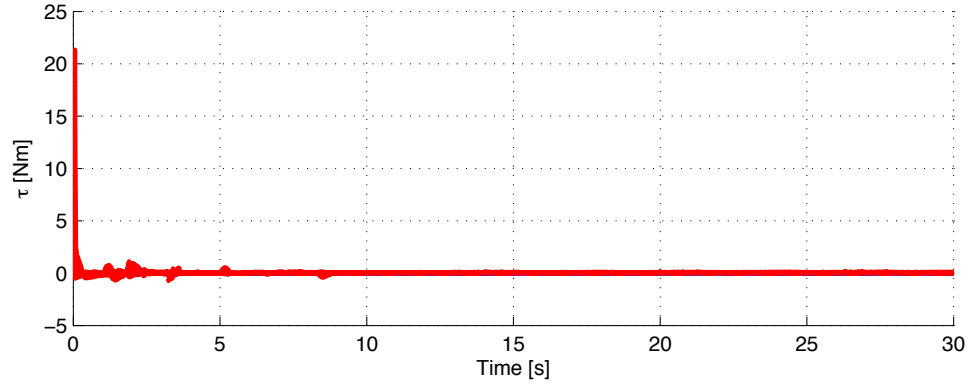

Figure 4.85: Torques of leaders and followers.

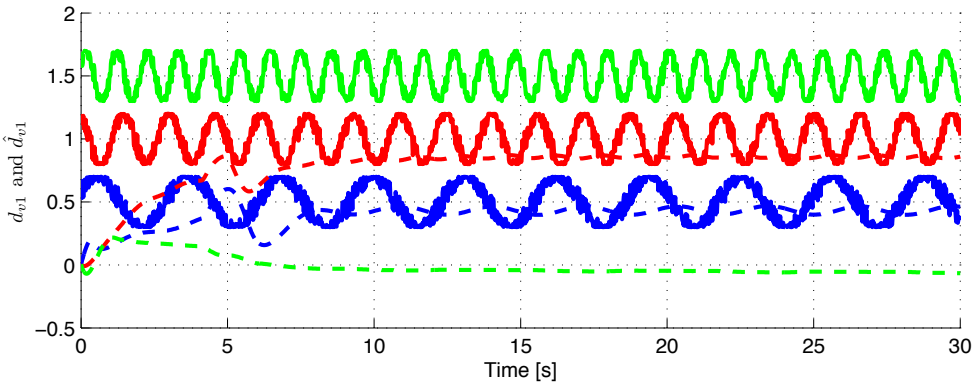

Figure 4.86: Disturbances and estimations of $\boldsymbol{d}_v$ of the leader quadrotor 1

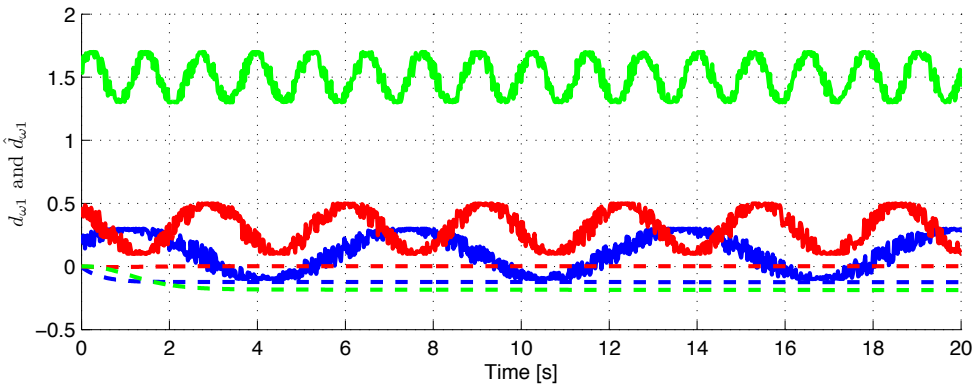

Figure 4.87: Disturbances and estimations of $\boldsymbol{d}_o$ of the leader quadrotor 1

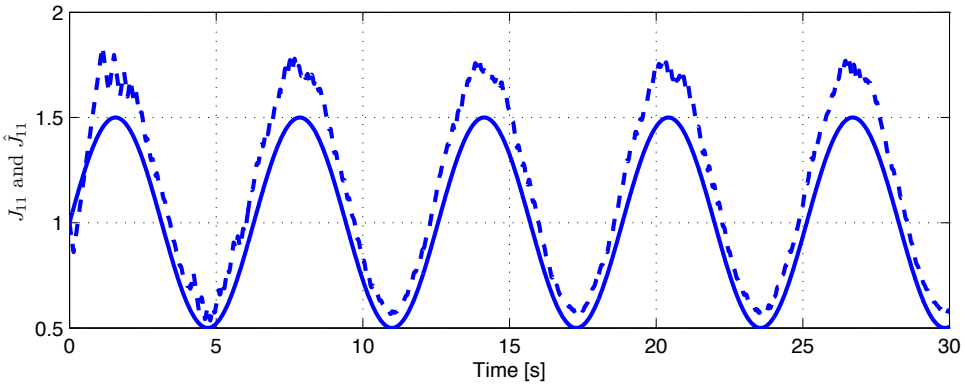

Figure 4.88: Uncertainty and estimation of mass of the leader quadrotor 1

4.5.4 Conclusion

An adaptive controller for leader-follower formation was presented. Uncertainty and external disturbances are solved by employing adaptive backstepping method. The simulation results demonstrated that the proposed controller works well with changing of unknown parameters and external disturbances. The avoidance function also performs well in both two cases, avoiding collision and keeping all the quadrotors in the sensing range. This avoidance function will be used in the next section for avoiding obstacles and collision.

4.6 Controller 5 - Formation of second order system

In the previous section, an adaptive controller for formation of leader-follower has been shown. The obstacle avoidance function uses the position information of quadrotors in the sensing range as the inputs for the avoidance function to avoid collision and keep all the quadrotors in the sensing range. However, all the formation form is fixed. In this section, a global controller

for a second order system is developed with the assumption that in the sensing range, the minimum distance to obstacles can be measured. It can be seen from previous section, the dynamics system of a quadrotor is usually separated into two subsystems, the translational subsystem and the rotational subsystem. After the intermediate control input force is calculated, the transformation coordinates via Lemma 2.3 generate the reference unit quaternion as the reference for the second subsystem. The second subsystem is a fully actuated system then it can be directly applied existing control design method to develop the control input for this subsystem. Second order system has the form of the translational subsystem so that it is chosen to expand the leader-follower formation in the case that the formation can be fixed, rotated around the formation center, expanded and moved along the reference formation.

4.6.1 Control objective

The dynamics of the second order system is written as in (4.164)

$$\begin{aligned} \dot{\boldsymbol{p}}_{ij} &= \boldsymbol{v}_{ij} \\ \dot{\boldsymbol{v}}_{ij} &= \boldsymbol{F}_{ij} \end{aligned} \tag{4.164}$$

where $ij \in \mathbb{N}$, $\mathbb{N}$ is the set of all vehicles in the group. All the other symbols in (4.164) are defined as in Section 2.1.
Before starting the formation control objective we impose the following assumption on the reference trajectories, communication and initial conditions between the vehicles in the group

Assumption 4.6.

1. *Let us define the formation of a group of quadrotors and the initial position of the leader quadrotor as follows*

$$\begin{aligned} \boldsymbol{L}_{LdLi} &= [x_{LdLi}\, y_{LdLi}\, z_{LdLi}]^T \\ \boldsymbol{p}_{Li}(t) &= [x_{i1}(t)\, y_{i1}(t)\, z_{i1}(t)]^T \end{aligned} \tag{4.165}$$

   where $\boldsymbol{L}_{Ldi}$ defines the formation shape of the leader vehicles and $\boldsymbol{p}_{Li}$ is position vector of the leader vehicles and it is defined as the first vehicle in each group. The follower dynamics then is defined as follows

$$\begin{aligned} \boldsymbol{L}_{F\_Ldij} &= [x_{F\_Ldij}\, y_{F\_Ldij}\, z_{F\_Ldij}]^T \\ \boldsymbol{p}_{F\_Lij}(t) &= [x_{F\_Lij}(t)\, y_{F\_Lij}(t)\, z_{F\_Lij}(t)]^T \end{aligned} \tag{4.166}$$

   where $\boldsymbol{L}_{F\_Ldij}$ defines the formation shape of the follower quadrotors and $\boldsymbol{p}_{F\_Lij}(t)$ is position vector of follower quadrotors in the $\boldsymbol{p}_{Li}$ group.

2. *The reference position trajectory $\boldsymbol{p}_d(t) = [x_d(t)\, y_d(t)\, z_d(t)]^T$ and the heading angle ψ_d are the based path for the leader vehicles to track. The reference trajectory, the formation of leader*

and follower are satisfied as follows

$$\begin{aligned} \left\|\boldsymbol{p}_{di}^{(k)}\right\| \leq \varepsilon_{0kd},\ \left\|\psi_{di}^{(k)}\right\| \leq \delta_{0kd}, \\ \left\|\boldsymbol{L}_{LdLi}^{(k)}\right\| \leq \varepsilon_{1kd},\ \left\|\boldsymbol{L}_{F\_Ldij}^{(k)}\right\| \leq \varepsilon_{2kd}, \end{aligned} \tag{4.167}$$

3. *Let us define*

$$\begin{aligned} \boldsymbol{p}_{ijmn} &= \boldsymbol{p}_{ij} - \boldsymbol{p}_{mn} \\ \boldsymbol{\alpha}_{ijmn} &= \tfrac{1}{2}\boldsymbol{p}_{ijmn}^T \boldsymbol{p}_{ijmn} \end{aligned} \tag{4.168}$$

where $ij \in \mathbb{N}_{mn}$, $\mathbb{N}_{mn}$ is the set of all vehicles and obstacles in the sensing range except the vehicle ij.

To avoid collision and keep all the vehicles in the sensing range, the collision avoidance function is chosen as follows

$$\beta_{ijmn} = k_\beta \frac{1 - h(\alpha_{ijmn}, \alpha_{ijmn}^S, \alpha_{ijmn}^S + \delta) - h(\alpha_{ijmn}, \alpha_{ijmn}^R - \delta, \alpha_{ijmn}^R)}{\alpha_{ijmn}} \tag{4.169}$$

where δ is a positive constant defined the working zone of the obstacle avoidance function.

Remark 4.6. *In the Assumption 4.6, property (1) is the definition for formation shape of the leaders and followers. Property (2) implies that the reference trajectory and formation are smooth. Property (3) illustrates a definition of an obstacle avoidance which guarantees capacity of communication and no collision among the vehicles.*

Control Objective 4.5. *Under the Assumption 4.6, first we design control input $\boldsymbol{F}_{Li}$ such that the Leader position vector $\boldsymbol{p}_{Li}(t)$ globally track the reference trajectory $\boldsymbol{p}_{Ldi}(t) = \boldsymbol{p}_d + \boldsymbol{L}_{LdLi}$. Then for each vehicle in the group, design control for the followers to track their references formed by vector $\boldsymbol{p}_{F\_Ldij}(t) = \boldsymbol{p}_{Li} + \boldsymbol{L}_{F\_Ldij}$. In more detail, for each vehicle F_Lij, design the control inputs $\boldsymbol{F}_{F\_Lij}$ such that the position vector $\boldsymbol{p}_{F\_Lij}(t)$ of the follower vehicle F_Lij track their reference trajectories $\boldsymbol{p}_{F\_Ldij}(t)$ while avoid collision with all other vehicles, obstacles and keep them in the sensing range. Specifically, we design the control inputs $\boldsymbol{F}_{Li}$ and $\boldsymbol{F}_{F\_Lij}$ such that*

$$\begin{aligned} &\lim_{t\to\infty} \left(\boldsymbol{p}_{Li}(t) - \boldsymbol{p}_{Ldi}(t)\right) = 0, \\ &\lim_{t\to\infty} \left(\psi_{Li}(t) - \psi_{di}(t)\right) = 0 \\ &\lim_{t\to\infty} \left(\boldsymbol{p}_{F\_Lij}(t) - \boldsymbol{p}_{F\_Ldij}(t)\right) = 0, \\ &\lim_{t\to\infty} \left(\psi_{F\_Lij}(t) - \psi_{Li}(t)\right) = 0 \\ &\|\boldsymbol{p}_{ij} - \boldsymbol{p}_{mn}\| \geq \alpha_{ijmn}^S \end{aligned} \tag{4.170}$$

for all $ij \in \mathbb{N}, ij \neq mn$ and $t \geq t_0 \geq 0$, the control design needs to keep all other states of the vehicle dynamics bounded for all initial conditions.

4.6.2 Control Design

To design control for the leader-follower formation satisfying the control objective 4.5, in first step, the controller for the leader tracking the predefined path is designed. After that the reference formation of followers is formed then the control inputs $\boldsymbol{F}_{Li}$ and $\boldsymbol{F}_{F\_Lij}$ are constructed.
We define the tracking errors as follows:

$$\begin{aligned}
\boldsymbol{p}_{eLi} &= \boldsymbol{p}_{Li} - \boldsymbol{p}_{Ldi}, \\
\boldsymbol{v}_{eLi} &= \boldsymbol{v}_{Li} - \boldsymbol{\alpha}_{vLi}, \\
\boldsymbol{p}_{eF_Lij} &= \boldsymbol{p}_{F_Lij} - \boldsymbol{p}_{F_Ldij}, \\
\boldsymbol{v}_{eF_Lij} &= \boldsymbol{v}_{F_Lij} - \boldsymbol{\alpha}_{vF_Lij},
\end{aligned} \tag{4.171}$$

where $\boldsymbol{\alpha}_{vLi}$ is a virtual control of leader velocity $\boldsymbol{v}_{Li}$ and $\boldsymbol{\alpha}_{vF\_Lij}$ is a virtual control of follower velocity $\boldsymbol{v}_{F\_Lij}$.
Differentiating both sides of (4.171) along (4.164), the error dynamics are expressed as

$$\begin{aligned}
\dot{\boldsymbol{p}}_{eLi} &= \boldsymbol{v}_{eLi} + \boldsymbol{\alpha}_{vLi} - \dot{\boldsymbol{p}}_{Ldi}, \\
\dot{\boldsymbol{v}}_{eLi} &= \boldsymbol{F}_{Li} - \dot{\boldsymbol{\alpha}}_{vLi} \\
\dot{\boldsymbol{p}}_{F_Lij} &= \boldsymbol{v}_{eF_Lij} + \boldsymbol{\alpha}_{vF_Lij} - \dot{\boldsymbol{p}}_{F_Lij}, \\
\dot{\boldsymbol{v}}_{eF_Lij} &= \boldsymbol{F}_{F_Lij} - \dot{\boldsymbol{\alpha}}_{vF_Lij}
\end{aligned} \tag{4.172}$$

where $\boldsymbol{F}_{Li}$ is the control input of the leader Li and $\boldsymbol{F}_{F\_Lij}$ is the control input of the follower F_Lij. In order to design these control inputs achieving the Formation control objective 4.5, we consider the following potential function:

$$V_{1a} = \frac{1}{2}\sum_{i=1}^{NL}\sum_{j=1}^{NF(i)}\left[\boldsymbol{p}_{eLi}^T\boldsymbol{p}_{eLi} + \sum_{ij\in\mathbb{N}_{ij}}\beta_{ijmn}\right] \tag{4.173}$$

where $\mathbb{N}_{ij}$ is the set containing all the vehicles and obstacles in the sensing range. NL is the number of leaders, and $NF(i)$ is the number of followers in the group i. β_{ijmn} is taken from (4.169) where α_{ijmn} is calculated from (4.168).
Differentiating both sides of (4.173) gives

$$\begin{aligned}
\dot{V}_{1a} &= \sum_{i=1}^{NL}\sum_{j=1}^{NF(i)}\left[\boldsymbol{p}_{eLi}^T\dot{\boldsymbol{p}}_{eLi} + \sum_{ij\in\mathbb{N}_{ij}}\beta'_{\text{ijmn}}\dot{\alpha}_{\text{ijmn}}\right] \\
&= \sum_{i=1}^{NL}\sum_{j=1}^{NF(i)}\left[\boldsymbol{p}_{eLi}^T\dot{\boldsymbol{p}}_{eLi} + \sum_{ij\in\mathbb{N}_{ij}}\beta'_{ijmn}\boldsymbol{p}_{ijmn}^T\dot{\boldsymbol{p}}_{ijmn}\right]
\end{aligned} \tag{4.174}$$

Noting that $\dot{\boldsymbol{p}}_{ijmn} = (\dot{\boldsymbol{p}}_{ij} - \dot{\boldsymbol{p}}_{Ldij}) - (\dot{\boldsymbol{p}}_{mn} - \dot{\boldsymbol{p}}_{Ldmn}) = \boldsymbol{v}_{eLij} - \boldsymbol{v}_{eLmn}$, we can write (4.174) as

follows

$$\begin{aligned}\dot{V}_{1a} &= \sum_{i=1}^{NL}\sum_{j=1}^{NF(i)}(\boldsymbol{p}_{eLi}^T + \sum_{ij\in\mathbb{N}_{ij}}\beta'_{ijmn}\boldsymbol{p}_{ijmn}^T)(\boldsymbol{v}_{eLi} + \boldsymbol{\alpha}_{vLi} - \dot{\boldsymbol{p}}_{Ldi}) \\ &= \sum_{i=1}^{NL}\sum_{j=1}^{NF(i)}\boldsymbol{\Omega}_{Li}^T(\boldsymbol{v}_{eLi} + \boldsymbol{\alpha}_{vLi} - \dot{\boldsymbol{p}}_{Ldi})\end{aligned} \tag{4.175}$$

where

$$\boldsymbol{\Omega}_{Li} = \boldsymbol{p}_{eLi} + \sum_{ij\in\mathbb{N}_{ij}}\beta'_{ijmn}\boldsymbol{p}_{ijmn} \tag{4.176}$$

The equation (4.175) suggests that we choose

$$\boldsymbol{\alpha}_{vLi} = -k_1\boldsymbol{\Omega}_{Li} + \dot{\boldsymbol{p}}_{Ldi} \tag{4.177}$$

To design the control input $\boldsymbol{F}_{Li}$, considering the following Lyapunov function

$$V_{2a} = V_{1a} + \frac{1}{2}\sum_{i=1}^{NL}\sum_{j=1}^{NF(i)}\boldsymbol{v}_{ei}{}^T\boldsymbol{v}_{ei} \tag{4.178}$$

Differentiating both sides of (4.178) gives

$$\dot{V}_{2a} = \sum_{i=1}^{NL}\sum_{j=1}^{NF(i)}\left[-k_1\boldsymbol{\Omega}_{Li}^T\boldsymbol{\Omega}_{Li} + \boldsymbol{v}_{ei}^T(\boldsymbol{F}_{Li} - \dot{\boldsymbol{\alpha}}_{vLi} + \boldsymbol{\Omega}_{Li})\right] \tag{4.179}$$

which suggests that we choose:

$$\boldsymbol{F}_{Li} = -k_2\boldsymbol{v}_{eLi} + \dot{\boldsymbol{\alpha}}_{vLi} - \boldsymbol{\Omega}_{Li} \tag{4.180}$$

For the follower group, the design process is similar as above. The control force $\boldsymbol{F}_{F\_Lij}$ is constructed by considering the following Lyapunov function

$$V_{1b} = \frac{1}{2}\sum_{i=1}^{NL}\sum_{j=1}^{NF(i)}\left[\boldsymbol{p}_{eF\_Lij}^T\boldsymbol{p}_{eF\_Lij} + \sum_{ij\in\mathbb{N}_{ij}}\beta_{ijmn}\right] \tag{4.181}$$

Differentiating both sides of (4.181) gives

$$\begin{aligned}\dot{V}_{1b} &= \sum_{i=1}^{NL}\sum_{j=1}^{NF(i)}\left[\boldsymbol{p}_{eF\_Lij}^T\dot{\boldsymbol{p}}_{eF\_Lij} + \sum_{ij\in\mathbb{N}_{ij}}\beta'_{\text{ijmn}}\dot{\alpha}_{\text{ijmn}}\right] \\ &= \sum_{i=1}^{NL}\sum_{j=1}^{NF(i)}\left[\boldsymbol{p}_{eF\_Lij}^T\dot{\boldsymbol{p}}_{eF\_Lij} + \sum_{ij\in\mathbb{N}_{ij}}\beta'_{ijmn}\boldsymbol{p}_{ijmn}^T\dot{\boldsymbol{p}}_{ijmn}\right]\end{aligned} \tag{4.182}$$

Noting that $\dot{\boldsymbol{p}}_{ijmn} = (\dot{\boldsymbol{p}}_{ij} - \dot{\boldsymbol{p}}_{F\_Ldij}) - (\dot{\boldsymbol{p}}_{mn} - \dot{\boldsymbol{p}}_{F\_Ldmn}) = \boldsymbol{v}_{eF\_Lij} - \boldsymbol{v}_{eF\_Lmn}$, we can write

(4.182) as follows

$$\begin{aligned}\dot{V}_{1b} &= \sum_{i=1}^{NL}\sum_{j=1}^{NF(i)}(\boldsymbol{p}_{eF\_Lij}^T + \sum_{ij\in\mathbb{N}_{ij}}\beta'_{ijmn}\boldsymbol{p}_{ijmn}^T)(\boldsymbol{v}_{eF\_Lij} + \boldsymbol{\alpha}_{vF\_Lij} - \dot{\boldsymbol{p}}_{F\_Ldij}) \\ &= \sum_{i=1}^{NL}\sum_{j=1}^{NF(i)}\boldsymbol{\Omega}_{F\_Lij}^T(\boldsymbol{v}_{eF\_Lij} + \boldsymbol{\alpha}_{vF\_Lij} - \dot{\boldsymbol{p}}_{F\_Ldij})\end{aligned} \tag{4.183}$$

where

$$\boldsymbol{\Omega}_{F\_Lij} = \boldsymbol{p}_{eF\_Lij} + \sum_{ij\in\mathbb{N}_{ij}}\beta'_{ijmn}\boldsymbol{p}_{ijmn} \tag{4.184}$$

The equation (4.183) suggests that we choose

$$\boldsymbol{\alpha}_{vF\_Lij} = -k_1\boldsymbol{\Omega}_{F\_Lij} + \dot{\boldsymbol{p}}_{F\_Ldi} \tag{4.185}$$

To design the control input $\boldsymbol{F}_{F\_Lij}$, considering the following Lyapunov function

$$V_{2b} = V_{1b} + \frac{1}{2}\sum_{i=1}^{NL}\sum_{j=1}^{NF(i)}\boldsymbol{v}_{eF\_Lij}{}^T\boldsymbol{v}_{eF\_Lij} \tag{4.186}$$

Differentiating both sides of (4.186) gives

$$\dot{V}_{2b} = \sum_{i=1}^{NL}\sum_{j=1}^{NF(i)}\left[-k_1\boldsymbol{\Omega}_{F\_Lij}^T\boldsymbol{\Omega}_{F\_Lij} + \boldsymbol{v}_{eF\_Lij}^T(\boldsymbol{F}_{F\_Lij} - \dot{\boldsymbol{\alpha}}_{vF\_Lij} + \boldsymbol{\Omega}_{F\_Lij})\right] \tag{4.187}$$

which suggests that we choose:

$$\boldsymbol{F}_{F\_Lij} = (-k_2\boldsymbol{v}_{\boldsymbol{eF\_Lij}} + \dot{\boldsymbol{\alpha}}_{vF\_Lij} - \boldsymbol{\Omega}_{F\_Lij}) \tag{4.188}$$

Substituting control inputs (4.180) and (4.188) into (4.172), we have the following closed loop system:

$$\begin{aligned}\dot{\boldsymbol{p}}_{eLi} &= \boldsymbol{v}_{eLi} - k_1\boldsymbol{\Omega}_{Li} \\ \dot{\boldsymbol{v}}_{eLi} &= -k_2\boldsymbol{v}_{eLi} - \boldsymbol{\Omega}_{\boldsymbol{Li}} \\ \dot{\boldsymbol{p}}_{eF\_Lij} &= \boldsymbol{v}_{eF\_Lij} - k_1\boldsymbol{\Omega}_{F\_Lij} \\ \dot{\boldsymbol{v}}_{eF\_Lij} &= -k_2\boldsymbol{v}_{eF\_Lij} - \boldsymbol{\Omega}_{\boldsymbol{F\_Lij}}\end{aligned} \tag{4.189}$$

The control design has been completed. We summarize the results in the following theorem.

Theorem 4.5. *Under Assumption 4.6, the formation control laws consisting of* (4.180) *and* (4.188) *for the vehicle ij achieve the Formation Control Objective 4.5, there is no collision between all the vehicles, the position $\boldsymbol{p}_{Li}$, and heading angle ψ_{Li} of the leader vehicle Li and the position $\boldsymbol{p}_{F\_Lij}$, and heading angle ψ_{F_Lij} of the follower vehicle F_Lij globally asymptotically track their reference*

trajectories $\boldsymbol{p}_{Ldi}$, ψ_{Ldi}, $\boldsymbol{p}_{F\_Ldij}$, *and* ψ_{F_Ldij}, *respectively.*

$$\begin{aligned}
&\lim_{t\to\infty}\left(\boldsymbol{p}_{Li}(t)-\boldsymbol{p}_{Ldi}(t)\right)=0,\\
&\lim_{t\to\infty}\left(\psi_{Li}(t)-\psi_{di}(t)\right)=0\\
&\lim_{t\to\infty}\left(\boldsymbol{p}_{F_Lij}(t)-\boldsymbol{p}_{F_Ldij}(t)\right)=0,\\
&\lim_{t\to\infty}\left(\psi_{F_Lij}(t)-\psi_{Li}(t)\right)=0\\
&\|\boldsymbol{p}_{ij}-\boldsymbol{p}_{mn}\|\geq\alpha^{S}_{ijmn}
\end{aligned}\tag{4.190}$$

and the closed loop system (4.189) *is forward complete.*

Proof. *See Appendix B.7.*

4.6.3 Simulation Results

In this section, we illustrate the effectiveness of the proposed formation control design through a numerical simulation. The number of leader $NL=4$ and $NF(i)=[4;4;4;4]$. The simulation is taken in seven cases with and without obstacles.
The initial conditions are taken as

$$\begin{aligned}
&\boldsymbol{p}_{ij}(0)=[(i-1)*R_1\quad(j-1)*R_1\quad 0]^T;\\
&\boldsymbol{v}_{ij}(0)=[0\,0\,0]^T
\end{aligned}\tag{4.191}$$

The reference path and formation of the leader and follower are chosen as follows

$$\begin{aligned}
&Ld_L1(:,i)=\boldsymbol{L}_{LdLi}=[RL0.sin((i-1).2.pi/(NL));RL0.cos((i-1).2.pi/(NL));0],\\
&\boldsymbol{L}_{F_Ldij}=[R0.sin((j-1).2.pi/(NF(i)-1));R0.cos((j-1).2.pi/(NF(i)-1));0],\\
&s=0.02.t,\\
&\boldsymbol{p}_{d1}=[15;2;4]\\
&\boldsymbol{p}_{d2}=[10.cos(0.1.s);10.sin(0.1.s);5],\\
&\boldsymbol{p}_{d3}=[10.cos(0.1.s);10.sin(0.1.s);5+s],
\end{aligned}\tag{4.192}$$

where $R_1=1.5m$, $R_0=3m$, at the first time, all vehicles are distributed on land in columns. The reference paths are a target point ($\boldsymbol{p}_{d1}$), a circle ($\boldsymbol{p}_{d2}$) and a helix ($\boldsymbol{p}_{d3}$).
The control gains are chosen as $|a_{ij}|=0.3m$, $|b_{ij}|=10m$, $\delta=.5m$, $k_1=2$, $k_2=5$. Simulation results are plotted in seven cases.
Case 1: The leaders are arranged on a rectangle and the followers are positioned on a triangle. The leader tracks a goal point $\boldsymbol{p}_{d1}$. The position of the leaders and followers in the formation is shown in the Figure 4.89. As can be seen from the Figure 4.90(a), 4.90(b), 4.91(a) and Figure 4.91(b) that all the position tracking errors are converged to the origin. The minimum

distance at 2s is about to safe area but there is no collision among vehicles.
Case 2: The leaders are arranged on a rectangle and the followers are positioned on a triangle and they rotate around their leader position. The position of leaders and followers is shown in Figure 4.92. From Figure 4.93(a), Figure 4.93(b), Figure 4.94(a) and Figure 4.94(b), one can see that all the position tracking errors are converged to the origin and there is no collision among vehicles.
Case 3: The rotation of the leaders around the reference point is added. The formation shape of leaders and followers arranged on a rectangle and triangle as in the case 2. The position of leaders and followers is shown in Figure 4.95. It can be seen from the Figure 4.96(a), Figure 4.96(b), and Figure 4.97(a) that all the position tracking errors are converged to the zero. The minimum distance among vehicles is greater than the safe radius as shown in Figure 4.97(b).
Case 4: Both leaders and followers rotate around their references. The leader formation is rotated around the reference point and the follower formation is rotated around its leader. The simulation of position of leaders and followers is plotted in Figure 4.98. The position tracking errors are plotted in Figure 4.99(a), Figure 4.99(b), and Figure 4.100(a). It is easy to see that all the position tracking errors are converged to the origin. The minimum distance among vehicles is greater than safe radius and there is no collision among them.
Case 5: The leader-follower formation tracking a helix path is added. Both leaders and followers rotate around their references. The leader formation is rotated around the reference point and the follower formation is rotated around its leader. The position of leaders and followers are plotted in Figure 4.101. The position tracking errors are plotted in Figure 4.102(a), Figure 4.102(b), and Figure 4.103(a). It can be seen from these figures that all the position tracking errors are converged to the zero. The minimum distance among vehicles is plotted in Figure 4.103(b). One can see that there is no collision among vehicles.
Case 6: The obstacles are added. The construction of these obstacles is generated randomly. These obstacles are arranged on a square with 6 rows and 6 columns. The distances between them is $2.5m$. The radius and height of obstacles are $rand(1)$ and $rand(6)$. The leader-follower formation are distributed at a reference point. Both leaders and followers rotate around their references. The position of leaders, followers and obstacles are plotted in Figure 4.105. The position tracking errors on x, y , z axis are plotted in Figure 4.104(a), Figure 4.104(b), and Figure 4.106(a). It can be seen from these figures that all the tracking errors tend to converge to zero. Some tracking errors are not converged to zero because at that time, the vehicles are closed to other vehicles or obstacles. It means that the obstacle avoidance function works effectively. This can be seen via Figure 4.106(b) that there is no collision among vehicles and obstacles.
Case 7: The obstacles are added and the construction of these obstacles is generated randomly. These obstacle's properties are chosen the same as case 6. The leader-follower formation tracks a circle path. Both leaders and followers rotate around their references. The position of leaders, followers and obstacles is plotted in Figure 4.107. The position tracking errors on x, y, z axis are plotted in Figure 4.104(a), Figure 4.104(b), and Figure 4.106(a). It can be seen from these

figures that all the tracking errors tend to converge to zero. Some tracking errors are still not converged to zero because at that time, the vehicles are closed to the other vehicles or obstacles. The minimum distance among vehicles and obstacles is greater than the safe radius. This can be seen via Figure 4.109(b) and there is no collision among vehicles and obstacles.
The simulation are plotted as follows:
Case 1: Leader follower formation of multiple leaders and followers where the leader formation distributes on a square shape and the follower formation arranges on a triangle. The goal point for the leader formation is $\boldsymbol{p}_{d1}$.

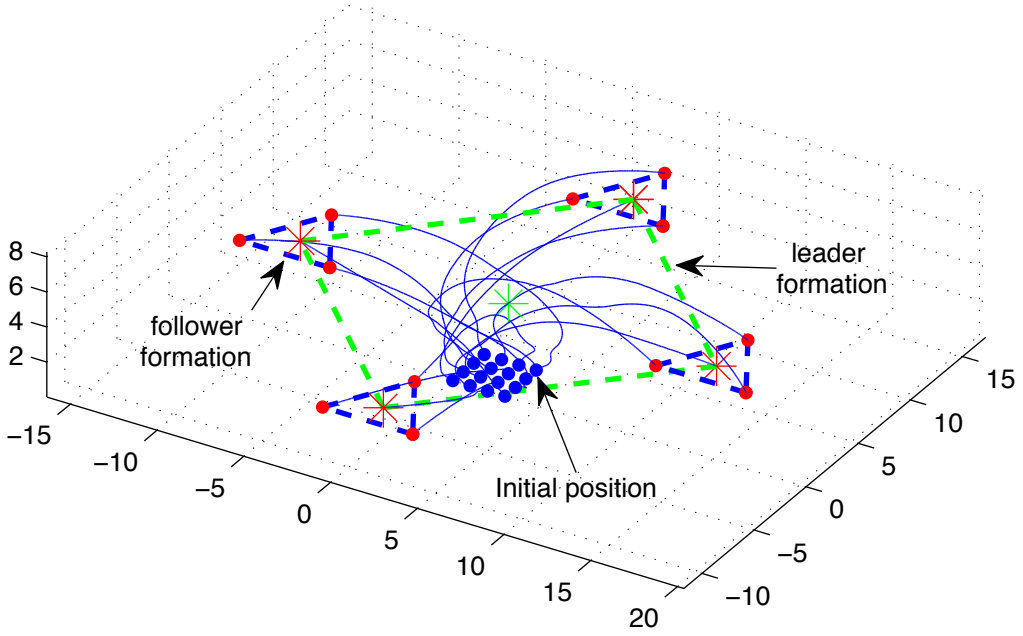

Figure 4.89: The leader-follower formation of of four leaders and three followers in each group distributed around a goal point

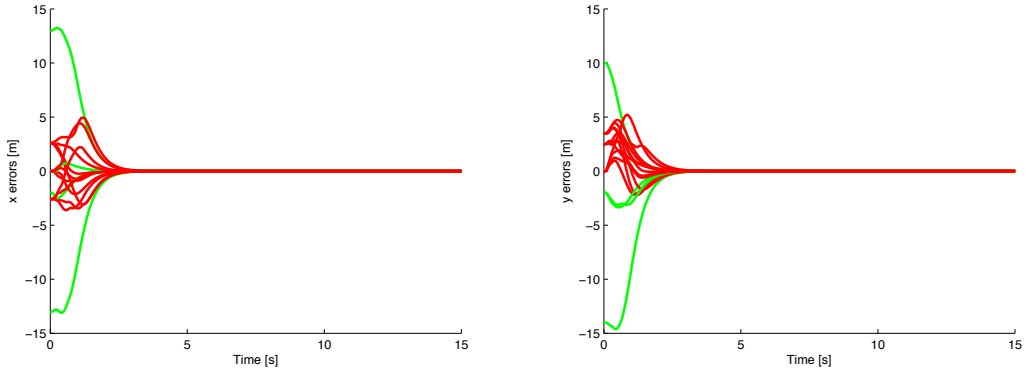

(a) Position tracking errors on x axis.

(b) Position tracking errors on y axis.

Figure 4.90: Position tracking errors on x and y axis.

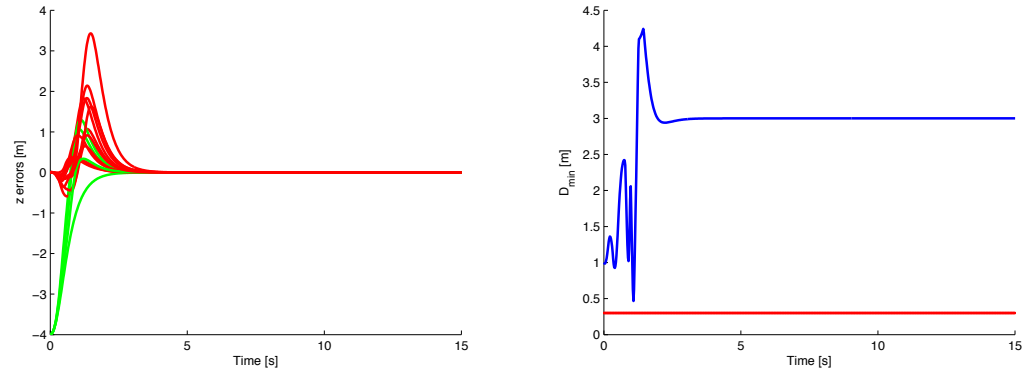

(a) Position tracking errors on z axis.

(b) Minimum distance among quadrotors.

Figure 4.91: Position tracking errors on z axis and the minimum distance among quadrotors in the formation.

Case 2: Leader follower formation of multiple leaders and followers where the leader formation distributes on a square shape and the follower formation arranges on a triangle. The goal point for the leader formation is $\boldsymbol{p}_{d1}$. The followers rotate around their leaders.

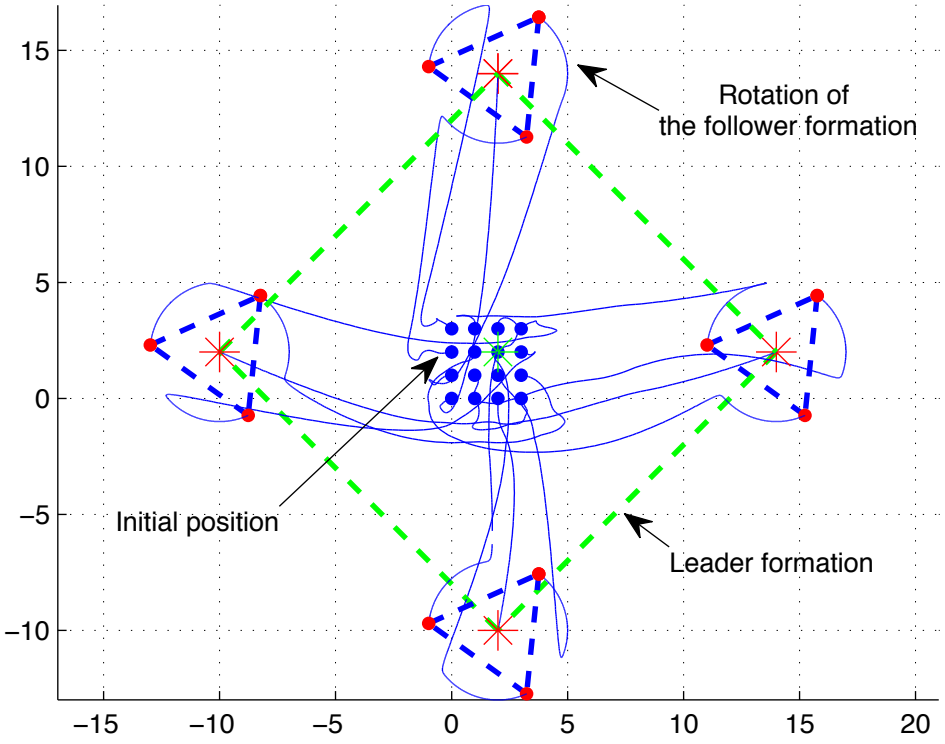

Figure 4.92: The leader-follower formation of of four leaders and three followers in each group distributed around a goal point

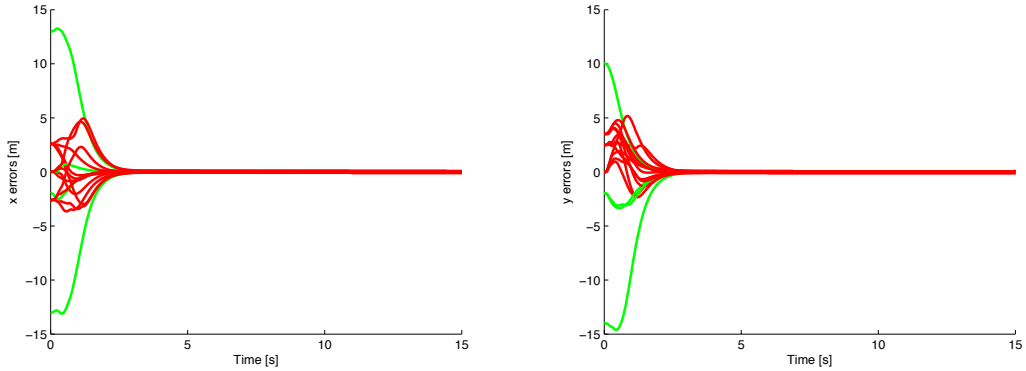

(a) Position tracking errors on x axis.

(b) Position tracking errors on y axis.

Figure 4.93: Position tracking errors on x and y axis.

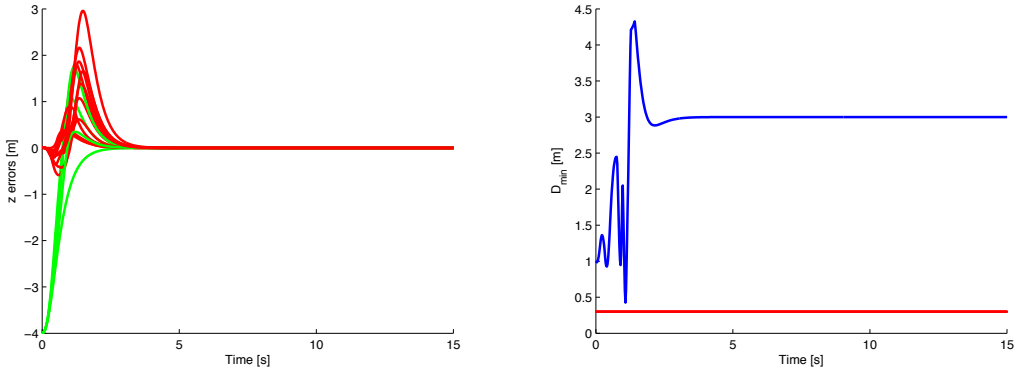

(a) Position tracking errors on z axis.

(b) Minimum distance among quadrotors

Figure 4.94: Position tracking errors on z axis and the minimum distance among quadrotors in the formation.

Case 3: Leader follower formation of multiple leaders and followers where the leader formation distributes on a square shape and the follower formation arranges on a triangle. The goal point for the leader formation is $\boldsymbol{p}_{d1}$. The leaders rotate around their reference point.

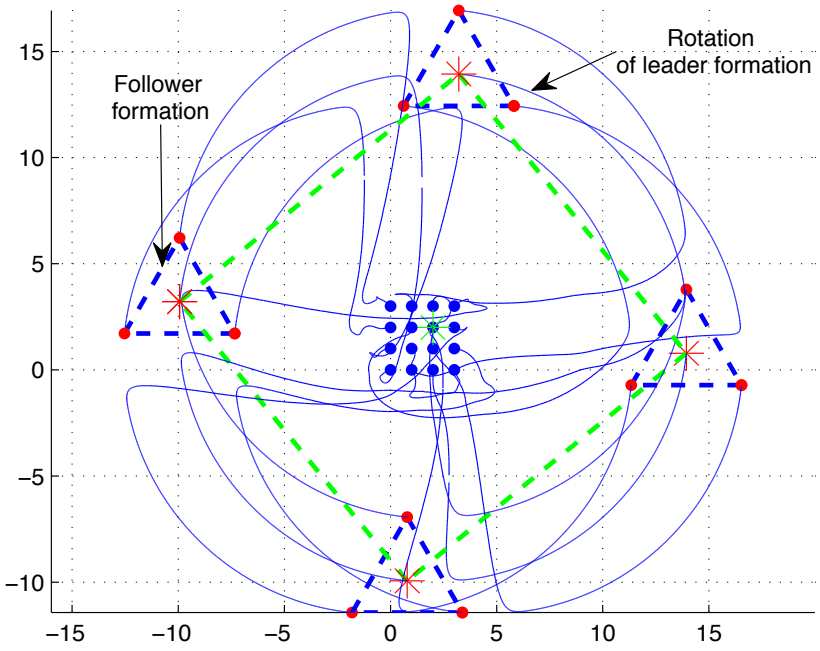

Figure 4.95: The leader-follower formation of of four leaders and three followers in each group distributed around a goal point

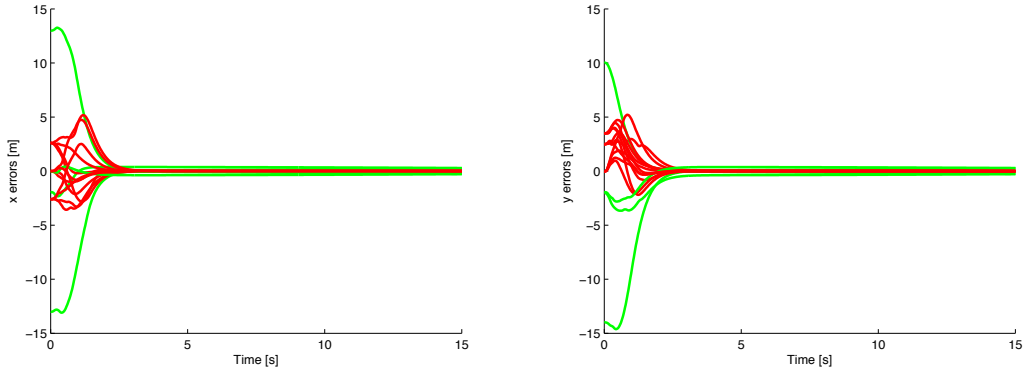

(a) Position tracking errors on x axis

(b) Position tracking errors on y axis.

Figure 4.96: Position tracking errors on x and y axis.

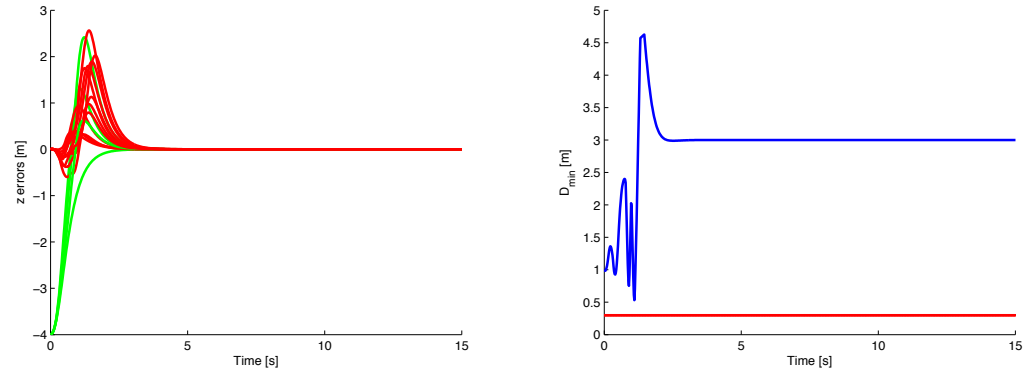

(a) Position tracking errors on z axis.

(b) Minimum distance among quadrotors

Figure 4.97: Position tracking errors on z axis and the minimum distance among quadrotors in the formation.

Case 4: Leader follower formation of multiple leaders and followers where the leader formation distributes on a square shape and the follower formation arranges on a triangle. The goal point for the leader formation is $\boldsymbol{p}_{d1}$. Both leaders and followers rotate around their references.

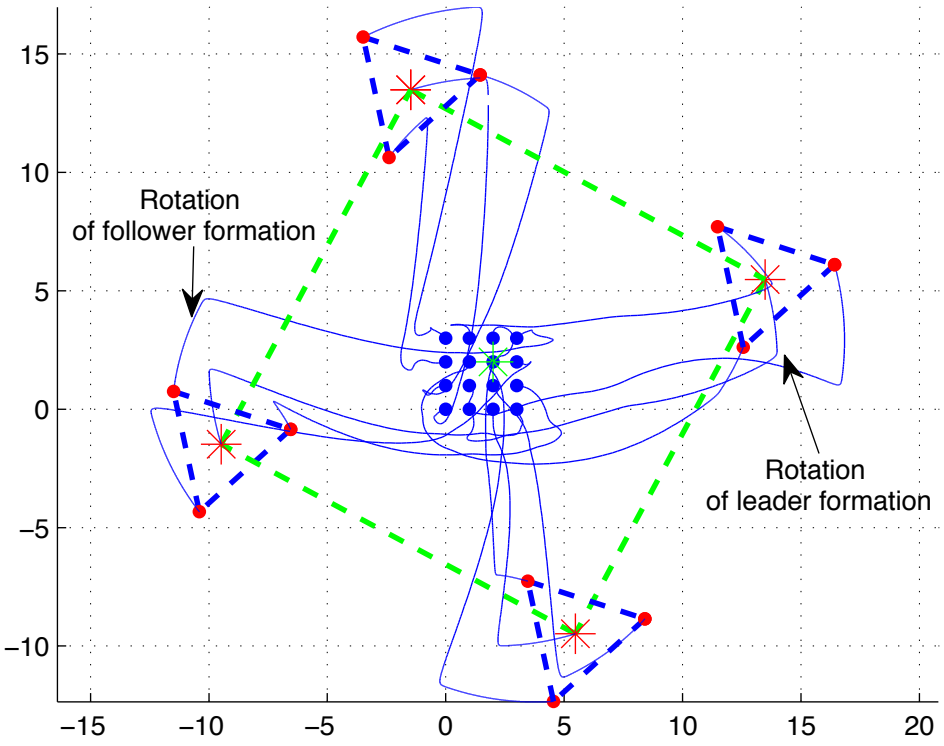

Figure 4.98: The leader-follower formation of of four leaders and three followers in each group distributed around a point

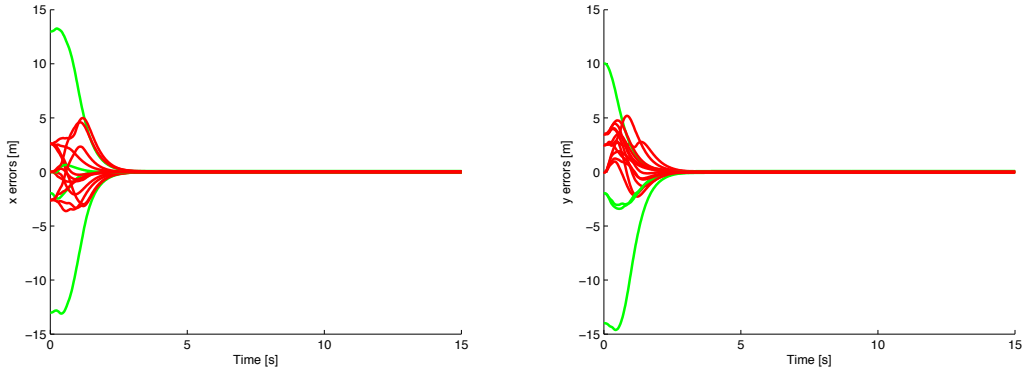

(a) Position tracking errors on x axis.

(b) Position tracking errors on y axis.

Figure 4.99: Position tracking errors on x and y axis.

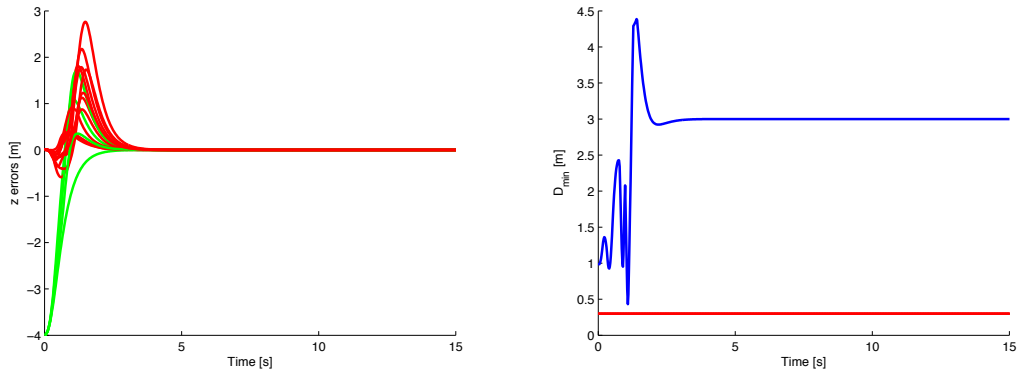

(a) Position tracking errors z axis.

(b) Minimum distance among quadrotors

Figure 4.100: Position tracking errors on z axis and the minimum distance among quadrotors in the formation.

Case 5: Leader follower formation of multiple leaders and followers where the leader formation distributes on a square shape and the follower formation arranges on a triangle. The reference path $\boldsymbol{p}_{d3}$ for the leaders is a helix. Both leaders and followers rotate around their references.

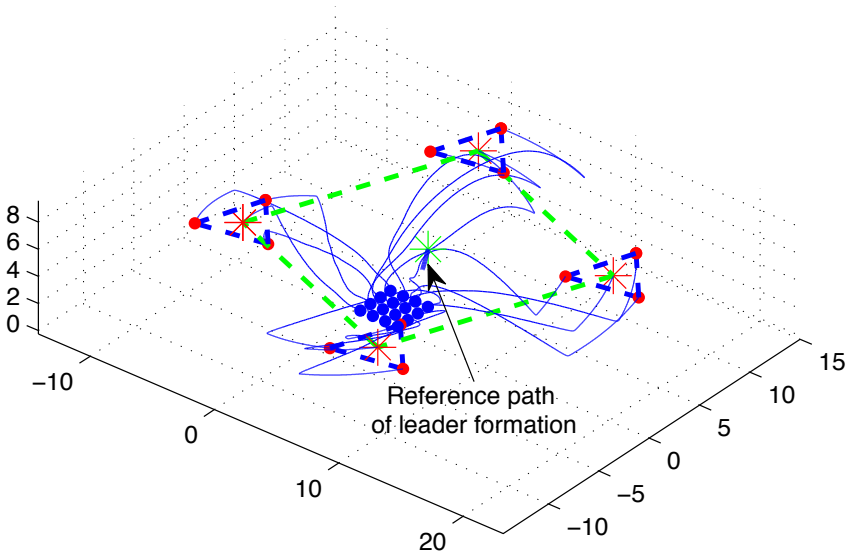

Figure 4.101: The leader-follower formation of of four leaders and three followers in each group distributed around their references

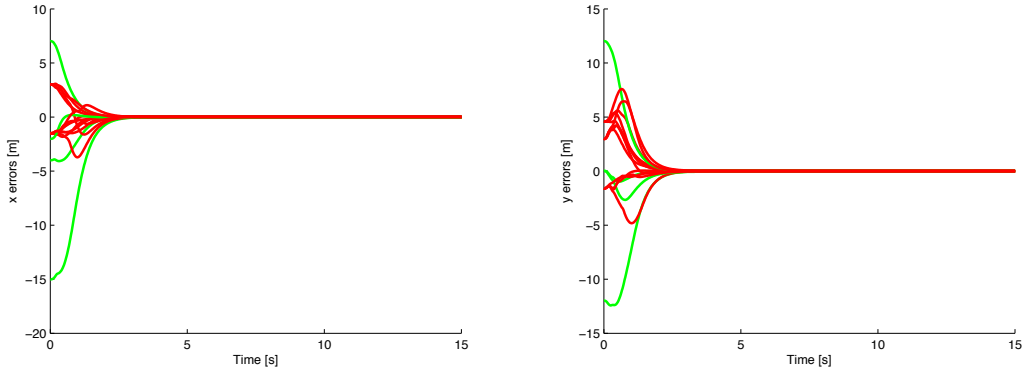

(a) Position tracking errors on x axis.

(b) Position tracking errors on y axis.

Figure 4.102: Position tracking errors on x and y axis.

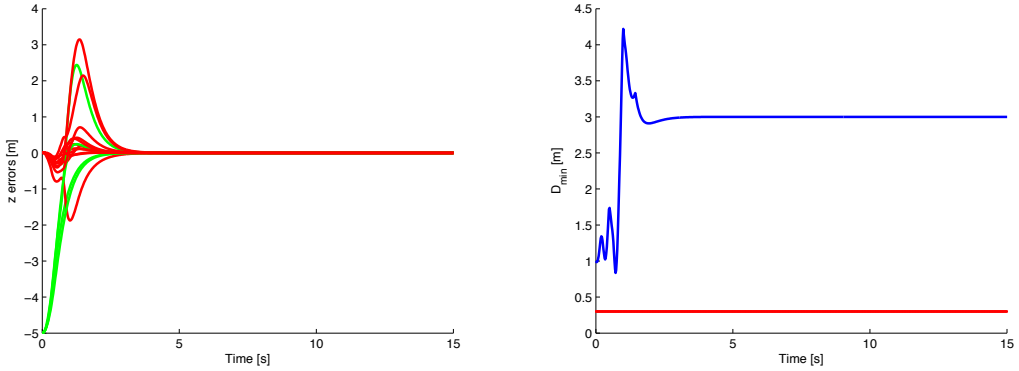

(a) Position tracking errors on z axis.

(b) Minimum distance among quadrotors

Figure 4.103: Position tracking errors on z axis and the minimum distance among quadrotors in the formation.

Case 6: Leader follower formation with obstacles. The reference path $\boldsymbol{p}_{d2}$ for the leaders is a circle. Both leaders and followers rotate around their references.

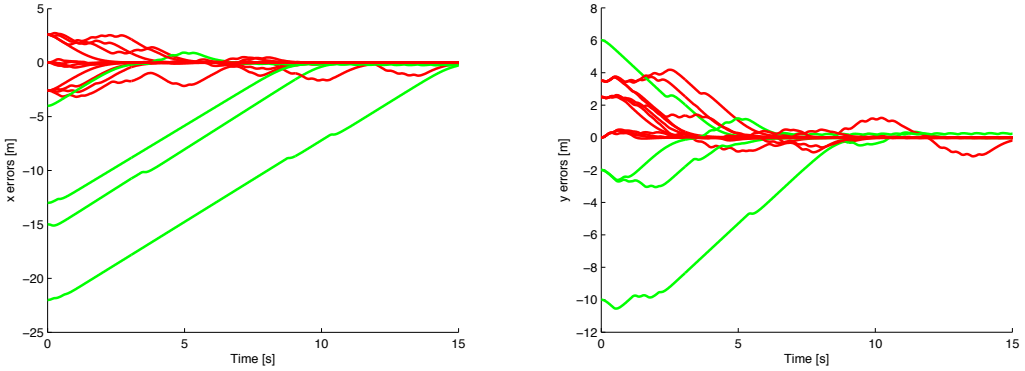

(a) Position tracking errors on x axis.

(b) Position tracking errors on y axis.

Figure 4.104: Position tracking errors on x and y axis.

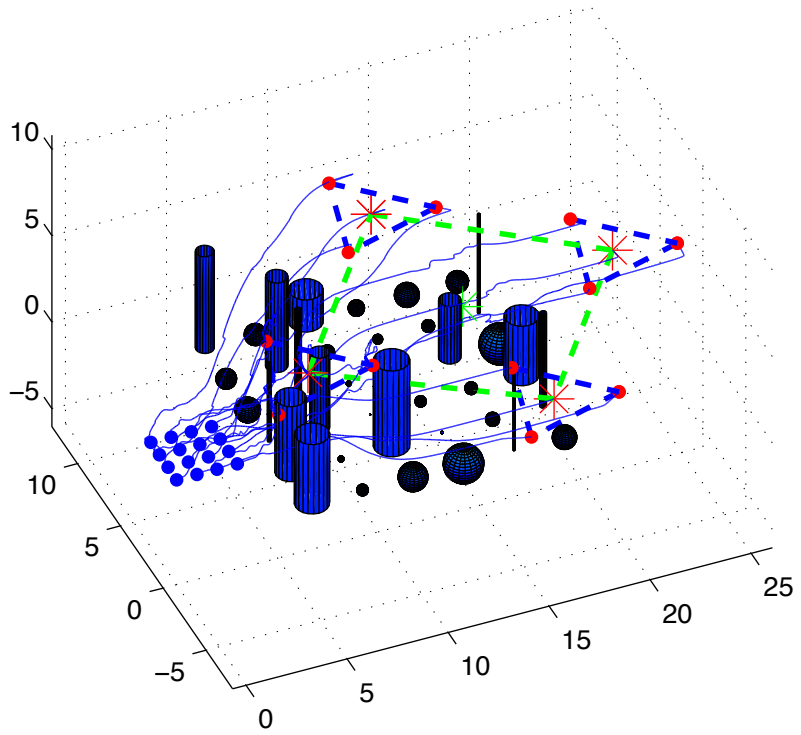

Figure 4.105: The leader-follower formation with obstacles

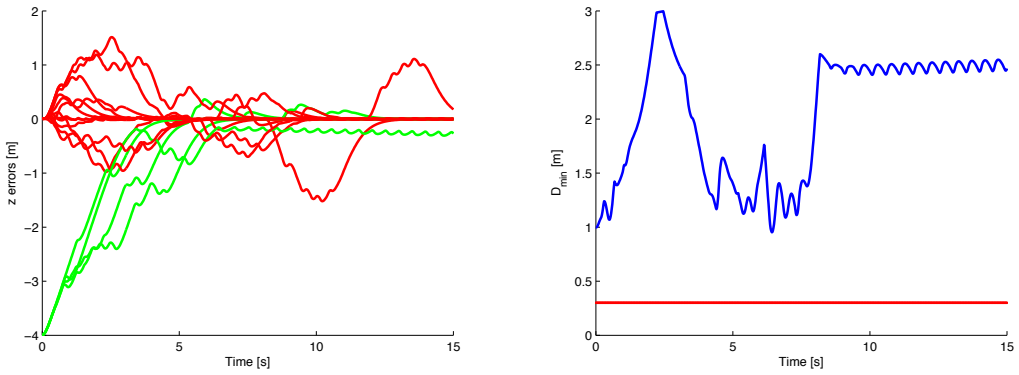

(a) Position tracking errors on z axis.

(b) Minimum distance among quadrotors

Figure 4.106: Position tracking errors on z axis and the minimum distance among quadrotors in the formation.

Case 7: Leader follower formation of multiple leaders and followers with obstacles. The reference path $\boldsymbol{p}_{d2}$ for the leaders is a circle. Both leaders and followers rotate around their references.

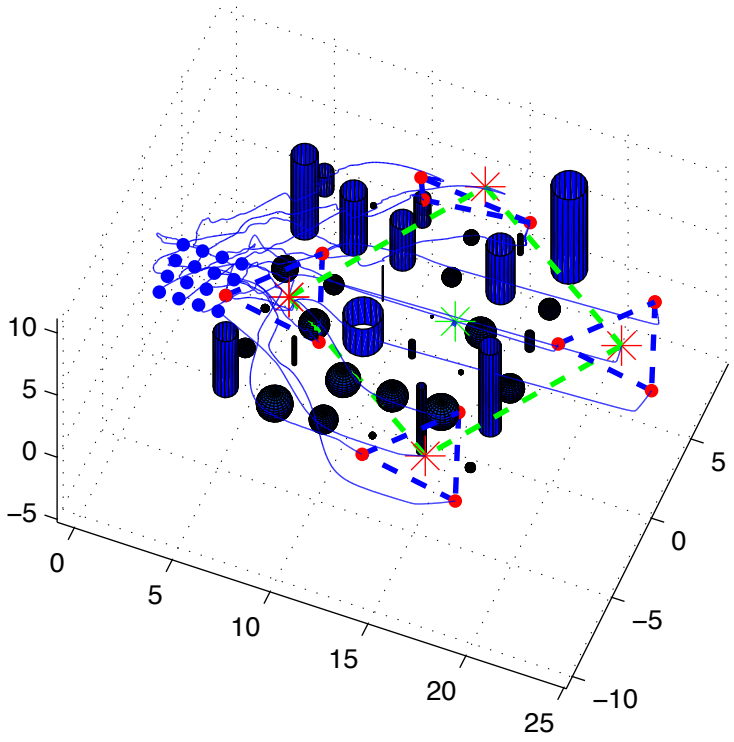

Figure 4.107: The leader-follower formation with obstacles.

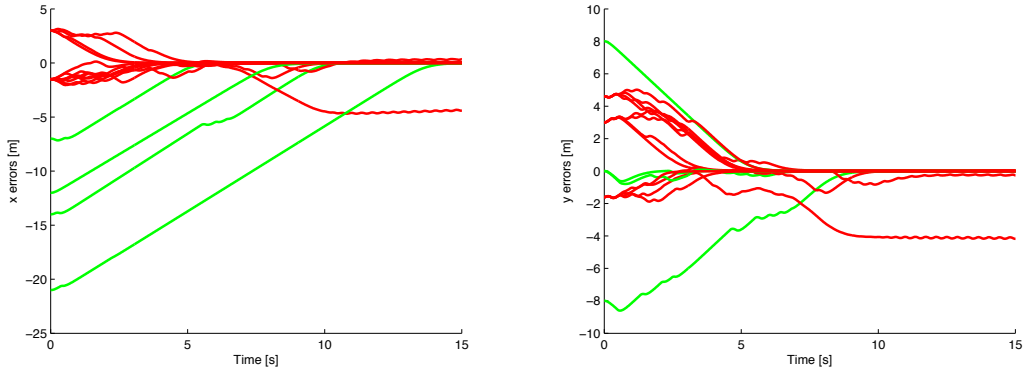

(a) Position tracking errors on x axis.

(b) Position tracking errors on y axis.

Figure 4.108: Position tracking errors on x and y axis.

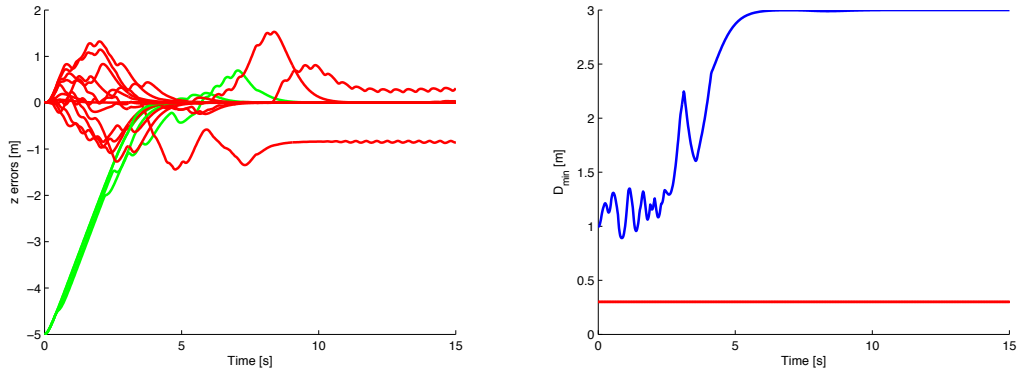

(a) Position tracking errors on z axis.

(b) Minimum distance among quadrotors

Figure 4.109: Position tracking errors on z axis and the minimum distance among quadrotors in the formation.

4.6.4 Conclusion

A leader-follower formation controller for second order system has been constructed. Seven cases of changing formation shape have been tested via simulations. Five first cases, obstacles are not included but the change of formation shape such as moving of follower around its leader or moving of leader and follower around its reference is simulated. In the last two cases, obstacles are added. The simulation results demonstrate that all the tracking errors converge to the origin and there is no collision among vehicles and obstacles.

4.7 Conclusion

Five formation controllers have been presented. For first third controllers, the virtual structure to form for the formation of quadrotors is developed. The first controller is an expansion of control for one quadrotor to multiple ones. In this controller, a transformation coordinate using conversion between quaternions and Euler angles is applied so that controller is developed for two subsystems, the translational and rotational subsystem. In addition to, the collision avoidance function constructing from a pairwise collision avoidance function is also embedded. The simulation results show that all the states converge to the origin and there is no collision among quadrotors in the formation. The second controller is being expanded by assuming that the linear velocity is unmeasured and the disturbance of the environment is added. By employing two observers, one for estimating the linear velocity and one for observing the environment disturbance, the formation controller is constructed. It is shown that the disturbance observer error converges to a ball centered at the origin and the velocity observer error also stabilizes to the zero. In the case the derivative of disturbance is equal zero, the disturbance error exponentially converges to zero. The simulation results illustrate that all the observer errors converge to zero. There is no collision among quadrotors and all the states stabilize to the origin. In the third controller, adaptive backstepping control design technique is employed. In comparing with the second controller, the estimations in this section do not reach to the real values. Instead of these, the tracking errors are eliminated by using the combination of the estimations and a energy function as presenting in the third controller. However, the third controller is dealt with the uncertainty in the quadrotor dynamics.

For the last two controllers, the fourth controller continuously uses the adaptive backstepping control design technique to develop a controller for a formation of leader-follower quadrotors and the fifth controller only concerns with the second order system. This second order system somehow has the form of the translational subsystem of a quadrotor dynamics. In the fourth controller, by using the leader-follower cooperation, an adaptive formation controller of leader-follower quadrotors has been developed. The update laws using the projection operator are constructed to avoid the finite escape time in the controller. A new collision avoidance function based on a smooth step function is also proposed and embedded. This function works quite well in both two cases: avoiding collision among quadrotors in the formation and keeping them in the sensing range. It can be seen that the fourth controller is a combination of virtual structure and leader-follower approach. The leaders usually track a moving object of virtual or actual vehicle and the followers cooperate tasks around the leaders. In the fourth controller, the leaders asymptotically track a predefined reference trajectory like the virtual structure approach, and the followers link with their leaders and form formation shapes. These formation shapes can be changed such as moving around a point, moving along a trajectory or expanding the whole group. Some tests in these cases are introduced in the fifth controller. The fifth controller is designed for a formation of leader-follower vehicles in the form of second order system. Seven cases have been tested with and without obstacles. For first five cases, the change of

formation shape is tested without obstacles. In the last two cases, the obstacles are included in the simulations. The simulation results show that the new collision avoidance function illustrates the effectiveness in avoidance of collision and obstacles.
The core of all the controllers is the thrust and attitude extraction algorithm. This algorithm transforms an underactuated system into two fully actuated systems which can directly apply any control design techniques to develop the controller for this kind of vehicles. This algorithm can be also applied for the vehicles on land or underwater.

CHAPTER

5

Thesis summary and future work

Contents

This chapter provides a summary of the work in the thesis and discusses some future research areas.

5.1 Thesis summary

The thesis consists of five chapters and two appendices. The first chapter presents an overview of formation control, formation control for VTOL UAVs, and control of a single VTOL UAV. In the chapter 2, the basic equations of a quadrotor and of multiple quadrotors in the form of Euler angles and quaternions have been described. Some mathematical tools using for developing the controllers in the chapter 3 and chapter 4 are also presented. The chapter 3 illustrates two controllers for an underactuted quadrotor. The first controller describing in Euler angles is designed. The drawback of Euler angle model is that there is singularity in the dynamics at the $\theta = \pi/2$. The thrust and attitude extraction algorithm in this controller is main idea to develop the global controller for single quadrotor and for formation of quadrotors in this thesis. The drawback in the Euler angles is overcome by using quaternions. The second controller employs the unit-quaternion in describing dynamics and uses adaptive backstepping control design technique to eliminate the affect of disturbance and uncertainty acting on the quadrotor. A new thrust and attitude extraction algorithm which transforms an underactuated system into two separated fully actuated subsystems is generated. This algorithm ensures that the control design process is easier and more simple. After this algorithm is applied, a thrust to force the quadrotor achieve the translational target and a reference attitude for the second subsystem are created. This algorithm is also embedded in formation controllers in the next chapter. Chapter 4 indicates five formation controllers divided into two group, the virtual structure (Section 4.2, 4.3, and 4.4) and the leader-follower group (Section 4.5, and 4.6). In both two group, the collision avoidance function based on pairwise smooth step function is embedded in the controllers. In the first group, virtual structure approach is applied to design the cooperation tasks for all quadrotors in the group tracking their references. All the equations of motion of quadrotor in Chapter 4 use quaternions for modeling. The first formation controller is designed for twelve quadrotors distributed on a circle shape while tracking their references. The collision avoidance function uses only the pushing force to put the other quadrotors far away. The simulation results show that this function works quite effectively and there is no collision among quadrotors in the formation. The new thrust and attitude extraction algorithm is also embedded in this controller. Moving to the second controller, the assumption, that the linear velocity and disturbance are unmeasured, is used. This controller uses two observers, one for linear velocity and one for disturbance to provide necessary signals for the controller. It is shown that all the observer values reach to the real ones. It is also shown that all the states are converged to the origin and there is no collision among quadrotors in the formation. The third controller is dealt with the uncertainty in the dynamics and the affect of environment disturbance. The adaptive backstepping technique is used. Unlike the previous controller, the estimations do not reach the real values. These values, obtained via control update laws, combine with a energy function to

eliminate the affect of uncertainty and disturbance on the quadrotors. The simulation results shows that this controller work well with the affect of uncertainty in the dynamics and environment disturbance. In the second group, leader-follower approach for formation of quadrotors is developed. The fourth controller continuously uses the adaptive backstepping control design technique to design control inputs. In this controller, the leader tracks a reference path like the virtual structure approach and the followers follow their leader and form their formation. The collision avoidance function in this controller is embedded with the pulling and pushing force so that the quadrotor in the formation can avoid collision among them and keep them in the sensing range. It can be seen from the simulation results that all the tracking errors converge to the zero under the affect of uncertainty and disturbance. The minimum distance satisfies the safe condition. There is no collision among quadrotors in the formation. In all above four controllers, the formation shape is fixed . To examine with the change of formation shape, the fifth controller for second order system is developed. Leader-follower formation is continuously applied. The change of formation shape of leaders and followers is simulated. The obstacles is also added in the simulation. The simulation results show that the collision avoidance function works quite effectively and there is no collision among vehicles and obstacles. The last two appendices present some proofs of lemma and theorem in this thesis.

5.2 Future work

The following issues are recommended for future works:

- Output-feedback control: Since the adaptive controllers in Chapter 3 and 4 use the state-feedback form to deal with the uncertainties and disturbances of the vehicle, it can be further exploited with adaptive control algorithms in the output-feedback form where some of the system states are not measured.
- Collision avoidance function: Although the collision avoidance function using in this thesis allows the vehicles in the formation avoid collision among them and with obstacles, somehow when the density of the vehicles and obstacles is increased, the position control objective may not be achieved. Expanding to the case when all the vehicles is connected, all the information can be exchange among connected vehicles. Then, the sensing range is expanded to the whole formation from which a more effective collision avoidance function may be created.
- An area which is not discussed in this thesis is the communication delay problem. This issue has been discussed in many research publications and it is one of issues in nonlinear time-delay systems. Observation and control for nonlinear time-delay systems are still open problems.
- Experimental work: Theory and practice are interrelated. It is of great practical interest to validate the controllers proposed in this thesis and to compare with existing ones in

experiments. The parameters of vehicle such as position and velocity, and the parameters of location or distance from the obstacles to the vehicle, size and movement speed of obstacles relative with the vehicle position are the main data needing to be determined. These values can be provided by sensors installed on/out of vehicles such as GPS, RADAR, Laser units, IMU,... Increase the accurate data to provide precise information about the position and velocity of the vehicle by using some kind of sensors is an interesting area. For example, using the vision-based sensors combining with GPS determines the current position of the vehicle while the GPS data is unavailable.

APPENDIX

A

Proof for Lemmas

A.1 Proof Of Lemma 2.2

To prove this Lemma, the conversion between quaternions and Euler angles is used. First we rewrite the the translational dynamics of a quadrotor in the Euler angles and quaternions as follows

$$\begin{aligned} \dot{\boldsymbol{p}} &= \boldsymbol{v} \\ \dot{\boldsymbol{v}} &= g\boldsymbol{e}_3 - \tfrac{1}{m} T \boldsymbol{R}_Q^T(\boldsymbol{Q}) \boldsymbol{e}_3 \end{aligned} \tag{A.1}$$

$$\begin{aligned} \dot{\boldsymbol{p}} &= \boldsymbol{v} \\ \dot{\boldsymbol{v}} &= g\boldsymbol{e}_3 - \tfrac{1}{m} T \boldsymbol{R}_\eta^T(\boldsymbol{\alpha}_Q) \boldsymbol{e}_3 \end{aligned} \tag{A.2}$$

where $\boldsymbol{R}_Q^T(\boldsymbol{Q})$ is a transformation in the unit-quaternion form. $\boldsymbol{R}_\eta^T(\boldsymbol{\alpha}_Q)$ is a transformation matrix, which is related through the functions of Euler angles. $\boldsymbol{\alpha}_Q = [\alpha_\phi \, \alpha_\theta \, \alpha_\psi]^T$ is an orientation vector in the earth-fixed frame where α_ϕ, α_θ and α_ψ are the roll, pitch and yaw angles, respectively. The transformation matrix in Euler angles is given by

$$\boldsymbol{R}_\eta(\boldsymbol{\alpha}_Q) = \begin{bmatrix} C\alpha_\theta C\alpha_\psi & -C\alpha_\phi S\alpha_\psi + S\alpha_\phi S\alpha_\theta C\alpha_\psi & S\alpha_\phi S\alpha_\psi + C\alpha_\phi S\alpha_\theta C\alpha_\psi \\ C\alpha_\theta S\alpha_\psi & C\alpha_\phi C\alpha_\psi + S\alpha_\phi S\alpha_\theta S\alpha_\psi & -S\alpha_\phi C\alpha_\psi + C\alpha_\phi S\alpha_\theta S\alpha_\psi \\ -S\alpha_\theta & S\alpha_\phi C\alpha_\theta & C\alpha_\phi C\alpha_\theta \end{bmatrix} \tag{A.3}$$

It is easy to see that the difference between the translational dynamics (A.2) and the translational dynamics (A.1) is the transformation matrix $\boldsymbol{R}_\eta^T(\boldsymbol{\alpha}_Q)$ and $\boldsymbol{R}_Q^T(\boldsymbol{Q})$. Thus the intermediate control force $\boldsymbol{F} = T\boldsymbol{R}_Q^T(\boldsymbol{Q})\boldsymbol{e}_3$ of (A.1) is also described as $\boldsymbol{F} = T\boldsymbol{R}_\eta^T(\boldsymbol{\alpha}_Q)\boldsymbol{e}_3$. Assuming that this control force achieves the translational control objective and ideally satisfies the heading reference angle ψ_d in which α_ψ is equal ψ_d.

Since $\boldsymbol{R}_\eta^T(\boldsymbol{\alpha}_Q)\boldsymbol{R}_\eta(\boldsymbol{\alpha}_Q) = \boldsymbol{I}_{3\times 3}$ and

$$T\boldsymbol{e}_3 = m\boldsymbol{R}_\eta(\boldsymbol{\alpha}_Q)\boldsymbol{F}, \tag{A.4}$$

we have

$$T = m \left\| \boldsymbol{F} \right\|, \tag{A.5}$$

The reference attitude $\boldsymbol{Q}_d$ is obtained through two steps, In the first step, the roll and pitch of the Euler angle vector $\boldsymbol{\alpha}_Q$ is calculated via the yaw angle α_ψ. In the next step, the attitude reference $\boldsymbol{Q}_d$ is obtained by using the conversion between quaternions and Euler angles. first we expand the term $\boldsymbol{R}_\eta(\boldsymbol{\alpha}_Q)$ by using (A.4) and $\boldsymbol{e}_3 = [0\,0\,1]^T$ as follows.

$$\begin{aligned} C\alpha_\theta C\alpha_\psi F_1 + C\alpha_\theta S\alpha_\psi F_2 - S\alpha_\theta F_3 &= 0 \\ \left[-C\alpha_\phi S\alpha_\psi + S\alpha_\phi S\alpha_\theta C\alpha_\psi\right] F_1 + \left[C\alpha_\phi C\alpha_\psi\right. & \\ \left. + S\alpha_\phi S\alpha_\theta S\alpha_\psi\right] F_2 + S\alpha_\phi C\alpha_\theta F_3 &= 0 \\ \left[S\alpha_\phi S\alpha_\psi + C\alpha_\phi S\alpha_\theta C\alpha_\psi\right] F_1 + \left[-S\alpha_\phi C\alpha_\psi\right. & \\ \left. + C\alpha_\phi S\alpha_\theta S\alpha_\psi\right] F_2 + C\alpha_\phi C\alpha_\theta F_3 &= T \end{aligned} \tag{A.6}$$

We choose $\alpha_\psi = \psi_d$ and calculate α_ϕ and α_θ depending on it. From the first equation of (A.6) we have

$$\alpha_\theta = \arctan\left(\frac{C\alpha_\psi F_1 + S\alpha_\psi F_2}{F_3}\right) \tag{A.7}$$

By multiplying the second equation of (A.6) with $-cos(\alpha_\phi)$ and the third equation of (A.6) with $sin(\alpha_\phi)$ then adding them together, we obtain

$$\alpha_\phi = \arcsin\left(\frac{S\alpha_\psi F_1 - C\alpha_\psi F_2}{T}\right) \tag{A.8}$$

Now we can use the conversion between quaternions and Euler angles to obtain the reference unit-quaternion vector $\boldsymbol{Q}_d$ as follows

$$\begin{aligned} T &= m\left\|\boldsymbol{F}\right\| \\ \boldsymbol{Q}_d &= \begin{bmatrix} C\frac{\alpha_\phi}{2}C\frac{\alpha_\theta}{2}C\frac{\alpha_\psi}{2} + S\frac{\alpha_\phi}{2}S\frac{\alpha_\theta}{2}S\frac{\alpha_\psi}{2} \\ S\frac{\alpha_\phi}{2}C\frac{\alpha_\theta}{2}C\frac{\alpha_\psi}{2} - C\frac{\alpha_\phi}{2}S\frac{\alpha_\theta}{2}S\frac{\alpha_\psi}{2} \\ C\frac{\alpha_\phi}{2}S\frac{\alpha_\theta}{2}C\frac{\alpha_\psi}{2} + S\frac{\alpha_\phi}{2}C\frac{\alpha_\theta}{2}S\frac{\alpha_\psi}{2} \\ C\frac{\alpha_\phi}{2}C\frac{\alpha_\theta}{2}S\frac{\alpha_\psi}{2} - S\frac{\alpha_\phi}{2}S\frac{\alpha_\theta}{2}C\frac{\alpha_\psi}{2} \end{bmatrix} \end{aligned} \tag{A.9}$$

A.2 Proof of Lemma 2.3

We first rewrite the tracking errors of nonlinear system (2.21) as follows

$$\begin{aligned} x_{1e} &= x_1 - x_d, \\ x_{2e} &= x_2 - \alpha_2 \end{aligned} \tag{A.10}$$

Differentiating both sides of (A.10) and using the control and update laws (2.22), we obtain the closed loop as follows

$$\begin{aligned} \dot{x}_{1e} &= -k_1 x_{1e} + x_{2e}, \\ \dot{x}_{2e} &= -k_2 x_{2e} - x_{1e} + \tilde{\theta}_1 u + \tilde{\theta}_2 \varphi(x) \end{aligned} \tag{A.11}$$

To prove that closed loop system (A.11) is globally asymptotically stable at the origin, we consider the following function

$$V = \tfrac{1}{2}x_{1e}^2 + \tfrac{1}{2}x_{2e}^2 + \tfrac{1}{2\gamma_1}\tilde{\theta}_1^2 + \tfrac{1}{2\gamma_2}\tilde{\theta}_2^2 \tag{A.12}$$

The first time derivative of V along solution of closed loop system (A.11) satisfies

$$\dot{V} = -k_1 x_{1e}^2 - k_2 x_{2e}^2 + \tilde{\theta}_1 \left(x_{2e} u + \frac{\dot{\tilde{\theta}}_1}{\gamma_1} \right) + \tilde{\theta}_2 \left(x_{2e} \varphi(x) + \frac{\dot{\tilde{\theta}}_2}{\gamma_2} \right) \tag{A.13}$$

we use

$$\begin{aligned} \dot{\hat{\theta}}_1 &= -\dot{\tilde{\theta}}_1 = proj(\gamma_1 x_{2e} u) \\ \dot{\hat{\theta}}_2 &= -\dot{\tilde{\theta}}_2 = \gamma_2 x_{2e} \varphi(x) \end{aligned} \tag{A.14}$$

Using (A.14) and projection operator's properties in (2.20) , the solution (A.13) can be rewritten as

$$\begin{aligned} \dot{V} &\leq -k_1 x_{1e}^2 - k_2 x_{2e}^2 + \tilde{\theta}_1 \left(x_{2e} u - \frac{\gamma_1 x_{2e} u}{\gamma_1} \right) + \tilde{\theta}_2 \left(x_{2e} \varphi(x) - \frac{\gamma_2 x_{2e} \varphi(x)}{\gamma_2} \right) \\ &\leq -k_1 x_{1e}^2 - k_2 x_{2e}^2 < 0 \quad \forall (x_{1e}, x_{2e}) \neq (0,0) \end{aligned} \tag{A.15}$$

which shows that the tracking error system (A.11) globally asymptotically converges to zero at origin.

A.3 Proof of Lemma 4.1

The proof of the disturbance observer can be seen in [DS10]. For more convenient , the disturbance observer is re-described. Let us first calculate the derivative of $\hat{\boldsymbol{d}}_i(t)$ as follows:

$$\begin{aligned} \dot{\hat{\boldsymbol{d}}}_i &= \dot{\boldsymbol{z}}_i + \boldsymbol{K}_{0i} \dot{\boldsymbol{G}}_{2i}^{-1}(\boldsymbol{x}_{1i}) \boldsymbol{x}_{2i} + \boldsymbol{K}_{0i} \boldsymbol{G}_{2i}^{-1}(\boldsymbol{x}_{1i}) \dot{\boldsymbol{x}}_{2i} \\ &= -\boldsymbol{K}_{0i} \boldsymbol{z}_i - \boldsymbol{K}_{0i} (\dot{\boldsymbol{G}}_{2i}^{-1}(\boldsymbol{x}_{1i}) \boldsymbol{x}_{2i} + \boldsymbol{G}_{2i}^{-1}(\boldsymbol{x}_{1i}) \boldsymbol{F}_{2i}(\boldsymbol{x}_{1i}, \boldsymbol{x}_{2i}, \boldsymbol{u}_i) + \boldsymbol{K}_{0i} \boldsymbol{G}_{2i}^{-1}(\boldsymbol{x}_{1i}) \boldsymbol{x}_{2i}) \\ &\quad + \boldsymbol{K}_{0i} \dot{\boldsymbol{G}}_{2i}^{-1}(\boldsymbol{x}_{1i}) \boldsymbol{x}_{2i} + \boldsymbol{K}_{0i} \boldsymbol{G}_{2i}^{-1}(\boldsymbol{x}_{1i}) \dot{\boldsymbol{x}}_{2i} \\ &= \boldsymbol{K}_{0i} (\boldsymbol{d}_i - \hat{\boldsymbol{d}}_i) = \boldsymbol{K}_{0i} \tilde{\boldsymbol{d}}_i \end{aligned} \tag{A.16}$$

Since $\tilde{\boldsymbol{d}}_i = \boldsymbol{d}_i - \hat{\boldsymbol{d}}_i$, using (A.16), we have:

$$\dot{\tilde{\boldsymbol{d}}}_i = \dot{\boldsymbol{d}}_i - \dot{\hat{\boldsymbol{d}}}_i = -\boldsymbol{K}_{0i} \tilde{\boldsymbol{d}}_i + \dot{\boldsymbol{d}}_i \tag{A.17}$$

Consider the Lyapunov function candidate

$$\tilde{V}_i = \frac{1}{2} \tilde{\boldsymbol{d}}_i^T \tilde{\boldsymbol{d}}_i \tag{A.18}$$

whose first time derivative along the solutions of (A.17) satisfies

$$\dot{\tilde{V}}_i = -\tilde{\boldsymbol{d}}_i^T \boldsymbol{K}_{0i} \tilde{\boldsymbol{d}}_i + \tilde{\boldsymbol{d}}_i^T \dot{\boldsymbol{d}}_i \tag{A.19}$$

Noting that

$$\begin{aligned} & \left(\tilde{\boldsymbol{d}}_i - \tfrac{1}{2\delta} \dot{\boldsymbol{d}}_i \right)^2 \geq 0 \\ \Leftrightarrow \quad & \tilde{\boldsymbol{d}}_i^T \tilde{\boldsymbol{d}}_i - \tfrac{\tilde{\boldsymbol{d}}_i^T \dot{\boldsymbol{d}}}{\delta} + \tfrac{1}{4\delta^2} \dot{\boldsymbol{d}}_i^T \dot{\boldsymbol{d}}_i \geq 0 \\ \Leftrightarrow \quad & \tilde{\boldsymbol{d}}_i^T \dot{\boldsymbol{d}}_i \leq \delta \tilde{\boldsymbol{d}}_i^T \tilde{\boldsymbol{d}} + \tfrac{1}{4\delta} \dot{\boldsymbol{d}}_i^T \dot{\boldsymbol{d}}_i \end{aligned} \tag{A.20}$$

Assume that $\dot{\boldsymbol{d}}_i \leq C_d$

$$\begin{aligned} \dot{\tilde{V}}_i &\leq -\tilde{\boldsymbol{d}}_i^T \left(\lambda_{\min}(\boldsymbol{K}_{0i}) - \delta\right) \tilde{\boldsymbol{d}}_i + \tfrac{1}{4\delta} \dot{\boldsymbol{d}}_i^T \dot{\boldsymbol{d}}_i \\ &\leq -2 \left(\lambda_{\min}(\boldsymbol{K}_{0i}) - \delta\right) \tilde{V}_i + \tfrac{1}{4\delta} C_d^2 \end{aligned} \tag{A.21}$$

where $\lambda_{min}(\boldsymbol{K}_{0i})$ is the minimum eigenvalue of the matrix $\boldsymbol{K}_{0i}$; δ is a positive constant such that $\lambda_{min}(\boldsymbol{K}_{0i}) - \delta$ is strictly positive; From (A.21), it is seen that $\tilde{V}_i$ exponentially converges to a ball centered the origin with the radius $R_{\tilde{V}_i} = \frac{C_d^2}{8\delta(\lambda_{min}(\boldsymbol{K}_{0i})-\delta)}$ as long as the solutions $\boldsymbol{x}_{1i}(t)$ and $\boldsymbol{x}_{2i}(t)$ exist. The existence of the solutions $\boldsymbol{x}_{1i}(t)$ and $\boldsymbol{x}_{2i}(t)$ is to be guaranteed by the design of the control input $\boldsymbol{u}_i$. This in turn means that the disturbance error $\tilde{\boldsymbol{d}}_i(t)$ exponentially converges to a ball centered at the origin with the radius $R_{\tilde{\boldsymbol{d}}_i} = \sqrt{\frac{1}{4\delta(\lambda_{min}(\boldsymbol{K}_{0i})-\delta)}} C_d$. Since $\lambda_{min}(\boldsymbol{K}_{0i})$ can be chosen arbitrarily large by choosing the matrix $\boldsymbol{K}_{0i}$, the radius $R_{\tilde{\boldsymbol{d}}_i}$ can be made arbitrarily small. In the case $C_d = 0$, the radius $R_{\tilde{\boldsymbol{d}}_i} = 0$ meaning that the disturbance error $\tilde{\boldsymbol{d}}_i(t)$ exponentially converges to zero.

APPENDIX

B

Proof for Theorems

B.1 Proof Of Theorem 3.1

It can be seen from (3.14) and (3.30) that $\dot{V}_2 \leq 0$ and $\dot{V}_4 \leq 0$. With the initial condition in Assumption 3.1, This implies that $V_2(t_0)$ and $V_4(t_0)$ are bounded. Thus, $V_2(t)$ and $V_4(t)$ are also bounded. Boundedness of $V_2(t)$ and $V_4(t)$ for all $t \geq t_0 \geq 0$ imply that of $\boldsymbol{p}_e$, $\boldsymbol{v}_e$, $\boldsymbol{\eta}_e$, and $\boldsymbol{\omega}_e$. Therefore the closed-loop system (3.31) is forward complete. It also implies that $(\psi(t) - \psi_d(t)) = 0$ and $\lim_{t\to\infty} (\boldsymbol{p}(t) - \boldsymbol{p}_d(t)) = 0$. This ends the proof.

B.2 Proof Of Theorem 3.2

To prove Theorem 3.2, we consider the following function

$$\begin{aligned} V &= \tfrac{1}{2}\boldsymbol{p}_e^T\boldsymbol{p}_e + \tfrac{1}{2}\boldsymbol{v}_e^T\boldsymbol{v}_e + \frac{\tilde{\boldsymbol{J}}_1^T\tilde{\boldsymbol{J}}_1}{2\gamma_{v1}} + \frac{\tilde{\boldsymbol{d}}_v^T\tilde{\boldsymbol{d}}_v}{2\gamma_{v2}} \\ &+ \tfrac{1}{2}\boldsymbol{q}_e^T\boldsymbol{q}_e + \tfrac{1}{2}\boldsymbol{\omega}_e^T\boldsymbol{\omega}_e + \frac{\tilde{\boldsymbol{J}}_2^T\tilde{\boldsymbol{J}}_2}{2\gamma_{\omega1}} + \frac{\tilde{\boldsymbol{d}}_\omega^T\tilde{\boldsymbol{d}}_\omega}{2\gamma_{\omega2}} \end{aligned} \tag{B.1}$$

using control and update laws in (3.38) and (3.44), and smooth saturation function and projection operator properties, the first derivative of V satisfies

$$\begin{aligned} V &\leq -k_1\boldsymbol{p}_e^T\boldsymbol{p}_e - k_2\boldsymbol{v}_e^T\boldsymbol{v}_e \\ &\quad +\tilde{\boldsymbol{J}}_1^T\left((\tilde{\boldsymbol{J}}_1^T)^{-1}\boldsymbol{v}_e^T\hat{\boldsymbol{J}}_1\boldsymbol{F}_d) - \tfrac{\gamma_{v1}(\hat{\boldsymbol{J}}_1^T)^{-1}(\boldsymbol{v}_e^T\hat{\boldsymbol{J}}_1\boldsymbol{F}_d)}{\gamma_{v1}}\right) \\ &\quad +\tilde{\boldsymbol{d}}_v^T\left(\boldsymbol{v}_e - \tfrac{\gamma_{v2}\boldsymbol{v}_e}{\gamma_{v2}}\right) \\ &\quad -k_3\boldsymbol{q}_e^T\boldsymbol{q}_e - k_4\boldsymbol{\omega}_e^T\boldsymbol{\omega}_e \\ &\quad +\tilde{\boldsymbol{J}}_2^T\left((\tilde{\boldsymbol{J}}_2^T)^{-1}\boldsymbol{\omega}_e^T\hat{\boldsymbol{J}}_2\boldsymbol{\tau}) - \tfrac{\gamma_{\omega1}(\hat{\boldsymbol{J}}_2^T)^{-1}(\boldsymbol{\omega}_e^T\hat{\boldsymbol{J}}_2\boldsymbol{\tau})}{\gamma_{\omega1}}\right) \\ &\quad +\tilde{\boldsymbol{d}}_\omega^T\left(\boldsymbol{\omega}_e - \tfrac{\gamma_{\omega2}\boldsymbol{\omega}_e}{\gamma_{\omega2}}\right) \\ &\leq -k_1\boldsymbol{p}_e^T\boldsymbol{p}_e - k_2\boldsymbol{v}_e^T\boldsymbol{v}_e - k_3\boldsymbol{q}_e^T\boldsymbol{q}_e - k_4\boldsymbol{\omega}_e^T\boldsymbol{\omega}_e \\ &< 0 \quad \forall(\boldsymbol{p}_e, \boldsymbol{v}_e, \boldsymbol{q}_e, \boldsymbol{\omega}_e) \neq (0,0,0,0). \end{aligned} \tag{B.2}$$

With the initial condition in Assumption 3.1, $V(t_0)$ is bounded. Thus, $V(t)$ is also bounded. Boundedness of $V(t)$ for all $t \geq t_0 \geq 0$ implies that of $\boldsymbol{p}_e$, $\boldsymbol{v}_e$, $\boldsymbol{q}_e$, and $\boldsymbol{\omega}_e$. Therefore the closed-loop system (3.45) is forward complete. Since $\lim_{t\to\infty} \boldsymbol{q}_e = 0$ implies that $(\psi(t) - \psi_d(t)) = 0$; It also shows that $\lim_{t\to\infty} (\boldsymbol{p}(t) - \boldsymbol{p}_d(t)) = 0$. This ends the proof.

B.3 Proof Of Theorem 4.1

From the Lyapunov candidates (4.20) and (4.31), we first consider the following Lyapunov function

$$V = V_2 + V_4 \tag{B.3}$$

Differentiating both sides of (B.3) and substituting with (4.21) and (4.32), yields,

$$\begin{aligned} \dot{V} &= \sum_{i=1}^{N} \left(-k_1 \boldsymbol{\Omega}_i^T \boldsymbol{\Omega}_i - k_2 \boldsymbol{v}_{ei}^T \boldsymbol{v}_{ei} - k_3 \boldsymbol{q}_{ei}^T \boldsymbol{G}_i \boldsymbol{G}_i^T \boldsymbol{q}_{ei} - k_4 \boldsymbol{\omega}_{ei}^T \boldsymbol{\omega}_{ei}\right), \\ &< 0 \quad \forall (\boldsymbol{\Omega}_i, \boldsymbol{v}_{ei}, \boldsymbol{q}_{ei}, \boldsymbol{\omega}_{ei}) \neq (0,0,0,0). \end{aligned} \tag{B.4}$$

With the initial condition in Assumption 4.2, $V(t_0)$ is bounded. Thus, $V(t)$ is also bounded. Boundedness of $V(t)$ for all $t \geq t_0 \geq 0$ implies that of $\boldsymbol{\Omega}_i$, $\boldsymbol{p}_{ei}$, $\boldsymbol{v}_{ei}$, $\boldsymbol{q}_{ei}$, and $\boldsymbol{\omega}_{ei}$. Therefore the closed-loop system (4.33) is forward complete. Since $\lim_{t\to\infty} \boldsymbol{q}_{ei} = 0$ implies that $(\psi_i(t) - \psi_d(t)) = 0$; It also shows that $\lim_{t\to\infty} (\boldsymbol{p}_i(t) - \boldsymbol{p}_{di}(t)) = 0$. This ends the proof.

B.4 Proof Of Theorem 4.2

The convergence of the linear velocity observer and disturbance observer has been proved as in Section 4.3.2.1 and Lemma A.3. Let we consider the following following Lyapunov function

$$V = V_2 + V_4 \tag{B.5}$$

Differentiating both sides of (B.5) and substituting with (4.63) and (4.74), yields,

$$\begin{aligned} \dot{V} &= \sum_{i=1}^{N} \left(-k_1 \boldsymbol{\Omega}_i^T \boldsymbol{\Omega}_i - k_2 \boldsymbol{v}_{ei}^T \boldsymbol{v}_{ei} - k_3 \boldsymbol{q}_{ei}^T \boldsymbol{G}_i \boldsymbol{G}_i^T \boldsymbol{q}_{ei} - k_4 \boldsymbol{\omega}_{ei}^T \boldsymbol{\omega}_{ei}\right), \\ &< 0 \quad \forall (\boldsymbol{\Omega}_i, \boldsymbol{v}_{ei}, \boldsymbol{q}_{ei}, \boldsymbol{\omega}_{ei}) \neq (0,0,0,0). \end{aligned} \tag{B.6}$$

With the initial condition in Assumption 4.3, $V(t_0)$ is bounded. Thus, $V(t)$ is also bounded. Boundedness of $V(t)$ for all $t \geq t_0 \geq 0$ implies that of $\boldsymbol{\Omega}_i$, $\boldsymbol{p}_{ei}$, $\boldsymbol{v}_{ei}$, $\boldsymbol{q}_{ei}$, and $\boldsymbol{\omega}_{ei}$. Therefore the closed-loop system (4.75) is forward complete. Since $\lim_{t\to\infty} \boldsymbol{q}_{ei} = 0$ implies that $(\psi_i(t) - \psi_d(t)) = 0$; It also shows that $\lim_{t\to\infty} (\boldsymbol{p}_i(t) - \boldsymbol{p}_{di}(t)) = 0$. This ends the proof.

B.5 Proof Of Theorem 4.3

Let we consider the following following Lyapunov function

$$V = V_2 + V_4 + \sum_{i=1}^{N} \left[\frac{\tilde{\boldsymbol{J}}_{1i}^T \tilde{\boldsymbol{J}}_{1i}}{2\gamma_{v1}} + \frac{\tilde{\boldsymbol{d}}_{vi}^T \tilde{\boldsymbol{d}}_{vi}}{2\gamma_{v2}} + \frac{\tilde{\boldsymbol{J}}_{2i}^T \tilde{\boldsymbol{J}}_{2i}}{2\gamma_{\omega 1}} + \frac{\tilde{\boldsymbol{d}}_{\omega i}^T \tilde{\boldsymbol{d}}_{\omega i}}{2\gamma_{\omega 2}} \right] \tag{B.7}$$

where V_2 and V_4 is taken from (4.94) and (4.106). Differentiating both sides of (B.7) and

substituting (4.96) , (4.108) and using control update laws (4.97), (4.109), yields

$$\begin{aligned}
\dot{V} &= \sum_{i=1}^{N} \left(-k_1 \boldsymbol{\Omega}_i^T \boldsymbol{\Omega}_i - k_2 \boldsymbol{v}_{ei}^T \boldsymbol{v}_{ei} - k_3 \boldsymbol{q}_{ei}^T \boldsymbol{G}_i \boldsymbol{G}_i^T \boldsymbol{q}_{ei} - k_4 \boldsymbol{\omega}_{ei}^T \boldsymbol{\omega}_{ei}\right), \\
&\quad + \sum_{i=1}^{N} \left(\tilde{\boldsymbol{J}}_{1i}^T \left((\tilde{\boldsymbol{J}}_{1i}^T)^{-1} (\boldsymbol{v}_{ei}^T \hat{\boldsymbol{J}}_{1i} \boldsymbol{F}_i) - \frac{\gamma_{v1} (\hat{\boldsymbol{J}}_{1i}^T)^{-1} (\boldsymbol{v}_{e1}^T \hat{\boldsymbol{J}}_{1i} \boldsymbol{F}_i)}{\gamma_{v1}} \right) + \tilde{\boldsymbol{d}}_{vi}^T \left(\boldsymbol{v}_{ei} - \frac{\gamma_{v2} \boldsymbol{v}_{ei}}{\gamma_{v2}} \right) \right) \\
&\quad + \sum_{i=1}^{N} \left(\tilde{\boldsymbol{J}}_{2i}^T \left((\tilde{\boldsymbol{J}}_{2i}^T)^{-1} (\boldsymbol{\omega}_{ei}^T \hat{\boldsymbol{J}}_{2i} \boldsymbol{\tau}_i) - \frac{\gamma_{\omega 1} (\hat{\boldsymbol{J}}_{2i}^T)^{-1} (\boldsymbol{\omega}_{ei}^T \hat{\boldsymbol{J}}_{2i} \boldsymbol{\tau}_i)}{\gamma_{\omega 1}} \right) + \tilde{\boldsymbol{d}}_{\omega i}^T \left(\boldsymbol{\omega}_{ei} - \frac{\gamma_{\omega 2} \boldsymbol{\omega}_{ei}}{\gamma_{\omega 2}} \right) \right) \\
&= \sum_{i=1}^{N} \left(-k_1 \boldsymbol{\Omega}_i^T \boldsymbol{\Omega}_i - k_2 \boldsymbol{v}_{ei}^T \boldsymbol{v}_{ei} - k_3 \boldsymbol{q}_{ei}^T \boldsymbol{G}_i \boldsymbol{G}_i^T \boldsymbol{q}_{ei} - k_4 \boldsymbol{\omega}_{ei}^T \boldsymbol{\omega}_{ei}\right), \\
&< 0, \quad \forall (\boldsymbol{\Omega}_i, \boldsymbol{v}_{ei}, \boldsymbol{q}_{ei}, \boldsymbol{\omega}_{ei}) \neq (0,0,0,0).
\end{aligned} \tag{B.8}$$

With the initial condition in Assumption 4.4, $V(t_0)$ is bounded. Thus, $V(t)$ is also bounded. Boundedness of $V(t)$ for all $t \geq t_0 \geq 0$ implies that of $\boldsymbol{\Omega}_i$, $\boldsymbol{p}_{ei}$, $\boldsymbol{v}_{ei}$, $\boldsymbol{q}_{ei}$, and $\boldsymbol{\omega}_{ei}$. Therefore the closed-loop system (4.110) is forward complete. Since $\lim_{t\to\infty} \boldsymbol{q}_{ei} = 0$ implies that $(\psi_i(t) - \psi_d(t)) = 0$; It also shows that $\lim_{t\to\infty} (\boldsymbol{p}_i(t) - \boldsymbol{p}_{di}(t)) = 0$. This ends the proof.

B.6 Proof Of Theorem 4.4

First we take the following Lyapunov function

$$\begin{aligned}
V &= V_{2a} + \tfrac{1}{2\gamma_{1v}} \tilde{J}_{1Li}^T \tilde{J}_{1Li} + \tfrac{1}{2\gamma_{2v}} \tilde{\boldsymbol{d}}_{vLi}^T \tilde{\boldsymbol{d}}_{vLi} \\
&\quad + V_{2b} + \tfrac{1}{2\gamma_{1v}} \tilde{J}_{1Fij}^T \tilde{J}_{1Fij} + \tfrac{1}{2\gamma_{2v}} \tilde{\boldsymbol{d}}_{vFij}^T \tilde{\boldsymbol{d}}_{vFij} \\
&\quad + V_4 + \tfrac{1}{2\gamma_{1\omega}} (\tilde{\boldsymbol{J}}_{Li}^{-1})^T (\tilde{\boldsymbol{J}}_{Li}^{-1}) + \tfrac{1}{2\gamma_{2\omega}} \tilde{\boldsymbol{d}}_{\omega Li}^T \tilde{\boldsymbol{d}}_{\omega Li} \\
&\quad + \tfrac{1}{2\gamma_{1\omega}} (\tilde{\boldsymbol{J}}_{Fij}^{-1})^T (\tilde{\boldsymbol{J}}_{Fij}^{-1}) + \tfrac{1}{2\gamma_{2\omega}} \tilde{\boldsymbol{d}}_{\omega Fij}^T \tilde{\boldsymbol{d}}_{\omega Fij}
\end{aligned} \tag{B.9}$$

Noting that

$$\begin{aligned}
&\dot{\tilde{J}}_{1(\cdot)} = -\dot{\hat{J}}_{1(\cdot)}, \\
&\dot{\tilde{\boldsymbol{d}}}_{\boldsymbol{v}(\cdot)} = -\dot{\hat{\boldsymbol{d}}}_{\boldsymbol{v}(\cdot)}, \\
&(\dot{\tilde{\boldsymbol{J}}}_{(\cdot)}^{-1}) = -(\dot{\hat{\boldsymbol{J}}}_{(\cdot)}^{-1}), \\
&\dot{\tilde{\boldsymbol{d}}}_{\boldsymbol{\omega}(\cdot)} = -\dot{\hat{\boldsymbol{d}}}_{\boldsymbol{\omega}(\cdot)}
\end{aligned} \tag{B.10}$$

where $(\cdot)$ stands for Li and Fij.

Differentiating both sides of (B.9), and using the results of (B.10), (4.130), (4.139) and (2.20)

, yields

$$\begin{aligned}\dot{V} &\leq \sum_{i=1}^{NL}\sum_{j=1}^{NF(i)}\left[-k_1\boldsymbol{\Omega}_{Li}^T\boldsymbol{\Omega}_{Li} - k_2{\boldsymbol{v}_{eLi}}^T\boldsymbol{v}_{eLi}\right] \\ &\quad + \sum_{i=1}^{NL}\sum_{j=1}^{NF(i)}\left[-k_1\boldsymbol{\Omega}_{Fij}^T\boldsymbol{\Omega}_{Fij} - k_2{\boldsymbol{v}_{eFij}}^T\boldsymbol{v}_{eFij}\right] \\ &\quad + \sum_{i=1}^{NL}\sum_{j=1}^{NF(i)}\left[-k_3\boldsymbol{q}_{eLi}^T\boldsymbol{G}_{Li}\boldsymbol{G}_{Li}^T\boldsymbol{q}_{eLi} - k_3\boldsymbol{q}_{eFij}^T\boldsymbol{G}_{F}ij\boldsymbol{G}_{Fij}^T\boldsymbol{q}_{eFij}\right] \\ &\quad + \sum_{i=1}^{NL}\sum_{j=1}^{NF(i)}\left[-k_4\boldsymbol{\omega}_{eLi}^T\boldsymbol{\omega}_{eLi} - k_4\boldsymbol{\omega}_{eFij}^T\boldsymbol{\omega}_{eFij}\right] \\ &< 0, \quad \forall(\boldsymbol{\Omega}_{Li}, \boldsymbol{v}_{eLi}, \boldsymbol{q}_{eLi}, \boldsymbol{\omega}_{eLi}) \neq (0,0,0,0) \text{ and } \forall(\boldsymbol{\Omega}_{Fij}, \boldsymbol{v}_{eFij}, \boldsymbol{q}_{eFij}, \boldsymbol{\omega}_{eFij}) \neq (0,0,0,0).\end{aligned} \tag{B.11}$$

meaning that

$$V(t) \leq V(t_0) \tag{B.12}$$

With the initial condition (2) in Assumption 4.5, $V(t_0)$ is bounded. Thus, $V(t)$ is also bounded. Boundedness of $V(t)$ for all $t \geq t_0 \geq 0$ implies that of $\boldsymbol{\Omega}_{Li}$,$\boldsymbol{\Omega}_{Fij}$, $\boldsymbol{v}_{eLi}$, $\boldsymbol{v}_{eFij}$, $\boldsymbol{q}_{eLi}$, $\boldsymbol{q}_{eFij}$, $\boldsymbol{\omega}_{eLi}$, and $\boldsymbol{\omega}_{eFij}$. Therefore the closed-loop system (4.157) is forward complete. Since $\lim_{t\to\infty} \boldsymbol{q}_{eLi} = 0$ implies that $(\psi_{Li}(t) - \psi_d(t)) = 0$ and $\lim_{t\to\infty} \boldsymbol{q}_{eFij} = 0$ implies that $\lim_{t\to\infty}(\psi_{Fij}(t) - \psi_{Li}(t)) = 0$; It also shows that $\lim_{t\to\infty}(\boldsymbol{p}_{Li}(t) - \boldsymbol{p}_{Ldi}(t)) = 0$ and $\lim_{t\to\infty}(\psi_{Fij}(t) - \psi_{Li}(t)) = 0$. This concludes the proof.

B.7 Proof Of Theorem 4.5

First we substitute the intermediate controls from (4.180) and (4.188) into (4.179) and (4.187) then we obtain

$$\begin{aligned}\dot{V}_{2a} &= \sum_{i=1}^{NL}\sum_{j=1}^{NF(i)}\left[-k_1\boldsymbol{\Omega}_{Li}^T\boldsymbol{\Omega}_{Li} - k_2\boldsymbol{v}_{eLi}^T\boldsymbol{v}_{eLi}\right], \\ &< 0, \quad \forall(\boldsymbol{\Omega}_{Li}, \boldsymbol{v}_{eLi}) \neq (0,0) \\ \dot{V}_{2b} &= \sum_{i=1}^{NL}\sum_{j=1}^{NF(i)}\left[-k_1\boldsymbol{\Omega}_{F\_Lij}^T\boldsymbol{\Omega}_{F\_Lij} - k_2\boldsymbol{v}_{eF\_Lij}^T\boldsymbol{v}_{eF\_Lij}\right] \\ &< 0, \quad \forall(\boldsymbol{\Omega}_{F\_Lij}, \boldsymbol{v}_{eF\_Lij}) \neq (0,0)\end{aligned} \tag{B.13}$$

this implies that

$$\begin{aligned}V_{2a}(t) &\leq V_{2a}(t_0), \\ V_{2b}(t) &\leq V_{2b}(t_0)\end{aligned} \tag{B.14}$$

With the initial condition in Assumption 4.6, $V_{2a}(t_0)$ and $V_{2b}(t_0)$ are bounded. Thus, $V_{2a}(t)$ and $V_{2b}(t)$ are also bounded. Boundedness of $V_{2a}(t)$ and $V_{2b}(t)$ for all $t \geq t_0 \geq 0$ implies that of $\boldsymbol{\Omega}_{Li}$, $\boldsymbol{\Omega}_{Fij}$, $\boldsymbol{v}_{eLi}$, and $\boldsymbol{v}_{eFij}$. Therefore the closed-loop system (4.189) is forward complete. It also shows that $\lim_{t\to\infty}(\boldsymbol{p}_{Li}(t) - \boldsymbol{p}_{Ldi}(t)) = 0$ and $\lim_{t\to\infty}(\boldsymbol{p}_{Fij}(t) - \boldsymbol{p}_{Li}(t)) = 0$. This concludes the proof.

APPENDIX

C

Publication list

International Conferences

- Nguyen Dang Hao, Boutayeb Mohamed and Hugues Rafaralahy, "Trajectory-tracking control design for an under-actuated quadrotor", the 13th European Control Conference (ECC) from the 24th to the 27th of June 2014 in Strasbourg, France.
- Nguyen Dang Hao, Boutayeb Mohamed and Hugues Rafaralahy, "Distributed controllers for multi-agent dynamical systems", SIAM (Society for Industrial and Applied Mathematics) Conference (10th EASIAM 2014) Thailand.
- Nguyen Dang Hao, Boutayeb Mohamed and Hugues Rafaralahy, "Global path tracking control for multiple quadrotors", The 2nd World Conference on Complex Systems (WCCS14), Agadir, Morocco.
- Nguyen Dang Hao, Boutayeb Mohamed and Hugues Rafaralahy, "Adaptive control for leader-follower formation of quadrotors", 3rd Workshop on Research, Education and Development of Unmanned Aerial Systems, Cancun, Mexico, November 2015.
- Nguyen Dang Hao, Boutayeb Mohamed and Hugues Rafaralahy, "Formation of leader-follower quadrotors in cluttered environment", The 2016 American Control Conference, July 2016, Boston, MA, USA. Submitted.

Preparing papers

- Nguyen Dang Hao, Boutayeb Mohamed and Hugues Rafaralahy, "Formation control of multiple quadrotors with limited sensing in cluttered environment", SIAM Journal on Control and Optimization (SICON). Preparing.

Commande de vol en formation d'une flotte de véhicules sous-actionnés

Nguyen Dang Hao

Résumé

Le contrôle de vol en formation se rapporte au contrôle de la trajectoire de plusieurs véhicules pour accomplir une tâche commune. La motivation du contrôle du vol en formation réside dans le fait que l'utilisation de plusieurs drones permet de réaliser des tâches plus complexes et que ne peut accomplir un drone unique. Les stratégies de commande de flotte de véhicules peuvent être classées en trois groupes principaux : la stratégie de vol type meneur-suiveur, celle basée sur comportement et l'approche utilisant un meneur virtuel. Chaque groupe se compose de différents véhicules et on suppose que les vehicules communiquent entre eux pour échanger des informations. Le contrôle de position pour des quadrirotors sous-actionnés ou des UAV VTOL a retenu l'intérêt de plusieurs chercheurs de la communauté scientifique. En raison de la nature sous-actionnée des UAV VTOL, l'attitude du système doit être utilisée afin de commander la position et la vitesse. En effet, la prise en compte des perturbations externes, des incertitudes sur la dynamique du système ainsi que l'objectif d'obtenir des résultats globaux rendent la synthèse de lois de commande plus difficile. Nous proposons, dans ce travail, un algorithme permettant l'extraction de l'attitude et une nouvelle formulation de la poussée pour la commande d'un drone. Cet algorithme utilise cette formulation de la force de poussée pour atteindre les objectifs en translation et utilise le vecteur quaternion unitaire comme consigne du sous-système en rotation. Cet algorithme est ensuite étendu au cas de la commande de vol en formation. Cinq contrôleurs de vol en formation sont développés et séparés dans deux groupes : l'approche structure virtuelle et l'approche meneur-suiveur. Les trois premiers contrôleurs de vol en formation utilisent l'approche structure virtuelle. La vitesse, les perturbations et les incertitudes de modèle dans la dynamique sont estimées par le biais d'un observateur et la technique de commande "backstepping" adaptative. La synthèse des deux derniers contrôleurs de vol en formation de vol est obtenue en utilisant l'approche meneur-suiveur. La formation utilisant cette approche pour des quadrirotors et pour le système du second degré est construite. Le changement de la configuration de la formation de vol est également simulé pour ces deux derniers contrôleurs de vol en formation. Dans chacun des cinq contrôleurs de vol en formation, la fonction d'évitement de collision construite à partir d'une fonction indicielle "lisse" est incluse. Cette fonction produit une force de poussée quand un quadrirotor évolue près des autres et d'une force de traction quand un quadrirotor évolue hors de la zone de détection. Les résultats de simulation prouvent que cette fonction d'évitement de collision fonctionne tout à fait correctement et qu'aucune collision entre les quadrirotors ni avec les obstacles ne se produit. En résumé, l'utilisation de la poussée, de l'algorithme d'extraction d'attitude et de la fonction d'évitement de collision, rend la synthèse des lois de commande plus facile et les résultats obtenus pour le vol en formation sont globaux.

Mots clés : quadrirotor, commande de vol en formation, systèmes non linéaires, véhicules sous-actionnés, drones

Formation control for a group of underactuated vehicles

Nguyen Dang Hao

Abstract

Formation control relates with the motion control of multiple vehicles to accomplish a common task. The motivation of formation control is because of the advantages achieved by using a formation of vehicles instead of a single one. Cooperative control approach can be cataloged into three main groups: leader-follower, behavior-based and virtual structure. Each group consists of individual vehicles and the communication allows the information be exchanged among vehicles. Position control for underactuated quadrotors or VTOL UAVs has been focused in several group in the research community. Due to the underactuated nature of VTOL UAVs, the system attitude must be used in order to control the position and velocity of the system. Moreover, the effect of external disturbance, uncertainty of the dynamics and the requirement of achieving the global results make the control design process more difficult. Developing from a global controller for a single quadrotor, a new thrust and attitude extraction algorithm is proposed. This algorithm allows transferring an intermediate control force to a thrust force to achieve the translational objective and an unit quaternion vector as a reference for the rotational subsystem. This algorithm is also embedded in the formation controller. Five formation controllers are developed and separated into two groups, virtual structure and leader-follower approach. The first three formation controllers are constructed by using the virtual structure approach. The unmeasured linear velocity, disturbance and uncertainty in the dynamics are solved by employing observer design and adaptive backstepping control design technique. The last two formation controllers are built by using the leader-follower approach. The leader follower formation for quadrotors and for second order system are constructed. The changing of formation shape in working time also is simulated in these last two formation controllers. In all five formation controllers, collision avoidance function constructed from a smooth step function is embedded. This function generates a pushing force when a quadrotor goes close to the others and a pulling force when a quadrotor travels out of the sensing range. The simulation results show that this collision avoidance function works quite effectively and there is no collision among quadrotors and obstacles. It can be summarized that by using the thrust and attitude extraction algorithm and the collision avoidance function, the control design process becomes easier and all the formation controllers achieve the global results.

Keywords: quadrotor, formation control, nonlinear systems, underactuated vehicles, UAV.

Bibliography

[Ark98] Ronald C Arkin, *Behavior-based robotics*, MIT press, 1998.

[AT09] A. Abdessameud and A. Tayebi, *Formation control of vtol-uavs*, Decision and Control, 2009 held jointly with the 2009 28th Chinese Control Conference. CDC/CCC 2009. Proceedings of the 48th IEEE Conference on, Dec 2009, pp. 3454–3459.

[AT10] Abdelkader Abdessameud and Abdelhamid Tayebi, *Global trajectory tracking control of vtol-uavs without linear velocity measurements*, Automatica **46** (2010), no. 6, 1053 – 1059.

[AT13] ———, *Motion coordination for vtol unmanned aerial vehicles*, Springer, 2013.

[BLH01] R.W. Beard, J. Lawton, and F.Y. Hadaegh, *A coordination architecture for spacecraft formation control*, Control Systems Technology, IEEE Transactions on **9** (2001), no. 6, 777–790.

[BM02] J.D. Boskovic and R.K. Mehra, *Multiple model-based adaptive reconfigurable formation flight control design*, Decision and Control, 2002, Proceedings of the 41st IEEE Conference on, vol. 2, Dec 2002, pp. 1263–1268 vol.2.

[BMF+11] A. Benini, A. Mancini, E. Frontoni, P. Zingaretti, and S. Longhi, *A simulation framework for coalition formation of unmanned aerial vehicles*, Control Automation (MED), 2011 19th Mediterranean Conference on, June 2011, pp. 406–411.

[BSZX12] Zhang Baoqun, Song Shenmin, Zheng Zhong, and Wei Xiqing, *Distributed coordinated formation control of multiple spacecraft with and without velocity measurements*, Control Conference (CCC), 2012 31st Chinese, July 2012, pp. 6105–6111.

[BVV11] F. Belkhouche, S. Vadhva, and M. Vaziri, *Modeling and controlling 3d formations and flocking behavior of unmanned air vehicles*, Information Reuse and Integration (IRI), 2011 IEEE International Conference on, Aug 2011, pp. 449–454.

[CL98] Tse Min Chen and R.C. Luo, *Integrated multi-behavior mobile robot navigation using decentralized control*, Intelligent Robots and Systems, 1998. Proceedings., 1998 IEEE/RSJ International Conference on, vol. 1, Oct 1998, pp. 564–569 vol.1.

[CLH+05] H. Choset, K. Lynch, S. Hutchinson, G. Kantor, W. Burgard, L. Kavraki, and S. Thrun, *Sampling-based algorithms*, pp. 197–267, MIT Press, 2005.

[CMSW11] Zhou Chao, Lei Ming, Zhou Shaolei, and Zhang Wenguang, *Collision-free uav formation flight control based on nonlinear mpc*, Electronics, Communications and Control (ICECC), 2011 International Conference on, Sept 2011, pp. 1951–1956.

[CS11] P. Calado and J. Sousa, *Leader-follower control of underwater vehicles over acoustic communications*, OCEANS, 2011 IEEE - Spain, June 2011, pp. 1–6.

[CSW12] Da Cai, Jian Sun, and Sentang Wu, *Uavs formation flight control based on behavior and virtual structure*, AsiaSim 2012 (Tianyuan Xiao, Lin Zhang, and Minrui Fei, eds.), Communications in Computer and Information Science, Springer Berlin Heidelberg, 2012, pp. 429–438 (English).

[DL12] Yanyan Dai and Suk-Gyu Lee, *The leader-follower formation control of nonholonomic mobile robots*, International Journal of Control, Automation and Systems **10** (2012), no. 2, 350–361.

[Do11] K.D. Do, *Relative formation control of mobile agent for gradient climbing and target capturing*, IEEE Transactions on Automatic Control **84** (2011), no. 6, 1098–1114.

[Do12] ———, *Formation control of underactuated ships with elliptical shape approximation and limited communication ranges*, Automatica **48** (2012), no. 7, 1380 – 1388.

[Do15] ———, *Coordination control of quadrotor vtol aircraft in three-dimensional space*, International Journal of Control **88** (2015), no. 3, 543–558.

[DP09] Khac Duc Do and Jie Pan, *Control of ships and underwater vehicles*, Springer, 2009.

[DP13] K.D. Do and J. Paxman, *Global tracking control of quadrotor vtol aircraft in three dimensional space*, Control Conference (AUCC), 2013 3rd Australian, Nov 2013, pp. 26–33.

[DS10] KhacDuc Do and Gerald Seet, *Motion control of a two-wheeled mobile vehicle with an inverted pendulum*, Journal of Intelligent and Robotic Systems **60** (2010), no. 3-4, 577–605 (English).

[EBOA04] D.B. Edwards, T.A. Bean, D.L. Odell, and M.J. Anderson, *A leader-follower algorithm for multiple auv formations*, Autonomous Underwater Vehicles, 2004 IEEE/OES, June 2004, pp. 40–46.

[EH01] M. Egerstedt and Xiaoming Hu, *Formation constrained multi-agent control*, Robotics and Automation, 2001. Proceedings 2001 ICRA. IEEE International Conference on, vol. 4, 2001, pp. 3961–3966 vol.4.

[EInE12] Aydin Eresen, Nevrez Imamoglu, and Mehmet ïċ½nder Efe, *Autonomous quadrotor flight with vision-based obstacle avoidance in virtual environment*, Expert Systems with Applications **39** (2012), no. 1, 894 – 905.

[HC08] Tianyun Huang and Xuebo Chen, *A geometric method of swarm robot formation controls*, Intelligent Control and Automation, 2008. WCICA 2008. 7th World Congress on, June 2008, pp. 3202–3206.

[JKW95] S.M. Joshi, A.G. Kelkar, and J.T.-Y. Wen, *Robust attitude stabilization of spacecraft using nonlinear quaternion feedback*, Automatic Control, IEEE Transactions on **40** (1995), no. 10, 1800–1803.

[Kha85] O. Khatib, *Real-time obstacle avoidance for manipulators and mobile robots*, Robotics and Automation. Proceedings. 1985 IEEE International Conference on, vol. 2, Mar 1985, pp. 500–505.

[Kha02] Hassan K. Khalil, *Nonlinear systems*, Prentice Hall, 2002.

[KK07] Seungkeun Kim and Youdan Kim, *Three dimensional optimum controller for multiple uav formation flight using behavior-based decentralized approach*, Control, Automation and Systems, 2007. ICCAS '07. International Conference on, Oct 2007, pp. 1387–1392.

[KKK95] Miroslav Krstic, Loannis Kanellakopoulos, and Petar Kokotovic, *Nonlinear and adaptive control design*, John Wiley and Sons, 1995.

[KKT09] Seungkeun Kim, Youdan Kim, and A. Tsourdos, *Optimized behavioural uav formation flight controller design*, Control Conference (ECC), 2009 European, Aug 2009, pp. 4973–4978.

[KS98] T.J. Koo and S. Sastry, *Output tracking control design of a helicopter model based on approximate linearization*, Decision and Control, 1998. Proceedings of the 37th IEEE Conference on, vol. 4, Dec 1998, pp. 3635–3640 vol.4.

[LaV06] Steven M. LaValle, *Planning algorithms*, Cambridge University Press, 2006.

[LF01] Naomi Ehrich Leonard and Edward Fiorelli, *Virtual leaders artificial potentials and coordinated control of groups*, Proccedings of the 40th IEEE Conference on decision and control, Orlando, Florida USA, 12/2001, pp. 2968–2973.

[Low11] Chang Boon Low, *A dynamic virtual structure formation control for fixed-wing uavs*, Control and Automation (ICCA), 2011 9th IEEE International Conference on, Dec 2011, pp. 627–632.

[Low14] ———, *A flexible virtual structure formation keeping control design for nonholonomic mobile robots with low-level control systems, with experiments*, Intelligent Control (ISIC), 2014 IEEE International Symposium on, Oct 2014, pp. 1576–1582.

[LRH+08] G. Lazea, R. Robotin, S. Herle, C. Marcu, and L. Tamas, *Mobile robots formation navigation with behavior based algorithms*, Automation, Quality and Testing, Robotics, 2008. AQTR 2008. IEEE International Conference on, vol. 2, May 2008, pp. 388–391.

[LSZ14] Shuang Liu, Dong Sun, and Changan Zhu, *A dynamic priority based path planning for cooperation of multiple mobile robots in formation forming*, Robotics and Computer-Integrated Manufacturing **30** (2014), no. 6, 589 – 596.

[MDTMC09] Hua Minh-Duc, Hamel T., Pascal Morin, and Samson Claude, *A control approach for thrust-propelled underactuated vehicles and its application to vtol drones*, Automatic Control, IEEE Transactions on **54** (2009), no. 8, 1837–1853.

[MS13] B. Madhevan and M. Sreekumar, *Tracking algorithm using leader follower approach for multi robots*, Procedia Engineering **64** (2013), 1426 – 1435, International Conference on Design and Manufacturing (IConDM2013).

[Muj09] Anusha Mujumdar, *Nonlinear geometric and differential geometric guidance of uavs for reactive collision avoidance*, Tech. report, Department of Aerospace Engineering Indian Institute of Science, 2009.

[OSM98] R. Olfati-Saber and A. Megretski, *Controller design for a class of underactuated nonlinear systems*, Decision and Control, 1998. Proceedings of the 37th IEEE Conference on, vol. 4, Dec 1998, pp. 4182–4187 vol.4.

[PAR05] R.C. Palat, A. Annamalau, and J.H. Reed, *Cooperative relaying for ad-hoc ground networks using swarm uavs*, Military Communications Conference, 2005. MILCOM 2005. IEEE, Oct 2005, pp. 1588–1594 Vol. 3.

[POT08] Jung Woo Park, Hyon Dong Oh, and Min Jea Tahk, *Uav collision avoidance based on geometric approach*, In SICE Annual Conference, 08/2008, pp. 2122–2126.

[PSH07] J. M. Pflimlin, P. Soueres, and T. Hamel, *Position control of a ducted fan VTOL UAV in crosswind*, International Journal of Control **80** (2007), 666–683.

[RCC+14] V. RoldÃ£o, R. Cunha, D. Cabecinhas, C. Silvestre, and P. Oliveira, *A leader-following trajectory generator with application to quadrotor formation flight*, Robotics and Autonomous Systems **62** (2014), no. 10, 1597 – 1609.

[RKPC02] D. Rathbun, S. Kragelund, A. Pongpunwattana, and B. Capozzi, *An evolution based path planning algorithm for autonomous motion of a uav through uncertain environments*, Digital Avionics Systems Conference, vol. 2, 2002, pp. 8D2–1 – 8D2–12 vol.2.

[Rob11] Andrew D. Roberts, *Attitude estimation and control of vtol uavs*, Ph.D. thesis, The University of Western Ontario, 2011.

[SB00] D.J. Stilwell and B.E. Bishop, *Platoons of underwater vehicles*, Control Systems, IEEE **20** (2000), no. 6, 45–52.

[SDFC01] P. Setlur, D. Dawson, Y. Fang, and B. Costic, *Nonlinear tracking control of the vtol aircraft*, Decision and Control, 2001. Proceedings of the 40th IEEE Conference on, vol. 5, 2001, pp. 4592–4597 vol.5.

[SH03] Karin Sigurd and Jonathan How, *Uav trajectory design using total field collision avoidance*, 2003.

[SHK+11] A. Sadowska, H. Huijberts, D. Kostic, N. van de Wouw, and H. Nijmeijer, *Formation control of unicycle robots using the virtual structure approach*, Advanced Robotics (ICAR), 2011 15th International Conference on, June 2011, pp. 365–370.

[Sho15] Khoshnam Shojaei, *Leader follower formation control of underactuated autonomous marine surface vehicles with limited torque*, Ocean Engineering **105** (2015), 196 – 205.

[SHP04] D.P. Scharf, F.Y. Hadaegh, and S.R. Ploen, *A survey of spacecraft formation flying guidance and control. part ii: control*, American Control Conference, 2004. Proceedings of the 2004, vol. 4, June 2004, pp. 2976–2985 vol.4.

[Shu93] Maicoim D. Shuster, *A survey of attitude representations*, The Journal of the Austronautical Sciences **41** (1993), no. 4, 439–517.

[STWZ10] Madhavan Shanmugavel, Antonois Tsourdos, Brian White, and Rafal Zbikowski, *Co-operative path planning of multiple uavs using dubins paths with clothoid arcs*, Control Engineering Practice **18** (2010), no. 9, 1084–1092.

[Tay08] A. Tayebi, *Unit quaternion-based output feedback for the attitude tracking problem*, Automatic Control, IEEE Transactions on **53** (2008), no. 6, 1516–1520.

[TDY09] K. Tulum, U. Durak, and S.K. Yder, *Situation aware uav mission route planning*, Aerospace conference, march 2009, pp. 1 –12.

[Tee92] Andrew R. Teel, *Global stabilization and restricted tracking for multiple integrators with bounded controls*, Syst. Control Lett. **18** (1992), no. 3, 165–171.

[TM06] A. Tayebi and S. McGilvray, *Attitude stabilization of a vtol quadrotor aircraft*, Control Systems Technology, IEEE Transactions on **14** (2006), no. 3, 562–571.

[Tsi98] P. Tsiotras, *Further passivity results for the attitude control problem*, Automatic Control, IEEE Transactions on **43** (1998), no. 11, 1597–1600.

[WKD91] J.T.-Y. Wen and K. Kreutz-Delgado, *The attitude control problem*, Automatic Control, IEEE Transactions on **36** (1991), no. 10, 1148–1162.

[YCLL08] Ben Yun, B.M. Chen, K.Y. Lum, and T.H. Lee, *A leader-follower formation flight control scheme for uav helicopters*, Automation and Logistics, 2008. ICAL 2008. IEEE International Conference on, Sept 2008, pp. 39–44.

[ZK12] An-Min Zou and K.D. Kumar, *Neural network-based distributed attitude coordination control for spacecraft formation flying with input saturation*, Neural Networks and Learning Systems, IEEE Transactions on **23** (2012), no. 7, 1155–1162.